Fibrin clot shields formation in tumor microenvironment driven by the procoagulant properties of cancer cells. Impact on the efficiency of anticancer therapy

Huong Chi Mai Tran

Sorbonne University

Doctorate School 394 Physiology, Pathophysiology and Therapeutics

Saint-Antoine Research Center - INSERM UMR_S 938

Cancer Biology and Therapeutics Team

Formation de boucliers de fibrine induite par les propriétés procoagulantes des cellules cancéreuses dans le microenvironnement tumoral

Étude de son impact sur l'efficacité du traitement anticancéreux

Fibrin clot shields formation in tumor microenvironment driven by the procoagulant properties of cancer cells

Impact on the efficiency of anticancer therapy

By Huong Chi Mai TRAN

Ph.D. Thesis in Molecular and Cellular Biology

Supervised by Pr. Grigorios GEROTZIAFAS

Presented and publicly defended on 19 June 2024

In front of a jury composed of:

Pr Alex DUVAL, as President

Pr Anna FALANGA, as Reviewer

Pr Laurence PANICOT-DUBOIS, as Reviewer

Pr Isabelle MAHÉ, as Examiner

Pr Cihan AY, as Examiner

Pr Grigorios GEROTZIAFAS, as Thesis Supervisor

"Un scientifique dans son laboratoire est non seulement un technicien : il est aussi un enfant placé devant des phénomènes naturels qui l'impressionnent comme des contes de fées."

"A scientist in their laboratory is not only a technician: they are also a child placed before natural phenomena that impress them like fairy tales."

Marie Skłodowska-Curie

ACKNOWLEDGEMENTS

First and foremost, I would like to express my gratitude to the members of the jury:

Professor **Alex DUVAL**, your presidency of the thesis jury was a profound honor for me. I deeply appreciate the trust and genuine interest you have shown in my work. Please accept my utmost respect and sincere gratitude.

Professor **Anna FALANGA** and Professor **Laurence PANICOT-DUBOIS**, I am immensely grateful to both of you for agreeing to participate in the evaluation of this work. Your invaluable contributions as reviewers have greatly enriched my thesis. I am truly thankful for the time and attention you dedicated to the critical reading of this manuscript. Please accept my heartfelt appreciation.

Professor **Isabelle MAHÉ** and Professor **Cihan AY**, I extend my heartfelt gratitude to you for accepting the responsibility of judging this work as examiners. Your expertise and insights are deeply appreciated. Thank you for your commitment to this process. Please accept my sincerest thanks and utmost respect.

I sincerely want to thank my thesis supervisor, Professor **Grigorios GEROTZIAFAS**. Words are not enough to express my gratitude for everything you have brought to me throughout this thesis. I am immensely grateful for your unwavering support, open-mindedness, and unwavering patience. Thank you for trusting me, for giving me the opportunity to work on this exciting project, which truly fueled my passion. I also would like to thank you for sharing your knowledge of hemostasis, your expertise, and your scientific spirit with me. I have not only enjoyed this work but also, and most importantly, the discussions we've had. It has been an incredible and enriching journey.

I extend my deepest gratitude to Doctor **Patrick VAN DREDEN** for your unwavering trust, support, encouragement, and generosity. Without you, I could not complete this journey.

I am deeply grateful to Professor **Marc VASSE** and Professor **Diane DAMOTTE** for their contributions to the annual thesis committee. Thank you for your availability, support, and

invaluable guidance that you have provided me throughout my professional journey. Please accept my heartfelt gratitude and utmost respect.

I would like to express my heartfelt thanks to **Diagnostica Stago**, for funding my thesis.

I also wish to convey my sincere appreciation to Doctor **Michèle SABBAH** for welcoming me into your team. Thank you for your support, guidance, and our always stimulating discussions.

To **Elisabeth MBEMBA**, the lab mom, I express my deepest gratitude. Thank you for your invaluable guidance, both professionally and personally. Your expertise in cell culture has been instrumental in my growth, and I am grateful for your numerous scientific insights and invaluable assistance in protocol development. Your unwavering support and comforting presence during both the good and challenging times have meant the world to me. Thank you for nurturing my growth and providing steadfast support.

To **Loula PAPAGEORGIOU**, without whom this incredible journey would not have begun, I extend my heartfelt thanks.

To all of my lab mates – **Rania, Lara, Aurélia, Lila, Élodie, and Chloé** - I am profoundly grateful for the countless enjoyable moments we've shared and the stimulating scientific discussions we've had. Thank you for your camaraderie and companionship.

To all of my dearest friends, **Khanh, Huyen,** and **Thu**, I extend my heartfelt gratitude. Thank you for always being there for me, for patiently listening to my complaints, my rambles, and my nonsensical musings.

To my family, especially **my parents**, I am deeply thankful. Thank you for your unwavering support and for instilling in me a love for science. Your encouragement of my curiosity has been invaluable. Thank you for teaching me to dream, to take risks, to be courageous, patient, and to believe in myself. Above all, thank you for your boundless love.

To **tata Bich and tonton Jean-Pièrre**, I am grateful beyond words for welcoming me into your home. Thank you for providing me with a sanctuary, a place of refuge when I am weary. Your support means the world to me.

To **tata Chau and tonton Trung**, your consistent presence in my life is deeply appreciated. Thank you for always being there.

And finally, to **my grandmother**, though you may no longer be with me physically, I feel your presence, love, and trust every day. Thank you for your enduring influence on my life.

ENGLISH ABSTRACT

Tumor microenvironment includes neo-vessels which brings in contact cancer cells with blood components including the proteins of the coagulation mechanism. Cancer cells express tissue factor (TF) and release TF-bearing micro-vesicles inducing a procoagulant state in their microenvironment. The formation of fibrin clot driven by the inherent procoagulant potential of cancer cells is an eventual consequence that, in the best of our knowledge, has not been explored. In the present PhD Thesis, we aimed to set-up a physiologically relevant experimental system of cancer cell cultures that includes human plasma allowing the investigation the formation of fibrin clot network, its structure, and its effect of the survival of cancer cells upon exposure to anticancer agents as well as on their migration.

Our work led to the set-up and validation of an original experimental system consisted of the culture of cancer cells in a conditioning media of human platelet poor plasma (PPP) diluted 10% in conventional culture media. The fibrin clot network formation process and structure upon coagulation activation by the inherent procoagulant potential of cancer cells were studied as follows:

- Pancreatic cancer cells (BXPC3), breast cancer cells triple negative (MDA-MB231) or positive to estrogen receptors (MCF7) were used to initiate coagulation.
- Their potential to trigger thrombin generation and their fibrinolytic activity were assessed.
- Scanning Electron Microscopy (SEM) and Laser Scanning Confocal Microscopy (LSCM) were used to study the fibrin clot structure and cancer cells' movement within the fibrin network.
- Paclitaxel (PTX) and 4-hydroxy-tamoxifen (4OHTam) were used to evaluate the impact of the cancer cell induced Fibrin Clot Shields (FCS) of the efficacy of the anticancer agents.

Cancer cells, particularly those with high procoagulant potential like BXPC3 and MDA-MB23 cells, induce the formation of dense fibrin networks with fine fibers, while MCF7 cells with lower procoagulant potential lead to the formation of thicker fibers. Exogenous TF further enhances the density of fibrin networks formed by MCF7 cells. Fibrin fibers are in contact with the cell membrane and the network has a structure like “bird’s nest” protecting the cells. Cancer cells demonstrate profibrinolytic activity and migrate within the fibrin scaffold, with BXPC3 and MCF7 cells moving in clusters and MDA-MB231 cells moving individually. The FCS decrease the efficiency of PTX and 4OHTam, indicating a protective effect against these anticancer agents.

Overall, this study reveals and highlights the critical role of cancer cells’ procoagulant signatures in shaping the fibrin clot network within the tumor microenvironment and influencing cancer cells’ behavior and response to therapies. The SEM images provide valuable insights into the architecture of the fibrin network and its interaction with cancer cells, supporting the notion of FCS as a protective mechanism against anticancer treatments.

Keywords: Cancer, thrombosis, microenvironment, D-dimer, fibrin, fibrinolysis

RÉSUMÉ EN FRANÇAIS (VERSION COURTE)

Le microenvironnement tumoral comprend des néovaisseaux qui mettent en contact les cellules cancéreuses avec les composants sanguins, y compris les protéines du mécanisme de coagulation. Les cellules cancéreuses expriment le facteur tissulaire (FT) et libèrent des microvésicules porteuses de FT, induisant un état procoagulant dans leur microenvironnement. La formation de caillots de fibrine, entraînée par le potentiel procoagulant inhérent des cellules cancéreuses, est une conséquence éventuelle qui, à notre connaissance, n'a pas été explorée. Dans la présente thèse de doctorat, nous avons cherché à établir un système expérimental physiologiquement pertinent de cultures de cellules cancéreuses incluant du plasma humain afin d'étudier la formation du réseau de caillots de fibrine, sa structure et son effet sur la survie des cellules cancéreuses lors de l'exposition à des agents anticancéreux ainsi que sur leur migration.

Ce travail a abouti à la mise en place et à la validation d'un système expérimental original consistant en une culture de cellules cancéreuses dans un milieu de conditionnement à base de plasma humain pauvre en plaquettes (PPP) dilué à 10 % dans un milieu de culture conventionnel. Le processus de formation et de structure du réseau de caillots de fibrine lors de l'activation de la coagulation par le potentiel procoagulant inhérent des cellules cancéreuses a été étudié comme suit :

- Des cellules cancéreuses du pancréas (BXPC3), des cellules cancéreuses du sein triple négatives (MDA-MB231) ou positives aux récepteurs d'œstrogènes (MCF7) ont été utilisées pour initier la coagulation.

- Leur capacité à déclencher la génération de thrombine et leur activité fibrinolytique ont été évaluées.

- La microscopie électronique à balayage (MEB) et la microscopie confocale à balayage laser (MCBL) ont été utilisées pour étudier la structure du caillot de fibrine et le mouvement des cellules cancéreuses au sein du réseau de fibrine.

- Le paclitaxel et le 4-hydroxy-tamoxifène ont été utilisés pour évaluer l'impact des boucliers de caillot de fibrine induits par les cellules cancéreuses sur l'efficacité des agents anticancéreux.

Les cellules cancéreuses, en particulier celles présentant un potentiel procoagulant élevé comme les cellules BXPC3 et MDA-MB231, induisent la formation de réseaux de fibrine denses avec des fibres fines, tandis que les cellules MCF7 avec un potentiel procoagulant plus faible conduisent à la formation de fibres plus épaisses. Le FT exogène renforce encore la densité des réseaux de fibrine formés par les cellules MCF7. Les fibres de fibrine sont en contact avec la membrane cellulaire et le réseau présente une structure de type "nid d'oiseau" protégeant les cellules. Les cellules cancéreuses démontrent une activité profibrinolytique et migrent à l'intérieur de l'échafaudage de fibrine, avec les cellules BXPC3 et MCF7 se déplaçant en amas et les cellules MDA-MB231 se déplaçant individuellement. Les boucliers de fibrine diminuent l'efficacité du paclitaxel et du 4-hydroxy-tamoxifene, indiquant un effet protecteur contre ces agents anticancéreux.

Dans l'ensemble, cette étude révèle et met en évidence le rôle critique des signatures procoagulantes des cellules cancéreuses dans le façonnage du réseau de caillots de fibrine dans le microenvironnement tumoral et l'influence sur le comportement des cellules cancéreuses et la réponse à la thérapie. Les images MEB fournissent des informations précieuses sur l'architecture du réseau de fibrine et son interaction avec les cellules cancéreuses, soutenant l'idée des boucliers de caillot de fibrine comme mécanisme protecteur contre les traitements anticancéreux.

Mots-clés : Cancer, thrombose, microenvironnement, D-dimères, fibrine, fibrinolyse

RÉSUMÉ EN FRANÇAIS (VERSION LONGUE)

Introduction

Les tumeurs solides sont des systèmes complexes, dominés par les interactions des cellules cancéreuses avec le microenvironnement, où les vaisseaux sanguins et les composants sanguins, y compris les protéines de coagulation, jouent un rôle important dans le développement et la métastase tumorale. La néoangiogenèse et la mimique vasculaire sont des processus essentiels stimulés par les cellules cancéreuses qui permettent l'approvisionnement en nutriments et en énergie de la tumeur. Certaines populations de cellules cancéreuses au sein de la tumeur sont en contact avec le sang, et par conséquent, avec les facteurs de coagulation et de fibrinolyse.

Les cellules cancéreuses expriment le facteur tissulaire (FT), le principal activateur de la coagulation sanguine qui induit la génération de thrombine, conduisant à la formation de caillots de fibrine. Le type histologique et l'agressivité des cellules cancéreuses sont liés à l'expression du FT et à leur potentiel procoagulant. De plus, les cellules cancéreuses libèrent des exosomes procoagulants portant du FT, qui amplifient le stimulus procoagulant dans le microenvironnement.

Le clivage du fibrinogène par la thrombine, la polymérisation des monomères de fibrine et la stabilisation du réseau de fibrine par le facteur XIII activé par la thrombine sont les étapes ultimes de l'activation de la coagulation conduisant à la formation de caillots. La fibrine est dégradée par la plasmine, suivant le clivage du plasminogène par l'activateur de plasmine urokinase (uPA) ou l'activateur de plasmine tissulaire (tPA). La fibrinolyse et le remodelage de la matrice extracellulaire sont des mécanismes clés dans le processus de métastase.

Le remodelage de la matrice extracellulaire par les cellules cancéreuses soutient la prolifération, la métastase, l'angiogenèse, la lymphangiogenèse et l'immunosuppression. La fibrine est un élément substantiel dans le microenvironnement tumoral, évident dans les spécimens pathologiques de tumeurs chez les patients. De plus, un lien a été établi entre le stade et l'agressivité du cancer et la quantité de fibrine dans le microenvironnement tumoral.

L'objectif de l'étude s'agit à étudier l'impact des propriétés procoagulantes des cellules cancéreuses sur la structure du caillot de fibrine et le comportement des cellules cancéreuses au sein du réseau de fibrine.

Matériels et Méthodes

Formation du Bouclier Caillot de Fibrine (BCL)

Deux méthodes de formation du BCL autour des cellules cancéreuses ont été testé :

Méthode 1 : Hydrogel de fibrine : Un hydrogel de fibrine a été fabriqué à partir de fibrinogène et thrombine purifié, avec différentes concentrations : 1 mg/ml Fibrinogène + 2 UI/ml Thrombine ; 1 mg/ml Fibrinogène + 4 UI/ml Thrombine ; 5 mg/ml Fibrinogène + 2 UI/ml Thrombine ; 5 mg/ml Fibrinogène + 4 UI/ml Thrombine. Les cellules ont été ensemencées à 24 heures auparavant pour adhésion, puis un hydrogel de 50 µm d'épaisseur a été déposé au-dessus.

Méthode 2 : Méthode du milieu conditionné au plasma pauvre en plaquettes (PPP) : La formation du réseau de fibrine a été induite en cultivant les cellules cancéreuses en présence de plasma pauvre en plaquettes (PPP) obtenu auprès de l'Établissement Français du Sang (Hôpital Saint-Antoine, Paris, France). Pour déterminer la dilution optimale du PPP dans le milieu de culture, la viabilité des cellules cancéreuses et leur capacité à induire la génération de thrombine ont été mesurées dans des dilutions sérielles de PPP, allant de 10% à 75%. La dilution de 10% a été sélectionnée pour être utilisée (ci-après appelé ***milieu conditionné PPP***). Dans cette condition, la viabilité des cellules était préservée, la génération de thrombine était mesurable et la formation du réseau de fibrine était garantie.

Évaluation de la génération de thrombine (GT)

Le test automatisé calibré du thrombogramme (Thrombinoscope™, Diagnostica Stago, Asnières, France) a été utilisé pour mesurer la génération de thrombine. Dans l'expérience de contrôle, la GT induite par une gamme de concentration du FT (de 0,5 à 20 pM) dans 10% de PPP a été étudiée. L'étude de la GT par les cellules cancéreuses ont été menée avec des cellules cancéreuses ont été ensemencées à une densité de $5x10^3$ cellules par puit. Du FT exogène (réactif PRP Reagent®, Diagnostica Stago, Asnières, France) a été ajouté aux cultures de cellules MCF7 dans un milieu conditionné PPP à une concentration finale de 1 pM.

Évaluation de la viabilité des cellules cancéreuses au sein du caillot de fibrine

La viabilité des cellules a été analysée par observation les cristaux de formazan en utilisant le test du MTT (bromure de 3-(4,5-diméthylthiazol-2-yl) -2,5-diphényltétrazolium) ; et par dosage colométrique en utilisant le test de résazurine.

Analyse de la structure du caillot de fibrine

La formation des BCF a été induite en utilisant la méthode PPP-milieu conditionné. L'analyse de la structure des BCF a été réalisé sur des images issues de la microscopie électronique à balayage (MEB). L'observation de la migration des cellules cancéreuses à l'intérieur des BCF ont été conduite en incorporant 2,5 µg/ml de fibrinogène couplé avec Alexa Fluor 488 dans le milieu conditionné PPP, avec un microscope confocale à balayage laser (MCBL).

Étude de la fibrinolyse

Les cellules ont été cultivées dans du milieu conditionné PPP ou 10% de PBS (expérience témoin). Les surnageants ont été collectés à des intervalles prédéfinis (0, 6, 10, 12, 14, 18, 24, 48 et 72 heures) pour la mesure des D-Dimères et du tPA en utilisant des méthodes ELISA.

Quantification de l'intensité de fluorescence

Les cellules dont les noyaux ont été marqués avec du Hoechst 33342 ont été cultivées par du milieu conditionné PPP, en présence ou en absence de 2,5 µg/ml de fibrinogène couplé avec Alexa Fluor 488. Les images ont été obtenues avec un microscope fluorescent, et l'intensité du canal vert a été mesurée et divisée par le nombre total de cellules dans chaque champ.

Efficacité des traitements anticancéreux en présence ou en absence de réseau de caillot de fibrine

Les cellules cancéreuses ont été exposées au paclitaxel (BXPC3, MDA-MB231 et MCF7) ou 4-hydroxy-tamixifène (4OHTam) (MCF7) à leurs IC50 correspondantes pendant 72 heurs, en absence ou en présence des BCF.

Résultats

Validation de la méthode de formation des BCF

Les cellules cultivées dans des hydrogels composés de 5 mg/ml de fibrinogène et de 2 UI/ml de thrombine ou de 5 mg/ml de fibrinogène et de 4 UI/ml de thrombine ont présenté une perte de viabilité d'environ 60% et 50%, respectivement. En revanche, l'hydrogel constitué de 1 mg/ml de fibrinogène et de 4 UI/ml de thrombine a augmenté la viabilité cellulaire d'environ 40%. Les cellules cultivées dans l'hydrogel de 1 mg/ml de fibrinogène et de 2 UI/ml de thrombine ont conservé une viabilité à des niveaux similaires à celles des cellules cultivées sans fibrine.

À la dilution de 10% de PPP, les trois lignées cellulaires ont présenté une viabilité et une prolifération acceptables. Dans cette condition, les cellules étaient capables à induire la GT, avec différents niveaux de potentiel dans l'ordre croissante : MCF7, BXPC3, et MDA-MB231. L'ajout du FT sur des cellules MCF7 les a rendus autant procoagulantes que les cellules BXPC3.

En utilisant la méthode du milieu conditionné PPP, les cellules cancéreuses ont été capable à induire la formation des BCF au bout de 2 heures, en présence de 10% PPP.

Caractéristiques structurelles du bouclier de caillot de fibrine - Impacts de FT et des cellules cancéreuses

L'augmentation des concentrations de FT dans le milieu conditionné PPP a entraîné une diminution des diamètres des fibres (0,104 ± 0,007 µm, 0,094 ± 0,003 µm et 0,091 ± 0,001 µm pour 0,5, 1 et 2 pM de FT respectivement) et de la taille des pores (0,093 ± 0,005 μm^2, 0,075 ± 0,003 μm^2 et 0,067 ± 0,001 μm^2 pour 0,5, 1 et 2 pM de FT respectivement). En revanche, l'augmentation des concentrations de FT a entraîné une augmentation du nombre d'intersections : 918 ± 76 en présence de 0,5 pM de FT, 1173 ± 52 avec 1 pM de FT et 1356 ± 24 intersections avec 2 pM de FT.

Les diamètres des fibres des caillots formés par les cellules MDA-MB231 étaient significativement plus petits que ceux formés par les cellules BXPC3 ou MCF7 [0,093 ± 0,002 µm contre 0,106 ± 0,004 µm ($p = 0,02$) et 0,141 ± 0,008 µm ($p < 0,001$) respectivement]. Les fibres du caillot de fibrine formé par les cellules MCF7 avaient un diamètre significativement plus grand que celles formées par les cellules BXPC3 ($p < 0,001$).

Les tailles des pores des caillots formés en présence de cellules MDA-MB231 (0,062 ± 0,006 μm^2) étaient significativement plus petites que celles formées en présence de cellules MCF7 (0,138 ± 0,029 μm^2, $p < 0,001$), mais pas par rapport à celles des cellules BXPC3 (0,087 ± 0,007 μm^2, $p = 0,09$). Les caillots formés en présence de cellules MCF7 présentaient une taille de pore significativement plus grande par rapport à ceux formés en présence de cellules BXPC3 ou MDA-MB231 ($p = 0,003$ et $p < 0,001$ respectivement).

Le nombre d'intersections des fibres de fibrine était significativement plus faible dans les caillots formés en présence de cellules MCF7 (539 ± 101) par rapport à ceux formés en présence de cellules MDA-MB231 ou BXPC3 (1177 ± 135 et 982 ± 96, $p = 0,001$ et $p = 0,01$ respectivement). Il n'y avait pas de différence significative dans le nombre d'intersections de fibrine entre les caillots formés en présence de cellules BXPC3 et de cellules MDA-MB231 ($p = 0,22$).

L'ajout de 1 pM de FT dans le milieu conditionné PPP de MCF7 a conduit à la formation de caillots similaires à ceux formés en présence de cellules BXPC3, en termes de diamètres de fibre (0,099 ± 0,010 µm contre 0,106 ± 0,004 µm respectivement, $p = 0,17$), de tailles de pores (0,095 ± 0,023 µm2 contre 0,087 ± 0,007 µm2 respectivement, $p = 0,56$) et de nombre d'intersections (1026 ± 385 contre 982 ± 96 respectivement, $p = 0,78$).

Migration des cellules cancéreuses au sein des BCF

Au début de l'expérience, les cellules cancéreuses ont formé une monocouche adhésive au fond de la plaque. Après la formation du caillot, l'observation par MEB a montré des amas de cellules sur la couche supérieure des caillots de fibrine. L'observation du caillot sous MCBL a révélé la présence de cellules BXPC3, MDA-MB231 ou MCF7 au fond, à l'intérieur et sur le dessus du caillot de fibrine. Ensuite, nous avons confirmé la vitalité de ces cellules et avons écarté la possibilité qu'elles soient des cellules mortes détachées de la plaque de culture et qu'elles soient ensuite piégées dans le caillot de fibrine. L'absence d'ADN condensé ou fragmenté dans les noyaux, l'intégrité des membranes cellulaires, le maintien de l'adhésion cellulaire, ont en outre confirmé le fait que les cellules à tous les niveaux du caillot étaient vivantes.

Ce résultat a été confirmé par la culture en 3D. Les cultures 3D de BXPC3 et MCF7 ont montré une expansion asymétrique en présence des BCF. Dans des régions distinctes des cultures

sphéroïdes initiales de BXPC3 et de MCF7, des formations en bourgeonnement sont apparues, indiquant un schéma de migration collective des cellules. L'ajout de FT exogène a renforcé l'invasion des cellules MCF7 dans le réseau de fibrine. Dans les cultures 3D de MDA-MB231, des cellules individuelles ont été identifiées le long des fibres de fibrine, indiquant une migration cellulaire suivant un modèle individuel.

Présence de la fibrine sur la membrane plasmique

La microscopie par fluorescence a révélé la présence de fibres de fibrine liées à la couche extracellulaire des membranes des cellules cancéreuses. Dans les cultures 3D, en utilisant un anticorps anti-fibrine spécifique qui reconnaissait spécifiquement la fibrine. Les lames transversales ont montré que seules les cellules situées sur la couche externe des sphéroïdes formés par les MCF7 ou les MDA-MB231 interagissaient avec la fibrine. En revanche, ce type d'interaction a été observé sur des cellules situées à la fois sur les couches externes et internes des sphéroïdes BXPC3.

Activité fibrinolytique des cellules cancéreuses

Dans l'expérience témoin, (cellules cultivées dans un milieu conditionné sans PPP), une libération progressive de tPA a été observée en présence de cellules BXPC3 ou MDA-MB231, mais pas en présence de cellules MCF7. Pendant la période d'observation, de faibles concentrations de tPA ont été mesurées dans le plasma (0,06 ± 0,04 ng/ml à t0 et 0,24 ± 0,07 ng/ml après 72 heures ; $p > 0,99$). En présence de PPP, la libération de tPA par les cellules BXPC3 ou MDA-MB231 a progressivement augmenté. À 72 heures, les niveaux de tPA libérés par les MDA-MB231 (3,77 ± 2,18 ng/ml) étaient significativement plus élevés par rapport à ceux libérés par les cellules MCF7 (0,14 ± 0,01 ng/ml, $p = 0,02$).

Dans l'expérience témoin, en absence de cellules cancéreuses, les niveaux de D-Dimère dans le milieu conditionné par PPP étaient de 0,09 ± 0,11 µg/ml après 72 heures. Après la formation du caillot de fibrine en présence de cellules BXPC3 ou MDA-MB231, une augmentation progressive de la D-Dimère a été observée. L'augmentation de la concentration en D-Dimère est devenue significative après 24 heures de formation du caillot pour les cellules BXPC3 ($p < 0,001$ par rapport à t0) et 14 heures pour les cellules MDA-MB231 ($p < 0,001$ par rapport à t0). En présence de cellules MDA-MB231 et BXPC3, les niveaux de D-Dimère ont continué à

augmenter jusqu'à 72 heures après la formation du caillot. En présence de cellules MCF7, après la formation du caillot de fibrine, aucune variation significative de la concentration en D-Dimère n'a été observée ($p > 0,99$ entre t0 et après 72 heures). À la fin de la période d'observation, la concentration maximale de D-Dimère en présence de BXPC3 et de MDA-MB231 était respectivement de 160,77 ± 46,39 µg/ml et de 56,19 ± 9,29 µg/ml.

Impact des BCF dans l'efficacité des agents anticancéreux

En appliquant le système expérimental conventionnel pour l'étude de l'efficacité des agents anticancéreux, sans fibrine, l'IC50 du paclitaxel était de 0,5 µM pour les cellules BXPC3 et de 0,1 µM pour les cellules MDA-MB231 et MCF7. L'IC50 du 4-hydroxy-tamoxifène était de 10 nM pour les cellules MCF7.

À 2 heures après la formation du caillot, l'ajout de paclitaxel à l'IC50 n'a pas entraîné de diminution détectable de la viabilité des cellules BXPC3, MDA-MB231 ou MCF7. De même, l'ajout de 4-hydroxy-tamoxifène n'a pas entraîné de diminution détectable de la viabilité des cellules MCF7.

À 24 heures après la formation du caillot, l'ajout de PTX à l'IC50 a entraîné une diminution de 50 % de la viabilité des cellules BXPC3.

À 24 heures après la formation du caillot, l'ajout de PTX à l'IC50 n'a pas entraîné de décès détectable des cellules MDA-MB213 ou MCF7. De même, l'ajout de 4OHTam n'a pas entraîné de mort détectable des cellules MCF7.

Discussion

La présente étude explore les caractéristiques qualitatives et quantitatives de la formation de caillots de fibrine lors de l'activation de la coagulation par les cellules cancéreuses exprimant le FT. Elle présente des preuves originales prouvant que les cellules cancéreuses conduisent à la formation d'un réseau de caillots de fibrine structuré comme un "nid d'oiseau" en contact avec les membranes des cellules cancéreuses. Les cellules cancéreuses avec leur propre signature procoagulante construisent le réseau de fibres qui fournit un échafaudage pour la migration. Le type histologique des cellules cancéreuses exprimant le FT et leur signature procoagulante sont des déterminants de l'architecture et des caractéristiques structurelles du réseau de fibres. Le

réseau de fibrine fonctionne comme une barrière protectrice contre les agents anticancéreux, tels que le paclitaxel et le 4-hydroxytamoxifène.

L'analyse des caractéristiques caractéristiques structurelles des BCF a révélé que les propriétés procoagulantes du microenvironnement jouent un rôle critique, qu'elles proviennent des propriétés procoagulantes des cellules cancéreuses elles-mêmes, telles que l'expression membranaire du FT, ou de la présence du FT dans le microenvironnement. En outre, nous avons démontré que les BCF servent d'échafaudage favorisant la migration des cellules cancéreuses et agissent comme une barrière physique, réduisant l'efficacité des agents anticancéreux.

Le rôle du bouclier de fibrine pourrait être d'un intérêt particulier dans la compréhension de la résistance aux thérapies anticancéreuses ciblées. Nos données permettent de proposer que les boucliers de fibrine générés par les propriétés procoagulantes des cellules cancéreuses pourraient représenter un nouveau mécanisme conduisant au développement de la résistance aux traitements anticancéreux qui mérite d'être étudié plus en détail.

Bien que les lymphocytes T conservent leur mobilité dans la fibrine (Zou et al., 2012), plus le caillot est ferme, plus il faut de temps aux cellules CAR-T pour le traverser (Ogunnaike et al., 2021). Ainsi, nous supposons que les boucliers de caillots de fibrine pourraient contribuer à l'épuisement des cellules CAR-T, qui est considéré comme un mécanisme majeur d'échec du traitement (Kouro et al., 2022 ; Zhu et al., 2022). Le rôle des boucliers de fibrine générés par les cellules cancéreuses dans le développement de la résistance aux traitements anticancéreux ciblés et aux thérapies par cellules CAR-T constitue un nouveau domaine d'intérêt potentiel.

En démêlant les mécanismes sous-jacents de l'interaction entre le microenvironnement tumoral et les boucliers de caillots de fibrine, nous pouvons obtenir des informations sur la manière dont ces interactions impactent l'efficacité des traitements ciblés. Cette connaissance pourrait finalement conduire au développement de stratégies visant à améliorer l'efficacité des thérapies anticancéreuses et à surmonter la résistance aux médicaments dans le traitement du cancer.

TABLE OF CONTENTS

ABBREVIATIONS

4OHTam	4-Hydroxy-Tamixifen / 4-Hydroxy-Tamixifène
A2AP	A2-Antiplasmin
A2M	A2-Macroglobulin
ADP	Adenosine Diphosphate
AMP	Adenosine Monophosphate
APC	Activated Protein C
AT	Antithrombin
ATP	Adenosine Triphosphate
BCL	Bouclier Caillot De Fibrine
BSA	Bovine Serum Albumin
BXPC3	Pancreatic Adenocarcinoma Cell Line
C/EBP	CCAAT-Enhancer-Binding Proteins
CAF	Cancer-Associated Fibroblasts
CAR-T cell	Chimeric Antigen Receptors T Cell
CAT	Cancer-Associated Thrombosis
CBP/p300	Co-Activator CREB-Binding Protein/P300 Protein
CTC	Circulating Tumor Cells
CTCF	CCCTC-Binding Factor
DMSO	Dimethyl Sulfoxide

DNA	Deoxyribonucleic Acid
EC	Endothelial Cells
ECM	Extracellular Matrix
EGFR	Epidermal Growth Factor Receptor
ELISA	Enzyme-Linked Immunosorbent Assay
EMT	Epithelial-Mesenchymal Transition
EPCR	Endothelial Protein C Receptors
ER	Estrogen Receptor
ET	Endothelin
ETP	Endogenous Thrombin Potential
EV	Extracellular Vesicles
FBS	Fetal Bovine Serum
FCS	Fibrin Clot Shield
FDP	Fibrin Degradation Products
Fg	Fibrinogen / Fibrinogène
FGA	Fibrinogen Alpha Chain
FGB	Fibrinogen Beta Chain
FGG	Fibrinogen Gamma Chain
FpA	Fibrinopeptide A
FpB	Fibrinopeptide B
FT	Facteur Tissulaire

GP	Glycoprotein
GR	Glucocorticoid Receptor
GT	Génération De Thrombine
HATs	Histone Acetyltransferases
HER2	Human Epidermal Growth Factor 2
HMDS	Hexamethyldisilazane
HMWK	High-Molecular-Weight Kininogen
HNF-1	Hepatocyte Nuclear Factor 1
HS	Heparan Sulfate
IC50	Half Maximal Inhibitory Concentration
ICAM-1	Intercellular Adhesion Molecule-I
IFN-γ	Interferon-Gamma
IGF	Insulin-Like Growth Factor
IL	Interleukin
KK	Kallikrein
KRAS	Kirsten Rat Sarcoma Virus
LSCM	Laser Scanning Confocal Microscopy
MCBL	Microscopie Confocale À Balayage Laser
MCF7	Non-Invasive Breast Adenocarcinoma Cell Line
MDA-MB231	Invasive Breast Adenocarcinoma Cell Line
MEB	Microscopie Électronique À Balayage

MMP	Matrix Metalloproteinases
MRI	Mean Rate Index
mRNA	Messenger Ribonucleic Acid
MTT	Bromure De 3-(4,5-Dimethylthiazol-2-Yl)-2,5-Diphenyltétrazolium
NET	Neutrophil Extracellular Traps
NO	Nitric Oxide
PAF	Platelet-Activating Factor
PAI-1	Plasminogen Activator Inhibitor Type-I
PAI-2	Plasminogen Activator Inhibitor Type-2
PAR	Protease-Activated Receptor
PBS	Phosphate-Buffered Saline
PF4	Platelet Factor 4
PGI2	Prostacyclin
PKK	Prekallikrein
PPL	Phospholipid
PPP	Platelet-Poor Plasma / Plasma Pauvre En Plaquette
PR	Progesterone Receptor
PS	Phosphatidylserine
PTEN	Phosphatase and Tensin Homolog
PTX	Paclitaxel
RBC	Red Blood Cell

ROS	Reactive Oxygen Species
SD	Standard Deviation
SDF-1	Stromal-Derived Factor-1
SEM	Scanning Electron Microscopy
Sp1	Specificity Protein 1
STAT3	Signal Transducer and Activator Of Transcription 3
TAFI	Thrombin Activated Fibrinolysis Inhibitor
TAM	Tumor-Associated Macrophages
TF	Tissue Factor
TFPI	Tissue Factor Pathway Inhibitor
TM	Thrombomodulin
TMB	3,3',5,5'-Tetramethylbenzidine
TNFα	Tumor Necrosis Factor Alpha
tPA	Tissue-Type Plasminogen Activator / Activateur De Plasmine Tissulaire
ttPeak	Time To Peak
TXA2	Thrombendothelinoxane A2
uPA	Urokinase-Type Plasminogen Activator / Activateur De Plasmine Urokinase
USF	Upstream Stimulatory Factor
VCAM-1	Vascular Cell Adhesion Molecule-I
VEGF	Endothelial Growth Factor
VTE	Venous Thromboembolism

vWF	von Willebrand Factor

LIST OF TABLES

LIST OF FIGURES

GENERAL INTRODUCTION

1. Hemostasis

1.1. Introduction

The term *hemostasis* is derived from *haemo-* (Neo Latin of *haimó*, meaning "*blood*", in Greek) and *-stasis* (*stagnation*) (Oxford English Dictionary, 2023). In the event of a vascular injury, hemostasis is a physiological mechanism that prevents blood loss while maintaining the integrity of blood vessels. Hemostasis consists of three phases:

- **Primary hemostasis:** the first response to vascular damages, leading to the activation, adhesion, and aggregation of platelets to the lesion, forming a platelet plug that minimize blood loss.
- **Coagulation:** a complex enzymatic system to expand and strengthen the clot, by polymerizing fibrin to form a fibrin network that captures other blood cells, ceasing hemorrhage.
- **Fibrinolysis:** degradation and dissolution of the fibrin clot, preventing it from excessive expand and total blockage of the vessel, allowing the wound healing process to repair the endothelial lesion.

Hemostasis must be strictly regulated, for it needs not only to be triggered and intensified in minimal time upon injury to minimize blood loss, but also to be prevented from being amplified more than necessary to avoid complete obstruction of blood flow. An imbalance between these forces leads to risks of either hemorrhage (hypocoagubility) or thrombosis (hypercoagubility).

1.2. Elements of hemostasis

1.2.1. Cellular elements

1.2.1.1. The endothelium

The *endothelium*, composed of a single layer of endothelial cells (EC), lines the inner surface of blood vessels (including arteries, veins, and capillaries) as well as the lymphatic system. These endothelial cells are anchored on one side to a connective tissue known as the *sub-endothelium*, while on the other side, they open to the lumen of the vessel.

The endothelium represents a large variety in term of structure and function base on the location and physiological condition. Their thickness could vary from 0.1 µm in capillaries to 1 µm in the aorta. Arteriolar ECs appear elongated and spindle-shaped; capillary ECs are irregularly shaped; postcapillary venular ECs appear large, elliptical, or irregular; whereas collecting venular ECs exhibit rounded morphology (Aird, 2007).

Structural heterogeneity of ECs could also be categorized as either continuous or discontinuous. Continuous endothelium may further be classified as fenestrated or nonfenestrated. Nonfenestrated continuous endothelium is typically found in the arteries, veins, and capillaries of organs such as the brain, skin, heart, and lungs. Fenestrated continuous endothelium is present in regions where there is an increased demand for filtration or transendothelial transport, such as in the capillaries of exocrine and endocrine glands, gastric and intestinal mucosa, choroid plexus, glomeruli, and a subset of renal tubules. Discontinuous endothelium is observed in specific sinusoidal vascular beds, notably in the liver (Aird, 2007).

The endothelium plays a crucial role in various physiological functions, including maintaining tissue homeostasis, regulating vessel permeability for exchanges of fluids, particles and soluble molecules, participating in immune and inflammatory responses, generating new vessels in case of wound healing and tumorigenesis (angiogenesis), and regulating hemostasis.

In its resting state, the endothelium, which is in constant contact with blood, exerts an antithrombotic activity, promoting unimpeded blood flow. Endothelial cells secrete nitric oxide (NO) and prostacyclin (PGI2), both serving as vasodilators while inhibiting platelet adhesion and aggregation. Ectonucleotidases, enzymes produced by endothelial cells, catalyze the dephosphorylation of ADP to AMP and eventually to adenosine, thereby preventing platelet aggregation.

The luminal membrane's thromboresistant characteristics is upheld through the expression of heparan sulfate (HS) and thrombomodulin (TM). HS facilitates the binding of antithrombin (AT), a potent coagulation inhibitor, to the endothelial surface, while TM modulates the activity of thrombin (FIIa) from a procoagulant to an anticoagulant state. Additionally, endothelial cells release Tissue Factor Pathway Inhibitor (TFPI), which neutralizes the enzymatic complex TF-FVIIa.

Furthermore, endothelial cells actively participate in fibrinolysis by secreting tissue-type plasminogen activator (tPA) and urokinase-type plasminogen activator (uPA). These activators transform plasminogen into plasmin, an enzyme crucial for degrading and dissolving fibrin clots, thereby aiding in the restoration of vascular patency and homeostasis (Félétou, 2011; Galley & Webster, 2004).

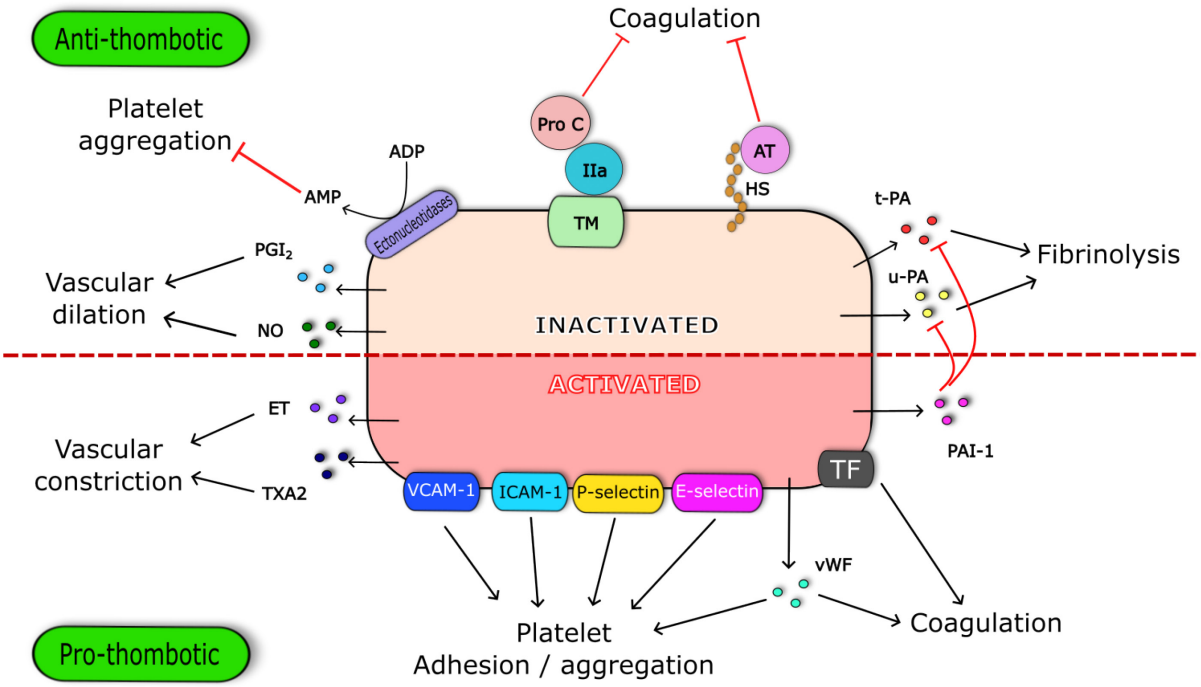

***Figure 1**: The dual roles of endothelial cell in hemostasis.*

Upon endothelial injury, dysfunction, or activation, endothelial cells undergo a phenotypic transition from an antithrombotic to a prothrombotic state. Vasoconstrictors such as thromboxane A2 (TXA2) and endothelin (ET) are secreted, leading to decreased blood flow (Félétou, 2011). In response to activation, endothelial cells unleash a significant release of von Willebrand factor (vWF), thereby amplifying platelet adhesion and aggregation (Lenting et al., 2015; Yau et al., 2015). Platelet activation and adhesion are further potentiated by the expression of platelet-activating factor (PAF) and various adhesion molecules including intercellular adhesion molecule-I (ICAM-1), vascular cell adhesion molecule-I (VCAM-1), E-selectin, and P-selectin (Félétou, 2011; Galley & Webster, 2004). Under pathological

conditions, endothelial cells become activated, exhibiting increased expression of Tissue Factor (TF), the primary initiator of blood coagulation, and plasminogen activator inhibitor type-I (PAI-1), which impedes fibrinolysis by inhibiting the activity of tissue-type plasminogen activator (tPA) and urokinase-type plasminogen activator (uPA). (Félétou, 2011; Yau et al., 2015).

1.2.1.2. The sub-endothelium

The *sub-endothelium* represents a connective tissue layer situated between the endothelium and the underlying smooth muscle cells. Comprising primarily fibroblasts and an extracellular matrix (ECM) network, the sub-endothelium serves as a naturally prothrombotic milieu due to its abundant content of collagen, von Willebrand factor (vWF) secreted by endothelial cells, and Tissue Factor (TF) expressed by both fibroblasts and smooth muscle cells.

Upon vascular injury or lesions, these constituents become exposed to the circulating blood, precipitating a series of events that include platelet adhesion, activation, aggregation, and initiation of the coagulation cascade. This cascade of events ultimately leads to the formation of a hemostatic plug or thrombus, crucial for the cessation of bleeding and the initiation of tissue repair processes.

1.2.1.3. Platelets

Platelets originate from the fragmentation of megakaryocytes, a process known as thrombopoiesis. Megakaryocytes undergo a process of duplication without dividing, leading to the formation of giant cells, with organelles organized into different compartments separated by inward plasma membrane. Upon shear stress from blood circulation, the megakaryocytes are fragmented into platelets.

Due to their origin, platelets are anucleate cells, incapable of protein synthesis. However, they contain in their cytoplasm the necessary elements to perform their functions in various types of organelles: dense granules and alpha granules, as well as lysosomes and glycosomes, and a few mitochondria:

- **Dense granules** (named after their density observed from electrons microscopy), rich in calcium, magnesium, and potassium, are the storage location for non-metabolic nucleotides (ADP, ATP, GTP, GDP), serotonin, and histamine.
- **Alpha granules** contain membrane proteins (αIIbβ3, GPIb-IX-V, GPVI, and P-selectin), hemostasis proteins (FV, FVIII, FXIII, protein S, antithrombin, TFPI, plasminogen, or α2-macroglobulin), adhesion proteins (fibrinogen, thrombospondin, vWF), chemokines, and growth factors such as Platelet factor 4 (PF4) or Insulin-like growth factor (IGF).

The platelet membrane is composed of an anionic phospholipid (PPL) bilayer, incorporating phosphatidylcholine, phosphatidylethanolamine, sphingosine, phosphatidylserine, and phosphatidylinositol. Additionally, a thin glycocalyx layer, housing glycoprotein (GP) receptors from the integrin family, envelops the platelets. These receptors play pivotal roles in platelet adhesion, activation, and aggregation during cell-extracellular matrix and cell-cell interactions.

In the bloodstream, platelets circulate in an inactive discoid form. Upon activation, they undergo a transformation to a more spherical shape, accompanied by pseudopod projections facilitated by the dynamic cytoskeleton, primarily composed of actin filaments. This activation prompts the release of granular contents, contributing to the support of blood coagulation processes.

1.2.1.4. Other cellular elements

Even though the initial thrombus only consists of a platelet plug, the polymerization of fibrin from the coagulation forms a fibrin network that captures other blood cells, like monocytes, and erythrocytes, resulting in a final solid clot. Monocytes upon stimulations from cytokines (such as IL-1 and TNFα), bacterial endotoxins, and antigens, could express TF.

1.2.2. Molecular elements

The following table (*Table 1*) summarize all of the molecular factors implicated in primary hemostasis, coagulation, and fibrinolysis.

***Table 1** : Hemostasis factors*

Factor	Name	Functions
I	Fibrinogen	Precursor of fibrin
II	Prothrombin	Activates platelets, FV, FVII, FVIII, FXI, FXIII, protein C Polymerizes fibrin
III	Tissue Factor (TF)	Co-factor of FVIIa
IV	Calcium	Required for coagulation factors to bind to PPL
V	Proaccelerin	Co-factor of FXa with which it forms the prothrombinase complex
VI	Old name of FVa	
VII	Proconvertin	Activates FIX, FX; increases rate of catalytic conversion of prothrombin into thrombin
VIII	Anti-hemophilia A	Co-factor of FIXa with which it forms the tenase complex

IX	Anti-hemophilia B	Activates FX, forms tenase complex with FVIIIa
X	Stuart	Activates FII, forms prothrombinase complex with Fva
XI	Rosenthal	Activates FIX
XII	Hagenman	Activates FXI, FVII, prekallikrein and plasminogen
XIII	Fibrin-stabilizing factor	Crosslinks fibrin
von Willebrand factor (vWF)		**In the sub-endothelium:** promotes platelets adhesion *via* GP1b/IX/V and platelet aggregation *via* GPIa, GPIIb/IIIa **In circulation:** stabilizes FVIIIa, protecting it from plasma proteolysis, transports FVIIIa to lesion, mediates platelet adhesion
Prekallikrein (PKK)	Fletcher Factor	Activates FXII and prekallikrein; cleaves HMWK
Kallikrein (KK)		Activates plasminogen

High-molecular-weight kininogen (HMWK)	Fitzgerald Factor	Supports reciprocal activation of FXII, FXI, and prekallikrein
Antithrombin III (AT)		Inhibits FIIa, FXa, FIXa, FXIa, and FXIIa
Protein C		Inactivates FVa and FVIIIa
Protein S		Co-factor for activated protein C (APC), inactive when bound to C4b-binding protein
Plasminogen		Converted to plasmin, lyses fibrin and other proteins
α2-Antiplasmin (A2AP)		Inhibits plasmin
α2-Macroglobulin (A2M)		Inhibits plasmin, kallikrein, and thrombin
Tissue-type plasminogen activator (tPA)		Activates plasminogen
Urokinase plasminogen activator (uPA)		Activates plasminogen

Plasminogen activator inhibitor-1 (PAI-1)	Inactivates tPA and uPA
Plasminogen activator inhibitor-2 (PAI-2)	Inactivates tPA and uPA

The majority of molecular factors implicated in coagulation are named with a Roman numeral (independently of the order in which these factors intervene in the coagulation mechanism), associated with the letter ***a*** when they are in their activated form.

These factors can be classified into two categories:

- **Serine protease enzymes** that exhibit proteolytic activity on their specific substrates. These factors transition from an inactive state (zymogen) to an active state (serine protease) following limited proteolysis.
- **Co-factors** that, upon activation by a limited proteolysis triggered by their specific activator, lack of proteolytic activity. They bind to a specific serine protease in the presence of calcium ions and PPL to form an enzymatic complex that enhances the proteolytic activity of the serine proteases. PPL and Ca^{2+} are therefore as essential as any protein factor.

1.3. Mechanism

1.3.1. Primary hemostasis

1.3.1.1. Vascular spasm

Under physiological conditions, the endothelium exhibits a continuous release of vasodilators including nitric oxide (NO) and prostacyclin (PGI2). However, following vascular injury, within the initial 30 seconds, the activated endothelium shifts its secretion profile towards vasoconstrictors such as endothelin (ET) and thromboxane A2 (TXA2). These vasoconstrictors act directly on the underlying smooth muscle cells, inducing their contraction. Consequently,

this contraction leads to a reduction in blood flow, facilitating the local accumulation of platelets at the site of injury.

1.3.1.2. Platelet adhesion

Platelets are recruited to the vessel lesion by adhesion to the sub-endothelium *via*:

- **Indirect binding** with the vWF as a link between collagen and the GP1b/V/IX on platelet membrane.
- **Direct binding** between ECM components from the sub-endothelium to platelet membrane.

Platelets exhibit a diverse array of integrins enabling their interaction with various sub-endothelial components. These include αIIbβ3 (fibrinogen receptor), αVβ3 (vitronectin receptor), α5β1 (fibronectin receptor), and α6β1 (laminin receptor) (Manon-Jensen et al., 2016).

Two principal receptors facilitate direct platelet interaction with exposed collagen: integrin α2β1 and glycoprotein (GP) VI (Thijs et al., 2010). Integrin α2β1 serves as the primary collagen receptor on both epithelial cells and platelets, demonstrating a robust affinity for fibril-forming collagens and binding capabilities to collagen type IV. Additionally, GPVI engages with adhesive extracellular matrix (ECM) components such as fibrin and laminin. GPVI exhibits selective reactivity towards collagens, particularly the larger fibril-forming types (types I and III), while showing limited affinity for type V collagen, which forms exclusively small fibrils (Manon-Jensen et al., 2016).

However, under conditions of elevated shear stress, as observed in arterioles, neither α2β1 nor GPVI alone, or in combination, is sufficient to facilitate platelet adhesion. Instead, this process requires the involvement of the GPIb/V/IX receptor complex, along with its primary ligand, von Willebrand factor (vWF). This interaction predominates, establishing stronger bonds between collagen and the α2β1 and GPVI receptors (Thijs et al., 2010).

Endothelial cells inherently produce the vWF, a glycoprotein critical for hemostasis. Within endothelial cells, vWF is synthesized and housed within specialized storage organelles known as Weibel–Palade bodies. Upon stimulation or injury, vWF is actively secreted into the

bloodstream on the luminal side of endothelial cells and into the sub-endothelial space on the basal side.

In the bloodstream, vWF assumes a coiled, inactive configuration, which serves to inhibit platelet adhesion and aggregation under normal conditions. Conversely, within the sub-endothelial matrix, vWF interacts with collagen fibers, extending into an elongated conformation that exposes binding sites crucial for platelet adhesion and aggregation (Ruggeri, 2007; Tomaiuolo et al., 2017; Yau et al., 2015).

During vascular injury, the exposure of collagen fibers within the sub-endothelial matrix triggers a cascade of events involving vWF and platelets. Activated endothelial cells release additional stores of vWF from Weibel–Palade bodies, augmenting the local concentration of vWF within the lesion site. The A3 domain of circulating vWF binds to various types of exposed collagen fibers within the sub-endothelium, effectively anchoring vWF to the lesion site. This binding event induces a conformational change in vWF, transitioning it from a coiled to an elongated fiber structure, thereby exposing the A1 domain critical for platelet binding and activation (Ruggeri & Mendolicchio, 2007). The interaction between A1 domain of vWF and GPVI of platelets tethers platelet to the lesion.

Interactions between platelets and the sub-endothelium induce the activation of platelets.

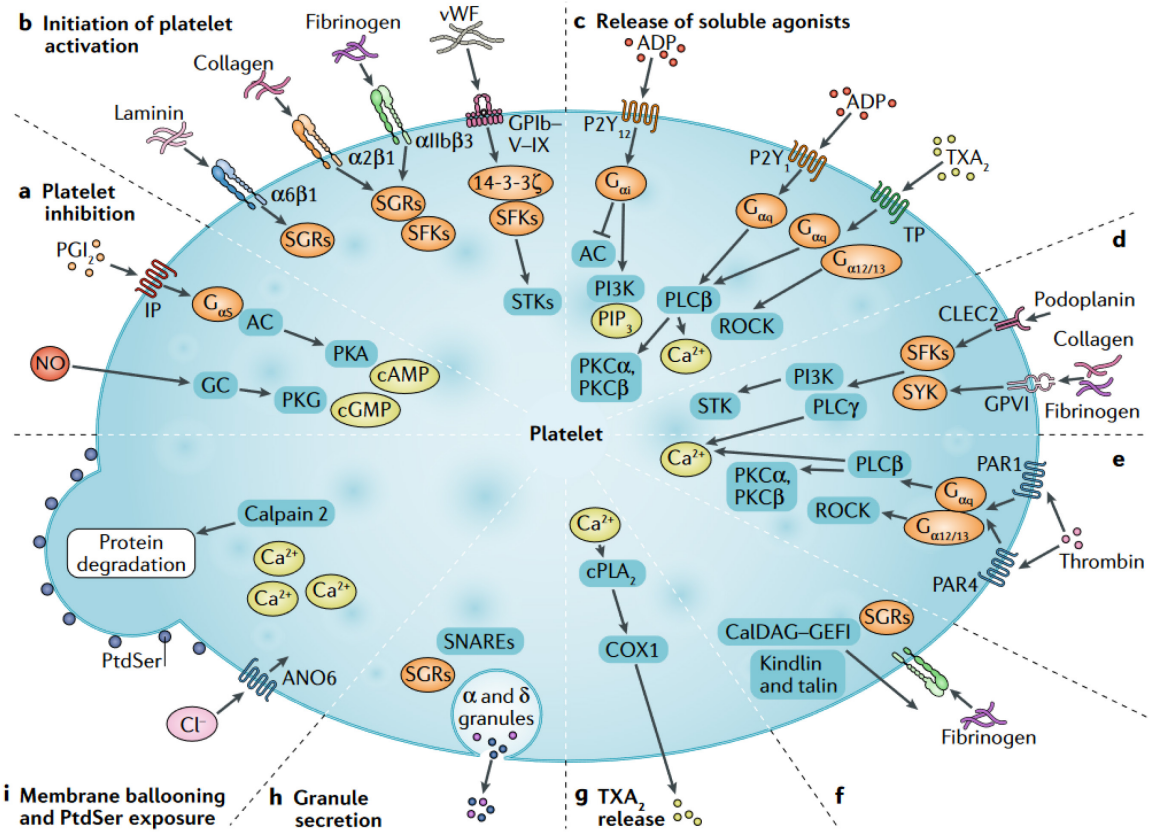

Figure 2 *: Platelet signaling* (van der Meijden & Heemskerk, 2019)

1.3.1.3. Platelet activation

The activation of platelets encompasses four primary processes: intracellular calcium flux, negative phospholipid translocation, granule release, and shape change (Rubenstein & Yin, 2018). It's essential to acknowledge that upon activation, these processes typically occur concurrently and can mutually reinforce the activation cascade as a whole.

Similar to most cells, resting platelets maintain a low cytosolic calcium concentration through the action of calcium pumps. In platelets, calcium is predominantly sequestered within dense granules. These calcium pumps, situated within the dense granule membrane, sustain the platelet cytosolic calcium concentration at approximately 100 nmol/L, while the calcium concentration within each dense granule reaches around 100 mmol/L. However, only a fraction

of this calcium content is released from platelets during coagulation, typically ranging between 10-100 μM.

Upon encountering an activating stimulus, the platelet cytosolic calcium concentration escalates by 2 to 3 orders of magnitude, primarily driven by the direct release of calcium stores from the dense granules. Analogous to many cell types, elevated cytosolic calcium levels trigger numerous cellular processes in platelets, including phospholipid translocation, α-granule release, shape change, membrane protein expression (e.g., translocation to the cell membrane), and activation of membrane proteins (e.g., adhesion proteins).

In the resting platelet membrane, phospholipid distribution is largely symmetrical, with phosphatidylserine predominantly confined to the inner leaflet. This asymmetry is maintained under resting conditions primarily through the actions of flippase, an integral membrane ATP-dependent phospholipid translocator. Another integral membrane protein, scramblase, plays a crucial role in equilibrating phospholipids across the cell membrane based on charge. In platelets, scramblase facilitates the exchange of phosphatidylserine from the inner leaflet to the outer leaflet, while phosphatidylcholine moves in the opposite direction. Notably, scramblase activation occurs concomitantly with the elevation of cytosolic calcium concentration upon platelet activation. Concurrently, increased cytosolic calcium levels deactivate flippase, thereby ensuring that the translocated phosphatidylserine remains exposed on the outer leaflet.

Another critical aspect of platelet function involves α-granule release. These granules harbor two platelet-specific proteins: platelet factor 4 and β-thromboglobulin, both capable of binding to heparin and neutralizing its anticoagulant effects. Approximately 20% of total coagulation factor V is sequestered within platelet α-granules, with the remainder circulating freely in plasma. Additionally, fibrinogen and vWF, adhesive proteins found within α-granules, modulate platelet aggregation and adhesion. P-selectin, meanwhile, facilitates the anchoring of platelets to endothelial cells and/or leukocytes, albeit indirectly through intermediate mediators between cells/receptors. Fusion of α-granules is contingent upon elevated cytosolic calcium levels and is frequently employed as a marker for platelet activation, often indicated by the expression of P-selectin.

Concurrently with the mentioned activation signals, platelets undergo significant shape changes. These alterations increase the likelihood of platelets encountering other platelets, coagulation proteins, or adhesive proteins, thereby facilitating coagulation, aggregation, and adhesion responses. Furthermore, increased platelet surface area resulting from shape change provides a larger interface for coagulation reactions, expediting the conversion of soluble fibrinogen into insoluble fibrin.

Contemporary insights into platelet activation reveal a nuanced framework wherein platelets undergo variable degrees of activation contingent on their proximity to the site of injury. The hemostatic clot architecture is delineated by a central domain populated by highly activated, densely aggregated, and degranulated platelets, surrounded by a peripheral region comprising less activated, loosely aggregated platelets. The heterogeneity in platelet activation is governed by the gradual spatial distribution of soluble platelet agonists such as thrombin, ADP, and TXA2 (Tomaiuolo et al., 2017).

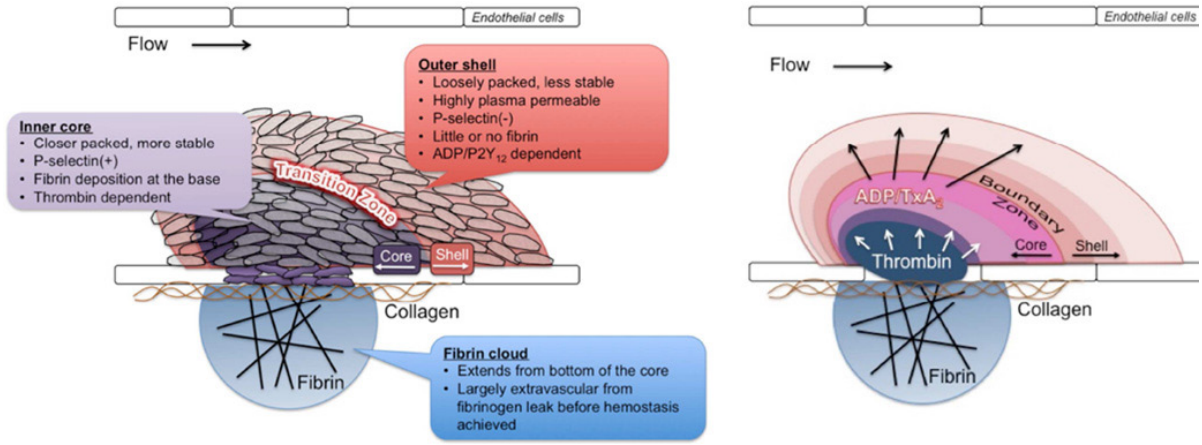

Figure 3 *: Architecture of activated platelet plug. (A): Spatial organization of various stages of activation inside of a platelet plug. (B): Spatial distribution of platelet agonists. (Tomaiuolo et al., 2017)*

The initial phase of reversible activation entails a morphological transition from a discoid to a spherical shape, coupled with the activation of αIIbβ3 integrin. The activated αIIbβ3 integrin

orchestrates platelet-platelet interactions, recruiting additional circulating platelets to the nascent thrombus.

Conversely, late activation events are irreversible and encompass diverse activities. The cell membrane undergoes flip-flop, exposing phospholipids (PPL) from the initially inner layer to the outer layer, thereby creating a platform for the assembly of coagulation enzymatic complexes. Simultaneously, granules are secreted, and their contents are released, contributing to the amplification of the coagulation response.

1.3.1.4. Platelet aggregation

Following the initial attachment and activation of platelets, a platelet plug is formed through platelet-to-platelet adherence during the expansion phase, attracting additional platelets from the bloodstream. This adherence primarily occurs via the binding of the plasma protein fibrinogen to αIIbβ3 integrin receptors. Each fibrinogen unit harbors two αIIbβ3 binding sites, facilitating platelet-to-platelet connections by engaging receptors on adjacent platelets. The process of platelet attraction and αIIbβ3-mediated adherence is contingent upon platelet activation induced by ADP release from platelet dense granules and TXA2 produced by platelets already adhered at the injury site. Thrombin activity also plays a contributory role in platelet activation. (Tomaiuolo et al., 2017).

1.3.2. Coagulation

1.3.2.1. Initiation

The initiation phase of blood coagulation commences with the activation of either the complex FVIIa/tissue factor (TF) or factor XII (FXII), culminating in the generation of the initial trace of thrombin (FIIa). Both TF and FXII possess the capacity to initiate coagulation, with TF exhibiting a higher rate of activity, rendering it the principal initiator.

Upon exposure to TF, which is consistently present in the sub-endothelium or on the membrane of cells expressing TF, in the presence of phospholipids (PPL) and calcium ions (Ca^{2+}), circulating factor VIIa (FVIIa) promptly forms an enzymatic complex with TF. This extrinsic tenase complex (FVIIa/TF/PPL/Ca^{2+}) initially activates factor X (FX) into factor Xa (FXa),

subsequently catalyzing the activation of factor IX (FIX) into factor IXa (FIXa). FIXa and FXa mutually activate each other, establishing an amplification loop, with FXa generating the initial trace of thrombin.

TF activity is regulated by circulating Tissue Factor Pathway Inhibitor (TFPI), secreted by endothelial cells. Coagulation activation by TF ensues only when sufficient TF is available to surpass TFPI inhibition. This regulatory mechanism serves to prevent activation in response to weak stimuli.

Concurrently, at a slower pace, FXII is activated by various factors, including collagen within the sub-endothelium. FXIIa subsequently activates circulating factor XI (FXI) and prekallikrein (PKK) into FXIa and kallikrein (KK), respectively. FXIa, in turn, activates FIX, complementing the initiation by TF. PK hydrolyzes FXII, creating a positive feedback loop.

The influence of FXIIa on coagulation is comparatively minor in contrast to TF, as FXII deficiency does not result in excessive bleeding (Konrath et al., 2021; Mailer et al., 2022). The activation of coagulation by FXII is most evident *ex vivo* when it is activated by negatively charged surfaces (e.g., kaolin, plastic, glass, etc…).

1.3.2.2. Amplification

Upon activation, FXa converts a small fraction of prothrombin (FII) to thrombin (FIIa). Despite its limited quantity, this initial thrombin is sufficient to trigger its own amplification cascade. Thrombin enhances platelet activation through interactions with protease-activated receptor 1 (PAR1) and protease-activated receptor 4 (PAR4). Activated platelets release their granules, liberating FV and FXI, both subsequently activated by thrombin. FXIa contributes to amplification by further activating FX. FVa forms the *prothrombinase complex* with FXa, phospholipids (PPL), and calcium ions (Ca^{2+}).

The initial trace of thrombin also catalyzes the activation of circulating FVIII. FVIIIa, in conjunction with FIXa, PPL, and Ca^{2+}, forms the *intrinsic tenase complex*. Notably, the intrinsic tenase complex activates FXa at a rate 50 times higher than the extrinsic tenase complex (He et

al., 2021). The formation of these two enzymatic complexes, prothrombinase and intrinsic tenase, initiates a surge in FXa generation, amplifying thrombin production.

Thrombin assumes multiple distinct roles within hemostasis:

- Cleavage of fibrinogen into fibrin monomers, initiating fibrin polymerization. Just 2% of the total thrombin generated suffices to trigger clot formation.
- Activation of factor XIII to factor XIIIa, facilitating crosslinking and stabilization of fibrin fibrils.
- Activation of Thrombin Activated Fibrinolysis Inhibitor (TAFI), an inhibitor of fibrinolysis.
- Positive feedback on its own production by augmenting platelet, FV, FVIII, and FXI activation.
- Inhibition of coagulation processes.

1.3.2.3. Inhibition

As previously stated, hemostasis is a finely regulated system deployed promptly upon vascular injury and maintained for the minimum duration necessary to prevent total obstruction of blood flow. It represents a delicate balance between activators and inhibitors, ensuring the swift and controlled resolution of vascular breaches.

The extension of hemostatic responses beyond the site of vascular injury is curtailed by the flowing blood, which facilitates the dilution of coagulation factors, and by various physiological inhibitor systems, primarily regulated by endothelial cells.

The pathways governed by natural coagulation inhibitors play a pivotal role in modulating thrombogenesis by impeding the activity of serine proteases or coagulation cofactors, thereby regulating thrombin generation. Dysfunctional natural inhibitor pathways lead to excessive thrombin generation, dissemination of activated factors, and catastrophic cessation of blood flow in tissues and organs.

Tissue Factor Pathway Inhibitor (TFPI), expressed by endothelial cells, is found both in the circulation and immobilized on the plasma membrane. TFPI forms a complex with activated

factor X (FXa), inhibiting its catalytic activity in thrombin generation. Furthermore, the TFPI/FXa complex interacts with the tissue factor (TF)/factor VIIa complex, forming a quaternary complex that inhibits the activity of TF/FVIIa. TFPI predominantly impairs coagulation through direct inhibition of FXa. The role of the TFPI/FXa/TF/FVIIa complex is limited to scenarios involving minimal stimuli.

Antithrombin (AT), a circulating glycoprotein, upon binding to its cofactor, heparin, inhibits the activity of factor IIa (thrombin), factor IXa, factor Xa, factor XIa, factor XIIa, and the TF/FVIIa complex. Heparins, belonging to the glycosaminoglycan family, are present on the endothelial cell membrane and in the extracellular matrix. Due to their anticoagulant properties, heparins extracted from mucosa or whole porcine intestines are industrially utilized as antithrombotic medications.

Another inhibitory mechanism involves thrombin, thrombomodulin (TM), protein C, endothelial protein C receptors (EPCR), and protein S. Endothelial cells express TM and EPCR on their membrane. Circulating protein C is converted to activated protein C (APC) through the interaction of thrombin with TM. In conjunction with the cofactor protein S, the interaction between APC and EPCR induces inhibition of factor Va and factor VIIIa.

2. Fibrin

2.1. Fibrinogen

2.1.1. Fibrinogen synthesis

Human fibrinogen is a substantial 340 kDa oligomeric glycoprotein composed of two symmetrical halves, each featuring three polypeptide chains: Aα, Bβ, and γ, with molecular weights of 67, 57, and 47 kDa, respectively (Wolberg, 2023). These chains are encoded by specific genes clustered within human chromosome 4: *FGA* for Aα, *FGB* for Bβ, and *FGG* for γ (Wolberg, 2023).

The primary site of synthesis is in hepatocytes, where fibrinogen mRNAs undergo splicing and translation, and the polypeptides undergo post-translational modifications. This synthesis occurs at a steady rate of 1.7–5 g per day, contributing to a substantial intracellular reserve

(Weisel & Litvinov, 2017). Following synthesis, fibrinogen is secreted into the bloodstream, where it circulates at high concentrations (2-4 mg/mL or 6-12 μM) with a relatively lengthy half-life of 4 days (Wolberg, 2023).

Fibrinogen synthesis is not limited to hepatocytes but extends to various other tissues, including lung and intestinal epithelium, bone marrow, brain, ovary, and different types of cancer cells:

- In lung epithelial cells, inflammation, via interleukin 6 (IL-6), prompts fibrinogen secretion, contributing to fibrosis (Guadiz et al., 1997; Simpson-Haidaris et al., 1998; Tomashefski et al., 1992).

- Within the intestinal epithelium, a subset of cells constitutively produces fibrinogen, which is then deposited in the extracellular matrix of the basement membrane. This deposition aids in fortifying the physical barrier against pathogens. Fibrin(ogen) accumulation, particularly evident in Crohn's disease specimens, suggests its involvement in both normal physiological conditions and pathological processes (Seltana et al., 2022).

- Granulosa cells have been observed to secrete fibrinogen during *in vitro* culture, although its specific role in ovarian function remains unclear (Parrott et al., 1993).

- While fibrinogen is typically undetectable in a healthy central nervous system, its abundant deposition occurs in various neurological diseases and traumatic injuries characterized by blood-brain barrier disruption. Consequently, fibrinogen serves as a reliable marker of blood-brain barrier integrity (McLarnon, 2022; Petersen et al., 2018).

- Fibrinogen expression has also been identified in various non-hepatic carcinoma cell lines originating from the lung, uterus, breast, and colon (Seltana et al., 2022).

Fibrinogen expression is regulated by both constitutive and inducible mechanisms, with IL-6 being a key inducer. The core transcription factors responsible for fibrinogen expression include hepatocyte nuclear factor 1 (HNF-1), members of the CCAAT-enhancer-binding proteins (C/EBP), and the upstream stimulatory factor (USF):

- As a transcriptional factor specifically expressed in hepatocytes, HNF-1 binds to its binding site on the promoter of *FGA* and *FGB*, leading to gene expression and basal secretion of fibrinogen in the liver.

- C/EBP proteins bind to the CCAAT (cytosine-cytosine-adenosine-adenosine-thymidine) box motif upstream of the promoters of *FGA*, *FGB*, and *FGG*. C/EBP participates in both basal and IL-6-induced production.

- USF is responsible for the regulation of *FGG* expression.

During inflammation, IL-6 signaling activates signal transducer and activator of transcription 3 (STAT3) by inhibiting its inhibitor. Subsequently, STAT3 binds to specific sites upstream of the promoters of *FGA*, *FGB*, and *FGG*, leading to increased fibrinogen production.

Glucocorticoids, as potent regulators of inflammation, are known to modulate the expression of genes that are induced by IL-6. The binding of glucocorticoids to the intracellular glucocorticoid receptor (GR) leads to the translocation of the ligand-receptor complex into the nucleus, where it activates transcription of downstream genes. Glucocorticoids are demonstrated to enhance IL-6-dependent *FGG* expression (Dittrich et al., 2012; Fuller & Zhang, 2001).

The expressions of *FGA*, *FGB*, and *FGG* are coordinated, for increasing gene expression of one lead to the overexpression of the other two, suggesting a common mechanism of regulation. The three fibrinogen genes are positioned continuously within a gene cluster and form a chromatin loop that is conserved across tetrapods. The cluster is flanked by two CCCTC-binding factor (CTCF) interaction sites. CTCF, a widely expressed zinc-finger protein, binds to the consensus DNA sequence CCGCGNGGNGGCAG and plays a role in looping genomic regions. Altering chromatin interactions by deleting the CTCF site at one edge of the cluster reduces the expression of *FGB* and *FGG* mRNA and decreases fibrinogen secretion (Espitia Jaimes et al., 2018). Since all of the three gene possess binding sites for C/EBP and STAT3, the chromatin loop ensures the spatial proximity of those binding sites, leading to simultaneous activation of the transcription of all of the three genes (**Figure 4**).

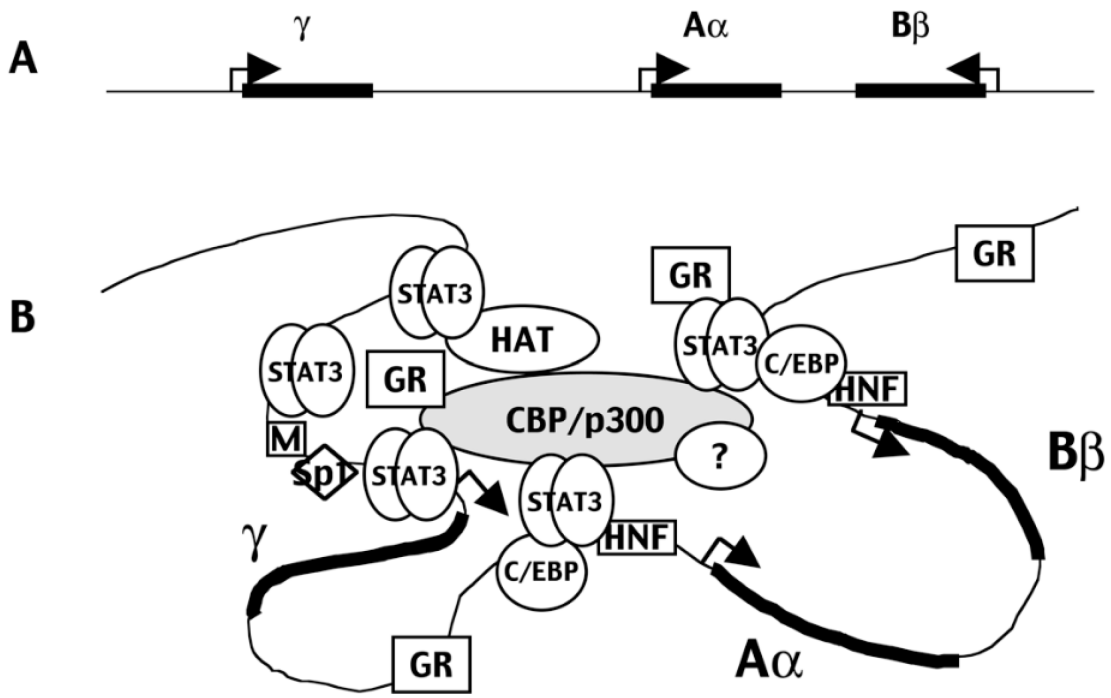

***Figure 4**: Regulation of fibrinogen genes. **(A)**: Position and transcriptional direction of FGA, FGB, and FGG genes (encoding the Aα, Bβ, and γ chains respectively). **(B)** Concordance regulation of fibrinogen expression. FGA and FGB promotors consist of hepatocyte nuclear factor 1 (HNF-1) and CCAAT-enhancer-binding proteins (C/EBP) binding sites. FGG promotors consists of the C/EBP binding sites and the upstream stimulatory factor (USF) binding site that binds to Specificity Protein 1 transcriptional factors (Sp1) and Major late transcription factor (M). Chromatin loop leads to spatial proximity of the promotors of FGA, FGB, and FGG. This proximity ensures the simultaneous binding of one molecule of co-activator CREB-binding protein/p300 protein (CBP/p300) to different molecules of transducer and activator of transcription 3 (STAT3), activating the transcription of all of the three fibrinogen genes at the same time via the C/EBP that bind to the promotor. CBP/p300 recruits the histone acetyltransferases (HATs) that modulate the chromatin structure, further enhancing gene expression. The binding of glucocorticoid receptor (GR) to the DNA also induces gene transcription (Fuller & Zhang, 2001).*

2.1.2. Fibrinogen structure

After translation, the three polypeptide chains are organized into various intermediate structures before assembling into the final hexameric glycoprotein form of fibrinogen. Initially, the chains combine to form Bβ-γ and Aα-γ intermediates, followed by Aα-Bβ-γ half-molecules. Eventually, they assemble into a 340-kDa hexameric glycoprotein consisting of two copies each of the three polypeptide chains $(A\alpha B\beta\gamma)_2$ (Wolberg, 2023). This assembly is stabilized by 29 disulfide bonds, which are concentrated in the central nodule of the fibrinogen molecule (Weisel & Litvinov, 2017).

Fibrinogen molecules possess an overall rod-like shape, measuring approximately 45 nm in length and 2–5 nm in thickness. Each fibrinogen molecule comprises two lateral D regions and one central E region, in the conformation of (D-E-D) (**Figure 5**). These regions contain both globular components and portions of α-helical coiled-coils, which serve to connect the lateral globules with the central one (Weisel & Litvinov, 2017).

The polypeptides within fibrinogen are arranged such that the N-terminus regions are located in the central E region. The C-terminus globular domains of the Bβ and γ chains, known as the βC and γC nodules, respectively, are situated in the D regions. The Aα chain extends into an unstructured αC connector and a partially structured αC domain (Wolberg, 2023).

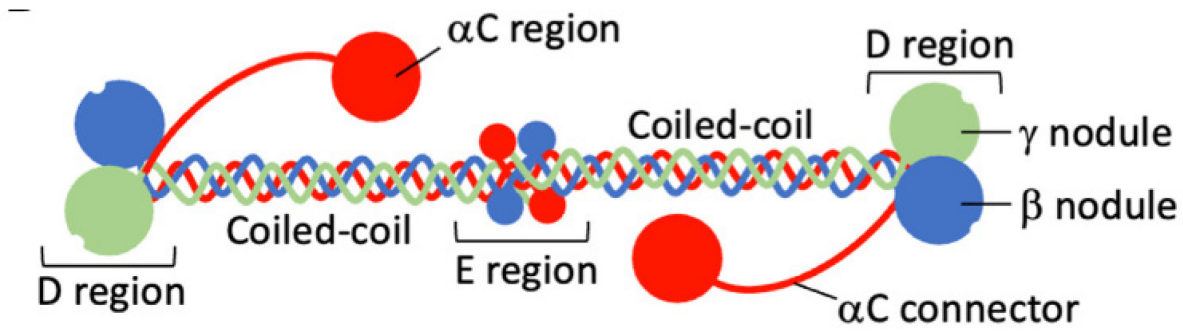

***Figure 5**: Structure of fibrinogen. The polypeptide chains Aα (red), Bβ (blue), and γ (green) are assembled into an hexameric molecule. Lateral D regions and central E regions each contains globular nodules. The N-terminus of each polypeptide chains are located in the central E region. The C-terminus of Bβ and γ chains are located in the lateral D regions. The C-terminus of Aα chains is organized into an unstructured αC connector and a partially structured αC domain (Wolberg, 2023).*

2.2. Fibrinoformation

Fibrin formation represents the final stage of the coagulation process, occurring subsequent to the conversion of prothrombin (FII) into active thrombin (FIIa), and serving to arrest hemorrhage by forming a crosslinked fibrin network. This process encompasses three main steps:

- Thrombin-mediated cleavage of fibrinogen into fibrin monomers.
- Assemblage of fibrin monomers into protofibrils.
- Crosslinking of protofibrils of fibrin to form a stable clot.

2.2.1. Fibrinogen cleavage

Fibrin formation is initiated when thrombin catalyzes the removal of two 16-residue-long peptides, fibrinopeptide A (FpA), from the N-termini of the Aα chains of fibrinogen, resulting

in the production of desA-fibrin monomer. The release of two 14-residue-long peptides, fibrinopeptide B (FpB), from the N-termini of the Bβ chains occurs at a slower rate (Litvinov et al., 2021). Upon removal of FpA and FpB, these chains are referred to as α and β. The nomenclature of chains Aα and Bβ specifies the cleavage of FpA and FpB from the α and β chains. The transformation of fibrinogen to fibrin can be described as $(A\alpha B\beta\gamma)_2 \rightarrow (\alpha\beta\gamma)_2 + 2$ FpA + 2 FpB.

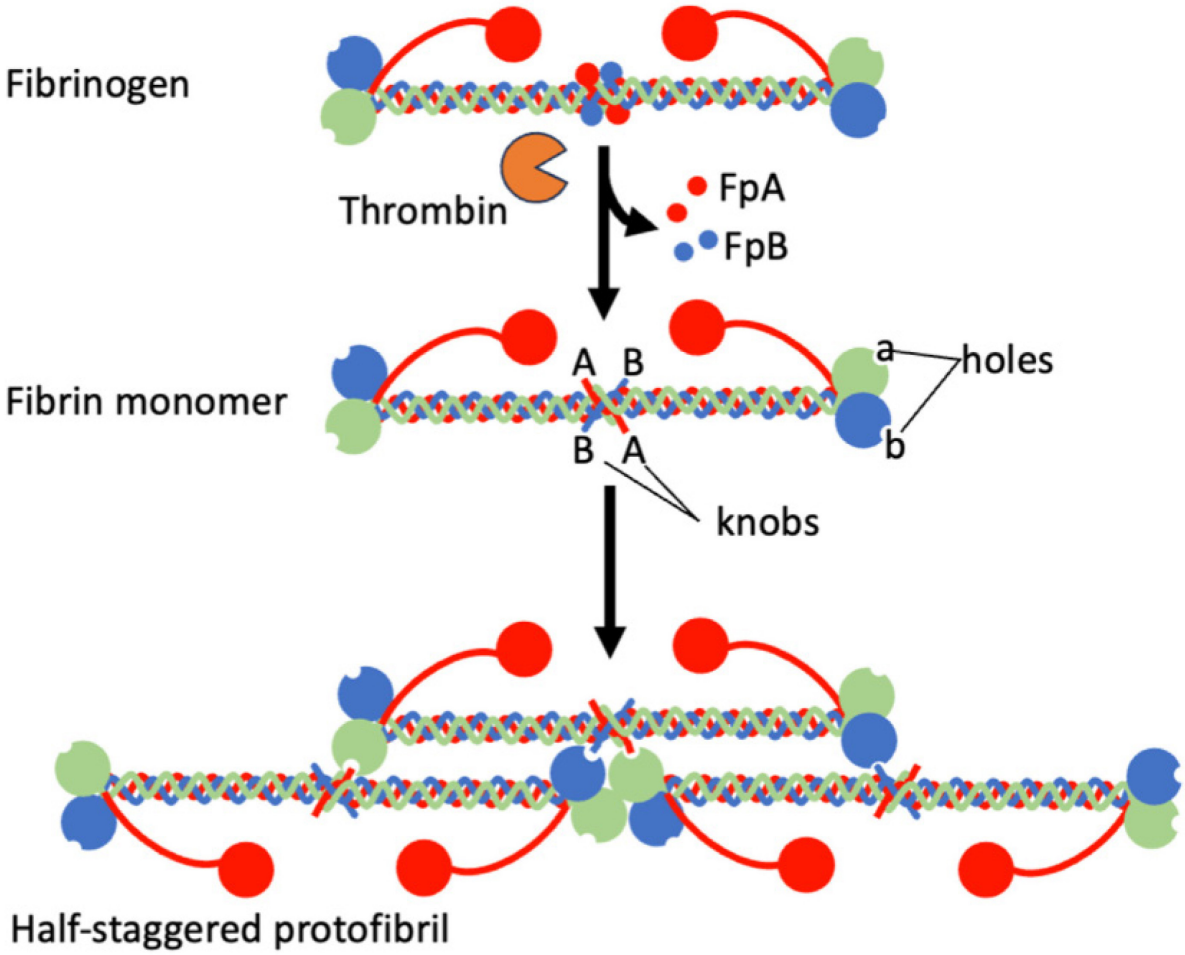

Figure 6: *Transformation of soluble fibrinogen to insoluble fibrin. Thrombin mediated the cleavage of Fibrinopeptide A (FpA) and Fibrinopeptide B (FpB) from the α and β chains, revealing the A and B knobs in the N-terminus of α and β chains, respectively, that are located in the central E region. Interactions between the A knob with a hole in the globular C-terminus of the γ chain initiates the formation of the protofibril. At a slower rate, the B knob interacts with the b hole in the globular C-terminus of the β chain (Wolberg, 2023).*

2.2.2. *Formation of fibrin protofibrils*

The enzymatic cleavage of FpA in fibrinogen results in exposure of the Gly-Pro-Arg motif, called the A knob, at the N-terminus of α chain located in the central E region. A binding pocket for the knob ‘A’ was identified as the hole ‘a’ located in the globular C-terminus of the γ chain in the lateral D region. The interaction between the A knob of one fibrinogen molecule and the 'a' hole of another fibrinogen molecule links the E region of one to the D region of the other, initiating fibrin polymerization.

At a slower rate, the cleavage of FpB reveals the Gly-His-Arg motif, called the B knob, at the N-terminus of the β chain in the central E region. The B knob binds to the b hole located in the globular C-terminus of the β chain of another fibrinogen molecule's D region.

Consequently, two D regions from two different fibrinogen molecules are attached to the E region of a third fibrinogen molecule, leading to the formation of a two-stranded trimer. The oligomeric strands grow longitudinally until they reach a length about 0.5-0.6 μm (20-25 monomers) (Chernysh et al., 2011) in the form of a of a double-stranded protofibril, comprising a straight twisted filament. Protofibrils aggregate laterally to form thicker fibers only when they reach this certain length (Weisel & Litvinov, 2017). The number of protofibrils per fiber can vary from two to several thousand.

As fibrin fibers thicken by lateral aggregation and grow in length, they also branch, resulting in a network. One branching mechanism is termed the "bilateral junction," where two protofibrils undergo incomplete lateral aggregation and diverge into two separate protofibrils, each of them giving rise to a new fiber. The second type, called "equilateral junction," forms when a fibrin monomer attached to the end of a protofibril via only one 'A:a' bond instead of two, allowing both the monomeric molecule and the protofibril to which it is bound to grow independently, forming two strands each.

2.2.3. *Fibrin crosslinking*

Fibrin is covalently crosslinked by activated factor XIII (FXIIIa). The zymogen form of factor XIII (FXIII) consists of two A subunits (FXIII-A_2) and two B subunits (FXIII-B_2), assembled

as a noncovalent heterotetramer (FXIII-A_2B_2). During coagulation, FXIII-A_2B_2 is activated by thrombin-mediated cleavage of the activation peptide from the FXIII-A subunits in the N-terminal. Subsequently, Ca^{2+} dissociates the inhibitory FXIII-B subunits, yielding fully activated FXIIIa (Byrnes et al., 2016).

The first sites to be crosslinked are the D regions from two adjacent monomers, forming a covalent bond between the C-terminal tails of γ chains, resulting in the formation of γ-γ dimers. Recent evidences support the notion that γ-γ crosslinking occurs mainly laterally between two molecules from the same strand rather than from two different strands (Rosenfeld et al., 2015; Zhmurov et al., 2016). FXIIIa forms similar bonds, albeit at a slower rate, between the αC regions to stabilize long αC polymers within protofibrils and in the inter-protofibril space. Crosslinking also occurs between fibrin α and γ chains, resulting in the formation of α-γ-heterodimers (Ząbczyk et al., 2021).

Crosslinking increases the compaction of fibrin monomers within the fiber, decreases the extensibility and elasticity of fibrin fibers, and increases fiber stiffness by 2-fold. It stabilizes fibrin branch points, protecting these regions from rupture (Wolberg, 2023). In the absence of FXIIIa, fibrin polymerization is reversible (Chernysh et al., 2012).

In addition to stabilizing fibrin fibers, FXIIIa also protects fibrin from fibrinolysis. Crosslinking of α2-antiplasmin and thrombin activatable fibrinolysis inhibitor (TAFI) to fibrin enables the retention of these inhibitors of fibrinolysis (Wolberg, 2023; Ząbczyk et al., 2021). Recently, FXIIIa was found to be able to crosslink histones released during neutrophil extracellular trap (NET) formation. Histones competitively inhibit plasmin to delay fibrinolysis, an effect enhanced by covalent crosslinking of histones to fibrin in a FXIIIa-dependent manner (Locke & Longstaff, 2021).

Additionally, FXIIIa also crosslink fibrin with fibronectin, vitronectin, thrombospondin, and collagen (Schroeder & Kohler, 2016).

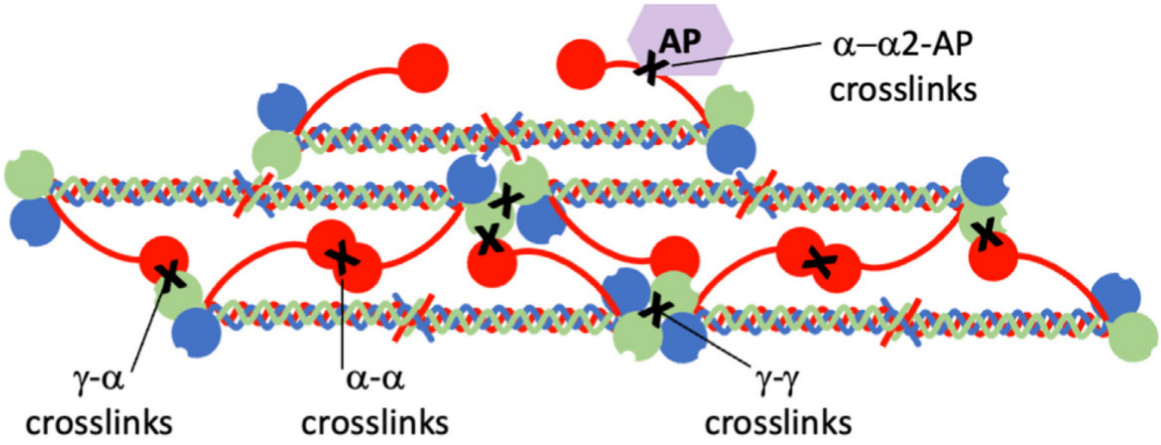

***Figure** 7: γ-γ, γ-α, α-α, and α-α2 antiplasmin (α2-AP) crosslinking generated by FXIIIa (Wolberg, 2023)*

2.3. Fibrin degradation

Following vessel injuries, coagulation is activated, resulting in the formation of a fibrin clot that clog the lesion, stopping hemorrhage. Once the bleeding is controlled, fibroblasts migrate to the lesion site and commence the wound healing process in which, fibrin is degraded and gradually replaced with fibronectin, collagens, and glycosaminoglycan (Dvorak, 2015). The degradation of the fibrin clot also permits the reestablishment of normal blood flow. Fibrin is degraded mainly by plasmin – a process known as fibrinolysis – and by a smaller activity, by matrix metalloproteinases (MMPs).

2.3.1. Plasmin-dependent fibrin degradation: fibrinolysis

Fibrinolysis initiates with the activation of plasminogen, converting it into its active form, plasmin. Plasmin then cleaves fibrin at lysine residues, resulting in the breakdown of fibrin into soluble fragments known as fibrin degradation products (FDP).

In clotted blood and plasma, fibrin is crosslinked by FXIIIa. Consequently, the smallest FDP fragment is the D-Dimer, formed from the crosslinking of two adjacent γ chains (Weisel & Litvinov, 2017). Measurement of D-Dimer levels serves as a direct indicator of fibrinolysis activity and an indirect indicator of fibrin formation.

Fibrin generated *in vitro* using purified fibrinogen and thrombin lacks FXIIIa-mediated crosslinking. As a result, the FDP from this fibrin does not contain D-Dimer and more closely resembles the products of proteolyzed fibrinogen.

2.3.1.1. Activators of fibrinolysis

The activators of plasminogen include the serine proteases tissue-type plasminogen activator (tPA), urokinase-type plasminogen activator (uPA), and bacterial proteins such as streptokinase and staphylokinase (Weisel & Litvinov, 2017).

Both tPA and staphylokinase are *bound to fibrin* and protected from rapid inhibition. tPA is synthesized by endothelial cells, neurons, glial cells, and cancer cells (Cesarman-Maus & Hajjar, 2005; Singh et al., 2023). Fibrin serves as a cofactor in the activation of plasmin by tPA. In the absence of fibrin, tPA functions as a weak activator of plasmin. When bound to fibrin, tPA demonstrates increased affinity for plasminogen, resulting in a twofold elevation in the conversion of plasminogen to plasmin (Singh et al., 2023).

Plasminogen and tPA attach to fibrin via the C-terminal lysine residue of fibrin. Upon activation, plasmin cleaves fibrin at the same lysine residue, revealing a new binding site and establishing a positive feedback loop. The number of tPA and plasminogen binding sites on fibrin can be increased by ultrasound-induced perturbation of fibrin clots, resulting in elevated the rate of lysis, which may serves as thrombolytic therapy (Chernysh et al., 2015).

Streptokinase and uPA are enzymes that lack fibrin selectivity, activating both plasminogen in the circulating blood and fibrin-bound plasminogen. uPA is expressed in various cell types, including endothelial cells, macrophages, renal epithelial cells, and certain tumor cells (Cesarman-Maus & Hajjar, 2005). Compared to tPA, uPA exhibits much lower affinity for

fibrin. However, uPA remains an effective plasminogen activator in both the presence and absence of fibrin (Chapin & Hajjar, 2015).

Upon activation, plasmin enhances the activity of activators by converting single-chain tPA and uPA into their two-chain counterparts, thereby providing positive feedback on its own activation. The activation of plasminogen by two-chain uPA is significantly increased in the presence of fibrin by approximately 10-fold (Cesarman-Maus & Hajjar, 2005), despite uPA not directly binding to fibrin. This phenomenon may indicate a conformational change in plasminogen upon interaction with fibrin. In contrast, single-chain uPA demonstrates considerable fibrin specificity but possesses an intrinsic plasminogen-activating capacity of less than 1% of that observed for two-chain uPA.

Although plasmin, tPA, and uPA are susceptible to neutralization by soluble circulating inhibitors, endothelial cell surfaces and fibrin thrombi provide protective environments that preserve their fibrinolytic activity. Various cell surface molecules, including plasminogen receptors, the uPA receptor (uPAR), and the annexin A2 complex, bind to plasminogen and/or its activators on endothelial cells, monocytes, and numerous other cell types.

Annexin A2 belongs to the annexin family of calcium-binding proteins. When present on the surface of endothelial cells and monocytes, annexin A2 forms a heterotetrameric complex with another protein, S100A10 (also known as p11). This complex acts as a profibrinolytic receptor, binding specifically to plasminogen and tPA, but not to uPA. The (annexin A2-S100A10) complex plays a crucial role in promoting the tPA-dependent activation of plasmin, irrespective of the presence of fibrin (Chapin & Hajjar, 2015).

2.3.1.2. Inhibitors of fibrinolysis

Circulating plasmin and plasminogen activators are counteracted by serine protease inhibitors, or serpins, which are present in excess concentrations in the bloodstream. Serpins form covalent complexes with their specific target enzymes, which are then cleared from circulation. The three key serpins involved in fibrinolysis are plasminogen activator inhibitor-1 (PAI-1), plasminogen activator inhibitor-2 (PAI-2), and α2-antiplasmin (A2AP) (Chapin & Hajjar, 2015).

- α2-antiplasmin (A2AP) is found in plasma or stored in platelet alpha granules. Plasmin released into the bloodstream or near a platelet-rich thrombus is promptly neutralized by A2AP. When plasmin binds to fibrin fibers, it is shielded from inhibition by A2AP (Singh et al., 2023).

- PAI-1, released into circulation from various cells such as endothelial cells, platelets, monocytes, macrophages, hepatocytes, and adipocytes, binds to tPA and uPA, effectively inhibiting their activity. PAI-1 expression is upregulated by inflammatory cytokines, and it is the most critical and rapidly acting physiological inhibitor of both tPA and uPA (Singh et al., 2023).

- PAI-2 serves as a major inhibitor of tPA and uPA during pregnancy, with its concentrations increasing as pregnancy progresses (Chapin & Hajjar, 2015).

Thrombin-activated fibrinolysis inhibitor (TAFI) is a non-serpin inhibitor of fibrinolysis that is activated by thrombomodulin-associated thrombin. TAFI removes C-terminal lysine and arginine residues from fibrin, thereby altering the binding of tPA and plasminogen to fibrin and impairing their activities (Cesarman-Maus & Hajjar, 2005).

Other non-serpin inhibitors include α2-macroglobulin, C1-esterase inhibitor, and members of the contact pathway of the coagulation cascade, which play minor roles in inhibiting plasmin.

2.3.2. Plasmin-independent fibrin degradation by Metalloproteinases

Aside from the plasminogen/plasmin systems, other enzymes can degrade fibrin, including several serine proteases and metalloproteinases.

Serine proteases hydrolyze peptide bonds in proteins, and a diverse array of these enzymes capable of denaturing fibrin are derived from various bacterial and fungal species such as *Streptococcus hemolyticus, Bacillus subtilis, Staphylococcus aureus, Arthrobotrys longa, Aspergillus versicolor, Penicillium sp, Rhizopus chinensis*, among others (Singh et al., 2023).

Matrix metalloproteinases (MMPs) are zinc-dependent serine proteases that cleave peptide bonds within the peptide backbone (endopeptidase), as opposed to exopeptidases that cleave at the ends of the peptide backbone (Singh et al., 2023). MMPs are expressed by various cell types, including epithelial, fibroblast, macrophages, myofibroblasts, and cancer cells, and are involved in extracellular matrix (ECM) remodeling by degrading ECM proteins such as collagens, laminin, and fibronectin (Mondal et al., 2020). Different MMPs are capable of denaturing fibrin, including MMP1, MMP3, MMP7, MMP9, and MMP14 (Ahmed et al., 2007; Bini et al., 1996; Dewyer et al., 2007; Hotary et al., 2002; Kumar et al., 2020). Particularly, MMP3 has been shown to degrade crosslinked D-Dimer into monomers of the D region (Bini et al., 1996).

2.4. Structural characteristics of fibrin network

Fibrin is a remarkably flexible polymer with unique mechanical properties. After its formation, fibrin contracts into a densely packed clot, effectively entrapping blood cells (Wolberg, 2023). However, when subjected to stress, fibrin clots tend to stretch rather than break. Crosslinking is crucial for enhancing the extensibility of fibrin fibers. Compared to non-crosslinked fibers, crosslinked fibrin fibers can be stretched to a greater extent before rupturing, contributing to their resilience. Non-crosslinked fibrin fibers can be stretched to 2.5-fold, and crosslinked fibrin fibers 3.3-fold, as compared to the 2.7-fold of spider silk (Pieters & Wolberg, 2019; Weisel & Litvinov, 2017). When fibrin fiber are stretched, the protofibrils slide across each other (Martinez-Torres et al., 2024). Consequently, mechanically stressed fibrin fibers are more resistant to fibrinolysis (Bucay et al., 2015).

Despite its elasticity, fibrin fibers can be ruptured under sufficient mechanical stress, leading to clot dislocation and embolism. The strength of fibrin fibers is influenced by factors such as the number of protofibrils compacted within each fiber, fiber diameter, and fiber length. When stress is applied to a fiber, it is distributed among all of the protofibrils within it (Hudson et al., 2010). Consequently, fibers with a higher number of protofibrils are stiffer and more resistant to mechanical breakage. Similarly, fibers with larger diameters and shorter lengths exhibit greater strength (Ramanujam et al., 2023).

The branching mechanism of fibrin fibers, where two strains originate from a single fiber, determines fiber diameter and length. Highly branched fibrin networks are associated with thinner and shorter fibers (Weisel & Litvinov, 2017). As a result, the density of branchpoints within the network influences clot stiffness (Ramanujam et al., 2023).

Different factors could influence the diameter of fibrin fiber (**Figure 8**):

- **Presence of red blood cells**: The presence of red blood cells (RBC) increases fiber diameters, as well as pore size, clot elasticity, and viscosity (Gersh et al., 2009).
- **Polymerization conditions**: The condition in which fibrin was polymerized. High NaCl and Ca^{2+} concentrations, as well as elevated pH lead to clots with thicker fiber (Litvinov et al., 2021; Pietsch et al., 2023).
- **Blood components**: Fibrin clots formed from platelet-poor plasma have finer fibers than fibrin clots formed with purified fibrinogen and thrombin (Risman, Belcher, et al., 2024).
- **Flow**: Under bi-directional flow, fibrin clots are polymerized with thick fiber that elongated in the direction of the flow as compared to clot formed in stasis (Campbell et al., 2010). However, under rotational flow, fibrin clots hace finer fibers in comparison to clots formed under stasis (Eyisoylu et al., 2024).
- **Factor XIIIa**: Crosslinking of protofibrils by factor XIIIa leads to highly compacted fibers with smaller diameters and increased resistance to fibrinolysis (Hethershaw et al., 2014).
- **Thrombin concentration**: Elevated thrombin concentrations also lead to decreased diameters of the fibers (Belcher et al., 2023; Domingues et al., 2016; Hotaling et al., 2015; Wolberg, 2023). This results in a differential spatial architecture of the fibrin clot, with dense structures in the center of the thrombus, where thrombin is more concentrated, and a looser structure in the periphery (Pieters & Wolberg, 2019).

- **Fibrinogen concentration**: High concentrations of fibrinogen lead to thicker fiber (Belcher et al., 2023; Risman, Belcher, et al., 2024; Weisel & Nagaswami, 1992). The presence of a common fibrinogen variant, fibrinogen γ' (γA/γ'), produced by alternative splicing of the γ-chain mRNA, which comprises up to 8% to 15% of total plasma fibrinogen concentration, results in the formation of loosely packed fibrin fibers with larger diameters (Domingues et al., 2016).

- **FXIIa**: Independently of thrombin, increased concentrations of FXIIa lead to fibrin clot with finer fibers (Konings et al., 2011)

In normal human plasma with a fibrinogen concentration of about 3 mg/ml, fibrin clot is highly porous, consisting of only 0.3 % protein and 99.7 % liquid by mass. Factors that can increase the pore sizes in fibrin network includes RBC, low concentrations of thrombin, FXIIIa, FXIIa, as well as high concentrations of fibrinogen (Gersh et al., 2009; Hethershaw et al., 2014; Konings et al., 2011; Weisel & Nagaswami, 1992; Wolberg, 2023). Small pores lead to poor perfusion and diffusion of fibrinolytic actors, thus delay the fibrinolysis process (Risman, Paynter, et al., 2024).

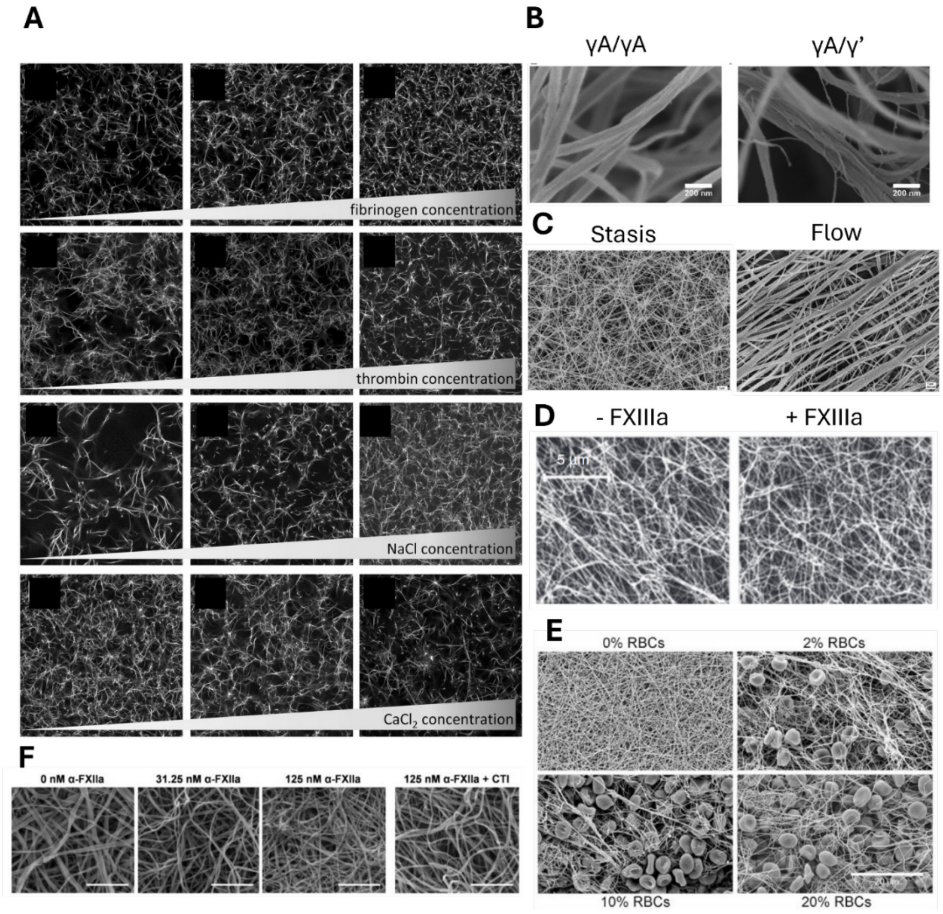

***Figure 8**: Factors that impact the structural characteristic of fibrin clot. **(A)** Fibrin clots formed from different concentrations of fibrinogen (1, 2, 3 mg/ml), thrombin (0.01, 0.05, 0.15 UI/ml), NaCl (60, 80, 120 mM) and $CaCl_2$ (1, 5, 10 mM) (Pietsch et al., 2023). **(B)** Fibrin clots formed from 1 mg/ml γA/γA or γA/γ' fibrinogen, 0.1 UI/ml thrombin, and 10 mM $CaCl_2$ (Domingues et al., 2016). **(C)** Fibrin clots formed from recalcified (10mM) platelet-free plasma in the presence of fibroblasts, under stasis and flow conditions (Campbell et al., 2010). **(D)** Fibrin clots formed with 1 mg/ml purified fibrinogen, 0.1 UI/ml thrombin, 2.5 mM $CaCl_2$, in the presence or absence of 6.7 µg/ml FXIII (Hethershaw et al., 2014). **(E)** Fibrin clots formed from recalcified platelet-free plasma (20mM), with addition of thrombin (0.5 UI/ml) and different concentration of red blood cells (RBC) (Gersh et al., 2009). **(F)** Fibrin clots formed from purified fibrinogen (1 mg/mL) with α-FXIIa (0-125 nM), thrombin (2.5 nM), and $CaCl_2$ (5 mM) in HEPES buffer (20mM HEPES, pH 7.4, 150mM NaCl). To inhibit α-FXIIa, corn trypsin inhibitor (CTI) (75 µg/mL) was added (Konings et al., 2011).*

3. Hypercoagubility in cancers

Thromboembolic events have been recognized since antiquity, but it was in 1865 that the physician Trousseau first identified the connection between cancer and thrombotic diseases, a relationship initially termed Trousseau's syndrome and now known as cancer-associated thrombosis (CAT). Today, CAT stands as the second leading cause of mortality among cancer patients (Farge et al., 2019). The risk of thrombosis development in individuals with cancer is notably elevated, ranging from 4 to 7 times higher compared to those without cancer (Khorana et al., 2020). Investigation into CAT has elucidated the mechanisms by which cancer contributes to thrombosis, uncovering the phenomenon of hypercoagulability in cancer cells.

Thrombosis occurs due to the imbalance between the anti- and pro-coagulant forces in the hemostasis system. In 1856, German physician Rudolf Virchow proposed a concept that would later be known as the Virchow Triad, citing three factors that can cause thrombosis:

- **Hypercoagubility:** Elevated level of coagulation factors in blood disturbs the balance of hemostasis.
- **Endothelial damage and activation:** The endothelium in its healthy, resting state, provides an anticoagulant and anti-platelet surface. Exposure of coagulation factors to the pro-coagulant sub-endothelium could be induced by injury of the vessel wall, or by the dysfunction of the endothelium. Activated endothelial cells release many coagulant factors, which contribute to the hypercoagubility.
- **Alteration in blood flow:** Stressors on the vessel wall regulate the production and secretion of endothelial defenses, including tPA, PGI2, and NO. Thus, blood flow controls vascular reactivity and limits platelet adhesion, aggregation, and fibrin formation to endothelial damage sites in the case of an endothelial injury.

This hypercoagulability manifests at both systemic and microenvironmental levels with the central role of cancer cells, by their procoagulant properties, and by their crosstalk with other cellular components.

3.1. Cancer cells' hypercoagubility

Tissue factor (TF) serves as the primary initiator of thrombin generation (Falanga et al., 2015). The procoagulant "fingerprint" of cancer cells refers to their ability to initiate and amplify thrombin generation. This concept implies that the nature and intensity of the procoagulant response vary depending on the histological characteristics of the cancer cells. For instance, the procoagulant potential exhibited by plasma cells in multiple myeloma differs from that of lung, breast, or pancreatic cancer cells (Gerotziafas et al., 2012; Marchetti et al., 2012; Papageorgiou et al., 2019). *In vitro* modeling studies have demonstrated that within the same histological type of cancer (e.g., breast cancer MCF7, MDA), the procoagulant potency varies based on the aggressiveness and metastatic potential of the cells (Gerotziafas et al., 2012). Moreover, it has been observed that chemotherapy-resistant MCF7 breast cancer cells exhibit significantly higher procoagulant potential compared to chemotherapy-sensitive MCF7 breast cancer cells (Rousseau, Van Dreden, Khaterchi, et al., 2015). In essence, published data indicate that the procoagulant fingerprint forms an integral part of the "biological identity" of cancer cells.

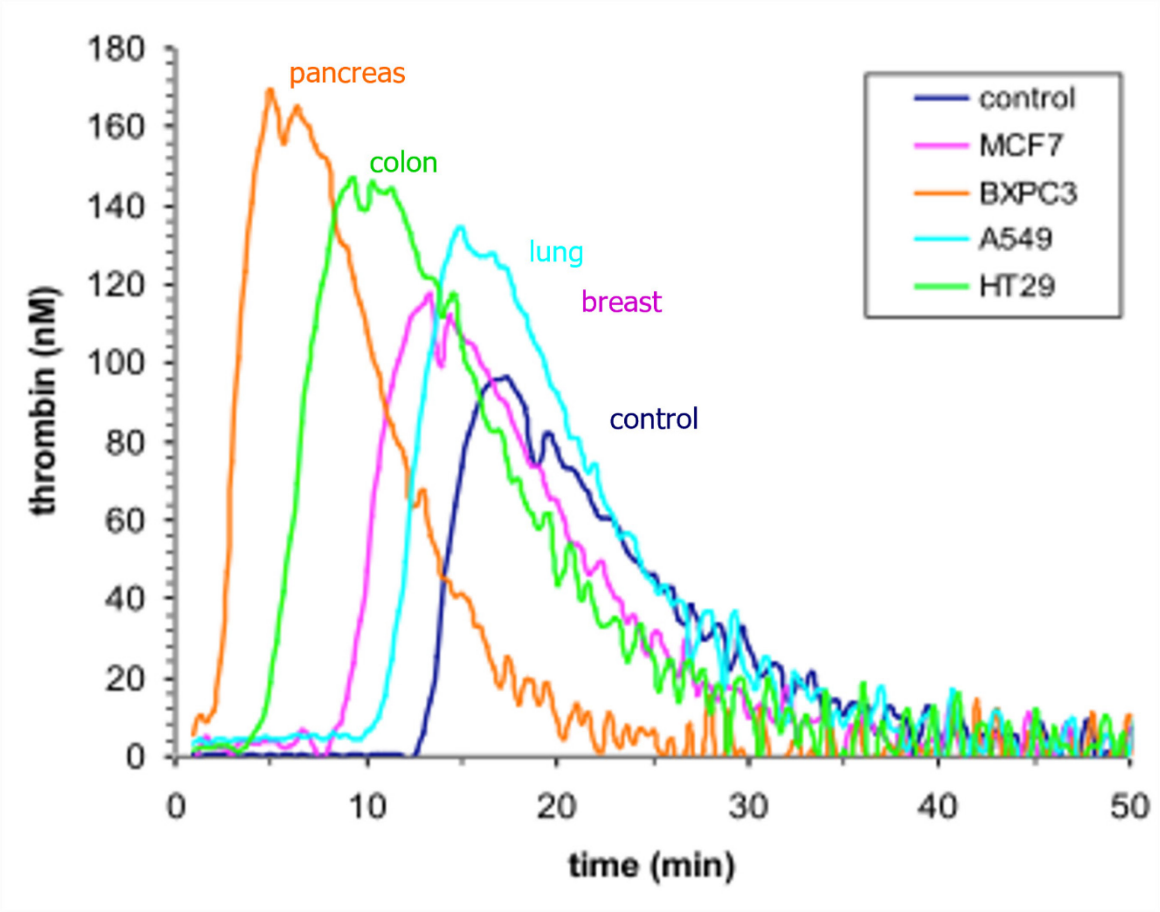

***Figure 9**: Thrombin generation profile from different cancer cell lines (Gerotziafas et al, 2012)*

The expression level of tissue factor (TF) correlates with the extent of tumor angiogenesis and malignancy. TF forms a complex with factor VII (FVII), leading to the activation of protease activated receptor 2 (PAR-2) signaling. This activation triggers calcium signaling and subsequently activates protein kinase C, mitogen-activated protein kinase, and phosphatidylinositol 3-kinase pathways, influencing tumor behavior by two mechanism (Han et al., 2014; Versteeg, 2015):

- Either by activation of the G protein, resulting in an increase in immune regulators, an increase in angiogenesis, and a decrease in apoptosis.

- Or by recruitment of beta-arrestins, which have an effect on cell migration. Direct activation of PAR-2 by the TF-VIIa complex also contributes to tumor proliferation through anti-apoptotic effects and the induction of various cytokines and other angiogenic regulators.

At the level of PAR 1 and 3, this activation requires the TF-VIIa-Xa complex and has an effect of increasing angiogenesis via an increase in P-selectin, vascular endothelial growth factor (VEGF), MMPs, IL-6, and 8, but also induces an increase in TF (Rickles et al., 2003).

TF expression, along with proangiogenic factors such as VEGF, plays a crucial role in determining the ability of cells from solid tumors (e.g., colon cancer) to engage in vascular mimicry processes (Sandrine et al., 2018). Alterations in the expression of tumor suppressor genes, such as Phosphatase and tensin homolog (*PTEN*) and *p53*, along with the upregulation of oncogenes like *EGFR* and *KRAS*, have been associated with dysregulated tissue factor (TF) expression in cancer cells (Galmiche et al., 2022; Miller et al., 2023)

Depending on the tumor type, certain types of cancer are also known to express factor VII and thrombin (Koizume et al., 2006, 2009; Yokota et al., 2009). Procoagulant FVIIa has been implicated in activating PAR2 signaling (Yokota et al., 2009). FVIIa has also been linked to the overexpression of β-catenin, which is involved in regulating T-cell inflammation and immunosuppression (Ruf & Graf, 2020). The TF-FVIIa-FXa complex is particularly crucial for Toll-like receptor 4-dependent regulation of interferon-controlled genes and the production of the tumor immune-evasion chemokine CCL22 (Liang et al., 2015).

Upregulation of tissue factor (TF) results in an excessive production of thrombin. Thrombin, acting as the pivotal enzyme in fibrin network formation, possesses potent platelet activation properties and induces cancer cell proliferation and migration via protease-activated receptors PARs. Among these, PAR-1, PAR-3, and PAR-4 are recognized as thrombin receptors, with PAR-1 being the primary mediator of thrombin's effects on tumor behavior, including tumor growth, metastasis, and angiogenesis (Coughlin, 2000). Thrombin signaling through PAR-1 has been implicated in promoting experimental pulmonary metastasis *in vivo* (B. Zhang et al., 2020). Moreover, thrombin activation of PAR-1 induces the secretion of pro-angiogenic factors by tumor cells and stimulates angiogenesis *in vivo* (Caunt et al., 2003).

3.2. Procoagulant extracellular vesicles

Extracellular vesicles (EVs) are micrometric structures secreted by all cells, including human cells, in a state of activation or apoptosis, as well as during conditions of stress (oxidative stress, hypoxia, inflammation) or under certain stimuli such as cytokines (TNF-alpha or IL-6) (Ayers et al., 2015). This family includes exosomes, microparticles, and apoptotic bodies, which differ in their formation and secretion mode, size, and content.

They are present in various biological fluids such as blood plasma, urine, pleural effusions, saliva, and breast milk (Kreimer et al., 2015). Initially considered as cellular "waste," they have quickly become a separate field of research after the discovery of their role as carriers and mediators in intercellular communication and immunity.

EVs contains numerous biomolecules, including proteins, lipids, and nucleic acids, which make capable of transmitting to other target cells (Colombo et al., 2014). Extracellular vesicles can interact directly with target cells via various mechanisms:

- Release of their content into the extracellular space.
- Contact using adhesion molecules, triggering intracellular signaling.
- Direct transfer of proteins to the cell surface (recycling).
- Membrane fusion, thereby releasing their cytosolic content into the recipient cell's cytoplasm. This results in the transfer not only of lipids and proteins but also of transcription factors and nucleic acids such as mRNAs or miRNAs.
- Or by endocytosis.

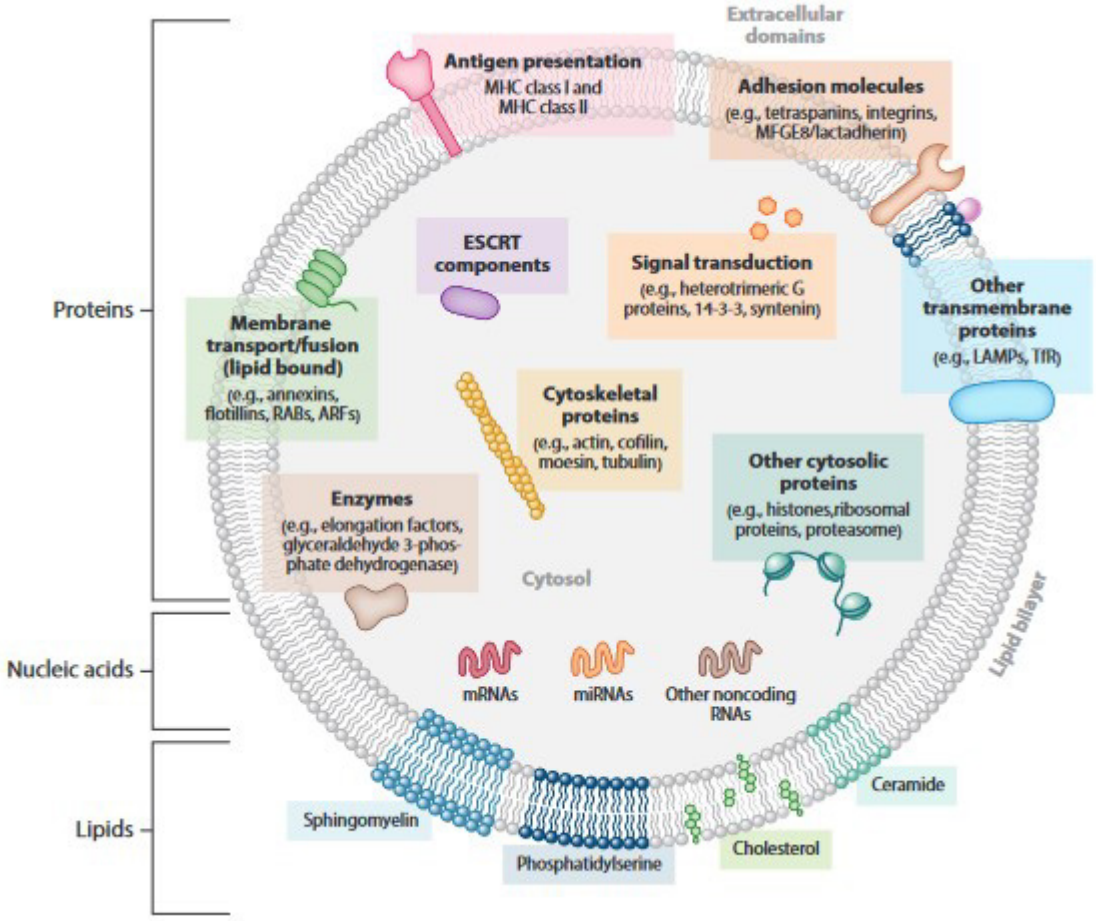

***Figure 10**: Composition of extracellular vesicle (Colombo et al, 2014)*

These EVs possess procoagulant properties that serve as a support for the procoagulant activity. Their main property lies in the provision of phosphatidylserine (PS), which is an anionic phospholipid exposed during the formation of microparticles. Due to its negative charge, it serves as a catalytic surface for the assembly of calcium-dependent coagulation factors and ultimately for the formation of the tenase complex, which is essential for the generation of thrombin.

In addition to PS, they can express TF on their surface, which serves as the trigger for the coagulation cascade through its interaction with activated factor VII. EVs reflect the molecular composition of their parent cells, including the presence of membrane proteins. Therefore, EVs derived from cancer cells that express TF would also carry TF on their membrane, with the procoagulant properties reflecting those of their parent cells (AmraneDjedidi et al., 2020; Rousseau, Van Dreden, Mbemba, et al., 2015).

The presence of circulating TF+ EVs and disseminated cancer cells during metastasis contributes to systemic CAT remote from the primary tumor site (Falanga et al., 2017). Within the tumor microenvironment, EVs derived from cancer cells not only initiate hypercoagulability by expressing tissue factor (TF) but also amplify it by serving as messengers between cancer cells and other cellular components, such as endothelial and immune cells.

3.3. Endothelial cells

The rapid proliferation of cancer cells presents a paradox: they require abundant oxygen and energy to support their growth, yet their uncontrolled division results in the formation of densely packed tumor masses with restricted access to oxygen and nutrients. To address this challenge, cancer cells stimulate the formation of new blood vessels, a process known as angiogenesis, as well as lymphatic vessels, termed neo-lymphangiogenesis, and induce vessel permeability, primarily through the expression of vascular endothelial growth factor (VEGF). Angiogenesis plays a pivotal role in tumor progression, and therapies targeting this process have demonstrated promising results (Eelen et al., 2020).

Angiogenesis is a phenomenon that primarily occurs during tissue repair to restore oxygen concentration or metabolite levels in certain tissues after ischemia or to meet increased demand, as seen in tumorigenesis. It involves the migration of activated endothelial cells from pre-existing vessels to form new vessels along a VEGF gradient established in response to hypoxic conditions. It occurs in several stages, including degradation of the extracellular matrix, proliferation and migration of endothelial cells, formation of initial tubules and neo-vessels, and finally, the formation and stabilization of the parenchymal cellular environment (recruitment of pericytes, synthesis of the extracellular matrix).

TF and thrombin have been shown to induce the recruitment of EC into the tumor stroma (Galmiche et al., 2022; Wahab et al., 2023). Once recruited, ECs undergo dysregulation mediated by reactive oxygen species (ROS), growth factors (such as TGFβ), and cytokines (such as IL-1), as well as EVs released by cancer-associated fibroblasts (CAFs), macrophages, and cancer cells. (Wahab et al., 2023). Cancer cell-derived extracellular vesicles (EVs) have also been demonstrated to activate ECs, thereby amplifying the hypercoagulability of the tumor microenvironment and promoting the recruitment of new ECs (AmraneDjedidi et al., 2020). Additionally, lymphangiogenesis is stimulated by coagulation, as thrombin cleaves and activates VEGF-C, a lymphangiogenic member of the VEGF family, after its release as an inactive precursor from the α-granules of platelets (Lim et al., 2019).

The activation of ECs exposes the von Willebrand factor (vWF) to circulating platelets, thereby enhancing its procoagulant activity. Additionally, vWF exposure in tumor-associated endothelial cells (TECs) serves to attract monocytes and neutrophils to the endothelium, thereby promoting leukocyte extravasation and inflammation. During the process of tumor extravasation, the physical interaction of tumor cells collaborates with TECs to activate them, creating an adhesive and procoagulant surface. Tumor-derived thrombin or tumor-secreted vascular endothelial growth factor (VEGF) plays a significant role in this process.

The regulation of endothelial barrier function and vascular permeability is crucial for controlling the extravasation of plasma and its macromolecular constituents. This regulation is primarily governed by intercellular junctions that create barriers within endothelial cells. There are two main types of intercellular junctions involved: adherent junctions and tight junctions. The number and arrangement of these junctions determine the permeability of the vasculature, which varies according to the specific needs of different organs and tissues (Claesson-Welsh et al., 2021).

Mediators that increase vascular permeability activate various kinases, phosphatases, and enzymatic activities, leading to the phosphorylation of junctional proteins and the formation of focal gaps between endothelial cells. This increased permeability is observed in numerous conditions, including asthma, inflammatory airway diseases, cancer, infections, *etc*… (Claesson-Welsh et al., 2021; Wautier & Wautier, 2022)

Cancer metastasis is favored by the enhancement of vascular permeability. Circulating tumor cells, moving in the microvasculature, tend to invade into stromal tissue at the location, where vascular permeability is enhanced. At least two mechanisms are involved in trans-endothelial permeability, vesicle transport, and migration through endothelial cell junctions. A tripeptide derived from collagen (proline–glycine–proline) promotes VE-cadherin phosphorylation and enhanced vascular permeability. Tumor cells can bind to endothelial cells and induce EC necrosis via a TNF receptor family mechanism. Tumor cells can also release a large number of molecules that affect EC permeability. Thrombin, heparanase, and matrix metalloproteinase (MMP), produced in inflammatory conditions, degrade the glycocalyx component, favoring tumor cell access to the EC surface (Wautier & Wautier, 2022). MMP17 originating from cancer-derived EVs has been shown to disrupt VE-cadherin-mediated adhesion, resulting in increased vascular permeability (K. Li et al., 2024). The production of the TF, by EC and/or macrophages, leads to factor X activation, which induces fibrin formation. Fibrinogen also has been considered a permeability factor (Angelidakis et al., 2023; Wautier & Wautier, 2022; Yu et al., 2021).

3.4. Platelets and red blood cells (RBC)

Vessel leakage facilitates not only the extravasation of cancer cells but also the infiltration of platelets and red blood cells into tumor tissues. Emerging evidence indicates that platelets can extravasate from vessels and aggregate within tumor tissues, playing versatile roles in cancer progression that promote tumor advancement.

The presence of tumor-infiltrating platelets has been correlated with poorer surgical outcomes (S.-R. Zhang et al., 2018), and their presence in the tumor microenvironment serves as an indicator for chemoresistance (Ishikawa et al., 2016; Saito et al., 2017). Furthermore, platelets recruited by tumor tissues play pivotal roles in tumor angiogenesis, growth, and metastasis.

Platelets play multifaceted roles in promoting tumor metastasis, including shielding tumor cells from immune surveillance, facilitating the epithelial-mesenchymal transition (EMT), aiding extravasation, and assisting in the establishment of metastatic niches. Within the tumor microenvironment, platelets secrete adenosine triphosphate (ATP), which promotes tumor-cell transendothelial migration and metastasis by activating endothelial P2Y2 receptors

(Schumacher et al., 2013). Moreover, platelet-secreted factors such as transforming growth factor-beta 1 (TGF-β1) and direct interactions with tumor cells activate signaling pathways such as TGF-β/Smad and nuclear factor (NF)-κB, leading to EMT, a key mechanism in metastasis (Krebs et al., 2017). Cancer cells cluster with activated platelets. Using the VEGF and MMPs secreted by the activated platelets, they degrade the ECM and loosen the endothelium, enter the blood stream, and transform into heterogeneous circulating tumor cells (CTC). This process allows cancer cells to enter the bloodstream, facilitating their dissemination to distant sites in the body (Wahab et al., 2023).

Activated platelets release angiogenesis-promoting factors like VEGF and stromal-derived factor-1 (SDF-1), fostering the formation of tumor-associated blood vessels (Stellos et al., 2008). Platelet-derived extracellular vesicles (EVs) also contribute to the observed vascular permeability in solid tumors and infiltrate the tumor microenvironment by transferring their miRNAs (Michael et al., 2017). Additionally, platelets can stimulate lymphangiogenesis by acting on lymphatic endothelial cells, as evidenced by the correlation between CD42b expression (a platelet marker) and lymphatic metastasis (Bertozzi et al., 2010).

In the tumor microenvironment, platelets interact with red blood cells (RBCs) via specific molecular interactions involving Fas ligand/Fas receptor, leading to increased thrombin generation. This interaction contributes to the procoagulant environment within the tumor microenvironment (Klatt et al., 2018). Additionally, RBCs play a positive role in regulating inflammation in the TME. Recent studies have demonstrated that RBCs contribute to the recruitment of CD45+ immune cells in mouse models implanted with blood clots of different cell compositions (Fan et al., 2020).

Furthermore, senescent RBCs within the tumor microenvironment serve as a significant source of iron delivered to tumor-associated macrophages (TAMs). This iron delivery favors the polarization of TAMs towards a tumoricidal (M1) phenotype, which can potentially enhance anti-tumor immune responses (Thielmann et al., 2019).

3.5. Immune cells

In tumor microenvironments, dense populations of tumor-infiltrating macrophages (TAMs) are often linked to unfavorable prognoses. TAMs typically exhibit two distinct phenotypes: M1, which is associated with tumor suppression and driven by interferon-gamma (IFN-γ), and M2, which promotes tumor growth and is driven by interleukin-4 (IL-4) and interleukin-13 (IL-13) (Mantovani et al., 2017).

During later stages of vascular dysfunction within tumors, TAMs undergo a transition from an M1 to an M2 phenotype, coinciding with increased permeability of tumor vessels. M2 TAMs contribute to the formation of abnormal blood vessels by supplying VEGF (Mathivet et al., 2017). Thrombin has been shown to directly influence TAM differentiation, as observed in ovarian cancer models, where exposure to thrombin induces NF-κB-driven transcription, increased production of the proinflammatory cytokine interleukin-8 (IL-8), and subsequent M2 differentiation (T. Zhang et al., 2010). Macrophages also differentiate into the M2 phenotype in the presence of fibrin via activation of the NF-κB pathway and expression of IL-8 (Mathivet et al., 2017). Recent study showed that cancer cells-derived EVs activated ECs, which in turn generated their own EVs containing numerous miRNA that induced the switch to the M2 phenotype in TAMs (Njock et al., 2022).

Furthermore, inflammatory monocytes expressing factor XIII (FXIII) interact with fibrin clots to promote the progression of lung squamous cell carcinoma (Porrello et al., 2018).

Myeloid cells expressing tissue factor (TF) initiate the coagulation cascade (Wahab et al., 2023). TAM-autonomous signaling through factor Xa (FXa) and protease-activated receptor 2 (PAR2), generated by infiltrating monocytic cells, contributes to the creation of an immunosuppressive environment by increasing the expression of programmed death-ligand 1 (PD-L1) on these cells (Graf et al., 2019). The infiltration of functional lymphocytes is crucial for the efficacity of Chimeric Antigenic Receptor - T (CAR-T) cells treatments.

3.6. Cancer-associated fibroblasts

Fibroblast cells play a crucial role in maintaining the structural integrity of the stroma and regulating interactions among various cellular components (Wahab et al., 2023). When exposed to cancer cell-derived transforming growth factor beta (TGFβ), fibroblasts undergo dedifferentiation and transform into cancer-associated fibroblasts (CAFs) (Shaashua et al., 2022). In the tumor microenvironment, CAFs contribute to tumor progression by promoting angiogenesis through tube formation, facilitating epithelial-mesenchymal transition (EMT) and subsequently, metastasis, and engaging in proinflammatory and immunosuppressive activities (Rimal et al., 2022).

CAFs also express TF. Specimens from early-stage breast cancer patients have shown that CAFs exhibit elevated levels of TF, thrombin, and PAR1 compared to normal breast fibroblasts. This suggests that procoagulant CAFs contribute to stromal hypercoagubility (Shaker et al., 2020). Thrombin, in addition to its role in coagulation, can stimulate the release of active TGF-β, thus creating a positive feedback loop that further promotes the transformation of normal fibroblasts into CAFs (Metelli et al., 2020).

HYPOTHESIS

The tumor microenvironment is characterized by a high procoagulant state, primarily driven by the expression of tissue factor (TF) by cancer cells, myeloid cells, and cancer-associated fibroblasts (CAFs) (Galmiche et al., 2022; Wahab et al., 2023). TF, the principal activator of blood coagulation, initiates thrombin generation, contributing to the hypercoagulable milieu within the tumor microenvironment. Variations in TF expression and procoagulant potential are associated with the histological type and aggressiveness of cancer cells (Gerotziafas et al., 2012; Rousseau, Van Dreden, Khaterchi, et al., 2015; Rousseau, Van Dreden, Mbemba, et al., 2015). Furthermore, cancer cells release TF-bearing exosomes, further amplifying the procoagulant stimulus in the microenvironment (Charpidou et al., 2024).

Cancer cells also enhance the procoagulant characteristics of the tumor microenvironment by activating endothelial cells (ECs) and platelets (AmraneDjedidi et al., 2020; Galmiche et al., 2022). The abundant presence of TF in the tumor microenvironment, exposed to blood coagulation factors due to processes such as angiogenesis, vascular mimicry, and vessel leakage, triggers coagulation and fibrin polymerization.

As a result, the presence of fibrin is a distinctive feature of the tumor microenvironment (Obonai et al., 2016; Starmans et al., 2015) (**Figure 11A-H**).

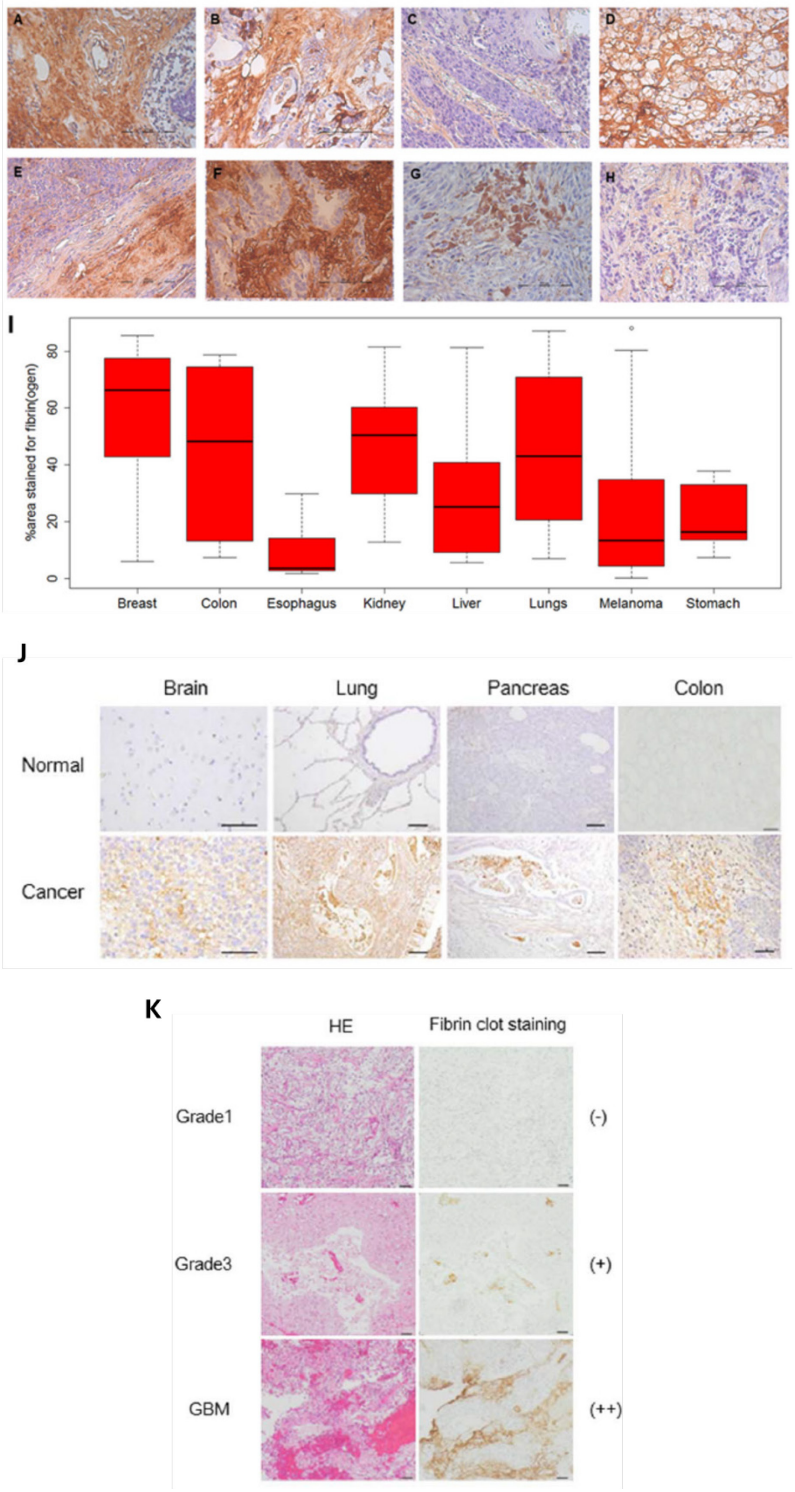

***Figure 11**: The presence of fibrin in tumor biopsies. Immunohistochemistry staining of fibrin in **(A)** breast, **(B)** colon, **(C)** esophagus, **(D)** kidney, **(E)** liver, **(F)** lungs, **(G)** melanoma, and **(H)** stomach tumor (Kirtane et al., 2017). **(I)** Occupation area of fibrin in cancer patients' specimens from different cancers (Kirtane et al., 2017). **(J)** Fibrin deposition in tumor in contrast with normal tissues (Hisada et al., 2013). **(K)** Fibrin immunostaining from glioblastoma in different grade of tumor progression (Hisada et al., 2013).*

Fibrin deposition is absent in normal tissue specimens but is evident in specimens from cancer patients (**Figure 11J**). Normal tissue specimens typically do not contain fibrin, whereas specimens from cancer patients show varying amounts of fibrin deposition (Hisada et al., 2013). The quantity of fibrin increases with cancer progression (Hisada et al., 2013) (**Figure 11K**), but the amount can vary widely between different types of cancer and among patients with the same type of cancer (Kirtane et al., 2017). For instance, fibrin deposition in breast cancer patients can occupy anywhere from 40% to 80% of the tumor area, while in colon cancer, the range is 10% to 80% (**Figure 11I**). This heterogeneity in fibrin quantity may be attributed to the non-uniform expression of TF in cancer patients.

Even though many studies had shed light on the presence and the quantification of fibrin in tumor microenvironment, little had been done to investigate the structural characteristics of fibrin networks in the tumor microenvironment.

Research examining the structure of fibrin clots formed from peripheral plasma in cancer patients has demonstrated distinct characteristics compared to clots formed from plasma of control subjects. Specifically, fibrin clots from cancer patient plasma exhibit finer fibers, smaller pores, and lower permeability (Gronostaj et al., 2013) (**Figure 12**). Since fibrin structure is influenced by thrombin concentration, which is regulated by tissue factor (TF) expression (Belcher et al., 2023), it is plausible to speculate that the procoagulant signature of cancer cells may impact the structural properties of fibrin networks within the tumor microenvironment.

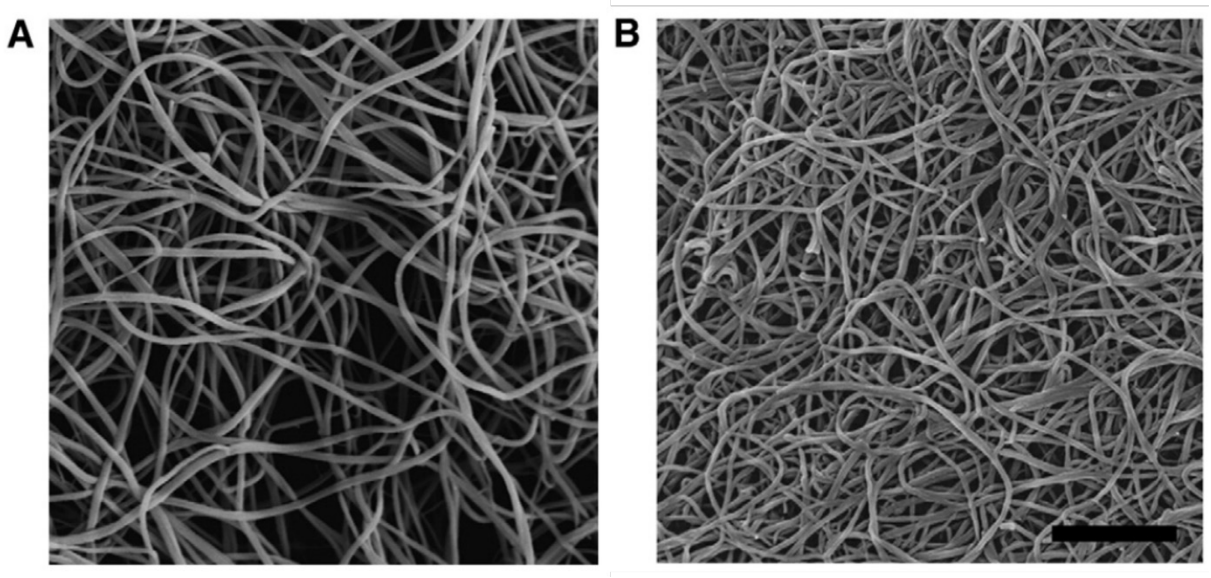

***Figure 12**: Scanning electron microscopy images of fibrin clots formed from **(A)** control subject and **(B)** cancer patient (Gronostaj et al., 2013). Scale bar represents 2 µm.*

Fibrin, as a significant component of the tumor extracellular matrix (ECM), undergoes remodeling, which supports various tumor-promoting processes such as proliferation, metastasis, angiogenesis, and immunosuppression. In wound healing scenarios, fibrin facilitates fibroblast and endothelial cell migration. Considering that cancer cells also possess fibrinolytic activity through the expression of urokinase plasminogen activator (uPA) or tissue plasminogen activator (tPA) (Saidak et al., 2021), it is conceivable that fibrin may play a role in cancer cell migration and invasion.

The observed low permeability of fibrin clots formed from cancer patients' plasma suggests that fibrin within the tumor microenvironment may act as a physical barrier, impeding the penetration of anticancer agents, particularly those reliant on ligand-receptor interactions such as targeted treatments.

Considering these findings, we hypothesize that the hypercoagulability exhibited by cancer cells, as evidenced by TF expression, serves as the primary driver of fibrin formation within the tumor microenvironment. Furthermore, we propose that the procoagulant fingerprint of cancer

cells could influence the structural characteristics of the tumor fibrin network, potentially impacting cancer cell migration and response to anticancer treatments.

OBJECTIVES

In the first objective of this PhD thesis, we aim to establish an experimental model wherein cancer cells are enveloped within a fibrin matrix. This experimental model must adhere to several crucial criteria:

- Ensuring the presence of cancer cells within the fibrin network to facilitate the study of their interaction with fibrin.
- Maintaining the viability and proliferative capacity of the cancer cells within the fibrin environment to simulate physiological conditions.
- Enabling the manipulation of the fibrin network's architecture to reflect varying degrees of thrombogenicity characteristic of the tumoral microenvironment across different cancers.
- Optionally, providing versatility for both two-dimensional (2D) and three-dimensional (3D) culture systems, allowing for the exploration of cell behavior in different spatial contexts. Compared to conventional 2D culture methods, 3D culture system offers a spatial architecture facilitating intricate cell-cell and cell-matrix interactions crucial for cellular functions and viability (Costa et al., 2016; Holle et al., 2016). By mimicking the spatial distribution, 3D cultures create gradients of essential nutrients, soluble factors, and oxygen, fostering a microenvironment akin to *in vivo* conditions. Consequently, cellular behaviors between 2D and 3D cultures exhibit substantial disparities. The utilization of 3D culture techniques is particularly advantageous in drug screening and pre-clinical testing due to their ability to replicate physiological conditions more faithfully than traditional 2D models (Langhans, 2018; Sensi et al., 2019; Stock et al., 2016). While 2D culture still holds significance in certain applications, the selection between these models hinges on specific research objectives, desired outcomes, and available resources. Thus, although the incorporation of 3D culture is not mandatory for our experimental model, its adoption presents opportunities for broader applications.

Two experimental models were investigated:

- Cell culture in fibrin hydrogel: A technique widely employed in tissue engineering and the culture of stem, neuronal, and endothelial cells. Fibrin was generated from purified fibrinogen and thrombin.
- Cell culture in media supplemented with platelet-poor plasma (PPP): Coagulation factors are supplied by PPP, and fibrin formation is induced by pre-existing Ca^{2+} in the culture media.

The final refined model will serve as a valuable tool for elucidating the intricate interplay between fibrin and cancer cells, shedding light on its significance in tumorigenesis and offering insights into potential therapeutic strategies.

In the second objective of this thesis, using the validated experimental model, our objectives are:

- Investigate the ability of cancer cells to induce the formation of fibrin clots.
- Assess the impact of cancer cells' procoagulant fingerprint on the structural characteristics of the fibrin clot.
- Examine the migration of cancer cells within the fibrin networks and evaluate the influence of the network's structure, as well as the fibrinolytic fingerprint of cancer cells, on cell mobility.
- Evaluate the impact of the fibrin network on the efficacy of anticancer agents, such as paclitaxel (a chemotherapeutic agent) and 4-hydroxy-tamoxifen (an inhibitor of the estrogen receptor).

MATERIALS AND METHODS

1. Cell culture

1.1. Cell lines

The initial studies conducted by our team have demonstrated that the procoagulant potential of cancer cells varies – at least - according to the histological type of cancer. For the present study, we initially assembled a panel of various cancer cell lines derived from solid tumors to investigate their procoagulant properties.

For comparison purpose, we pre-defined the following criteria for cell line selection :

- **Variety in inter-histology type:** the selected cell lines should come from two different types of cancer.
- **Variety in intra-histology type:** the selected cell lines should issued from the same type of cancer, but differ in term of subtype/phenotype.
- **Variety in prothrombotic cancer associated potential:** the selected cell lines should represent cancer type associated with high or low/moderate risk of cancer associated thrombosis.
- **Variety in procoagulant potential:** the selected cell lines should display different of procoagulant potency, in terms of TF expression.

Based on those criteria, the studied tumors were pancreatic adenocarcinoma and breast adenocarcinoma and the selected cell lines were the pancreatic cancer BXPC3 cells and the breast cancer cell lines MCF7 and MDA-MB231.

1.1.1. Pancreatic adenocarcinoma cell line BXPC3

Pancreatic adenocarcinoma cell line BXPC3 (ATCC CRL-1687) was obtained from ATCC (Virginia, USA). Originally derived from pancreatic tissue obtained from a 61-year-old Caucasian female patient diagnosed with adenocarcinoma in 1980, BXPC3 cells display epithelial morphology and have a doubling time ranging from 48 to 60 hours (Tan et al., 1986). BXPC3 cells display high procoagubility, as demonstrated by their elevated expression of

Tissue Factor (TF) and potency of thrombin generation in normal human plasma, as well as their production of TF+ extracellular vesicles.

For the purposes of this study, BXPC3 cells were maintained in RPMI-1640 GlutaMAX medium supplemented with 10% Fetal Bovine Serum (FBS) and 1% Penicillin/Streptomycin, and cultured under standard conditions at 37°C, 5% CO_2, and 100% humidity.

1.1.2. Breast adenocarcinoma cell line MDA-MB231

Invasive breast adenocarcinoma cell line MDA-MB231 (ATCC HTB-26) was obtained from ATCC (Virginia, USA). Derived from the pleural effusion of a 51-years-old Caucasian patient with metastatic breast adenocarcinoma in 1973, MDA-MB231 cells display epithelial morphology and possess a doubling time ranging from 25 to 30 hours (Cailleau et al., 1974). Characterized by the absence of estrogen (ER), progesterone (PR), and human epidermal growth factor 2 (HER2) receptors, MDA-MB231 cells serve as a valuable model for triple-negative breast cancer (ER-, PR-, HER2-). Furthermore, their diminished expression of E-cadherin renders them a representative model for highly invasive breast cancer (Welsh, 2013). MDA-MB231 cells highly express TF, both on their plasma membrane and in extracellular vesicles, inducing elevated levels of thrombin generation.

In this study, MDA-MB231 cells were cultured in either DMEM GlutaMAX media *containing 4.5 g/l D-glucose*, or RPMI-1640 GlutaMAX media, both supplemented with 10% FBS, and 1% Penicillin/Streptomycin, at 37°C, 5% CO_2 and 100% humidity.

1.1.3. Breast adenocarcinoma cell line MCF7

Non-invasive breast adenocarcinoma cell line MCF7 (ATCC HTB-22) was obtained from ATCC (Virginia, USA). Originating from the pleural effusion of a 69-year-old Caucasian patient in 1973, MCF7 cells, despite their metastatic origin, exhibit non-invasive behavior both in *in vitro* and in xenograft models. Renowned for their high expression of estrogen receptors (ER), MCF7 cells serve as a pivotal tool in preclinical assessments of antiestrogen therapies such as tamoxifen and aromatase inhibitors, as well as in elucidating mechanisms of drug

resistance (Welsh, 2013). MCF7 cells express a very minimal amount of TF, making them the lowest in terms of procoagulant properties across the three selected cell lines.

It is noteworthy that phenol red, a commonly employed pH indicator in culture media, shares structural similarities with certain nonsteroidal estrogens. Consequently, phenol red-containing media exerts partial estrogenic stimulation, leading to a two-fold increase in cell proliferation and a three-fold rise in progesterone receptor content compared to cells cultured in phenol red-free media (Berthois et al., 1986). Hence, it is preferable to use a phenol red-free media in studies that imply hormonal treatments.

Another potential source of artefact in studies involving estrogen receptor modulators is the presence of estradiol in fetal bovine serum (FBS). The concentration of estradiol in FBS varies widely among different batches and manufacturers, compromising reproducibility. To mitigate these issues, two solutions are proposed:

- Utilizing phenol red-free media supplemented with dextran-coated charcoal-treated FBS devoid of all hormones, alongside a consistent concentration of exogenous estradiol tailored to physiological levels based on the study design. Physiological concentrations of estradiol range from 30 to 400 pg/ml in premenopausal women and from 0 to 30 pg/ml in postmenopausal women (Hultin, 2012).
- Utilizing phenol red-free media supplemented with regular FBS. At the standard 10% dilution typically used in cell culture, the final concentration of estradiol in FBS aligns with the normal range observed in premenopausal women. However, for reproducibility, it is preferable to use FBS from the same batch for throughout the study.

In this work, MCF7 cells were cultured in RPMI-1640 media, *in the absence of red phenol*, supplemented with 10% FVS, 1% Penicillin/Streptomycin, 5 mM of L-glutamine, at 37°C, 5% CO_2 and 100% humidity.

1.1.4. Conclusion

Characteristics of the three selected cell lines are summarized in the following table:

Table 2: Characteristics of BXPC3, MDA-MB231, and MCF7 cell lines

	BXPC3	MDA-MB231	MCF7
Histology type	Pancreatic adenocarcinoma	Breast adenocarcinoma	Breast adenocarcinoma
Phenotype	Epithelial	Epithelial ER-, PR-, HER2- E-cadherin-, N-cadherin+, Claudin-1-	Epithelial ER+, PR+, HER2+ E-cadherin+, N-cadherin-, Claudin-1+
Procoagulant properties	Highly procoagulant	Highly procoagulant	Lowly procoagulant
Invasivity	Highly invasive	Highly invasive	Non-invasive

1.2. Cell Passaging

Adherent cell cultures were maintained by regular passaging upon reaching 80% confluency. To achieve these levels of confluency, cells were initially rinsed with phosphate-buffered saline (PBS) followed by trypsinization with 0.25% trypsin EDTA for 3-5 minutes at 37°C, 5% CO_2, and 100% humidity within the incubator. Subsequently, detached cells were collected and pelleted by centrifugation at 1300 rpm for 5 minutes, following a PBS wash. The resultant cell pellet was then resuspended in fresh culture media. Cell viability was evaluated using trypan blue staining, and only cultures exhibiting a mortality rate below 2% were deemed suitable for experimentation.

1.3. Cryopreservation

Cells were cryopreserved in a freezing medium comprising 10% dimethyl sulfoxide (DMSO) in fetal bovine serum (FBS), achieving a final concentration of $1x10^6$ cells/ml, and stored at -80°C for 24 hours prior to transfer to liquid nitrogen for long-term preservation.

For cell recovery, cryovials were thawed in a 37°C water bath and subsequently transferred to pre-warmed culture media for centrifugation at 1300 rpm for 5 minutes to eliminate the DMSO-containing freezing media. Thawed cells were then resuspended in fresh culture media and seeded into a 75 cm^2 culture flask (Falcon™, Corning, New York, USA). Following a 24-hour incubation period, the culture media was replaced to eliminate any residual DMSO.

Cells were utilized for experiments for a maximum of 10 passages following thawing to ensure optimal cellular functionality.

2. 3-dimensentional (3D) cell culture

Cells were seeded at a density of $3x10^3$ cells per well in low-attachment 96-well plates (Nucleon Sphera, Thermo Fisher, Massachusetts, USA) with a volume of 100 µl per well. Media renewal was achieved by exchanging 50 µl of old media with an equal volume of fresh media. Spheroids were harvested for experimentation upon reaching a maturity of 4 days.

3. Fibrin formation

In the first part of the study, we set-up and validated a new method the evaluation of the clot structure formed following the initiation of coagulation by cancer cells.

3.1. Conventional Hydrogel method for fibrin formation

Hydrogel of fibrin was prepared by combining different concentration of fibrinogen and thrombin. Fibrinogen (Diagnostica Stago, Asnières, France) was used at 1 mg/ml and 5 mg/ml. Human thrombin (Diagnostica Stago, Asnières, France) was used at 2 UI/ml and 4 UI/ml.

For 2D-culture, cells were seeded at the density of density of $5x10^3$ cells/well in each well of the 96-well microplate for 24 hours for adherence, then the supernatant was discarded, and 16 µl of the hydrogel preparation was deposed on the cells. The plate was next placed in the incubator for fibrin polymerization. After 2 hours, a hydrogel of fibrin with 500 µm of thickness was formed and 100 µl of culture media were added to each well.

For 3D-culture, 4-days old cancer spheroids were developed in the ultra-low attachment plate. A volume of 16 µl of the hydrogel preparation was deposed into each well of another flat bottom 96-wells plate. The plate was next placed in the incubator for fibrin polymerization. After 2 hours, a hydrogel of fibrin with 500 µm thickness formed and Cancer spheroids were transferred from the ultra-low attachment plate to the hydrogel, using aspiration by micropipette, 100 µl of culture media was added to each well.

3.2. PPP-conditioned media method

A new method for the study of fibrin clot structure formed upon coagulation activation by cancer cells was set up according to the following protocol:

- Fibrin network formation was induced by culturing cancer cells in the presence of normal human platelet poor plasma (PPP). The PPP was obtained from the French Blood Establishment (Saint Antoine Hospital, Paris, France).
- **For 2D-culture**, cells were seeded at $5x10^3$ cells/well in each well of the 96-wells plate, or $3x10^5$ cells/well on glass coverslips, in the 12-wells plate, for 24 hours for adherence. Subsequently, conditioned media was replaced with fresh media supplement with 10% PPP.
- **For 3D-culture**, cancer spheroids were growth in the ultra-low attachment plate. At 4-days old, 50 µl of the conditioned media was removed from each well and replaced with 50 µl of fresh media supplemented with 20% PPP. The final concentration of PPP in each well was thus 10%.

In a first step of the elaboration of the experimental procedure we determined the dilution of PPP in RPMI-1640 which warranted a significant thrombin generation and solid fibrin network

without compromising cancer cell viability and proliferation rate as compared to the standard culture with RPMI-1640 (conventional media). The optimal dilution of PPP in the RPMI-1640 media was found to be situated to 10% (data are shown in the Results section). This conditioned media is called "*PPP-conditioned media*" to be distinguished by the conventional culture media (RPMI-1640).

4. Assessment of thrombin generation

The Calibrated Automated Thrombogram® was used to assess thrombin generation in normal PPP and in the PPP-conditioned media triggered by the cancer cells. Thrombin generation test allows for the continuous registration of the amount of thrombin generated following the initiation of coagulation (by addition of $CaCl_2$) in platelet-poor or platelet-rich plasma.

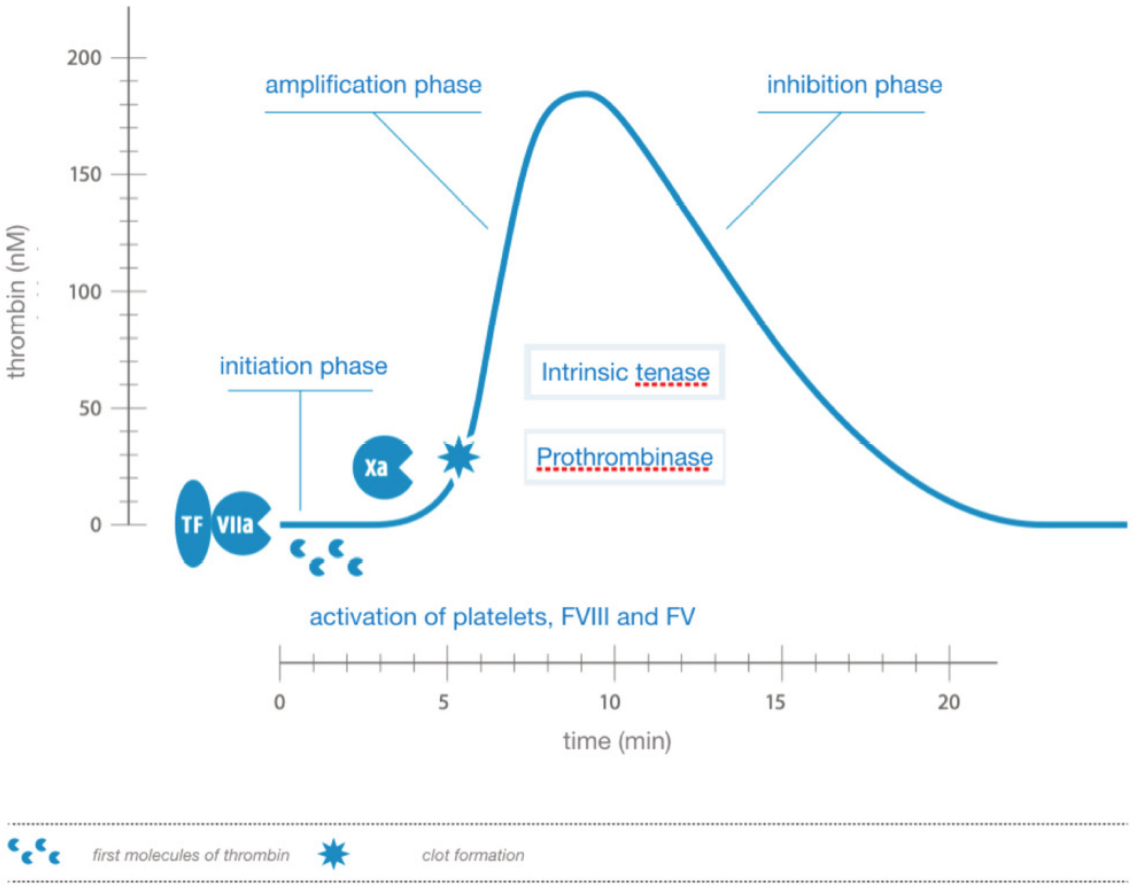

***Figure 13**: The kinetics of thrombin generation (Gerotziafas et al., 2018)*

The concurrent use of a calibrator in the plasma being tested enables quantitative expression of the generated thrombin. The key parameters of the thrombogram include:

- **Lag-time:** the latency period corresponding to the initiation phase of thrombin generation (expressed in minutes)
- **Peak**: the maximum concentration of generated thrombin (expressed in nM)
- **Time to peak (ttpeak)**: the time required to reach the maximum concentration of thrombin (expressed in minutes)

- **Endogenous Thrombin Potential (ETP):** The endogenous potential of thrombin or the area under the curve representing the enzymatic activity performed by active thrombin molecules in plasma (expressed in nM/min)
- **Mean Rate Index (MRI):** The average rate of the propagation phase of thrombin generation, calculated by the formula: MRI = peak/(ttpeak-lag-time); (expressed in nM/min)

For thrombin generation in the presence of increasing concentration of TF, the PPP-Reagent HIGH (Diagnostica Stago, Asnières, France) was diluted in the STA® Owren-Koller buffer (Diagnostica Stago, Asnières, France) to yield final concentrations in PPP of 0.5 pM, 1 pM, 2 pM, 3 pM, 4 pM, and 5pM of TF. In each well of a 96-wells microplate, 80 µl of PPP conditioned media (PPP diluted at 10% in RPMI) were added to 20 µl of TF solution. Then, thrombin generation was initiated by the addition of 20 µl triggering solution comprising $CaCl_2$ (16.7 mM final concentration) and a fluorogenic substrate of thrombin (Z-Gly-Gly-Arg-AMC, 417 mM final concentration). Among thrombogram parameters, the lag-time, the ETP and Peak were analyzed.

For the assessment of thrombin generation in the presence of cancer cells the following procedure was applied: cells were seeded at a density of $5x10^3$ cells/well in each well of the 96-well microplate. PBS buffer (20 µl) was mixed with 80 µl of PPP-conditioned media (PPP diluted at 10% in culture media) and then, thrombin generation was assessed as described above.

In a separate series of experiments, a volume of 20 µl of solution of exogenous TF (PRP Reagent **High**®, Diagnostica Stago, Asnières, France) was added to MCF7 cells cultures (as described above) yielding a final concentration of 1 pM. Thrombin generation was initiated by the addition of 20 µl triggering solution comprising $CaCl_2$ (16.7 mM final concentration) and a fluorogenic substrate of thrombin (Z-Gly-Gly-Arg-AMC, 417 mM final concentration). Among thrombogram parameters, the lag-time, endogenous thrombin potential (ETP) and Peak were analyzed.

5. Viability and proliferation assessment of cancer cells within the fibrin clot

5.1. MTT assay

For MTT [3-(4,5-dimethylthiazol-2-yl)-2,5-diphenyltetrazolium bromide] assay, cells were seeded at $12.5x10^4$ cells/ml in chambered coverglass (Nunc, Thermo Fischer, Massachusetts, USA). Fibrin clot was formed with PPP as described above, with the addition of 25 µg/ml of fluorescent Fibrinogen (Thermo Fisher, Massachusetts, USA). After 24 hours incubation, a MTT solution (4 g/l). Images of formazan crystals and fibrin networks were obtained with a fluorescent microscope (EVOS, Thermo Fisher, Massachusetts, USA).

The MTT assay is based on the concept that mitochondrial activities of viable cells convert soluble MTT of color yellow to purple crystals of formazan (**Figure 14**).

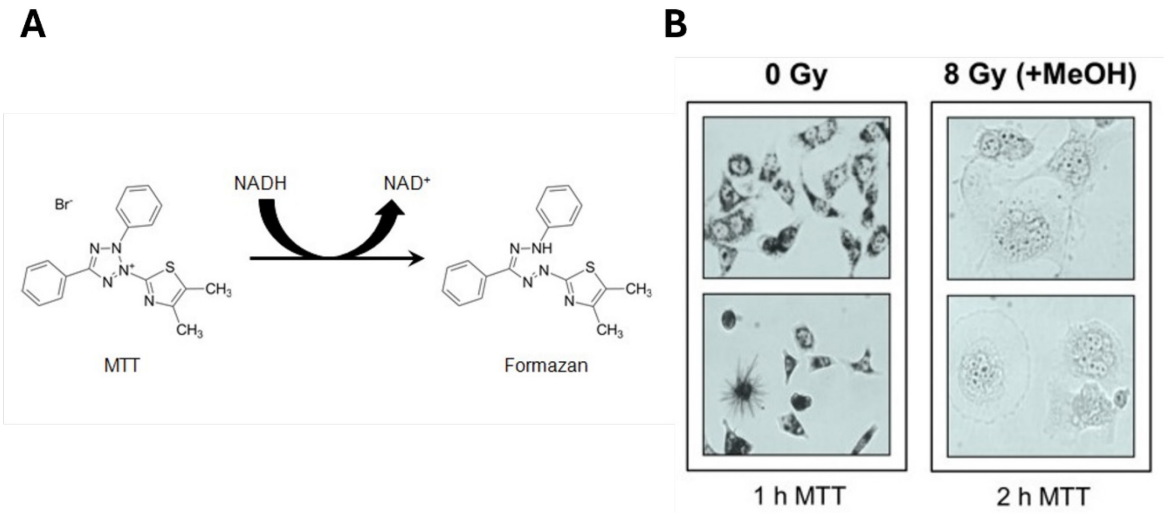

Figure 14: *Principle of the MTT assay. (A) Transformation of yellow soluble 3-(4,5-dimethylthiazol-2-yl)-2,5-diphenyltetrazolium bromide (MTT) into purple formazan crystals under the mitochondrial metabolic activities (Riss et al, 2016). (B) Qualification evaluation of cell viability using the MTT assay. Viable multinucleated giant cancer cells HCT116p53−/− non-treated with ionizing radiation are able to induce formazan crystal formation after 1 hour of incubation with MTT. In another experiment, cell death was induced by 8 Gy of radiation, followed by arrestation of metabolic activity with methanol (MeOH). Dead cells are unbale to produce formazan crystal after 2 hours of incubation with MTT (Mirzayans et al, 2017).*

Classical MTT assay involve solubilization of the formazan crystals and absorbance reading at 570 nm. Subsequently, the DOs are **normalized with control condition** to relatively quantify cell viability. However, this method has a limitation due to the presence of fibrin, which impairs the dissolution of formazan crystals. In the absence of fibrin, most of the crystals are dissolved after 4 hours of incubation with DMSO in at 25°C. However, in the presence of fibrin, a significant proportion of crystals are still present, even after 8 hours of incubation with DMSO at 37°C and in agitation (**Figure 15**).

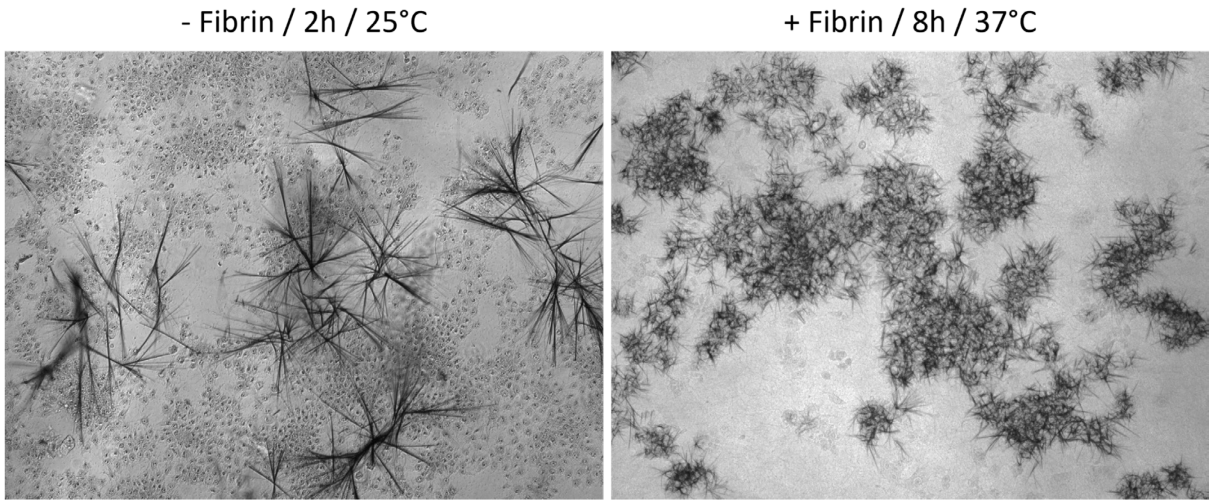

***Figure 15**: Fibrin interference with the dissolution of formazan crystals in the MTT assay. BXPC3 cells were cultured in the absence or presence of fibrin, by employing conventional media and PPP-conditioned media respectively, for 24 hours. Subsequently, cells were incubated with the MTT reagent for 4 hours to induce for formation of formazan crystals. DMSO was used for the solubilization of the crystals, with different incubation time and temperature: 2 hours at 25°C for dissolution in the absence of fibrin, and 8 hours at 37°C in the presence of fibrin.*

Despite this limitation, MTT assay could still be employed for qualification evaluation. Viable cells could still be individually identified under simple phase-contrast microscopy, as evidenced by the presence of formazan crystals.

5.2. Resazurin assay

To overcome the above-described limitation of the MTT method, a second assay was used for quantification of cell viability within the fibrin network. The Resazurin assay is based on the concept that mitochondrial activities of viable cells reduce the blue resazurin substrate to the pink fluorescent resorufin product. Resazurin assay is widely used in fibrin hydrogel model to assess the cell viability (Fernández et al., 2013; Giannotti et al., 2013; Kniebs et al., 2021;

Sharma et al., 2015), where MTT assay tends to underestimate cell viability due to undissolved crystals (**Figure 16**).

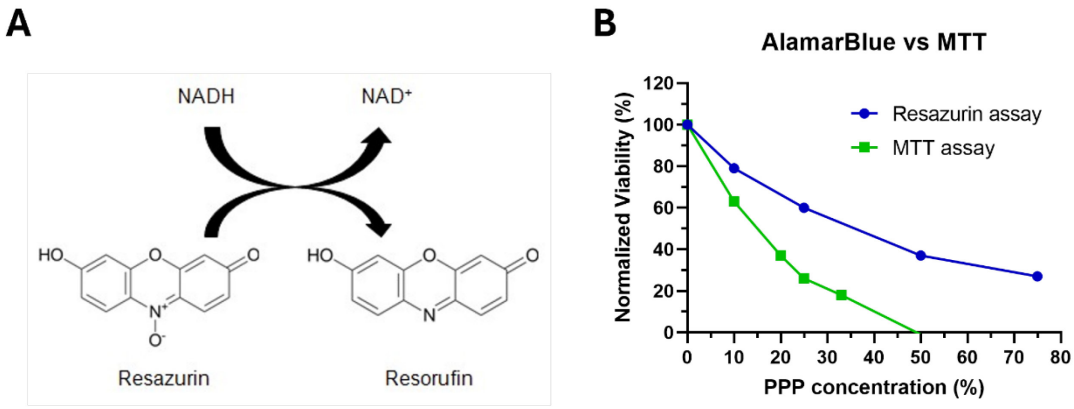

***Figure 16**: Principle of the Resazurin assay. **(A)** Transformation of blue resazurin into pink resorufin under the mitochondrial metabolic activities (Riss et al, 2016). **(B)** Comparison between the efficiency of MTT and Resazurin assay on assessing cell viability inside of fibrin clot. 5x10³ BXPC3 cells were cultured in each well of the 96-well microplate, in the presence of different concentration of PPP, for 24 hours, before cell viability was measured using either MTT or Resazurin assay. Cell viability was normalized with cell cultured in the absence of PPP.*

Cell viability was studied by adding Resazurin solution to the final concentration of 0.2 mg/ml to each well, followed by incubation for 4 hours at 37°C, and fluorescence measurement at excitation/emission lengths at 530/590 nm.

5.2.1. Cell viability assessment

5.2.1.1. For the hydrogel method

In a control experiment, cancer cells were cultured for 24 hours in the presence of increasing of Fg (1 or 5 mg/ml) or thrombin (2 or 4 IU/ml). Subsequently, cell viability was assessed using

the Resazurin assay. Fluorescent intensity was measured and normalized with cells cultured in normal conditions.

In another experiment, cancer cells were cultured in fibrin hydrogel made from different combinations of thrombin and fibrinogen: 1 mg/ml Fg + 2 UI/ml FIIa; 1 mg/ml Fg + 4 UI/ml FIIa; 5 mg/ml Fg + 2 UI/ml FIIa; 5 mg/ml Fg + 4 UI/ml FIIa. Subsequently, cell viability was assessed using the Resazurin assay. Fluorescent intensity was measured and normalized with cells cultured in normal conditions.

5.2.1.2. For the PPP method

Cells were cultured in culture media supplemented with different concentration of PPP from 0% to 100% for 24 hours. Subsequently, cell viability was assessed using the Resazurin assay. Fluorescent intensity was measured and normalized with cells cultured in the absence of PPP.

5.2.2. Cell proliferation assessment

For control experiment **in the absence of PPP**, cells were seeded at $2x10^3$ cells/well in each well of the 96-wells plate for 24 hours for adherence. Subsequently, conditioned media was replaced with fresh media supplemented with 10% PBS. Resazurin solution was added at either immediately (t0), or after 24, 48, and 72 hours. Fluorescent intensity was measured and normalized with t0.

For cells cultured **in the presence PPP**, cancer cells were seeded at $2x10^3$ cells/well in each well of the 96-wells plate for 24 hours for adherence. Subsequently, conditioned media was replaced with fresh media supplemented with 10% PPP. Resazurin solution was added at either immediately (t0), or after 24, 48, and 72 hours. Fluorescent intensity was measured and normalized with t0.

6. Microscopy analysis of fibrin clot network

6.1. Laser Scanning Confocal Microscopy (LSCM)

6.1.1. In 2D culture

Cells were cultured in a 12-wells plate ($3x10^5$ cells/well), on glass coverslips (Φ 18 mm), for 24 hours. Two protocols were tested, using fluorescent fibrinogen, or immunostaining with an anti-fibrin antibody:

***Table 3**: Protocol for visualization of FCS using LSCM.*

<table>
<tr><th></th><th>Protocol A</th><th>Protocol B</th></tr>
<tr><td>Day 1</td><td colspan="2">Cells were seeded at $3x10^5$ cells/well on glass coverslip, in the 12-wells plate.</td></tr>
<tr><td rowspan="2">Day 2</td><td colspan="2">Nuclei staining with Hoechst 33342 for 20 min, at 37°C.</td></tr>
<tr><td>Conditioned media was replaced with fresh media, supplemented with 10% PPP and 2.5 µg/ml fluorescent Fg.</td><td>Conditioned media was replaced with fresh media, supplemented with 10% PPP.</td></tr>
<tr><td>Day 3</td><td colspan="2">Conditioned media was carefully removed.

Fixation: Fibrin clots were fixed with 4% paraformaldehyde for 20 min at room temperature (RT), then washed for 3 times in PBS.</td></tr>
</table>

	Fibrin clots were mounted on slides, using a mounting media.	**Saturation**: Clots were saturated with 1% Bovine serum albumin (BSA) for 1 hour at RT, in agitation. **Primary antibody**: Clots were incubated with anti-fibrin antibody diluted at 1/300 in 1% BSA, at 4°C, overnight, in agitation.
Day 4	The slides were sealed using nail polish. Fibrin clots were ready for observation.	**Secondary antibody**: Clots were washed 3 times in 1% BSA, then incubated with secondary antibody, diluted at 1/500 in 1% BSA, at RT, for 4 hours, in agitation. After 3 washes with PBS, clots were mounted on slides, using a mounting media.
Day 5		The slides were sealed using nail polish. Fibrin clots were ready for observation.

Images were obtained with FV3000 microscope (Olympus, Tokyo, Japan). Z positions for z-stack imaging were determined manually. Imaris software (version 10.1.0, Oxford Instruments) and Fiji (version 1.54f, NIH, USA) was used for deconvolution, and 3D reconstruction.

6.1.2. In 3D culture

Cancer cells were growth in conventional media. Nuclei were stained using Hoechst 33342 (Thermo Fischer, Massachusetts, USA) before cells were harvested for the formation of spheroids. Spheroids were growth in the ultra-low attachment plate. At 4-days old, 50 µl of the conditioned media was removed from each well and replaced with 50 µl of fresh media supplemented with 20% PPP. The final concentration of PPP in each well was thus 10%. 24 hours after exposition to the PPP-conditioned media, fibrin clot shields with spheroids inside were fixed with 4% of paraformaldehyde for 1 hour at 25°C, on a rotator to ensure deep penetration.

Subsequently, specimens were washed with PBS and blocked with 4% of Bovine Serum Albumin (BSA) for 1 hour at 25°C, on a rotator. Staining solution was prepared, with 4% BSA, 1/200 primary anti-fibrin antibody (MilliporeSigma, Massachusetts, USA), and 1/500 nano-secondary antibody (Proteintech, Illinois, USA). Samples were incubated with the staining solution for 72 hours at 4°C on a rotator.

After the staining, samples were washed with PBS and placed in a chambered glass slide for observation with LSCM.

6.2. Scanning Electron Microscopy (SEM)

Cells were seeded in a 12-wells plate at density of $3x10^5$ cells/well, on glass coverslips (Φ 18 mm), for 24 hours, before replacing their culture media with a media supplemented with 10% PPP. After 24 hours, culture media was carefully removed.

Clots were rinsed with PBS before being immersed overnight at 4°C in a fixative solution of 2% EM-grade glutaraldehyde in 0.1 M cacodylate buffer pH 7.4 (Agar Scientific or Delta Microscopies). The samples were then rinsed with 0.1 M cacodylate buffer. Then, samples were

incubated for 20 minutes in 0.1 M cacodylate buffer containing 1% osmium tetroxide (Delta Microscopies, Mauressac, France), thoroughly rinsed with distilled water, and dehydrated using a graded concentration of ethanol (50% - 70% - 90% - 100%). Samples were immersed in a 1:1 mixture of ethanol and hexamethyldisilazane (HMDS), before pure HMDS, followed by drying in a vacuum desiccator. Finally, samples were mounted on stubs, platinum-sputtered (ACE600, Leica microsystems, Nanterre, France), and inspected with a 3 kV high-resolution Field-Emission SEM (GeminiSEM500, Zeiss, Perigny, France) with a 20 µm objective aperture diameter. Secondary electrons were collected with in-lens or Everhart-Thornley detectors and scan speed and line integration were adjusted during observation.

Fiber diameters, pore sizes and the number of intersections were calculated using the Fiji software (version 1.53t), using the DiameterJ plugin, as described elsewhere (Daraei et al., 2021; Hotaling et al., 2015). Briefly, images obtained from SEM is segmented, then analyzed for structure characterization.

6.2.1. Segmentation

The aim of this step is to separate the objects to be analyzed from the background. To achieve this, the image undergoes a transformation into a binary representation, where white pixels denote the targeted fibers while black pixels indicate the background. This conversion is executed through the application of 24 distinct segmentation algorithms, systematically grouped into three categories: Traditional, Mixed, and Statistical Region Merging methodologies. Consequently, a set of 24 segmented output images is generated from a single input image. The onus lies upon the user to discern and select the optimal segmented image from this array for subsequent analysis.

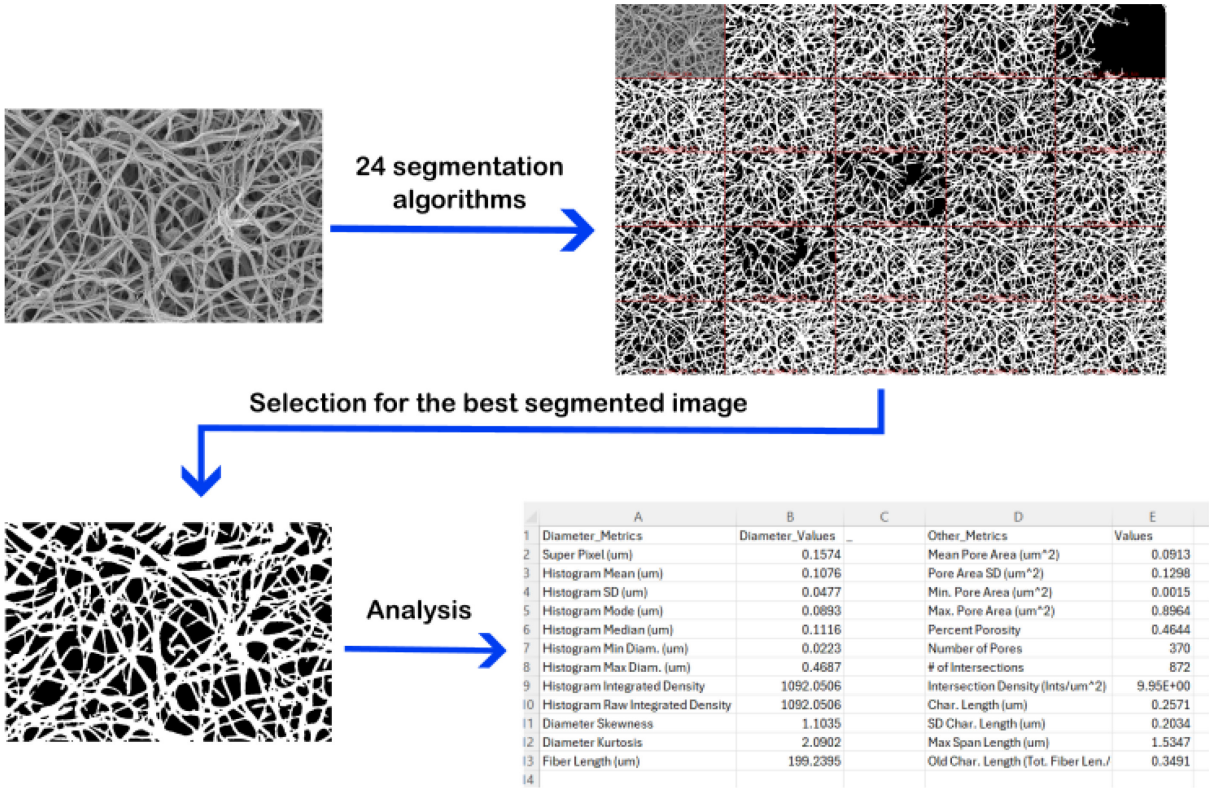

	A	B	C	D	E
1	Diameter_Metrics	Diameter_Values	_	Other_Metrics	Values
2	Super Pixel (um)	0.1574		Mean Pore Area (um^2)	0.0913
3	Histogram Mean (um)	0.1076		Pore Area SD (um^2)	0.1298
4	Histogram SD (um)	0.0477		Min. Pore Area (um^2)	0.0015
5	Histogram Mode (um)	0.0893		Max. Pore Area (um^2)	0.8964
6	Histogram Median (um)	0.1116		Percent Porosity	0.4644
7	Histogram Min Diam. (um)	0.0223		Number of Pores	370
8	Histogram Max Diam. (um)	0.4687		# of Intersections	872
9	Histogram Integrated Density	1092.0506		Intersection Density (Ints/um^2)	9.95E+00
10	Histogram Raw Integrated Density	1092.0506		Char. Length (um)	0.2571
11	Diameter Skewness	1.1035		SD Char. Length (um)	0.2034
12	Diameter Kurtosis	2.0902		Max Span Length (um)	1.5347
13	Fiber Length (um)	199.2395		Old Char. Length (Tot. Fiber Len./	0.3491
14					

***Figure 17** : Pipeline for the analysis of the structure of fibrin network, using Scanning Electron Microscopy image and the DiameterJ plugin.*

Segmentation necessitates rigorous execution to minimize bias, as it can introduce artifacts into the analysis. Notably, in images, fibers and pores located in lower layers may appear smaller due to perspective distortion. To mitigate this distortion, segmentation should exclusively consider fibers present in the topmost layer of the clot.

Daraei et al., in their 2021 study comparing automated analysis utilizing DiameterJ and manual analysis, have underscored the significant impact of pixel size and algorithm selection on the analysis. Pixel size, synonymous with scale in digital image analysis, denotes the actual distance represented by a single pixel. Higher magnification yields smaller pixel sizes, while lower magnification yields larger pixel sizes.

DiameterJ algorithms tend to underestimate diameter values in images with smaller pixel sizes and overestimate diameters in images with larger pixel sizes. Algorithms such as S2, M2, and M1 exhibit optimal performance for datasets with smaller pixels, while algorithms such as M4, S4, S8, and T4 fare better for datasets with larger pixels.

The authors delineated two plausible reasons for this discrepancy:

- Firstly, segmentation algorithms tend to bundle closely positioned fibers into larger fibers, thereby inflating measured fiber diameters, an effect that increases with pixel size.
- Secondly, during image processing with smaller pixel sizes, segmentation algorithms may incorporate deeper fibers within the clot but depict them as thin and incomplete.

In summary, the authors advocated for images with a pixel size of approximately 8 to 10 nanometers (equivalent to a magnification of at least 10,000X) and recommend employing algorithms M1–M3, M5–M7, T1–T3, T5, T6, S1–S3, and S5–S7 for optimal segmentation outcomes.

6.2.2. Analysis

DiameterJ automatically analyzes segmented images, using different algorithms.

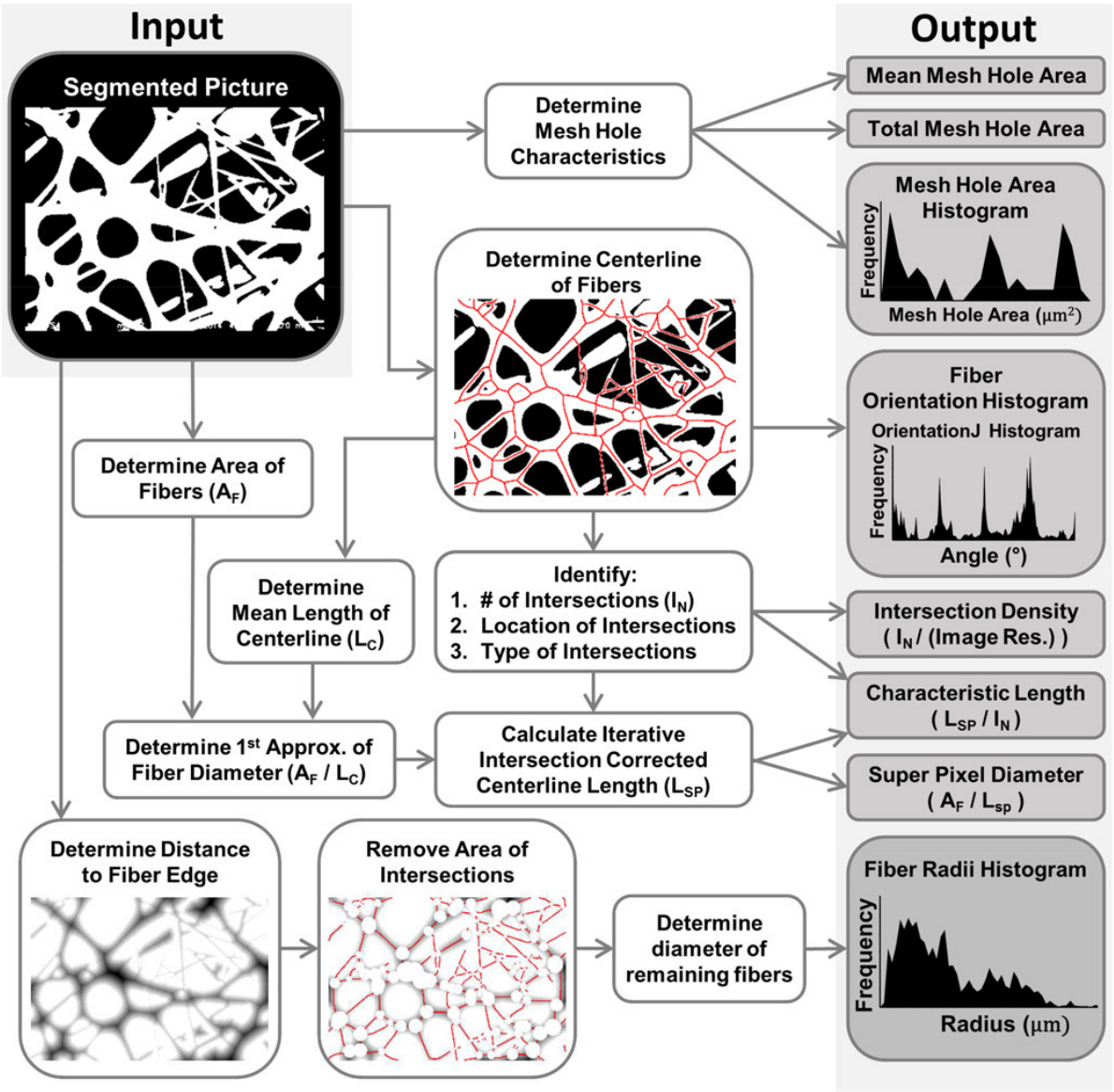

***Figure 18**: Pipeline for analysis of segmented image within DiameterJ (Hotaling et al., 2015).*

While DiameterJ provides an analysis of porosity by computing the ratio of pore area to the total image area, this metric inadequately represents the true porosity of the structure. As elucidated in the Segmentation section, analysis should solely focus on the top layer of the clot, as fibers in deeper layers may appear diminished in size due to perspective effects.

Consequently, the porosity calculated by DiameterJ exclusively pertains to the top layer and overlooks considerations of deeper layers and the thickness of the clot.

Acknowledging the limitations inherent in the plugin, we have opted to confine our analysis to fiber diameter, mean pore area, and the number of intersections. These parameters offer a more comprehensive insight into the structural characteristics of the material.

7. Study of fibrinolysis

Cells were cultured in a 12-well plate ($3x10^5$ cells/well) for 24 hours before replacing the culture media with either PPP-conditioning media or 10% PBS in the conventional conditioning media (control). Cell-free media with 10% of PPP was used as a control. Supernatants were collected at predefined intervals (0, 6, 10, 12, 14, 18, 24, 48, and 72 hours) for D-Dimers and tPA measurement using commercially available ELISA methods (Asserachrom D-Di and Asserachrom tPA from Diagnostica Stago, Asnières, France). The assays were performed according to the manufacturer's instructions. Briefly, 200 µl of the pure supernatant or diluted in diluent buffer were deposited and incubated for 2 hours in each well. After 5 washes, an anti-D-Dimer or anti-tPA antibody coupled to peroxidase was added, followed by another 2-hour incubation. After 5 washes, 3,3',5,5'-tetramethylbenzidine (TMB) was added. The reaction was stopped by the addition of H_2SO_4. The absorbance was measured at 450 nm (Tecan Infinite 200 Pro Spectrophotometer – Microplate reader, Männedorf, Suisse).

8. Fluorescence intensity quantification

Cells were cultured in a 12-wells plate ($3x10^5$ cells/well), on glass coverslips (Φ 18 mm), for 24 hours, then nuclei were marked with Hoechst 33342 (Thermo Fischer, Massachusetts, USA) and culture media was replaced by PPP-conditioning media in the presence or absence of 2.5 µg/ml of Fibrinogen coupled with Alexa Fluor 488 (Thermo Fisher, Massachusetts, USA). After incubation for 24 hours, fibrin clots were removed, and the remaining cells on the coverslip were fixed with 4% paraformaldehyde in PBS, washed 3 times in PBS, and mounted between coverslip and slide.

Images were obtained with a fluorescent microscope (Olympus IX83, Olympus, Tokyo, Japan). Cell Detection plugins in QuPath software (version 0.4.1) was used to isolate each individual cell base on the blue channel. Then the intensity of the green channel was measured and divided by the total number of cells. No threshold nor any contrast/brightness adjustments were conducted.

9. Study of cancer cell migration within the fibrin clot shield

Cancer cell migration in fibrin clot shield was observed in both 2D and 3D culture.

In 2D culture, observation of the surface of the fibrin clot was assessed with SEM. The presence of cancer cells within fluorescent fibrin clot was observed with LCSM. The viability of cells in different locations within the fibrin clot was observed via the presence of formazan crystals using the MTT assay as described above.

In 3D culture, Images of spheroids were taken at 0, 24, 48, and 72 hours after exposition with PPP-conditioned media with a brightfield microscope.

10. Anticancer treatments in the presence or absence of Fibrin Clot Shield

The anticancer effect of paclitaxel and 4-hydroxy-tamoxifen (4OHTam) was studied using the experimental procedure described above for i*n vitro* evaluation of the efficiency of the anticancer agents and in the presence of fibrin clot. In the control experiment, the efficacy of the anticancer agents on cancer cell viability was studied using the conventional experimental procedure (Berthois et al., 1986; Liebmann et al., 1993).

10.1. Conventional model for the evaluation of the efficiency of anticancer agents

Cancer cells were cultured at conditioning media followed by addition of the studied anticancer agents (Liebmann et al., 1993). Herein BXPC3, MDA-MB231 and MCF7 cells were cultured in a 96-wells plate ($3x10^3$ cells/well) for 24 hours in conditioned media (RPMI-1640) to achieve

maximum cell adhesion. Subsequently, the conditioned media was replaced by a new solution of RPMI-1640 with the studied anticancer agents: paclitaxel (Taxol®) from Thermo Fisher (Massachusetts, USA) for the BXPC3, MDA-MB231 and MCF7 cells or 4-hydroxy-tamoxifen (4OHTam) obtained from Selleckchem, (Texas, USA) for the MCF7 at increasing concentrations. In the control experiment, cancer cells were treated with DMSO instead of anticancer agents. The concentration of the anticancer agents that reduced the viability of cancer cells by 50% (IC50) as compared to the control condition (witout any addition of anticancer agents) was calculated after exposure for 72h.

10.2. Fibrin clot shield model for the evaluation of the efficiency of anticancer agents

BXPC3, MDA-MB231 and MCF7 cells were cultured in a 96-wells plate ($3x10^3$ cells/well) for 24 hours in conventional conditioned media (RPMI-1640) in order to achieve maximum cell adhesion. Subsequently, the conventional conditioned media was replaced by PPP-conditioned media (50 µL) and clot formation was formed. In 2h, or 24h, after the addition of the PPP-conditioned media and following visual confirmation of clot formation, 50 µL of PPP-conditioned media containing the studied anticancer agents at the IC50 final concentration (calculated for the total volume of the PPP-conditioned media). In the control experiment, cancer cells were treated with DMSO instead of the anticancer agents. The cell viability was measured after 72h of exposure to anticancer the agents and compared to the control condition.

11. Statistical analysis

Statistical analysis was conducted using GraphPad Prism (version 9.5.1, GraphPad Software Inc, California, USA). Data were first verified for normal distribution. In case of normal distribution, parametric ANOVA test was used. Non-parametric Kruskal-Wallis test, followed by a post-hoc study, was used in case of non-normal distribution. The threshold for statistical significance is 0.05.

RESULTS

1. Set-up and validation of experimental system for the study of the formation and structure of fibrin clot network induced by cancer cells

1.1. Impact of fibrin hydrogel on cancer cells' viability

We examined four combinations comprising two different concentrations of thrombin (2 UI/ml and 4 UI/ml) and two concentrations of fibrinogen (1 mg/ml and 5 mg/ml) to assess their impact on BXPC3 cell viability.

After 24h, the exposure of BXPC3 cells to 1 mg/ml or 5 mg/ml fibrinogen resulted to 40% and 60% cell death, respectively. The exposure of BXPC3 cells to thrombin (2 UI/ml or 4 UI/ml) did not significantly impact cell viability (***Figure* 19A**).

After 24 hours of clot formation, cell viability was evaluated and compared to cells grown without fibrin hydrogel. Maintaining fibrinogen concentration constant, increasing thrombin concentration resulted in enhanced cell viability. Cells cultured in hydrogels composed of 5 mg/ml fibrinogen and thrombin 2 UI/ml or fibrinogen 5 mg/ml and thrombin 4 UI/ml exhibited approximately 60% and 50% loss in viability, respectively. Conversely, the hydrogel consisting of fibrinogen 1 mg/ml fibrinogen and thrombin 4 UI/ml thrombin increased cell viability by approximately 40%. Cells cultured in fibrinogen 1 mg/ml and thrombin 2 UI/ml hydrogel retained viability at levels similar to cells cultured without fibrin (***Figure* 19B**).

1.2. Impact of PPP on cell viability and proliferation

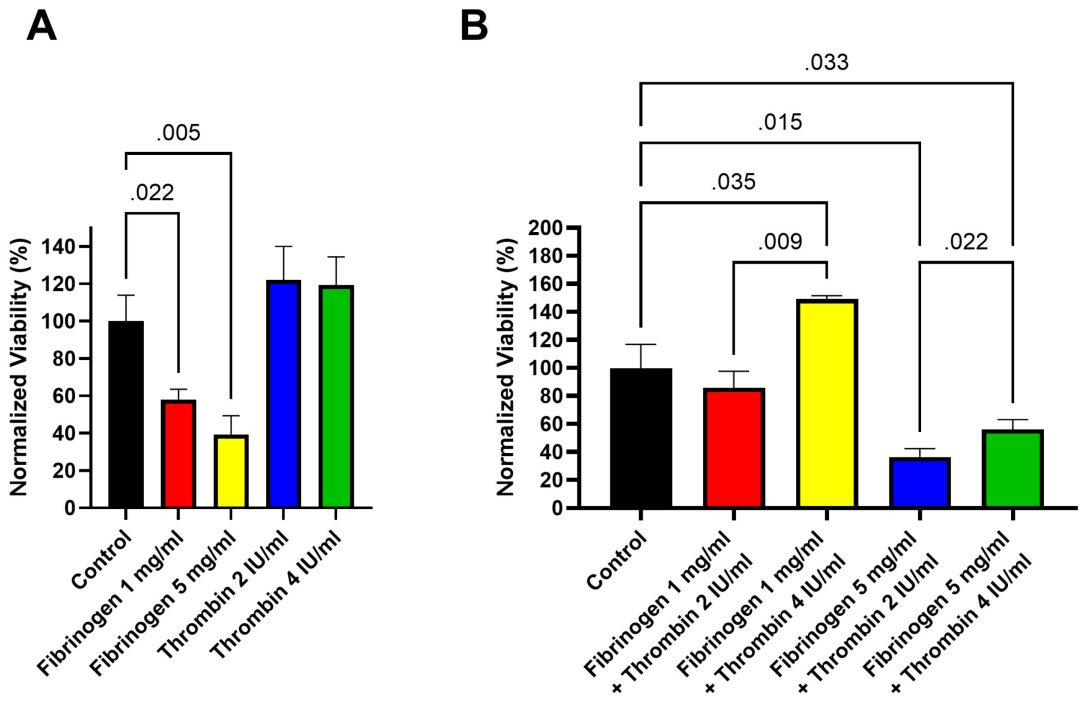

***Figure 19**: Optimization of the culture of BXPC3 cells in fibrin hydrogel. Data represented as Mean ± SD of 3 independent experiments. (A): Impact of fibrinogen (Fg) and thrombin (FIIa) on the viability of BXPC3 cells after 24 hours of exposure. (B): Viabilities of BXPC3 cells in the absence (Control), and presence of fibrin hydrogel made from different combinations of Fg and FIIa.*

Cancer cell lines BXPC3, MDA-MB231, and MCF7 were cultured with PPP at varying concentrations in the conditioning media (RMPI-1640), and respective viabilities were assessed after 24 hours of exposure. As anticipated, increasing PPP concentrations resulted in decreased cell viability (***Figure* 20**). However, at the dilution of 10% PPP, all three cell lines exhibited acceptable viability.

Regarding proliferation, MDA-MB231 cells showed the same proliferation rate in the presence of 10% PPP as compared to in the absence of PPP (***Figure* 20C**). BXPC3 cells have the same proliferation rate for the first 48 hours (***Figure* 20B**). From 48 to 72 hours, BXPC3 showed higher proliferation rate in 10% PPP as compared to in the absence of PPP. MCF7 cells have a

slower proliferation rate in the first 48 hours. From 48 to 72 hours, the proliferation rate was similar to cells cultured in the absence of PPP (***Figure*** **20D**).

The 10% concentration of PPP in the conditioned media (PPP-conditioned media) was selected for further experiments since it warranted the viability of cancer cells.

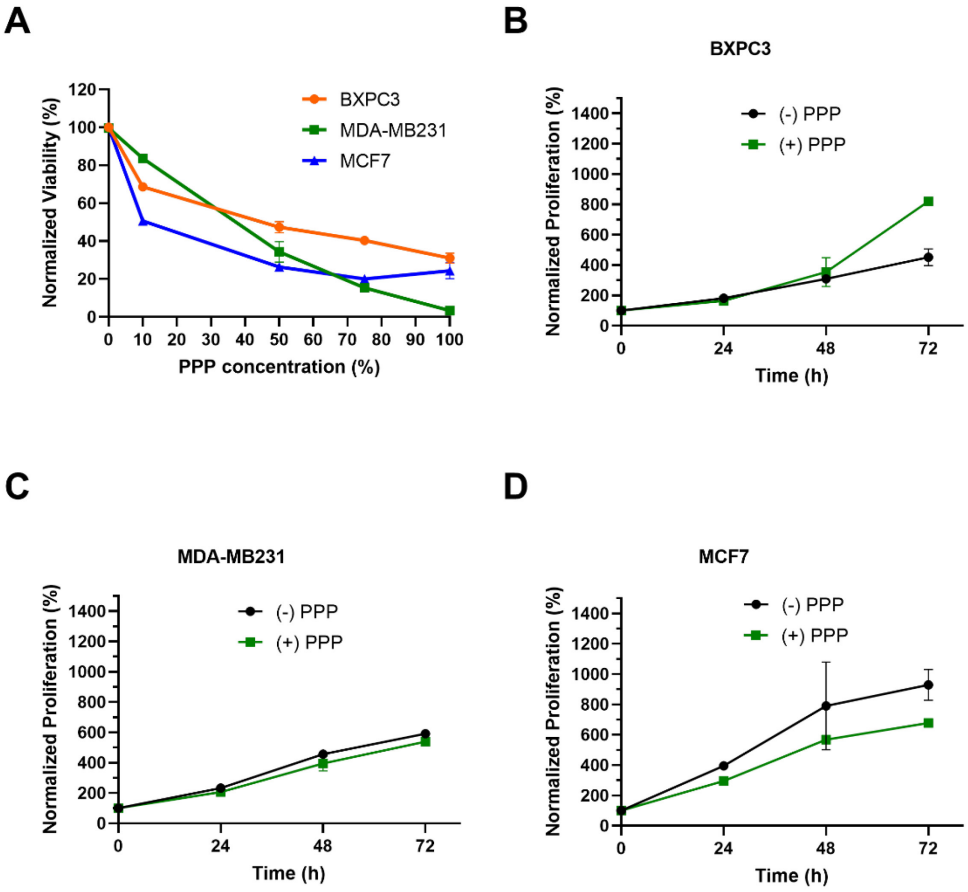

***Figure 20**: Cancer cell viability and proliferation in the presence of PPP. Data represented as Mean ± SD of 3 independent experiments. **(A)**: Cancer cells viability in different dilutions of PPP in culture media after 24 hours of exposure, normalized with cell viability in the absence of PPP. **(B)**: Proliferation of BXPC3 cells in the presence and absence of 10% PPP within 72 hours of exposure, normalized with cell viability at the time of PPP addition. **(C)**: Proliferation of MDA-MB231 cells in the presence and absence of 10% PPP within 72 hours, normalized with cell viability at the time of PPP addition. **(D):** Proliferation of MCF7 cells in the presence and absence of 10% PPP within 72 hours, normalized with cell viability at the time of PPP addition.*

1.3. Thrombin generation trigger by TF in PPP-conditioned media

Thrombin generation in 10% PPP, employing various concentrations of Tissue Factor (TF), was investigated. In the absence of additional TF, no thrombin generation activity was detected in the RPMI-1640 culture media supplemented with 10% PPP (**Figure 21A**).

Thrombin generation increased as TF concentrations raised from 0.5 pM to 3 pM. Between 3 pM and 4 pM TF, thrombin generation peaked, subsequently decreased as TF concentration reached 5 pM. While the lag time continued to decrease with increasing TF concentration (**Figure 21B**), Endogenous Thrombin Potential (ETP) and Peak values reached their maximum at 4 pM TF, declining thereafter at 5 pM of TF (**Figure 21C, D**).

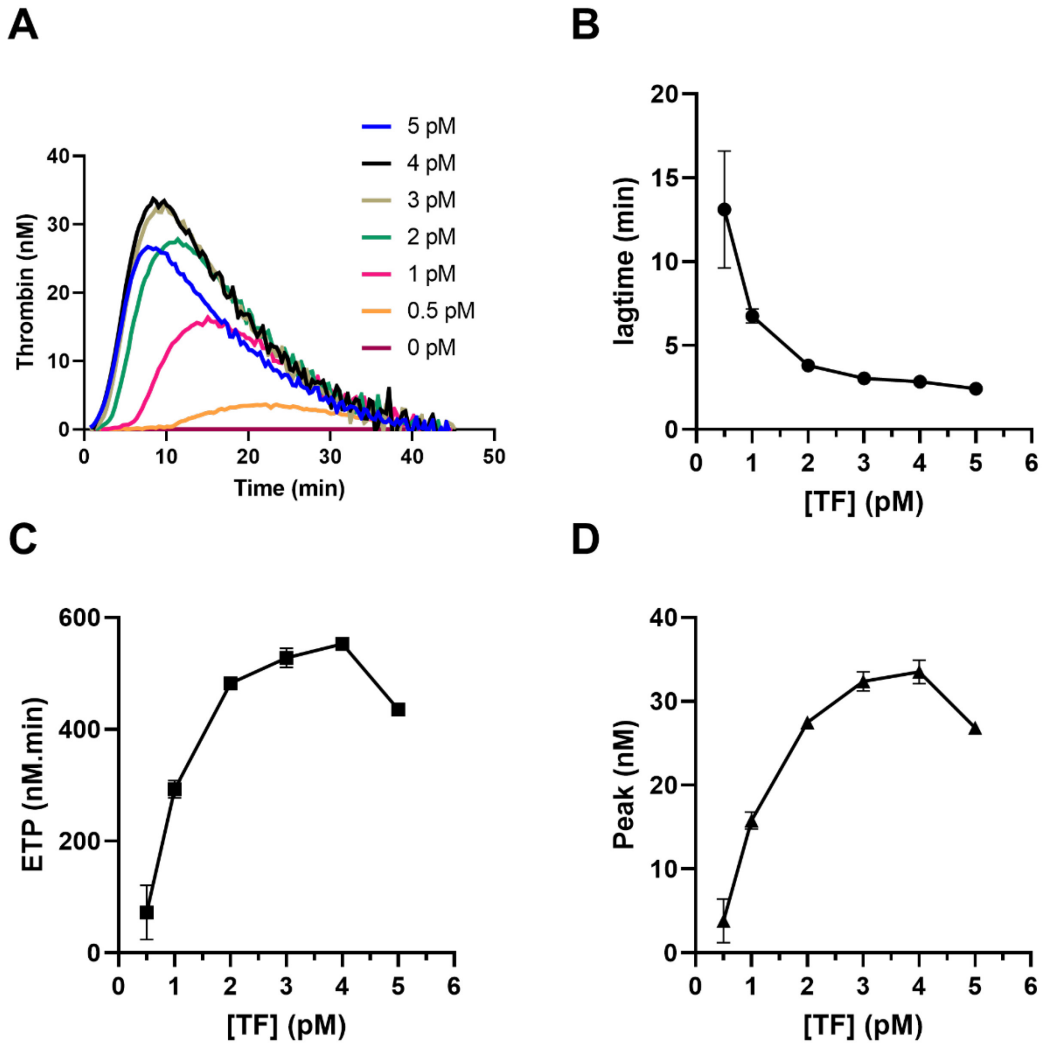

***Figure 21**: Thrombin generation in 10% of normal Platelet Poor Plasma (PPP) diluted in culture media, triggered by increasing concentrations of Tissue Factor (TF). **(A)**: Thrombin generation in 10% PPP diluted in the RPMI-1640 media. Data represented as Mean curve of 3 independent experiments. **(B)**: Lag time of thrombin generation in 10% PPP diluted in the RPMI-1640 media. **(C)**: Endogenous Thrombin Potential (ETP) of thrombin generation in 10% PPP diluted in the RPMI-1640 media. **(D)**: Peak of thrombin generation in 10% PPP diluted in the RPMI-1640 media.*

1.4. Thrombin generation triggered by cancer cells in 10% of PPP

The ability of cancer cells to induce thrombin generation in PPP-conditioned media was investigated.

MDA-MB231 cells could be cultured in various media, including L-15, DMEM, or RPMI-1640. The manufacturer (Gibco) specifies that the Ca^{2+} concentration is 0.4 mM in RPMI-1640 and 1.8 mM in DMEM. Given Ca^{2+} concentration influences thrombin generation in pure PPP, its impact in 10% PPP was examined. Thrombin generation induced by MDA-MB231 in 10% PPP diluted in RPMI-1640 and DMEM media was studied. In RPMI-1640 media, MDA-MB231 cells exhibited longer lag time and higher ETP and Peak compared to DMEM (***Figure* 22A-D**). As BXPC3 and MCF7 cells were cultured in RPMI-1640, it was chosen for MDA-MB231 to enable comparison across the three cell lines.

Thrombin generation in the presence of BXPC3, MDA-MB231, or MCF7 cells in PPP-conditioned media was analyzed. In the control experiment (recalcification of PPP-conditioned media in the absence of cancer cells), no detectable thrombin generation was observed (***Figure* 22E**). The presence of cancer cells led to significant thrombin generation compared to the control. The BXPC3 and MDA-MB231 cells had a similar effect on thrombin generation at the same cell number. Conversely, with an equivalent number of MCF7 cells, the lag time was 3.5 times longer, and the ETP and Peak were 80% lower compared to BXPC3 cells (***Figure* 22E**). In the experiment with the MCF7 cells, the addition of exogenous TF (1 pM) amplified thrombin generation at levels similar to those observed in the presence of BXPC3 cells.

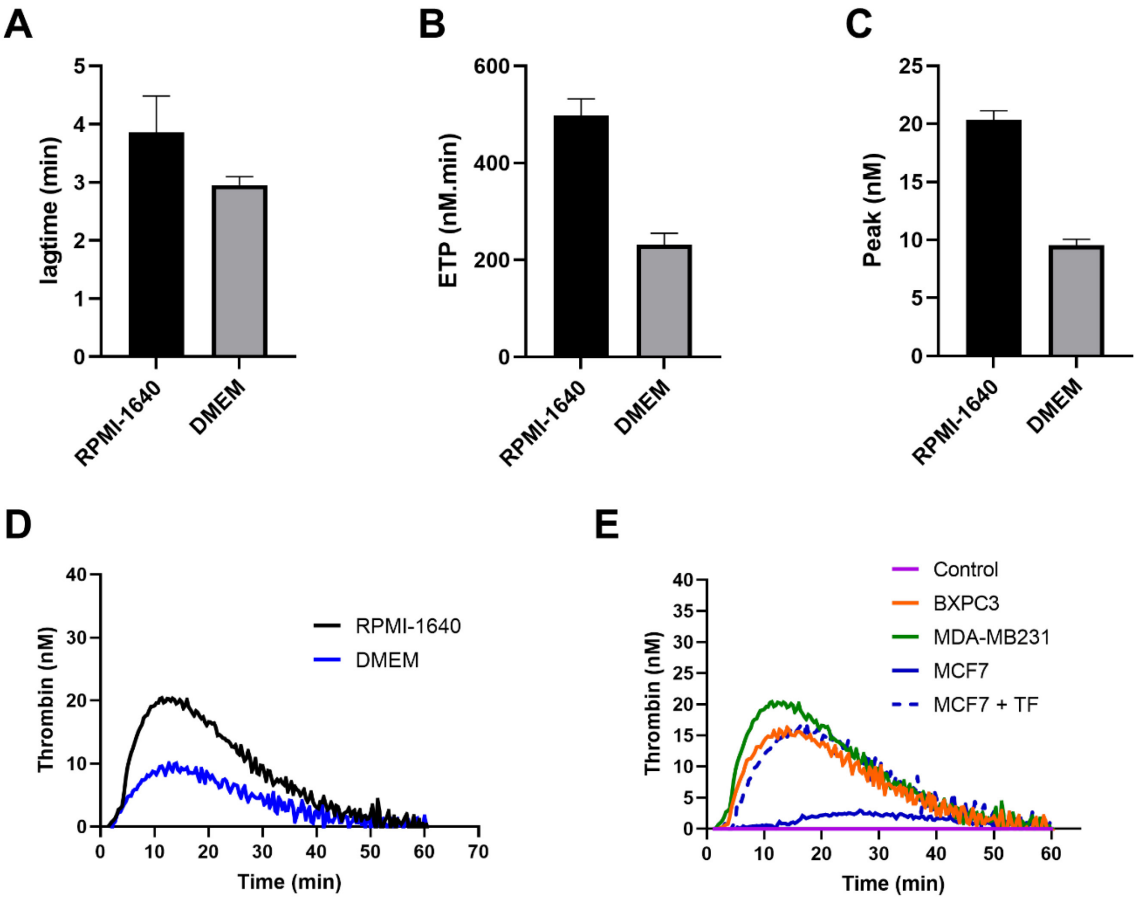

***Figure 22**: Thrombin generation by cancer cells in the presence of PPP-conditioned media **(A-D)**: Comparison of thrombin generation potency of MDA-MB231 in 10% PPP diluted in different media, RPMI-1640 and DMEM. **(A)**: Lag times of thrombin generation by MDA-MB231 cells in 10% of PPP in RPMI-1640 media as compared to in DMEM media. **(B)**: ETP of thrombin generation by MDA-MB231 cells in 10% of PPP in RPMI-1640 media as compared to in DMEM media. **(C)**: Peak of thrombin generation by MDA-MB231 cells in 10% of PPP in RPMI-1640 media as compared to in DMEM media. **(D)**: Thrombin generation by MDA-MB231 cells in 10% of PPP in RPMI-1640 media as compared to in DMEM media. **(E)**: Thrombin generation by BXPC3, MCF7, MCF7 cells in the presence of 1 pM TF, and MDA-MB231 cells in 10% of PPP in RPMI-1640 media, as compared to the Control experiment (in the absence of cancer cells).*

1.5. Fibrin formation in PPP-conditioned media

Given that the three studied cell lines demonstrate both viability and the ability to induce thrombin generation in 10% PPP in RPMI-1640 media, this condition was selected to attempt fibrin clot formation.

Cancer cells were seeded, and fibrin formation was initiated according to the procedures described in the Materials and Methods section. Two hours after exposure to PPP-conditioned media, cancer cells successfully induced the formation of a robust fibrin clot. Cells were seeded on glass coverslips to facilitate harvesting with forceps (**Figure 23**).

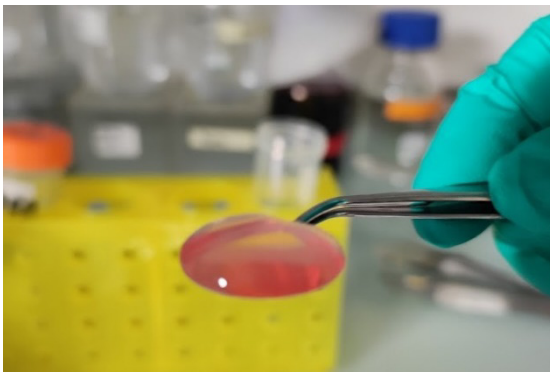

***Figure 23**: Fibrin clot formed by MDA-MB231 cells after 2 hours.*

1.6. Structural characteristics of fibrin clot shield – Impacts of TF and cancer cells

Fibrin clot shields' structure was observed and analyzed using SEM. Increase of TF concentrations in PPP-conditioned media resulted in decrease of fiber diameters (0.104 ± 0.007 µm, 0.094 ± 0.003 µm and 0.091 ± 0.001 µm for 0.5, 1 and 2 pM of TF respectively) and pore size (0.093 ± 0.005 μm^2, 0.075 ± 0.003 μm^2, and 0.067 ± 0.001 μm^2 for 0.5, 1 and 2 pM of TF respectively). On the other hand, the augmentation of TF concentrations resulted in increase of the number of intersections: 918 ± 76 in the presence of 0.5 pM TF, 1173 ± 52 in 1 pM TF and 1356 ± 24 intersections in 2 pM of TF. For each parameter of fibrin clot produced in the presence of 2 pM TF the difference was significant ($p<0.05$) as compared to the corresponding

of the clot produced in the presence of 0.5 pM. Detailed comparisons are depicted in **Figure 24A, C-E.**

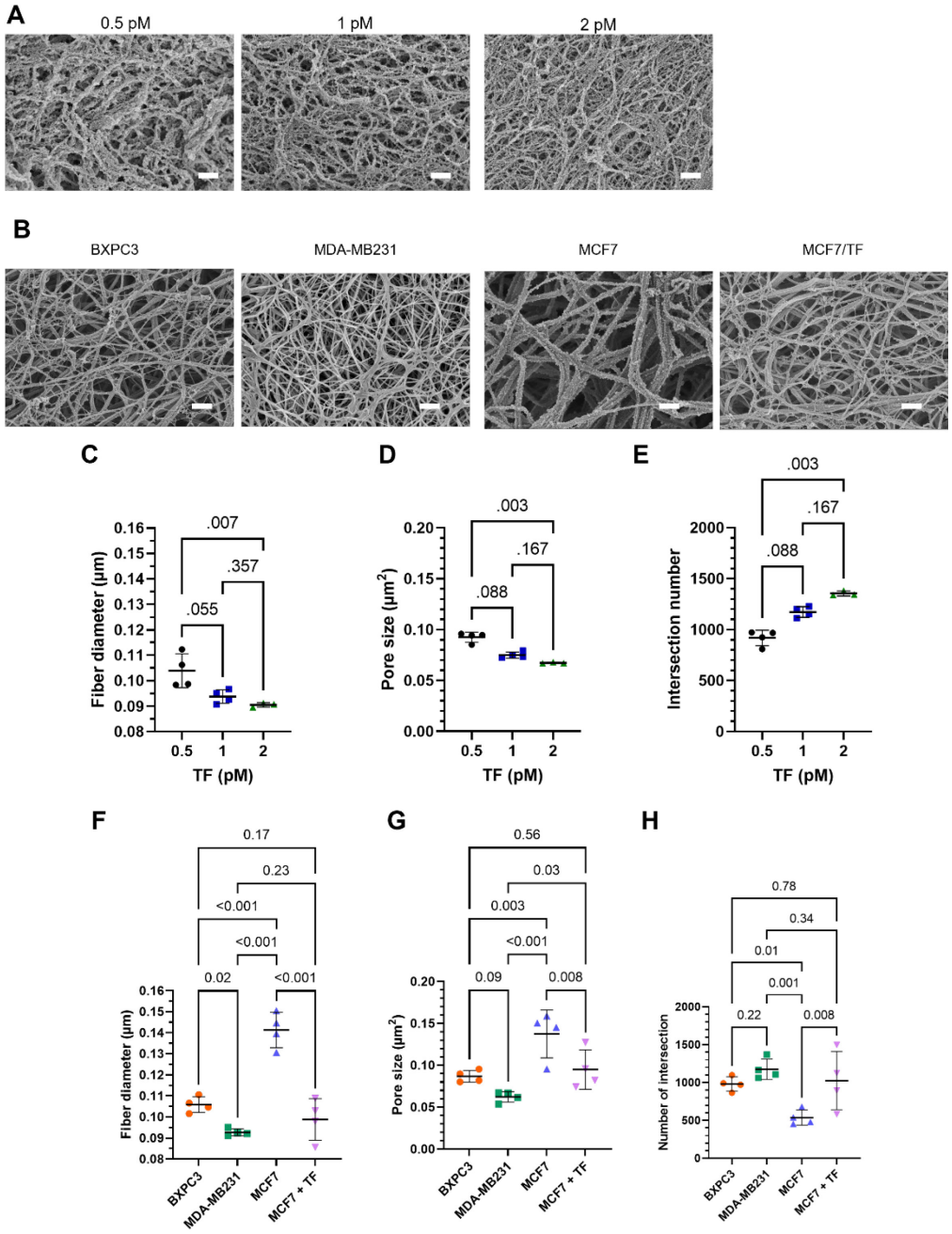

***Figure 24**: Impact of TF and cancer cells on the structure of fibrin clot in PPP-conditioned media (PPP diluted 10% in RPMI-1640). **(A)**: SEM images of the fibrin network formed 2 hours after triggering coagulation with various concentrations of TF. **(B)**: Images of SEM of the network formed after clotting in PPP-conditioned media in the presence of cancer cells (BXPC3, MDA-MB231, MCF7) or MCF7 + 1 pM TF. **(C - H)**: Analysis of the structure of fibrin network using images obtained from SEM. Each data point represents the mean value of an independent experiment. Scale bars: 1 µm. Bars represent Mean ± SD. SEM: scanning electron microscopy. SD: standard deviation.*

The structural characteristics of the fibrin network varied among the three studied cancer cell lines (**Figure 24B, F-H**).

The fiber diameters of clots formed by MDA-MB231 cells were significantly smaller than those formed by BXPC3 or MCF7 cells [0.093 ± 0.002 µm versus 0.106 ± 0.004 µm ($p = 0.02$) and 0.141 ± 0.008 µm ($p < 0.001$) respectively]. The fibers of fibrin clot formed by MCF7 cells had a significantly larger diameter than those formed by BXPC3 cells ($p < 0.001$) (**Figure 24F**).

The pore sizes of clots formed in the presence of MDA-MB231 cells (0.062 ± 0.006 μm^2) were significantly smaller than those formed in the presence of MCF7 cells (0.138 ± 0.029 μm^2, $p< 0.001$), but not to those of BXPC3 cells (0.087 ± 0.007 μm^2, $p = 0.09$). Clots formed in the presence of MCF7 cells showed a significantly larger pore size compared to those formed in the presence of BXPC3 or MDA-MB231 cells ($p = 0.003$ and $p< 0.001$ respectively) (**Figure 24G**).

The number of fibrin fiber intersections was significantly lower in clots formed in the presence of MCF7 cells (539 ± 101) compared to those formed in the presence of MDA-MB231 or BXPC3 cells (1177 ± 135 and 982 ± 96, $p = 0.001$ and $p = 0.01$ respectively). There was no significant difference in the number of fibrin intersections between clots formed in the presence of BXPC3 cells and MDA-MB231 cells ($p = 0.22$) (**Figure 24H**).

The addition of 1 pM TF into MCF7 PPP-conditioned media led to the formation of clots that were similar to those formed in the presence of BXPC3 cells, in terms of fiber diameters (0.099 ± 0.010 µm versus 0.106 ± 0.004 µm respectively, $p = 0.17$), pore sizes (0.095 ± 0.023 μm^2 versus 0.087 ± 0.007 μm^2 respectively, $p = 0.56$) and the number of intersections (1026 ± 385 versus 982 ± 96 respectively, $p = 0.78$) (**Figure 24F-H**).

1.7. Observation of fibrin network using LSCM

Two methods for visualization by LSCM of fibrin clot was tested: by using fluorescent fibrinogen (Protocol A), or by using anti-fibrin antibody (Protocol B). Both methods yield good results, as the clots were observed with fibrous structure (**Figure 25**).

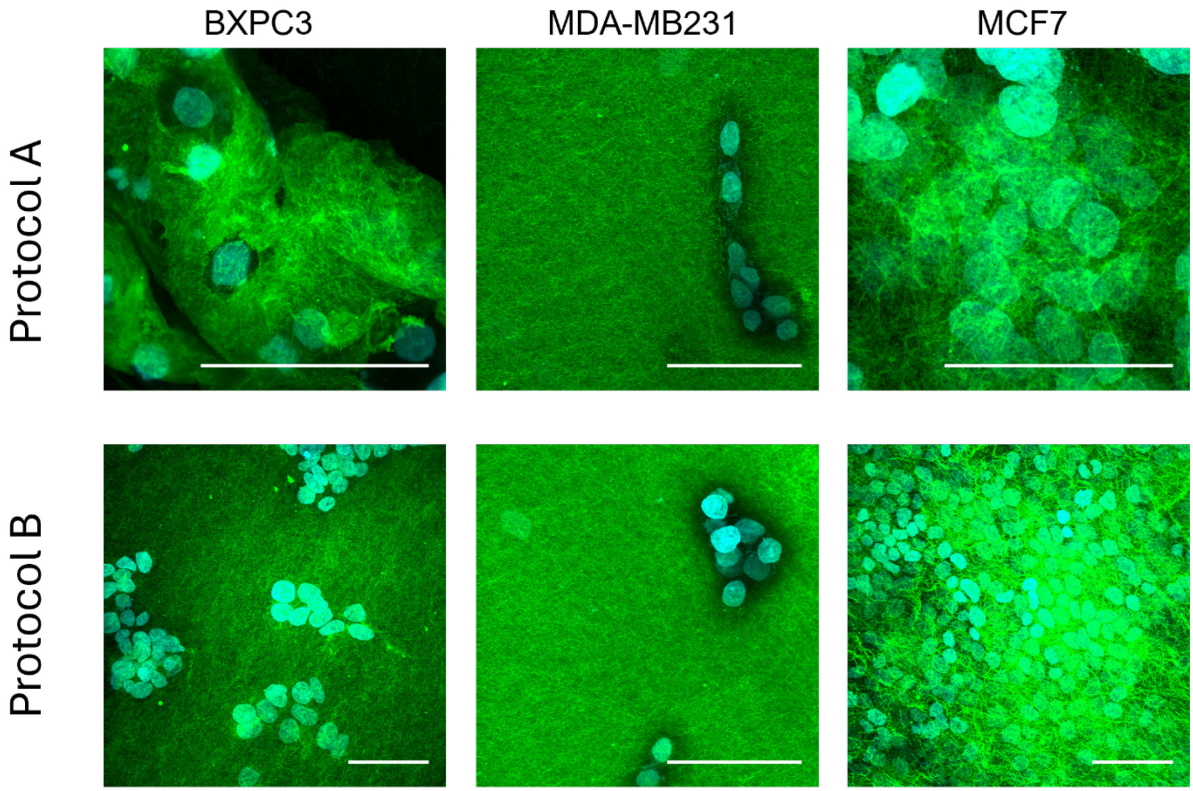

***Figure 25**: Images of fibrin clots formed by cancer cells in 10% PPP using fluorescent Fg (Protocol A), and anti-fibrin antibody (Protocol B). Nuclei are in cyan, and fibrin in green. Scale bars represented 50 µm.*

1.8. Application 3D culture

Efforts were made to encapsulate cancer spheroids in fibrin hydrogel, but due to the low expression of adhesion proteins like E-cadherin in MDA-MB231 cells, their spheroids proved exceedingly fragile and prone to disintegration during transfer. Conversely, attempts with BXPC3 and MCF7 cells yielded successful encapsulation (**Figure 26**).

Efforts were made to encapsulate cancer spheroids in fibrin using the PPP method. Through this approach, we successfully formed a fibrin network surrounding our cancer spheroids (**Figure 26**).

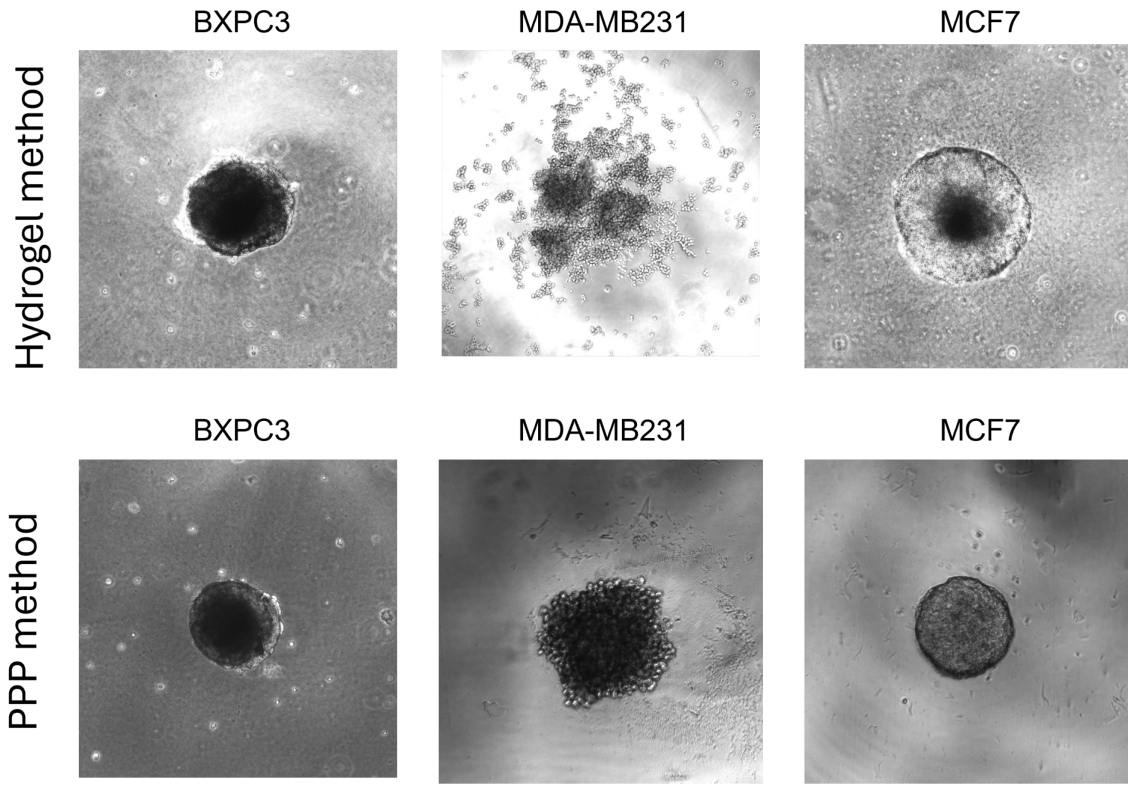

Figure 26: Cancer spheroids in fibrin.

2. Fibrin clot shield in the tumoral microenvironment

2.1. Cancer cell mobility into the fibrin clot

In the beginning of the experiment cancer cells formed an adhesive monolayer at the bottom of the well. After clot formation, the observation by SEM showed of clusters of cells on the top layer of fibrin clots (**Figure 27C**).

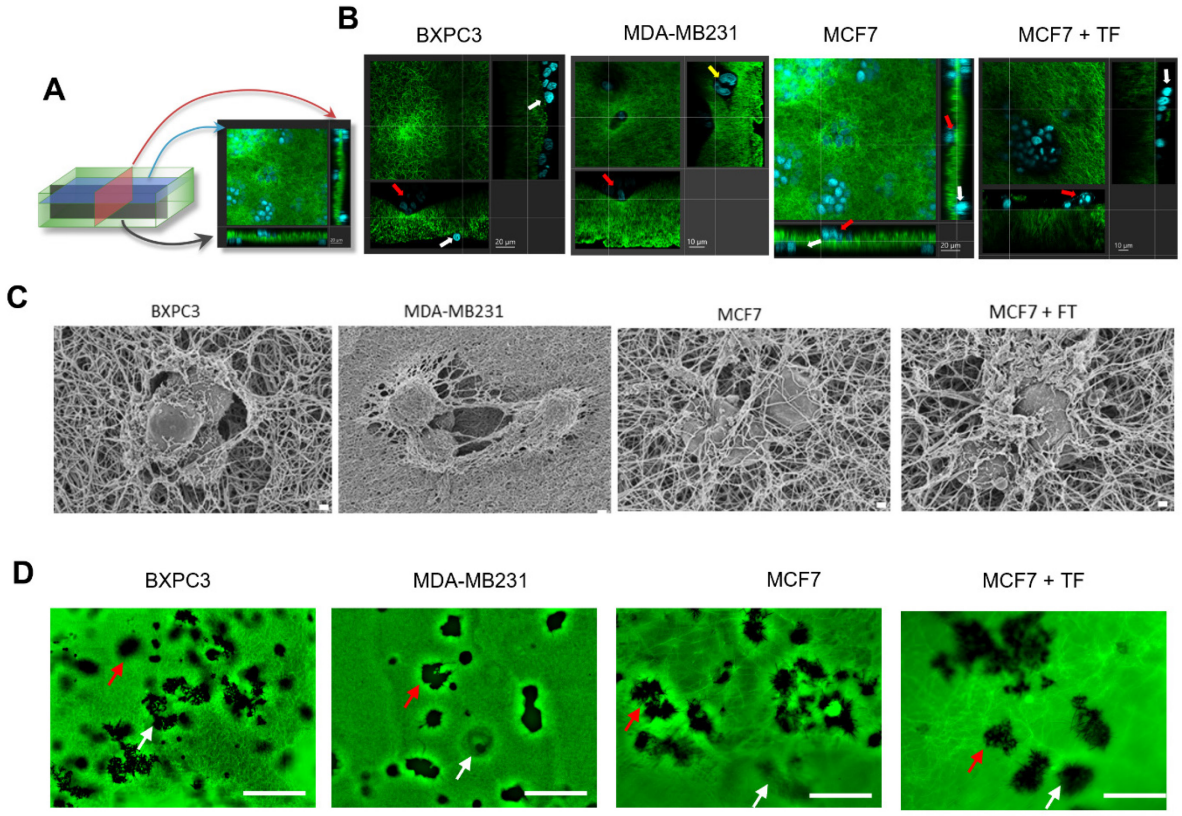

***Figure 27**: Migration into fibrin clot of cancer cells from bottom to top layers. **(A)**: Schema of orthogonal slides. **(B)**: Orthogonal slides of fibrin clot formed from different cell lines. Cyan: nuclei. Green: Fibrin. White arrows: cells at bottom layer. Red arrows: cells at op layer. Yellow arrows: cells in the middle. **(C)**: Cancer cells found on the top layer of the fibrin clot network. Scale bars: 2 µm. **(D)**: Formazan crystals formed by cells in the bottom (white arrows) and top (red arrows) of fibrin clots. Scale bars: 50 µm. Images are representative of 4 independent experiments.*

Clot observation under Laser Scanning Confocal Microscopy (LSCM) revealed the presence of BXPC3, MDA-MB231, or MCF7 cells at the bottom, inside, and on top of the fibrin clot (**Figure 27B**).

Afterwards we confirmed the vitality of these cells and ruled out the possibility that they were dead cells detached from the culture plate and subsequently been trapped within the fibrin clot. The viability of cells located at the top and at the bottom layers of the clot, was assessed with the MTT assay. These cells maintained their metabolic activities as documented by the ability to induce the formation of formazan crystals (**Figure 27D**). Additionally, the absence of condensed or fragmented DNA in the nuclei (**Figure 27B**), the intactness of the cell membranes, and the maintenance of cell-cell adhesion (**Figure 27C**), further substantiated that cells at all levels of the clot were alive.

2.2. 3D spheroid cultures: Cancer cell invasion into fibrin clot

At 72 hours after clot formation, the invasion of BXPC3, MDA-MB231, and MCF7 cells within the fibrin network was confirmed by the observation with phase-contrast microscopy of 3D spheroids (**Figure 28**). In the control experiment performed in 3D cultures in conventional media (absence of PPP), cancer spheroids exhibited a symmetrical increase in size while they conserved the spherical shape. The shape of the 3D cultures of cancer cells was different in the PPP-conditioned media. The BXPC3 and MCF7 3D cultures showed and asymmetric expansion. In distinct regions of the initial spheroid cultures of BXPC3 and MCF7 cells, budding appeared indicating a pattern of collective invasion of the cells. The addition of exogenous TF enhanced the invasion of MCF7 cells within the fibrin network.

In, 3D cultures of MDA-MB231, single cells were identified along the fibrin fibers indicating a cell invasion that followed an individual pattern.

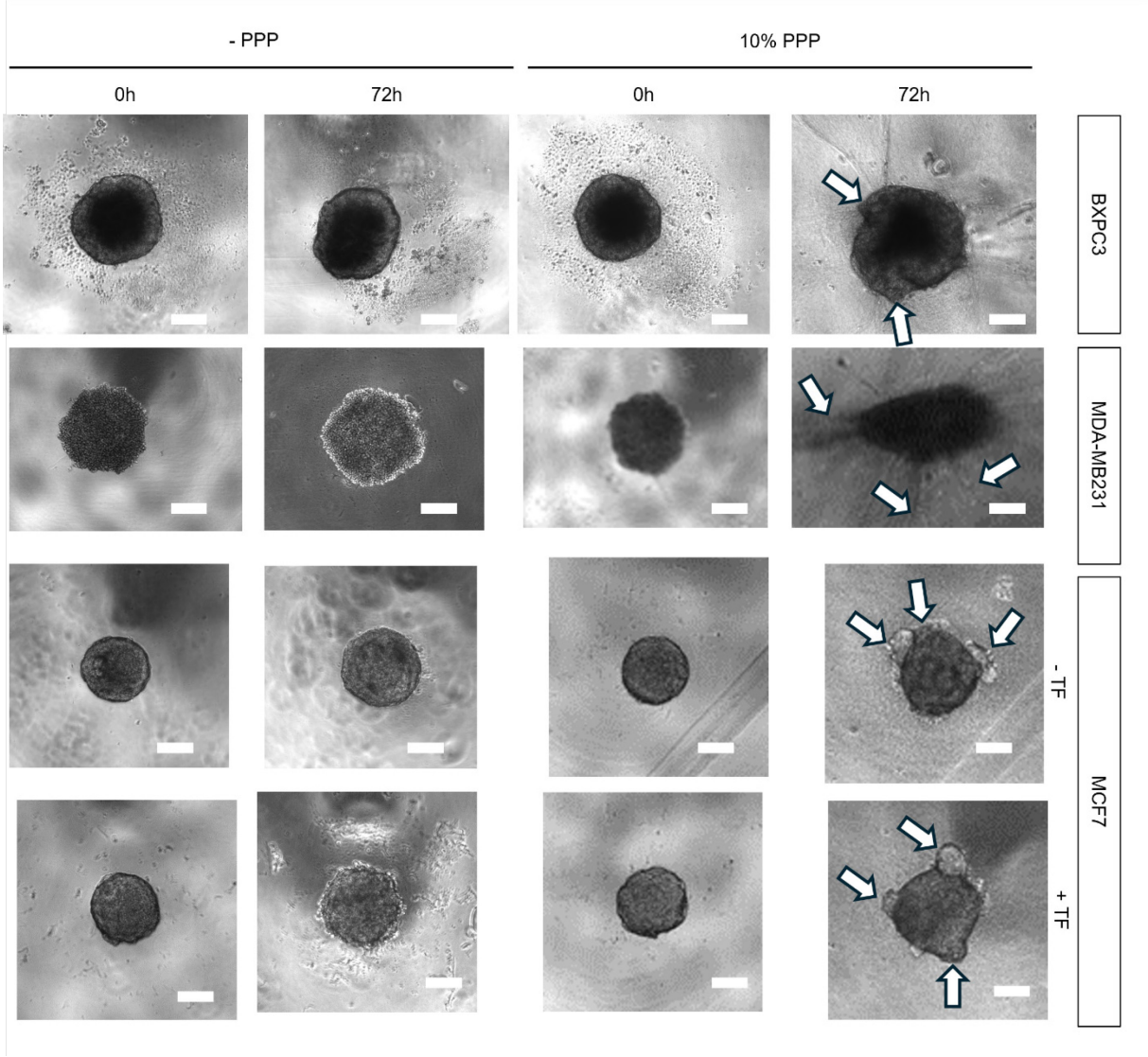

***Figure 28**: Invasion of BXPC3, MDA-MB231, and MCF7 from 3D from spheroid cultures towards the fibrin network. Images were taken at the beginning of the experiment (t0) and 72h after triggering coagulation in PPP-conditioned media and were compared with images taken in 3D cultures in conventional conditioned media. Arrows indicate the invasion regions. Scale bars represent 200 µm. Images are representative of 4 independent experiments. - TF: no exogenous addition of TF.*

+ TF: exogenous addition of TF (1 pM).

2.3. Presence of fibrin on the membrane of cancer cells

Fluorescence microscopy revealed the presence of fibrin fibers bound at the extracellular layer of the cancer cell membranes (**Figure 29**).

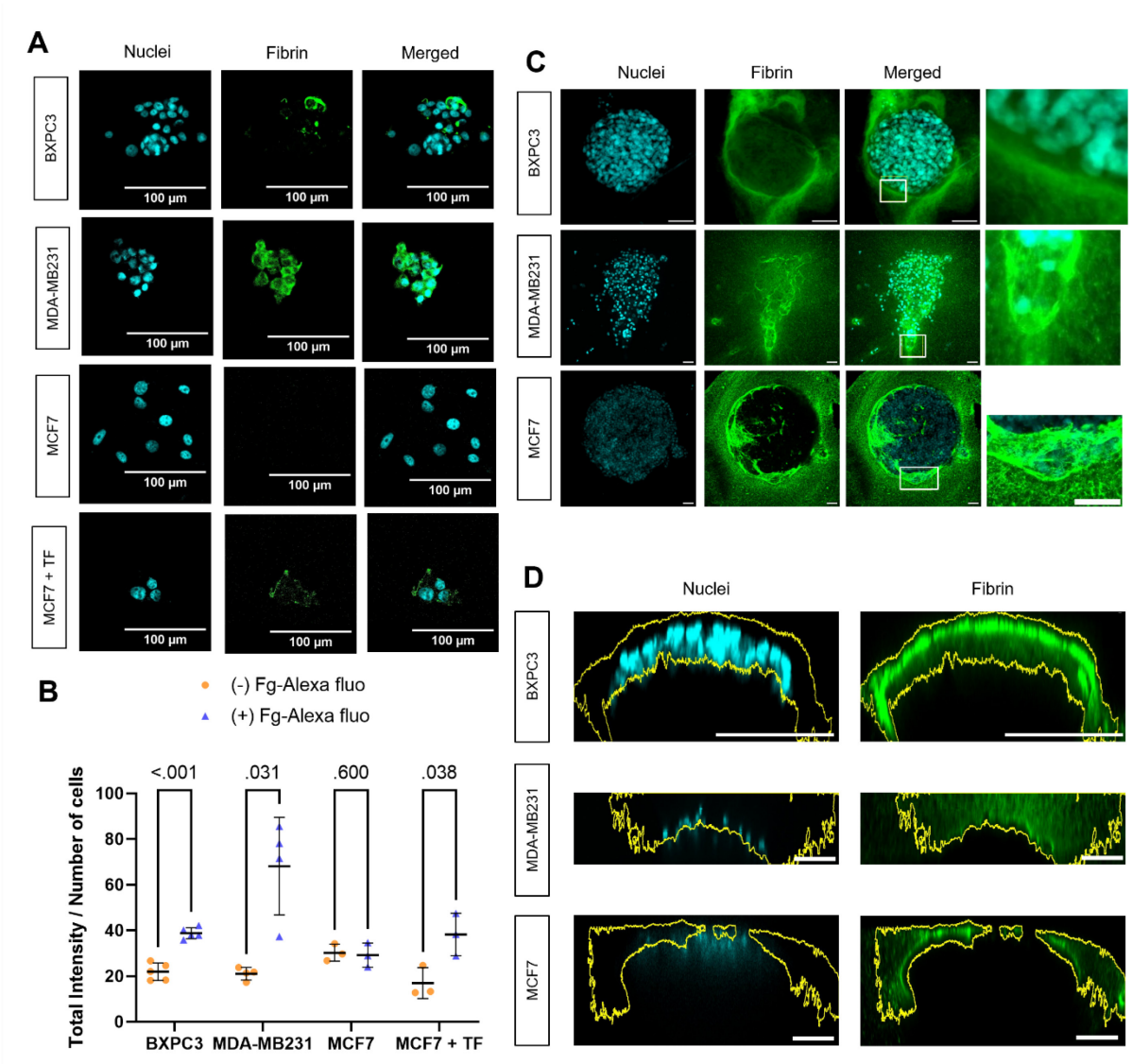

***Figure 29**: Fibrin deposit on cancer cell membrane. **(A)**: Detection of fibrin deposit on the cell membrane after 24h of culture in the PPP-conditioned media, using 2.5 µg/ml of Fibrinogen coupled with Alexa Fluor 488 (in green). Nuclei were marked with Hoechst 33442 (in cyan). Scale bar represents 50 µm. **(B)**: Fibrin deposit on cell membrane after 24h was quantified by fluorescence intensity. The total fluorescence intensity of the green channel was normalized to the total number of cells. Each data point represents the mean value of each field from three independent experiments. Bars are Mean ± SD). **(C)**: Detection of fibrin fibers on cell membrane in cancer cell spheroids, using anti-fibrin antibody. Scale bars represent 50 µm. **(D)**: Transversal slides of cancer cells spheroids. Yellow lines represent regions where fibrin was detected. Scale bars represent 100 µm.*

In the 2D-culture model using fluorescent fibrinogen, the superposition of green and cyan channels demonstrated that fibrin was located at the extracellular layer of the cell membrane (**Figure 29A**). Quantification of the fluorescence intensity at the extracellular layer of cell membrane after careful removal of the clot confirmed that thrombin generation induced by BXPC3 or MDA-MB231 cells leaded to fibrin deposition on the cell membrane. No signs of fibrin deposition were found in the experiment with MCF7 cells in the 2D-culture model, using fluorescent fibrinogen (**Figure 29B**). The exogenous addition of TF induced detectable fibrin deposition on the extracellular layer of the cytoplasmic membrane of MCF7 cells.

An attempt to confirm that the fluorescent signal observed was fibrin and not its degradation products using an anti-fibrin antibody was made, however, due the low adherence of cells on glass coverslips, most of the cells were eliminated after many of washing steps in the immunofluorescence procedure.

The presence of fibrin on the cell membrane was further confirmed by immunofluorescence observation in 3D cultures, using a specific anti-fibrin antibody that specifically recognized fibrin. Transversal slides showed that exclusively the cells located on the outer layer of the spheroids formed by the MCF7 or MDA-MB231 interacted with fibrin (**Figure 29D**). In contrast, this type of interaction was found on cells located at both the outer and inner layers of BXPC3 spheroids (**Figure 29D**).

2.4. Profibrinolytic signature of cancer cells and kinetics of fibrin clot lysis

In the control experiment (cells cultured in conditioned media without PPP), a progressive release of tPA was observed with BXPC3 or MDA-MB231 cells, but not with MCF7 cells. At 72 hours of incubation, MDA-MB231 cells released a 4-fold higher concentration of tPA as compared to BXPC3 cells. The time required to observe a detectable increase of tPA secretion was 14 hours for MDA-MB231 cells ($p < 0.001$ between t0 and 14 hours) and 72 hours ($p < 0.001$ between t0 and 72 hours) for BXPC3 cells (**Figure 30A**).

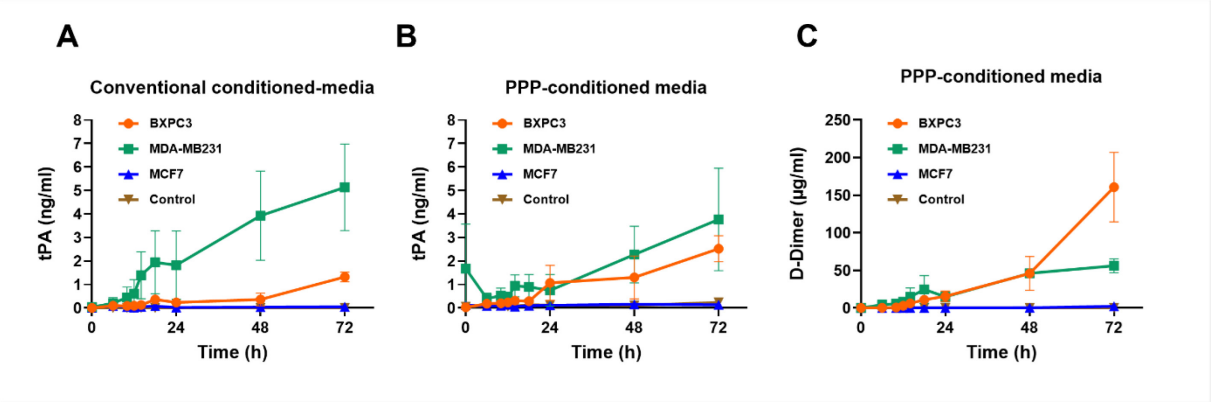

***Figure 30**: Distinct fibrinolytic potential of BXPC3, MDA-MB213 and MCF7 cells. Control experiment: conditioned media without cells. Data are shown ad Mean ± SD; of 3 experiments. **(A)**: Secretion of tPA from cancer cells (BXPC3, MDA-MB231, MCF7) cultured in conventional conditioned media. **(B)** Secretion of tPA from cancer cells (BXPC3, MDA-MB231, MCF7) cultured in PPP-conditioned media. **(C)** Release of D-Dimer in PPP-conditioned media in the control experiment and in the presence of BXPC3, MDA-MB231, or MCF7 cells.*

During the observation period tiny concentrations of tPA were measured in plasma (0.06 ± 0.04 ng/ml at t0 and 0.24 ± 0.07 ng/ml after 72h; $p > 0.99$) (**Figure 30B**). In the presence of PPP, the release of tPA by BXPC3 or MDA-MB231 cells progressively increased. At 72 hours, the levels of tPA released by MDA-MB231 (3.77 ± 2.18 ng/ml) were significantly higher as compared to those released by MCF7 cells (0.14 ± 0.01 ng/ml, $p = 0.02$) (**Figure 30B**).

In the control experiment, in the absence of cancer cells, the levels of D-Dimer in PPP-conditioned media were 0.09 ± 0.11 µg/ml after 72 hours (**Figure 30C**). Following fibrin clot formation in the presence of BXPC3 or MDA-MB231 cells, a progressive increase in D-Dimer was observed. The increase in D-Dimer concentration became significant after 24 hours from clot formation for BXPC3 cells ($p < 0.001$ as compared to t0) and 14 hours for MDA-MB231 cells ($p < 0.001$ as compared to t0) (**Figure 30C**). In the presence of MDA-MB231 and BXPC3 cells, the levels of D-Dimer continued to increase up to 72 hours from clot formation. In the

presence of MCF7 cells, after fibrin clot formation, no significant changes in D-Dimer concentration were observed ($p > 0.99$ between t0 and after 72h). At the end of the observation period, the maximum concentration of D-Dimer in the presence of BXPC3 and MDA-MB231 was 160.77 ± 46.39 μg/ml and 56.19 ± 9.29 μg/ml, respectively.

2.5. Fibrin clot shields induced resistance to the anticancer agents.

Applying the conventional experimental system for the study of the efficacy of anticancer agents, without fibrin, the IC50 of paclitaxel was 0.5 μM for BXPC3 and 0.1 μM for MDA-MB231 and MCF7 cells. The IC50 of 4-hydroxy-tamoxifen was 10 nM for MCF7 cells.

At 2h after the clot formation, the addition of paclitaxel at the IC50 did not induce any detectable decrease of the viability of the BXPC3, MDA-MB213 or MCF7 cells. Similarly, the addition of 4-hydroxy-tamoxifen did not induce any detectable decrease of the viability of the MCF7 cells (**Figure 31**).

At 24h after the clot formation, the addition of PTX at the IC50 resulted in 50% decrease of viability of BXPC3 cells (**Figure 31A**).

At 24h after the clot formation, the addition of PTX at the IC50 did not induce any detectable death to the MDA-MB213 or MCF7 cells. Similarly, the addition of 4OHTam did not induce any detectable death to the MCF7 cells (**Figure 31B, C, D**).

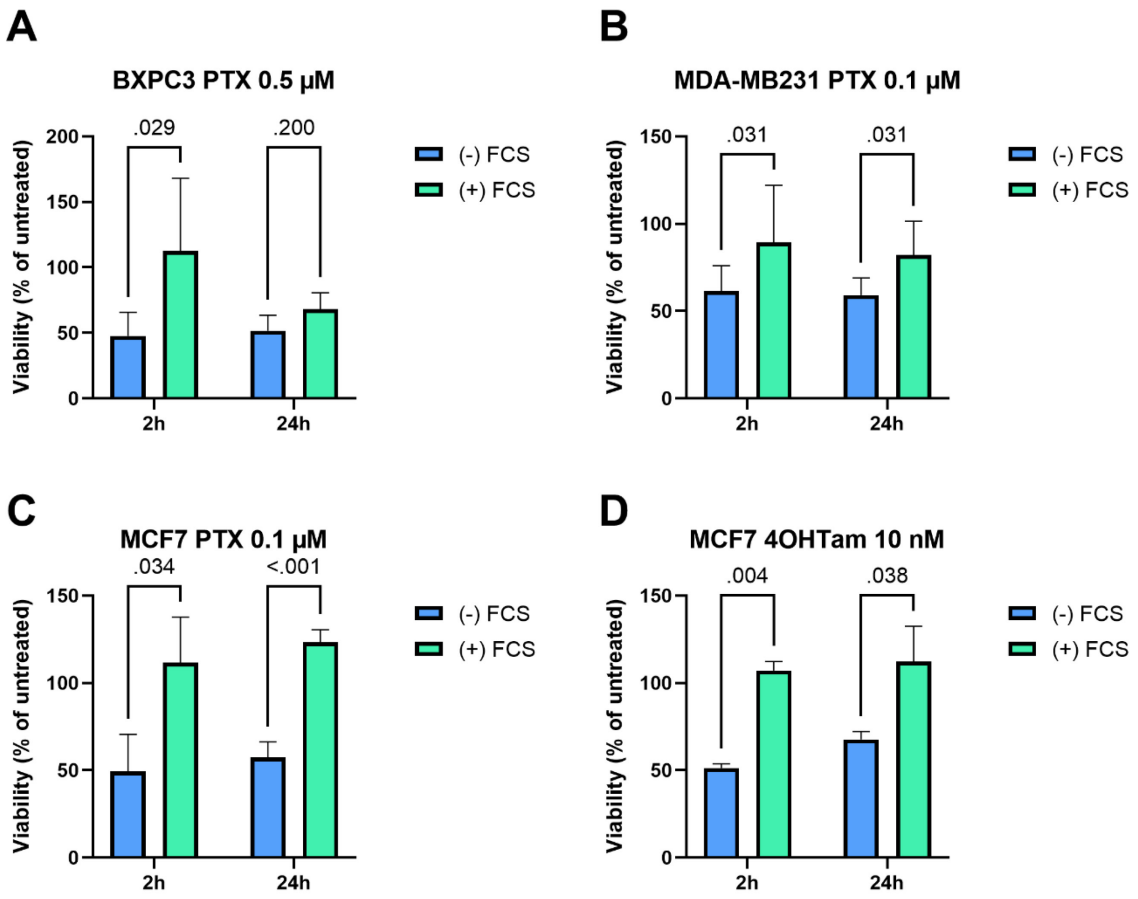

***Figure 31**: Impact of the Fibrin Clot Shield (FCS) on the efficiency of anticancer treatments. Data were represented as Mean ± SD of 3 independent experiments. **(A)** Viability of BXPC3 cells after 72 hours of treatment with 0.5 µM of paclitaxel (PTX) in the presence or absence of 10% PPP. PTX was introduced either at 2, or at 24 hours after FCS formation. **(B)** Viability of MDA-MB231 cells after 72 hours of treatment with 0,1 µM of PTX in the presence or absence of 10% PPP. PTX was introduced either at 2, or at 24 hours after FCS formation. **(C)** Viability of MCF7 cells after 72 hours of treatment with 100 nM of PTX in the presence or absence of 10% PPP. PTX was introduced either at 2, or at 24 hours after FCS formation. **(D)** Viability of MCF7 cells after 72 hours of treatment with 10 nM of 4-Hydroxy-Tamoxifen (4OHTam) in the presence or absence of 10% PPP. PTX was introduced either at 2, or at 24 hours after FCS formation. Values are Mean ± SD of 3 independent experiments.*

DISCUSSION

The link between cancer and thrombosis has been recognized for over a century, dating back to Armand Trousseau's observations of an association between gastric cancer and venous thromboembolism (VTE) in the 19th century. Since then, research in this area has grown significantly, with numerous studies shedding light on the mechanisms underlying the heightened thrombotic risk in cancer patients.

Several factors contribute to the activation of blood coagulation and the increased risk of thrombosis in cancer patients. Surgical procedures, chemotherapy, and radiotherapy are all associated with thrombotic events (Grover et al., 2021). Additionally, pro-inflammatory cytokines such as TNFα, IL1, IL6, IL8, IL12, and IFNγ, released by cancer cells, play a role in activating the endothelium, platelets, and leukocytes, leading to vascular damage and the formation of neutrophil extracellular traps (NETs) (Falanga & Marchetti, 2023; Herre et al., 2023). Moreover, cancer cells have been shown to express tissue factor (TF) and produce TF-containing extracellular vesicles (AmraneDjedidi et al., 2020; Galmiche et al., 2022; Rees et al., 2023).

As a consequence, the tumor microenvironment is inherently prothrombotic, leading to the deposition of fibrin in histological specimens from cancer patients. However, just as TF expression is diverse from one cancer cell line to another (Rousseau et al., 2017a), the quantity of fibrin present in tumors varies widely, ranging from 10% to 80% across different types of cancer and even among patients with the same cancer type (Kirtane et al., 2017). While the role of fibrin in inducing hypoxia, cell migration, and angiogenesis has been established early on (Dvorak, 1986), little attention has been given to the relationship between the procoagulant properties of cancer cells and the characteristics of fibrin, and how these interactions influence cancer cells' survival and progression.

In this study, we established an original experimental model to investigate the interplay between cancer cells and the blood coagulation mechanism leading to the formation of a fibrin clot network. Using this model, we demonstrated that thrombin generation and fibrin network formation are driven by the specific procoagulant signature of cancer cells. The expression of TF in cancer cells induces thrombin generation, resulting in the formation of Fibrin Clot Shields

(FCS) around the cancer cells. For the first time, we visualized the architecture of the fibrin network originating from the membranes of cancer cells using Scanning Electron Microscopy.

Analysis of the structural characteristics of the FCSs revealed that the procoagulant properties of the microenvironment play a critical role, whether derived from the procoagulant properties of cancer cells themselves, such as membrane expression of TF, or from the presence of TF in the microenvironment. This was demonstrated by experiments involving the exogenous addition of TF in the presence of MCF7 cells. Additionally, we found that FCSs serve as a scaffold that supports cancer cell migration and act as a physical barrier, reducing the efficacy of anticancer agents such as paclitaxel and 4-hydroxy-tamoxifen.

The initial phase of our study consists of the establishment of an experimental model comprising cancer cells and FCS, by comparing two methods: conventional fibrin hydrogel, and PPP-conditioned media.

As the final product of coagulation in respond to vascular injury, fibrin is a critical temporary component within the extracellular matrix (ECM) components in the wounded area and as such, plays an important role in tissue repair and endothelial cells (EC) migration during angiogenesis (Dvorak, 1986). In fundamental research, fibrin hydrogel is used as an experimental model for angiogenesis (Blache & Ehrbar, 2018; Helms et al., 2022; Matveeva et al., 2022; Tiruvannamalai Annamalai et al., 2016). Due to its role in facilizing the wound healing process and its biodegradability by fibrinolysis, fibrin, in its hydrogel form, has emerged as a versatile sealant in diverse clinical contexts (Blache & Ehrbar, 2018; Chung et al., 2015; Creste et al., 2020; Sanz-Horta et al., 2023).

The fabrication of fibrin hydrogel consists of the combination of purified thrombin and fibrinogen, with optional addition of aprotinin to inhibit the activities of proteases secreted by various cell types. Typically, concentrations of fibrinogen and thrombin range from 1-5 mg/ml and 1-5 IU/ml, respectively. The structural characteristics, permeability, and stiffness of fibrin hydrogel can be readily adjusted by varying the concentrations of fibrinogen and thrombin (Belcher et al., 2023; Dey et al., 2021; Heilala et al., 2023).

Our findings reveal that each component of the fibrin hydrogel can impact cell viability. Increasing the concentration of fibrinogen alone led to a reduction in cell viability, with significantly lower viability observed in hydrogels fabricated from 5 mg/ml fibrinogen compared to 1 mg/ml. While thrombin alone did not significantly affect cell viability, hydrogels fabricated from 4 UI/ml thrombin increased cell viability as compared to those from 2 UI/ml.

Thrombin has been demonstrated to induce cell proliferation via protease-activated receptor (PAR) signaling not only in cancer cells (Rees et al., 2023), but also in other cell types such as fibroblasts (Sébert et al., 2018), smooth muscle cells (Burzynski et al., 2023), or macrophages (Ukan et al., 2022). As excess thrombin is bound to fibrin fibers while maintaining its activity in all hydrogels (Haynes et al., 2017), plasma, and whole blood models (Crossen et al., 2023; S. Zhu et al., 2018), fibrin clot serves as a reservoir for thrombin. This phenomenon suggests that hydrogels made with a higher concentration of thrombin may promote higher cell viability, as confirmed by our data. Out of the four combinations of fibrinogen and thrombin tested, hydrogels made with (1 mg/ml fibrinogen + 2 UI/ml thrombin) allowed cancer cells to maintain the same viability as that of cells cultured in the absence of fibrin hydrogel.

The hydrogel model offers the advantage of modulating fibrin hydrogel structure by varying fibrinogen and thrombin concentrations, allowing observation of the impact of different fibrin clot structures on the same cell line. However, modifications to this formulation may affect cell viability and introduce potential artifacts in result interpretation. Additionally, as fibrin clot formation relies on exogenous fibrinogen and thrombin and not on the expression of TF in cancer cells, it is impossible to study the influence of cancer cells on fibrin clot structure using this model.

Cancer cells have demonstrated the ability to initiate clot formation through thrombin generation in pure platelet-poor plasma (PPP), as evidenced by the Calibrated Automated Thrombogram (CAT) assay (Gerotziafas et al., 2012). While immediate fibrin formation can be induced by exposing cancer cells to recalcified PPP, maintaining cell culture in this environment is not possible. Despite PPP containing essential adhesion factors, hormones, lipids, and minerals necessary for cell growth, the absence of a carbon source renders pure PPP unsuitable for cell culture.

Thus, our objective is to devise a strategy that involves supplementing culture media with an optimal amount of PPP to facilitate fibrin formation while ensuring cell viability (the PPP-conditioned media method). However, diluting PPP in the culture media also results in the dilution of coagulation factors and inhibitors. Thus, optimization of the PPP concentration was imperative to strike a balance between on the one hand ensuring sufficient thrombin generation and promoting fibrin formation, and on the other hand, preserving cell viability.

Our experiments showed that in 10% dilution of PPP in conditioned media (RPMI-1640), BXPC3, MDA-MB231, and MCF7 cells maintained satisfactory viability and proliferation rates as compared to their normal conditions in RPMI-1640 without any addition of PPP. Consequently, we selected this concentration of 10% PPP (PPP-conditioned media) to assess the cancer cells' ability to induce thrombin generation and fibrin clot formation.

In control experiments with increasing TF concentrations in PPP-conditioned media, the impact of TF on lag time was evident, with lag time shortening as TF concentration increased. However, ETP and Peak reached their maxima at 3 and 4 pM of TF, respectively, then decreased at 5 pM TF concentration, suggesting a threshold effect on thrombin generation activity in PPP-conditioned media where clotting factors, including prothrombin (factor II) were decreased by 90%.

In pure PPP, Ca^{2+} enhances thrombin generation up to 15.4 mM, maintains consistent levels from 15.4 to 19.2 mM, and inhibits thrombin generation at concentrations above 19.2 mM (Parunov et al., 2017). Our results demonstrated that in PPP-conditioned media (10% dilution of PPP in RPMI), 1.8 mM Ca^{2+} in the presence of MDA-MB231 cells yielded lower thrombin generation activity than 0.4 mM. These results demonstrated the importance of culture media selection. Culture media formulations are not always disclosed by manufacturers, and in some cases, there are too many different calcium salts, rendering the estimation of Ca^{2+} concentration inaccurate. Hence, in order to compare our 3 studied cell lines, we decided to use the same culture media (RPMI-1640) for the three studied cancer cell lines.

Investigating thrombin generation process triggered by the three studied cancer cell lines, BXPC3, MDA-MB231, and MCF7, revealed that all were capable of inducing thrombin

generation in PPP-conditioned media at the concentration of 10%, with increasing potency observed from MCF7 to BXPC3 and MDA-MB231, respectively.

Multiple lines of evidence from experiments in an original culture system in the presence of human PPP, show for the first time that the procoagulant signature of cancer cells determines the quality and structure of fibrin clot network.

Two methods were employed to observe the FCS generated by cancer cells: Laser Scanning Confocal Microscopy (LSCM) to explore different layers of FCS, and Scanning Electron Microscopy (SEM) to investigate at high resolution the architecture and structural aspect of FCS.

To observe the fibrin clot using LSCM, we explored the feasibility of two methods: fluorescent fibrinogen and anti-fibrin antibody. Both methods yield a good image of the clot. While the immunostaining method using an anti-fibrin antibody is more time-consuming, it offers greater flexibility. Commercially fluorescent fibrinogens are only available in two options of spectral wavelengths: 650/668 nm (far red channel), and 495/519 nm (green channel). Since anti-fibrin antibody could be recognized by a wider range of secondary antibodies, it offers more flexibility in case of co-immunostaining with other proteins.

The structural characteristics of the fibrin clot were evaluated according to established criteria based on fiber thickness, pore size, and the number of intersections (Daraei et al., 2021; W. Li et al., 2016). Thrombin generation triggered by the high TF expressing cells BXPC3 or MDA-MB231, resulted in a more robust clot structure with thinner fibers, smaller pores, and a higher number of intersections as compared to those obtained following coagulation activation by the low TF expressing MCF7 cells. The exogenous addition of TF to the MCF7 experimental microenvironment resulted in thrombin generation levels comparable to those observed in the experiment with the BXPC3 cells. Accordingly, the fibrin network displayed a similar architecture and structure to that observed in the presence of BXPC3 cells. The analysis of SEM images, obtained by the addition of exogenous TF in the PPP-conditioned media (in the absence of cells), showed that the strengthening of the fibrin network was correlated with the concentration of TF and the increase in thrombin generation.

To the best of our knowledge, the present study provides for the first-time electron microscopy images of the architecture of the cancer cell-initiated fibrin network and its interaction with the cell membranes. This network develops in the form of "bird's nest" being in contact with the extracellular layer of the cell membrane. We suppose that fibrin fibers could cover specific receptors at the membrane of cancer cells which are potential aims of targeted anticancer therapies. This hypothesis must be investigated in appropriately designed studies.

Many groups have worked on the impact of fibrinogen and thrombin concentration on the structure of fibrin clot by combining purified fibrinogen and thrombin, or by adding fibrinogen and/or thrombin to PPP (Belcher et al., 2023; Blombäck & Okada, 1982; Ramanujam et al., 2023; Wolberg, 2007). However, to the limit of our knowledge, the are no studies on the impact of TF expressed by cancer cells on the fibrin formation process, even though TF is a major trigger of thrombin generation, and it is well established that cancer cells express abundantly this protein. Many studies have showed results on the impact of thrombin on the structure of fibrin clot: increased thrombin concentration leads to clots with finer fibers, and smaller pores (Belcher et al., 2023; Dey et al., 2021; Domingues et al., 2016; Weisel & Nagaswami, 1992; Wolberg, 2007). However, to the limit of our knowledge, the impact of TF-driven thrombin generation on the structure of the fibrin network remains poorly studied. The BXPC3, MDA-MB231, and MCF7 cells exhibit different procoagulant potential – determined by different levels of TF expression which results in different intensities of thrombin generation. For example, BXPC3, of MDA-MB231 cells, expressing higher levels of TF lead to thrombin generation marked by shorter initiation phase, more rapid propagation phase and higher Peak as compared to MCF7 cells that express low levels of TF (Gerotziafas et al., 2012; Rousseau et al., 2017b).

Our data demonstrated the impact of the procoagulant properties of the tumoral microenvironment, either from cancer cells themselves, or from exogenous TF, could impact the structural characteristics of FCS. Since TF concentration is the determinant factor in this model, it is possible to generate FCS with different architecture on the same cell line, by varying the concentration of TF, as we demonstrated by adding exogenous TF on MCF7 cells. Other possibilities include induced overexpression of TF, and incorporation of TF+ extracellular

vesicles. We therefore conclude that the PPP-conditioning model is suitable to study the interaction between cancer cells and the FCS.

Accordingly, we hypothesized that the proper procoagulant potential of cancer cells could impact the structure of the fibrin clot which, subsequently could function as a protecting barrier against the effect of anticancer agents.

In the second part of the study, we explored the impact of the FCS on cancer cells migration and the efficacity of anticancer agents paclitaxel and 4OHTam.

The stiffness of the extracellular matrix is recognized as a factor that leads to poor perfusion and hinders the infiltration of anti-cancer agents and CAR-T cells (Henke et al., 2020; Huang et al., 2021; M. Li et al., 2022; Mushtaq et al., 2018; Yeow et al., 2019). Indeed, our study shows for the first time that the fibrin clot network generated by the cancer cells acts as a barrier offering a protection against the anticancer agents. Fibrin clot network acting as a shield abrogated the anticancer efficacy of either a conventional chemotherapeutic agent such as paclitaxel, or a targeted anticancer agent like tamoxifen.

Indeed, FCS in fresh clot (formed within 2 hours prior to exposure) completely abrogated the effect of paclitaxel on the viability of the three studied cancer cell lines. In contrast, exposure of cells with older FCS (formed 24 hours prior to exposure) resulted in distinction between its efficacy against BXPC3 cells on the one hand and MDA-MB213 and MCF7 on the other. In the former case the older clot did not lose its effect whereas in the latter case the protection by the FCS persisted.

An analysis of fibrinolytic activities of cancer cells offered an explanation for this observation. The D-Dimer, as a specific fibrin degradation product following plasmin generation, is an indicator of the fibrinolytic process. Increased levels of D-Dimer are associated with the stage and the aggressiveness of the cancer and are recognized as a prognostic factor for cancer recurrence and resistance to the anticancer therapy (J. Li et al., 2021; Liu et al., 2015; Ma et al., 2021).

Our results show that under steady-state conditions and following the initiation of thrombin generation and fibrin network formation, MDA-MB231 and BXPC3 cells, but not MCF7 cells,

secrete tPA. The steady increase in tPA secretion observed with BXPC3 and MDA-MB231 cells is correlate with their doubling time (Cailleau et al., 1974, 1978; Tan et al., 1986), suggesting that this increase is due to the increase in cell number by proliferation. This supports earlier studies that have documented the inherent pro-fibrinolytic activity in cancer cells (Galmiche et al., 2022; Saidak et al., 2021). While the tPA secreted after 72 hours by MDA-MB231 cells is greater than that by BXPC3 in 10% PBS, no significant difference was observed in 10% PPP. The impact of PPP on cell proliferation was different between BXPC3 and MDA-MB231 cells and this might be a possible explanation of this finding.

The lysis of the fibrin network formed by MDA-MB231 or BXPC3 cells, as evidenced by the increase in D-Dimer, corresponds to the release of tPA. While the secretion of tPA in MDA-MB231 cells surpassed that in BXPC3 cells, the rate of increase in D-Dimer levels in the former was notably slower than that observed in the latter. This observation is consistent with previous studies indicating that the lysis of clots composed of finer fibers is a prolonged process compared to clots formed by thicker fibers (Hethershaw et al., 2014; Mullin et al., 2006).

Neither significant tPA release nor a substantial increase in D-Dimer were observed in fibrin clots formed by MCF7 cells. Considering that MCF7 cells were found within the fibrin clot at a distance from the original adhesive layer, we hypothesize that they employ an alternative, plasminogen-independent pathways for fibrin degradation. Indeed, various matrix metalloproteinases (MMPs) have the capacity to degrade not only fibrin but also D-Dimer (Alexander et al., 2016; Bini et al., 1996, 1999; Hotary et al., 2002). The expression of MMP-14 by MCF7 cells (Di et al., 2016) could constitute this alternative fibrinolytic pathway, offering an explanation for the absence of any detectable D-Dimer.

The differences of the fibrinolytic potency among the BXPC3 cells and the MDA-MM231 and the MCF7 cells could be the origin of the effect of the formation of the FCSs on the efficacy of paclitaxel. We conclude that in the presence of potent fibrinolytic activity of BXPC3 cells, the FCS lost their protective action after 24 hours due to degradation. In weaker, or in total absence, of fibrinolytic activity, as was the case of MDA-MB231 and MCF7 cells, FCS could still offer their protection against the anticancer agents. These results are in accordance with the data from previous studies (Kirtane et al., 2017; Seo et al., 2018, 2021) which showed that the

combination of fibrinolytic agents with anticancer treatments increased the efficiency of the latter's.

A recent study showed that preoperative treatment (neoadjuvant) with chemotherapy offered better outcomes with lower relapse than postoperative (adjuvant) treatment in colon cancer patients (Morton et al., 2023). Since the postoperative wound healing process results in fibrin deposit, we could hypothesize that the presence of fibrin explained relapse in patients receiving adjuvant therapy.

Extracellular matrix remodeling is an integral component of the migration and invasion process in cancer (Lintz et al., 2017; Majidpoor & Mortezaee, 2021). The fibrinolytic properties of cancer cells offer to them the capability to break down fibrin, facilitating their invasion of adjacent tissues (Dvorak, 1986; Dvorak et al., 1983; Kwaan & Lindholm, 2019).

It is well established that fibrin serves as a scaffold supporting cancer cell adhesion and migration (Dvorak, 1986). Our study provides evidence confirming this concept and further demonstrates that cancer cells, via their inherent procoagulant properties, construct the fibrin scaffold utilized for their invasion. Cell imaging using LSCM of fibrin clots revealed that BXPC3, MDA-MB231, or MCF7 cells detached from the initial adhesive monolayer and traversed through the fibrin network. Within the 24-hour observation period, living cells were identified at a distance from the cell layer, within, and on the top of the clots. This phenomenon has been observed by Andrade et al, who showed that breast cancer cells migrate within fibrin bundles formed in the presence of platelets (Andrade et al., 2017). According to this study platelets are a source of TGF-β and VEGF which induced the migration of breast cancer cells. Our study demonstrates that migration of pancreatic or breast cancer cells within the fibrin network occurs in the absence of platelets. Consequently, we hypothesis that the presence of fibrin scaffolds and/or the serine proteases of blood coagulation (i.e. activated factors X, IX, VII or thrombin) in concert with the inherent profibrinolytic activity of the cells, play a pivotal role in the selection of migrating cancer cells within the fibrin clot and the formation of distal colonies.

The 3D spheroid cultures of the three studied cancer cell lines also confirmed that the cells invaded and moved within the fibrin network. MDA-MB231 cells exhibited individual

movement into the fibrin clot, whereas BXPC3 and MCF7 cells demonstrated collective movement and this is in accordance with previous findings (De Pascalis & Etienne-Manneville, 2017; Friedl & Gilmour, 2009; Lintz et al., 2017; Lüönd et al., 2021; Majidpoor & Mortezaee, 2021). According to a recent study, cancer cells move through the fibrin network by expressing ICAM-1 and forming a fibrinogen-dependent bridge (Angelidakis et al., 2023).

In conclusion, the present study provides original data showing that the inherent procoagulant signature of cancer cells lead to the formation of a fibrin clot, with a structure that is influenced by thrombin generation potency. The FCSs offer a protection against the conventional chemotherapeutic agent paclitaxel or the targeted anticancer agent 4-hydroxy-tamoxifen.

PERSPECTIVES

In 10% of PPP, thrombin generation's ETP and Peak reached their highest levels with 3 pM and 4 pM TF, and subsequently decreased when TF concentration was augmented to 5 pM. Similarly, thrombin generation induced by MDA-MB231 in the DMEM media yielded lower ETP and Peak as compared to the RPMI-1640 media, despite being 4-fold more concentrated in Ca^{2+}. The effect of increasing concentrations of Ca^{2+} on inducing a bell-shaped dose-response curve in thrombin generation in pure PPP was reported (Parunov et al., 2017), although the authors offered no explanation. The mechanism that explains these observations needed to be further investigated.

While our PPP-conditioned media model provides a flexible method to culture cells within a modifiable fibrin network, reflecting various levels of thrombogenicity in the tumor microenvironment by adjusting TF expression, it does have notable limitations. Firstly, it lacks the presence of other cellular constituents typically found in the tumor microenvironment. Secondly, it operates within a static closed system, leading to the depletion of nutrients and coagulation factors over time.

In our current study, the absence of continuous renewal of coagulation factors while fibrin clot shields are exposed to cells that possess high fibrinolytic activity such as BXPC3 and MDA-MB231 cells, means that the fibrin clot shield may degrade over time. The introduction of a system for the continual renewal of coagulation factors could ensure the sustained recreation of the fibrin clot shield, enhancing the longevity of the model.

Additionally, fibrin networks formed under flow have thicker fibers than those formed in static condition, with the fibers orientated in the direction of the flow (Campbell et al., 2010), which makes them less susceptible to fibrinolysis (Varjú et al., 2011).

Microfluidics has emerged as a promising approach to address these challenges by facilitating the delivery of nutrient supplies and removal of waste through the generation of microflows. In a recent study (Angelidakis et al., 2023), MDA-MB231 cells, along with endothelial cells and fibroblasts were encapsulated within a fibrin hydrogel in a microfluidic chamber. Subsequently, culture media supplemented with PPP were perfused through the fibrin clot, leading to observed angiogenesis. This innovative approach offers a potential solution to enhance the physiological relevance of our PPP-conditioned media model.

An exploration of the involvement of other cellular components in the structure of fibrin clot shields could provide valuable insights. In non-cancer experimental systems, erythrocytes, platelets, neutrophil extracellular traps, and TF-expressing activated monocytes have been shown to support thrombin generation and increase clot viscosity (Guedes et al., 2018; Sun et al., 2023). In a tumoral context, platelets and red blood cells may infiltrate the tumor due to increased vessel permeability (Antunes et al., 2011; Wu et al., 2023; Yin et al., 2015; S.-R. Zhang et al., 2018). As activated platelets express procoagulant phospholipids necessary for the formation of the enzymatic complexes (extrinsic and intrinsic tenase and prothrombinase) that drive and amplify thrombin generation to the propagation phase, they might contribute to the formation of more dense and firm fibrin networks in the tumoral microenvironment. Further investigations into the impact of platelets and red blood cells on the structure of fibrin clots formed by cancer cells could be conducted using our experimental model with platelet-rich plasma or whole blood. This approach may offer a more comprehensive understanding of the intricate interactions within the tumor microenvironment and their influence on fibrin clot formation.

Considering the multifaceted interactions within the tumor microenvironment, endothelial cells could play a crucial role. TF-containing cancer cell-derived extracellular vesicles have been shown to activate endothelial cells, making them procoagulant (AmraneDjedidi et al., 2020). Conversely, the expression of tissue factor pathway inhibitor (TFPI) as a coagulation inhibitor may counteract fibrin clot formation. Investigating the impact of endothelial cells on the structure of fibrin clot shields in a direct co-culture model involving cancer cells, endothelial cells, and plasma, could provide valuable insights.

Furthermore, previous research has highlighted the significance of the co-present of cancer and endothelial cells in promoting angiogenesis. For instance, a study by Andrade et al. (2017) demonstrated that co-culture of fibroblasts and endothelial cells with patient-derived triple-negative breast cancer cells in the presence of platelet-rich plasma led to a higher number of vessel-like formations, as compared to co-culture with patient-derived luminal B breast cancer cells, despite similar levels of VEGF-A secretion. Given that MDA-MB231 cells represent a triple-negative model and MCF7 cells represent a luminal A model (Holliday & Speirs, 2011), it's plausible to hypothesize that the structure of fibrin clot shields may indeed play a role in

angiogenesis. Further investigation into this hypothesis could provide valuable insights into the complex interplay between cancer cells, endothelial cells, and fibrin clot formation in the context of tumor angiogenesis.

A translational approach that correlates the quantification of fibrin deposits in patient histological specimens with the procoagulant profile of patient-derived cancer cells and the structural characteristics of fibrin clot shields could provide valuable clinical insights. By analyzing patient samples, such as tumor tissue sections, and assessing the amount of fibrin deposition, along with profiling the procoagulant properties of cancer cells derived from those patients, we could gain a deeper understanding of the relationship between fibrin clot formation and cancer progression. Moreover, integrating information about the structural characteristics of fibrin clot shields formed by patient-derived cancer cells could further enhance our understanding of the tumor microenvironment. This approach could potentially identify patterns or signatures associated with specific cancer types or stages, paving the way for personalized diagnostics and therapeutic strategies.

Our results confirmed that the presence of TF is a factor that indirectly via thrombin generation impacts the structure of fibrin clot. We could hypothesis that when MCF7 cells overexpress TF, or when they are exposed to the microparticles expressing TF, they could induce the formation of firmer clots. This hypothesis worth further consideration.

The role of fibrin clot shields could be of particular interest in the comprehension of the resistance to the targeted anticancer therapies. Our data allow to propose that fibrin clot shields generated by the own procoagulant properties of cancer cells might represent a new mechanism leading to the development of resistance to the anticancer treatments. This hypothesis merits to be further investigated.

To correlate the clot's structure to chemoresistance, an experimental approach could involve supplementing low-expressing cell lines like MCF7 with varying concentrations of TF and observing alterations in IC50 values. Additionally, our data indicate that degradation of fibrin clot shields might enhance the efficacy of anticancer agents, suggesting potential benefits in exploring combination therapies that integrate anticancer agents with fibrinolytic strategies.

The quantitative estimation of fibrin network structural and mechanical characteristics (pore diameter, fibrin fiber diameter and number of intersections as well as clot elasticity) and the establishment of thresholds related to either the response to the treatment or the aggressivity and the migration of the cells could be of importance either for pharmacological studies on the efficacy of new anticancer agents or in the evaluation of the risk of treatment failure in patients.

Inducing resistance to chemotherapeutic agents through prolonged exposure to low concentrations is a commonly employed *in vitro* method for generating chemo-resistant cell lines (Amaral et al., 2019). Given our results, along with supporting studies (Seo et al., 2018, 2021), which reveal the hindrance of chemotherapeutic agents doxorubicin and paclitaxel penetration by fibrin clot shields, we could hypothesize that sustained exposure of cancer cells to suboptimal concentration of anticancer agents in the presence of fibrin clots may induce cancer cell resistance over time.

It is well established that the efficacy of the targeted anticancer treatments relies on ligand-receptor interactions. The presence of the fibrin clot shields in the tumor microenvironment and in the conformation of the "bird's nest" enveloping the cancer cells, as evidenced by SEM analysis, could decrease the accessibility of the targeted anticancer agents towards their targets. Our data allows to hypothesis that cancer cell induced fibrin clot shields might influence the access of CAR-T cells towards their cellular targets.

Although T-lymphocytes maintain their mobility in fibrin (Zou et al., 2012), the firmer the clot, the longer it would take for CAR-T cells to traverse it (Ogunnaike et al., 2021). Thus, we assume that fibrin clot shields might contribute to CAR-T cells exhaustion which is considered as a major mechanism of treatment failure (Kouro et al., 2022; X. Zhu et al., 2022). The role of cancer cell generated fibrin clot shields in the development of the resistance to targeted anticancer treatments and CAR-T cell therapies raises as a potential new field of interest.

Cancer continues to pose a significant global health burden, with 20 million new cases and 9.7 million deaths reported worldwide in 2022 (Bray et al., 2024), making it the second leading cause of mortality. Despite considerable efforts and advancements in research and the development of new anti-cancer therapies, drug resistance remains a major obstacle, leading to relapses and unfavorable outcomes.

In recent years, targeted therapies such as monoclonal antibodies or CAR-T cells have emerged as promising approaches for cancer treatment. However, their effectiveness in solid tumors remains limited compared to hematologic cancers (Qin & Xu, 2022). Understanding how alterations in the coagulant properties of the tumor microenvironment influence the formation and characteristics of fibrin clot shields, and their relation to the efficacy of targeted treatments, is crucial for overcoming the challenges posed by anticancer therapies.

By unraveling the mechanisms underlying the interaction between the tumor microenvironment and fibrin clot shields, we can gain insights into how these interactions impact the efficacy of targeted treatments. This knowledge may ultimately lead to the development of strategies to enhance the effectiveness of anticancer therapies and overcome drug resistance in cancer treatments.

REFERENCES

Ahmed, T. A. E., Griffith, M., & Hincke, M. (2007). Characterization and inhibition of fibrin hydrogel-degrading enzymes during development of tissue engineering scaffolds. *Tissue Engineering*, *13*(7), 1469–1477. https://doi.org/10.1089/ten.2006.0354

Aird, W. C. (2007). Phenotypic Heterogeneity of the Endothelium. *Circulation Research*, *100*(2), 158–173. https://doi.org/10.1161/01.RES.0000255691.76142.4a

Alexander, K., Banos, A., Abro, S., Hoppensteadt, D., Fareed, J., Rees, H., & Hopkinson, W. (2016). Levels of matrix metalloproteinases in arthroplasty patients and their correlation with inflammatory and thrombotic activation processes. *Clinical and Applied Thrombosis/Hemostasis*, *22*(5), 441–446. https://doi.org/10.1177/1076029616639704

Amaral, M. V. S., Portilho, A. J. D. S., Silva, E. L. D., Sales, L. D. O., Maués, J. H. D. S., Moraes, M. E. A. D., & Moreira-Nunes, C. A. (2019). Establishment of Drug-resistant Cell Lines as a Model in Experimental Oncology: A Review. *Anticancer Research*, *39*(12), 6443–6455. https://doi.org/10.21873/anticanres.13858

AmraneDjedidi, R., Rousseau, A., Larsen, A. K., Elalamy, I., Van Dreden, P., & Gerotziafas, G. T. (2020). Extracellular vesicles derived from pancreatic cancer cells BXPC3 or breast cancer cells MCF7 induce a permanent procoagulant shift to endothelial cells. *Thrombosis Research*, *187*, 170–179. https://doi.org/10.1016/j.thromres.2019.09.003

Andrade, S. S., Sumikawa, J. T., Castro, E. D., Batista, F. P., Paredes-Gamero, E., Oliveira, L. C., Guerra, I. M., Peres, G. B., Cavalheiro, R. P., Juliano, L., Nazário, A. P., Facina, G.,

Tsai, S. M., Oliva, M. L. V., & Girão, M. J. B. C. (2017). Interface between breast cancer cells and the tumor microenvironment using platelet-rich plasma to promote tumor angiogenesis—Influence of platelets and fibrin bundles on the behavior of breast tumor cells. *Oncotarget*, *8*(10), Article 10. https://doi.org/10.18632/oncotarget.15170

Angelidakis, E., Chen, S., Zhang, S., Wan, Z., Kamm, R. D., & Shelton, S. E. (2023). Impact of fibrinogen, fibrin thrombi, and thrombin on cancer cell extravasation using in vitro microvascular networks. *Advanced Healthcare Materials*, *12*(19), 2202984. https://doi.org/10.1002/adhm.202202984

Antunes, R. F., Brandão, C., Maia, M., & Arosa, F. A. (2011). Red blood cells release factors with growth and survival bioactivities for normal and leukemic T cells. *Immunology and Cell Biology*, *89*(1), 111–121. https://doi.org/10.1038/icb.2010.60

Ayers, L., Nieuwland, R., Kohler, M., Kraenkel, N., Ferry, B., & Leeson, P. (2015). Dynamic microvesicle release and clearance within the cardiovascular system: Triggers and mechanisms. *Clinical Science (London, England: 1979)*, *129*(11), 915–931. https://doi.org/10.1042/CS20140623

Belcher, H. A., Guthold, M., & Hudson, N. E. (2023). What is the diameter of a fibrin fiber? *Research and Practice in Thrombosis and Haemostasis*, *7*(5), 100285. https://doi.org/10.1016/j.rpth.2023.100285

Berthois, Y., Katzenellenbogen, J. A., & Katzenellenbogen, B. S. (1986). Phenol red in tissue culture media is a weak estrogen: Implications concerning the study of estrogen-

responsive cells in culture. *Proceedings of the National Academy of Sciences of the United States of America*, *83*(8), 2496–2500.

Bertozzi, C. C., Hess, P. R., & Kahn, M. L. (2010). Platelets: Covert regulators of lymphatic development. *Arteriosclerosis, Thrombosis, and Vascular Biology*, *30*(12), 2368–2371. https://doi.org/10.1161/ATVBAHA.110.217281

Bini, A., Itoh, Y., Kudryk, B. J., & Nagase, H. (1996). Degradation of cross-linked fibrin by matrix metalloproteinase 3 (stromelysin 1): Hydrolysis of the γ gly 404−ala 405 peptide bond. *Biochemistry*, *35*(40), 13056–13063. https://doi.org/10.1021/bi960730c

Bini, A., Wu, D., Schnuer, J., & Kudryk, B. J. (1999). Characterization of stromelysin 1 (MMP-3), matrilysin (MMP-7), and membrane type 1 matrix metalloproteinase (MT1-MMP) derived fibrin(ogen) fragments D-dimer and D-like monomer: NH2-terminal sequences of late-stage digest fragments. *Biochemistry*, *38*(42), 13928–13936. https://doi.org/10.1021/bi991096g

Blache, U., & Ehrbar, M. (2018). Inspired by Nature: Hydrogels as Versatile Tools for Vascular Engineering. *Advances in Wound Care*, *7*(7), 232–246. https://doi.org/10.1089/wound.2017.0760

Blombäck, B., & Okada, M. (1982). Fibrin gel structure and clotting time. *Thrombosis Research*, *25*(1), Article 1. https://doi.org/10.1016/0049-3848(82)90214-6

Bray, F., Laversanne, M., Sung, H., Ferlay, J., Siegel, R. L., Soerjomataram, I., & Jemal, A. (2024). Global cancer statistics 2022: GLOBOCAN estimates of incidence and

mortality worldwide for 36 cancers in 185 countries. *CA: A Cancer Journal for Clinicians*. https://doi.org/10.3322/caac.21834

Bucay, I., O'Brien, E. T., Wulfe, S. D., Superfine, R., Wolberg, A. S., Falvo, M. R., & Hudson, N. E. (2015). Physical determinants of fibrinolysis in single fibrin fibers. *PloS One*, *10*(2), e0116350. https://doi.org/10.1371/journal.pone.0116350

Burzynski, L. C., Morales-Maldonado, A., Rodgers, A., Kitt, L. A., Humphry, M., Figg, N., Bennett, M. R., & Clarke, M. C. H. (2023). Thrombin-activated interleukin-1α drives atherogenesis, but also promotes vascular smooth muscle cell proliferation and collagen production. *Cardiovascular Research*, *119*(12), 2179–2189. https://doi.org/10.1093/cvr/cvad091

Byrnes, J. R., Wilson, C., Boutelle, A. M., Brandner, C. B., Flick, M. J., Philippou, H., & Wolberg, A. S. (2016). The interaction between fibrinogen and zymogen FXIII-A2B2 is mediated by fibrinogen residues γ390-396 and the FXIII-B subunits. *Blood*, *128*(15), 1969–1978. https://doi.org/10.1182/blood-2016-04-712323

Cailleau, R., Olivé, M., & Cruciger, Q. V. (1978). Long-term human breast carcinoma cell lines of metastatic origin: Preliminary characterization. *In Vitro*, *14*(11), 911–915. https://doi.org/10.1007/BF02616120

Cailleau, R., Young, R., Olivé, M., & W. J. Reeves, J. (1974). Breast Tumor Cell Lines From Pleural Effusions. *JNCI Journal of the National Cancer Institute*, *53*(3), 661. https://doi.org/10.1093/jnci/53.3.661

Campbell, R. A., Aleman, M., Gray, L. D., Falvo, M. R., & Wolberg, A. S. (2010). Flow profoundly influences fibrin network structure: Implications for fibrin formation and clot stability in haemostasis. *Thrombosis and Haemostasis*, *104*(6), 1281–1284. https://doi.org/10.1160/TH10-07-0442

Caunt, M., Huang, Y.-Q., Brooks, P. C., & Karpatkin, S. (2003). Thrombin induces neoangiogenesis in the chick chorioallantoic membrane. *Journal of Thrombosis and Haemostasis: JTH*, *1*(10), 2097–2102. https://doi.org/10.1046/j.1538-7836.2003.00426.x

Cesarman-Maus, G., & Hajjar, K. A. (2005). Molecular mechanisms of fibrinolysis. *British Journal of Haematology*, *129*(3), 307–321. https://doi.org/10.1111/j.1365-2141.2005.05444.x

Chapin, J. C., & Hajjar, K. A. (2015). Fibrinolysis and the Control of Blood Coagulation. *Blood Reviews*, *29*(1), 17–24. https://doi.org/10.1016/j.blre.2014.09.003

Charpidou, A., Gerotziafas, G., Popat, S., Araujo, A., Scherpereel, A., Kopp, H.-G., Bironzo, P., Massard, G., Jiménez, D., Falanga, A., Kollias, A., & Syrigos, K. (2024). Lung Cancer Related Thrombosis (LCART): Focus on Immune Checkpoint Blockade. *Cancers*, *16*(2), 450. https://doi.org/10.3390/cancers16020450

Chernysh, I. N., Everbach, C. E., Purohit, P. K., & Weisel, J. W. (2015). Molecular mechanisms of the effect of ultrasound on the fibrinolysis of clots. *Journal of Thrombosis and Haemostasis: JTH*, *13*(4), 601–609. https://doi.org/10.1111/jth.12857

Chernysh, I. N., Nagaswami, C., Purohit, P. K., & Weisel, J. W. (2012). Fibrin clots are equilibrium polymers that can be remodeled without proteolytic digestion. *Scientific Reports*, *2*, 879. https://doi.org/10.1038/srep00879

Chernysh, I. N., Nagaswami, C., & Weisel, J. W. (2011). Visualization and identification of the structures formed during early stages of fibrin polymerization. *Blood*, *117*(17), 4609–4614. https://doi.org/10.1182/blood-2010-07-297671

Chung, E., Rytlewski, J. A., Merchant, A. G., Dhada, K. S., Lewis, E. W., & Suggs, L. J. (2015). Fibrin-based 3D Matrices Induce Angiogenic Behavior of Adipose-derived Stem Cells. *Acta Biomaterialia*, *17*, 78–88. https://doi.org/10.1016/j.actbio.2015.01.012

Claesson-Welsh, L., Dejana, E., & McDonald, D. M. (2021). Permeability of the endothelial barrier: Identifying and reconciling controversies. *Trends in Molecular Medicine*, *27*(4), 314–331. https://doi.org/10.1016/j.molmed.2020.11.006

Colombo, M., Raposo, G., & Théry, C. (2014). Biogenesis, secretion, and intercellular interactions of exosomes and other extracellular vesicles. *Annual Review of Cell and Developmental Biology*, *30*, 255–289. https://doi.org/10.1146/annurev-cellbio-101512-122326

Costa, E. C., Moreira, A. F., de Melo-Diogo, D., Gaspar, V. M., Carvalho, M. P., & Correia, I. J. (2016). 3D tumor spheroids: An overview on the tools and techniques used for their analysis. *Biotechnology Advances*, *34*(8), 1427–1441. https://doi.org/10.1016/j.biotechadv.2016.11.002

Coughlin, S. R. (2000). Thrombin signalling and protease-activated receptors. *Nature*, *407*(6801), 258–264. https://doi.org/10.1038/35025229

Creste, C. F. Z., Orsi, P. R., Landim-Alvarenga, F. C., Justulin, L. A., Golim, M. de A., Barraviera, B., & Ferreira, R. S. (2020). Highly Effective Fibrin Biopolymer Scaffold for Stem Cells Upgrading Bone Regeneration. *Materials*, *13*(12), 2747. https://doi.org/10.3390/ma13122747

Crossen, J., Shankar, K. N., & Diamond, S. L. (2023). Investigating thrombin-loaded fibrin in whole blood clot microfluidic assay via fluorogenic peptide. *Biophysical Journal*, *122*(4), 697. https://doi.org/10.1016/j.bpj.2023.01.008

Daraei, A., Pieters, M., Baker, S. R., de Lange-Loots, Z., Siniarski, A., Litvinov, R. I., Veen, C. S. B., de Maat, M. P. M., Weisel, J. W., Ariëns, R. A. S., & Guthold, M. (2021). Automated fiber diameter and porosity measurements of plasma clots in scanning electron microscopy images. *Biomolecules*, *11*(10), Article 10. https://doi.org/10.3390/biom11101536

De Pascalis, C., & Etienne-Manneville, S. (2017). Single and collective cell migration: The mechanics of adhesions. *Molecular Biology of the Cell*, *28*(14), 1833–1846. https://doi.org/10.1091/mbc.e17-03-0134

Dewyer, N. A., Sood, V., Lynch, E. M., Luke, C. E., Upchurch, G. R., Wakefield, T. W., Kunkel, S., & Henke, P. K. (2007). Plasmin inhibition increases MMP-9 activity and decreases vein wall stiffness during venous thrombosis resolution. *The Journal of Surgical Research*, *142*(2), 357–363. https://doi.org/10.1016/j.jss.2007.03.064

Dey, M., Ayan, B., Yurieva, M., Unutmaz, D., & Ozbolat, I. T. (2021). Studying tumor angiogenesis and cancer invasion in a three-dimensional vascularized breast cancer micro-environment. *Advanced Biology*, *5*(7), 2100090. https://doi.org/10.1002/adbi.202100090

Di, D., Chen, L., Wang, L., Sun, P., Liu, Y., Xu, Z., & Ju, J. (2016). Downregulation of human intercellular adhesion molecule-1 attenuates the metastatic ability in human breast cancer cell lines. *Oncology Reports*, *35*(3), 1541–1548. https://doi.org/10.3892/or.2016.4543

Dittrich, A., Khouri, C., Sackett, S. D., Ehlting, C., Böhmer, O., Albrecht, U., Bode, J. G., Trautwein, C., & Schaper, F. (2012). Glucocorticoids increase interleukin-6-dependent gene induction by interfering with the expression of the suppressor of cytokine signaling 3 feedback inhibitor. *Hepatology (Baltimore, Md.)*, *55*(1), 256–266. https://doi.org/10.1002/hep.24655

Domingues, M. M., Macrae, F. L., Duval, C., McPherson, H. R., Bridge, K. I., Ajjan, R. A., Ridger, V. C., Connell, S. D., Philippou, H., & Ariëns, R. A. S. (2016). Thrombin and fibrinogen γ′ impact clot structure by marked effects on intrafibrillar structure and protofibril packing. *Blood*, *127*(4), 487–495. https://doi.org/10.1182/blood-2015-06-652214

Dvorak, H. F. (1986). Tumors: Wounds that do not heal. *New England Journal of Medicine*, *315*(26), Article 26. https://doi.org/10.1056/NEJM198612253152606

Dvorak, H. F. (2015). Tumors: Wounds that do not heal—redux. *Cancer Immunology Research*, *3*(1), 1–11. https://doi.org/10.1158/2326-6066.CIR-14-0209

Dvorak, H. F., Senger, D. R., & Dvorak, A. M. (1983). Fibrin as a component of the tumor stroma: Origins and biological significance. *CANCER AND METASTASIS REVIEW*, *2*(1), Article 1. https://doi.org/10.1007/BF00046905

Eelen, G., Treps, L., Li, X., & Carmeliet, P. (2020). Basic and Therapeutic Aspects of Angiogenesis Updated. *Circulation Research*, *127*(2), 310–329. https://doi.org/10.1161/CIRCRESAHA.120.316851

Espitia Jaimes, C., Fish, R. J., & Neerman-Arbez, M. (2018). Local chromatin interactions contribute to expression of the fibrinogen gene cluster. *Journal of Thrombosis and Haemostasis: JTH*, *16*(10), 2070–2082. https://doi.org/10.1111/jth.14248

Eyisoylu, H., Hazekamp, E. D., Cruts, J., Koenderink, G. H., & de Maat, M. P. M. (2024). Flow affects the structural and mechanical properties of the fibrin network in plasma clots. *Journal of Materials Science: Materials in Medicine*, *35*(1), 8. https://doi.org/10.1007/s10856-024-06775-1

Falanga, A., & Marchetti, M. (2023). Cancer-associated thrombosis: Enhanced awareness and pathophysiologic complexity. *Journal of Thrombosis and Haemostasis*, *21*(6), 1397–1408. https://doi.org/10.1016/j.jtha.2023.02.029

Falanga, A., Russo, L., Milesi, V., & Vignoli, A. (2017). Mechanisms and risk factors of thrombosis in cancer. *Critical Reviews in Oncology/Hematology*, *118*, 79–83. https://doi.org/10.1016/j.critrevonc.2017.08.003

Falanga, A., Schieppati, F., & Russo, D. (2015). Cancer Tissue Procoagulant Mechanisms and the Hypercoagulable State of Patients with Cancer. *Seminars in Thrombosis and Hemostasis*, *41*(7), 756–764. https://doi.org/10.1055/s-0035-1564040

Fan, Q., Ma, Q., Bai, J., Xu, J., Fei, Z., Dong, Z., Maruyama, A., Leong, K. W., Liu, Z., & Wang, C. (2020). An implantable blood clot-based immune niche for enhanced cancer vaccination. *Science Advances*, *6*(39), eabb4639. https://doi.org/10.1126/sciadv.abb4639

Farge, D., Frere, C., Connors, J. M., Ay, C., Khorana, A. A., Munoz, A., Brenner, B., Kakkar, A., Rafii, H., Solymoss, S., Brilhante, D., Monreal, M., Bounameaux, H., Pabinger, I., Douketis, J., Ageno, W., Ajauro, F., Al-Aboudi, K. R., Alcindor, T., … Yamada, N. (2019). 2019 international clinical practice guidelines for the treatment and prophylaxis of venous thromboembolism in patients with cancer. *The Lancet Oncology*, *20*(10), e566–e581. https://doi.org/10.1016/S1470-2045(19)30336-5

Félétou, M. (2011). *The Endothelium: Part 1: Multiple Functions of the Endothelial Cells—Focus on Endothelium-Derived Vasoactive Mediators*. Morgan & Claypool Life Sciences. http://www.ncbi.nlm.nih.gov/books/NBK57149/

Fernández, A., Ramos, J., López, M., Pérez, P., Santín, E., Llorente, L., Diebold, Y., & Iglesias, F. J. (2013). Proliferation of porcine conjunctival fibroblasts in fibrin-based scaffolds using alamar blue assay. *Investigative Ophthalmology & Visual Science*, *54*(15), 1387.

Friedl, P., & Gilmour, D. (2009). Collective cell migration in morphogenesis, regeneration and cancer. *Nature Reviews Molecular Cell Biology*, *10*(7), Article 7. https://doi.org/10.1038/nrm2720

Fuller, G. M., & Zhang, Z. (2001). Transcriptional Control Mechanism of Fibrinogen Gene Expression. *Annals of the New York Academy of Sciences*, *936*(1), 469–479. https://doi.org/10.1111/j.1749-6632.2001.tb03534.x

Galley, H. F., & Webster, N. R. (2004). Physiology of the endothelium. *British Journal of Anaesthesia*, *93*(1), 105–113. https://doi.org/10.1093/bja/aeh163

Galmiche, A., Rak, J., Roumenina, L. T., & Saidak, Z. (2022). Coagulome and the tumor microenvironment: An actionable interplay. *Trends in Cancer*, *8*(5), 369–383. https://doi.org/10.1016/j.trecan.2021.12.008

Gerotziafas, G. T., Galea, V., Mbemba, E., Khaterchi, A., Sassi, M., Baccouche, H., Prengel, C., van Dreden, P., Hatmi, M., Bernaudin, J. F., & Elalamy, I. (2012). Tissue factor over-expression by human pancreatic cancer cells BXPC3 is related to higher prothrombotic potential as compared to breast cancer cells MCF7. *Thrombosis Research*, *129*(6), 779–786. https://doi.org/10.1016/j.thromres.2011.07.049

Gersh, K. C., Nagaswami, C., & Weisel, J. W. (2009). Fibrin network structure and clot mechanical properties are altered by incorporation of erythrocytes. *Thrombosis and Haemostasis*, *102*(6), 1169–1175. https://doi.org/10.1160/TH09-03-0199

Giannotti, S., Trombi, L., Bottai, V., Ghilardi, M., D'Alessandro, D., Danti, S., Dell'Osso, G., Guido, G., & Petrini, M. (2013). Use of autologous human mesenchymal stromal

cell/fibrin clot constructs in upper limb non-unions: Long-term assessment. *PloS One*, *8*(8), e73893. https://doi.org/10.1371/journal.pone.0073893

Graf, C., Wilgenbus, P., Pagel, S., Pott, J., Marini, F., Reyda, S., Kitano, M., Macher-Göppinger, S., Weiler, H., & Ruf, W. (2019). Myeloid cell–synthesized coagulation factor X dampens antitumor immunity. *Science Immunology*, *4*(39), eaaw8405. https://doi.org/10.1126/sciimmunol.aaw8405

Gronostaj, K., Richter, P., Nowak, W., & Undas, A. (2013). Altered plasma fibrin clot properties in patients with digestive tract cancers: Links with the increased thrombin generation. *Thrombosis Research*, *131*(3), Article 3. https://doi.org/10.1016/j.thromres.2012.11.033

Grover, S. P., Hisada, Y. M., Kasthuri, R. S., Reeves, B. N., & Mackman, N. (2021). Cancer therapy associated thrombosis. *Arteriosclerosis, Thrombosis, and Vascular Biology*, *41*(4), 1291–1305. https://doi.org/10.1161/ATVBAHA.120.314378

Guadiz, G., Sporn, L. A., & Simpson-Haidaris, P. J. (1997). Thrombin cleavage-independent deposition of fibrinogen in extracellular matrices. *Blood*, *90*(7), 2644–2653.

Guedes, A. F., Carvalho, F. A., Domingues, M. M., Macrae, F. L., McPherson, H. R., Sabban, A., Martins, I. C., Duval, C., Santos, N. C., & Ariëns, R. A. (2018). Impact of γ'γ' fibrinogen interaction with red blood cells on fibrin clots. *Nanomedicine (London, England)*, *13*(19), 2491–2505. https://doi.org/10.2217/nnm-2018-0136

Han, X., Guo, B., Li, Y., & Zhu, B. (2014). Tissue factor in tumor microenvironment: A systematic review. *Journal of Hematology & Oncology*, *7*, 54. https://doi.org/10.1186/s13045-014-0054-8

Haynes, L. M., Orfeo, T., Mann, K. G., Everse, S. J., & Brummel-Ziedins, K. E. (2017). Probing the Dynamics of Clot-Bound Thrombin at Venous Shear Rates. *Biophysical Journal*, *112*(8), 1634–1644. https://doi.org/10.1016/j.bpj.2017.03.002

He, S., Cao, H., Thålin, C., Svensson, J., Blombäck, M., & Wallén, H. (2021). The Clotting Trigger Is an Important Determinant for the Coagulation Pathway In Vivo or In Vitro-Inference from Data Review. *Seminars in Thrombosis and Hemostasis*, *47*(1), 63–73. https://doi.org/10.1055/s-0040-1718888

Heilala, M., Lehtonen, A., Arasalo, O., Peura, A., Pokki, J., Ikkala, O., Nonappa, Klefström, J., & Munne, P. M. (2023). Fibrin Stiffness Regulates Phenotypic Plasticity of Metastatic Breast Cancer Cells. *Advanced Healthcare Materials*, *12*(31), 2301137. https://doi.org/10.1002/adhm.202301137

Helms, F., Zippusch, S., Theilen, J., Haverich, A., Wilhelmi, M., & Böer, U. (2022). An encapsulated fibrin-based bioartificial tissue construct with integrated macrovessels, microchannels, and capillary tubes. *Biotechnology and Bioengineering*, *119*(8), 2239–2249. https://doi.org/10.1002/bit.28111

Henke, E., Nandigama, R., & Ergün, S. (2020). Extracellular matrix in the tumor microenvironment and its impact on cancer therapy. *Frontiers in Molecular Biosciences*, *6*, 160. https://doi.org/10.3389/fmolb.2019.00160

Herre, M., Cedervall, J., Mackman, N., & Olsson, A.-K. (2023). Neutrophil extracellular traps in the pathology of cancer and other inflammatory diseases. *Physiological Reviews*, *103*(1), 277–312. https://doi.org/10.1152/physrev.00062.2021

Hethershaw, E. L., Cilia La Corte, A. L., Duval, C., Ali, M., Grant, P. J., Ariëns, R. A. S., & Philippou, H. (2014). The effect of blood coagulation factor XIII on fibrin clot structure and fibrinolysis. *Journal of Thrombosis and Haemostasis*, *12*(2), Article 2. https://doi.org/10.1111/jth.12455

Hisada, Y., Yasunaga, M., Hanaoka, S., Saijou, S., Sugino, T., Tsuji, A., Saga, T., Tsumoto, K., Manabe, S., Kuroda, J., Kuratsu, J., & Matsumura, Y. (2013). Discovery of an uncovered region in fibrin clots and its clinical significance. *Scientific Reports*, *3*(1), Article 1. https://doi.org/10.1038/srep02604

Holle, A. W., Young, J. L., & Spatz, J. P. (2016). In vitro cancer cell–ECM interactions inform in vivo cancer treatment. *Advanced Drug Delivery Reviews*, *97*, 270–279. https://doi.org/10.1016/j.addr.2015.10.007

Holliday, D. L., & Speirs, V. (2011). Choosing the right cell line for breast cancer research. *Breast Cancer Research*, *13*(4), 215. https://doi.org/10.1186/bcr2889

Hotaling, N. A., Bharti, K., Kriel, H., & Simon, C. G. (2015). DiameterJ: A Validated Open Source Nanofiber Diameter Measurement Tool. *Biomaterials*, *61*, 327–338. https://doi.org/10.1016/j.biomaterials.2015.05.015

Hotary, K. B., Yana, I., Sabeh, F., Li, X.-Y., Holmbeck, K., Birkedal-Hansen, H., Allen, E. D., Hiraoka, N., & Weiss, S. J. (2002). Matrix metalloproteinases (MMPs) regulate fibrin-

invasive activity via MT1-MMP–dependent and –independent processes. *The Journal of Experimental Medicine*, *195*(3), 295–308. https://doi.org/10.1084/jem.20010815

Huang, J., Zhang, L., Wan, D., Zhou, L., Zheng, S., Lin, S., & Qiao, Y. (2021). Extracellular matrix and its therapeutic potential for cancer treatment. *Signal Transduction and Targeted Therapy*, *6*(1), Article 1. https://doi.org/10.1038/s41392-021-00544-0

Hudson, N. E., Houser, J. R., O'Brien, E. T., Taylor, R. M., Superfine, R., Lord, S. T., & Falvo, M. R. (2010). Stiffening of Individual Fibrin Fibers Equitably Distributes Strain and Strengthens Networks. *Biophysical Journal*, *98*(8), 1632–1640. https://doi.org/10.1016/j.bpj.2009.12.4312

Hultin, S. (2012). Mosby's Manual of Diagnostic and Laboratory Tests (4th edn). *Annals of Clinical Biochemistry*, *49*(4), 415–415. https://doi.org/10.1258/acb.2012.201207

Ishikawa, S., Miyashita, T., Inokuchi, M., Hayashi, H., Oyama, K., Tajima, H., Takamura, H., Ninomiya, I., Ahmed, A. K., Harman, J. W., Fushida, S., & Ohta, T. (2016). Platelets surrounding primary tumor cells are related to chemoresistance. *Oncology Reports*, *36*(2), 787–794. https://doi.org/10.3892/or.2016.4898

Khorana, A. A., Cohen, A. T., Carrier, M., Meyer, G., Pabinger, I., Kavan, P., & Wells, P. (2020). Prevention of venous thromboembolism in ambulatory patients with cancer. *ESMO Open*, *5*(6), e000948. https://doi.org/10.1136/esmoopen-2020-000948

Kirtane, A. R., Sadhukha, T., Kim, H., Khanna, V., Koniar, B., & Panyam, J. (2017). Fibrinolytic enzyme co-therapy improves tumor perfusion and therapeutic efficacy of

anticancer nanomedicine. *Cancer Research*, *77*(6), 1465–1475. https://doi.org/10.1158/0008-5472.CAN-16-1646

Klatt, C., Krüger, I., Zey, S., Krott, K.-J., Spelleken, M., Gowert, N. S., Oberhuber, A., Pfaff, L., Lückstädt, W., Jurk, K., Schaller, M., Al-Hasani, H., Schrader, J., Massberg, S., Stark, K., Schelzig, H., Kelm, M., & Elvers, M. (2018). Platelet-RBC interaction mediated by FasL/FasR induces procoagulant activity important for thrombosis. *The Journal of Clinical Investigation*, *128*(9), 3906–3925. https://doi.org/10.1172/JCI92077

Kniebs, C., Luengen, A. E., Guenther, D., Cornelissen, C. G., Schmitz-Rode, T., Jockenhoevel, S., & Thiebes, A. L. (2021). Establishment of a Pre-vascularized 3D Lung Cancer Model in Fibrin Gel—Influence of Hypoxia and Cancer-Specific Therapeutics. *Frontiers in Bioengineering and Biotechnology*, *9*. https://doi.org/10.3389/fbioe.2021.761846

Koizume, S., Jin, M.-S., Miyagi, E., Hirahara, F., Nakamura, Y., Piao, J.-H., Asai, A., Yoshida, A., Tsuchiya, E., Ruf, W., & Miyagi, Y. (2006). Activation of cancer cell migration and invasion by ectopic synthesis of coagulation factor VII. *Cancer Research*, *66*(19), 9453–9460. https://doi.org/10.1158/0008-5472.CAN-06-1803

Koizume, S., Yokota, N., Miyagi, E., Hirahara, F., Nakamura, Y., Sakuma, Y., Yoshida, A., Kameda, Y., Tsuchiya, E., Ruf, W., & Miyagi, Y. (2009). Hepatocyte nuclear factor-4-independent synthesis of coagulation factor VII in breast cancer cells and its inhibition by targeting selective histone acetyltransferases. *Molecular Cancer Research: MCR*, *7*(12), 1928–1936. https://doi.org/10.1158/1541-7786.MCR-09-0372

Konings, J., Govers-Riemslag, J. W. P., Philippou, H., Mutch, N. J., Borissoff, J. I., Allan, P., Mohan, S., Tans, G., ten Cate, H., & Ariëns, R. A. S. (2011). Factor XIIa regulates the structure of the fibrin clot independently of thrombin generation through direct interaction with fibrin. *Blood*, *118*(14), 3942–3951. https://doi.org/10.1182/blood-2011-03-339572

Konrath, S., Mailer, R. K., & Renné, T. (2021). Mechanism, Functions, and Diagnostic Relevance of FXII Activation by Foreign Surfaces. *Hämostaseologie*, *41*(6), 489–501. https://doi.org/10.1055/a-1528-0499

Kouro, T., Himuro, H., & Sasada, T. (2022). Exhaustion of CAR T cells: Potential causes and solutions. *Journal of Translational Medicine*, *20*(1), 239. https://doi.org/10.1186/s12967-022-03442-3

Krebs, A. M., Mitschke, J., Lasierra Losada, M., Schmalhofer, O., Boerries, M., Busch, H., Boettcher, M., Mougiakakos, D., Reichardt, W., Bronsert, P., Brunton, V. G., Pilarsky, C., Winkler, T. H., Brabletz, S., Stemmler, M. P., & Brabletz, T. (2017). The EMT-activator Zeb1 is a key factor for cell plasticity and promotes metastasis in pancreatic cancer. *Nature Cell Biology*, *19*(5), 518–529. https://doi.org/10.1038/ncb3513

Kreimer, S., Belov, A. M., Ghiran, I., Murthy, S. K., Frank, D. A., & Ivanov, A. R. (2015). Mass-spectrometry-based molecular characterization of extracellular vesicles: Lipidomics and proteomics. *Journal of Proteome Research*, *14*(6), 2367–2384. https://doi.org/10.1021/pr501279t

Kumar, L., Planas-Iglesias, J., Harms, C., Kamboj, S., Wright, D., Klein-Seetharaman, J., & Sarkar, S. K. (2020). Activity-dependent interdomain dynamics of matrix metalloprotease-1 on fibrin. *Scientific Reports*, *10*(1), 20615. https://doi.org/10.1038/s41598-020-77699-3

Kwaan, H. C., & Lindholm, P. F. (2019). Fibrin and fibrinolysis in cancer. *Seminars in Thrombosis and Hemostasis*, *45*(04), 413–422. https://doi.org/10.1055/s-0039-1688495

Langhans, S. A. (2018). Three-dimensional in vitro cell culture models in drug discovery and drug repositioning. *Frontiers in Pharmacology*, *9*, 6. https://doi.org/10.3389/fphar.2018.00006

Lenting, P. J., Christophe, O. D., & Denis, C. V. (2015). von Willebrand factor biosynthesis, secretion, and clearance: Connecting the far ends. *Blood*, *125*(13), 2019–2028. https://doi.org/10.1182/blood-2014-06-528406

Li, J., Wang, Y., Li, J., & Che, G. (2021). Prognostic value of pretreatment D-dimer level in small-cell lung cancer: A meta-analysis. *Technology in Cancer Research & Treatment*, *20*, 1533033821989822. https://doi.org/10.1177/1533033821989822

Li, K., Xue, W., Lu, Z., Wang, S., Zheng, J., Lu, K., Li, M., Zong, Y., Xu, F., Dai, J., Yang, Y., & Sun, J. (2024). Tumor-derived exosomal ADAM17 promotes pre-metastatic niche formation by enhancing vascular permeability in colorectal cancer. *Journal of Experimental & Clinical Cancer Research : CR*, *43*, 59. https://doi.org/10.1186/s13046-024-02991-3

Li, M., Zhang, Y., Zhang, Q., & Li, J. (2022). Tumor extracellular matrix modulating strategies for enhanced antitumor therapy of nanomedicines. *Materials Today Bio*, *16*, 100364. https://doi.org/10.1016/j.mtbio.2022.100364

Li, W., Sigley, J., Pieters, M., Helms, C. C., Nagaswami, C., Weisel, J. W., & Guthold, M. (2016). Fibrin fiber stiffness is strongly affected by fiber diameter, but not by fibrinogen glycation. *Biophysical Journal*, *110*(6), 1400–1410. https://doi.org/10.1016/j.bpj.2016.02.021

Liang, H. P. H., Kerschen, E. J., Hernandez, I., Basu, S., Zogg, M., Botros, F., Jia, S., Hessner, M. J., Griffin, J. H., Ruf, W., & Weiler, H. (2015). EPCR-dependent PAR2 activation by the blood coagulation initiation complex regulates LPS-triggered interferon responses in mice. *Blood*, *125*(18), 2845–2854. https://doi.org/10.1182/blood-2014-11-610717

Liebmann, J. E., Cook, J. A., Lipschultz, C., Teague, D., Fisher, J., & Mitchell, J. B. (1993). Cytotoxic studies of paclitaxel (Taxol) in human tumour cell lines. *British Journal of Cancer*, *68*(6), 1104–1109.

Lim, L., Bui, H., Farrelly, O., Yang, J., Li, L., Enis, D., Ma, W., Chen, M., Oliver, G., Welsh, J. D., & Kahn, M. L. (2019). Hemostasis stimulates lymphangiogenesis through release and activation of VEGFC. *Blood*, *134*(20), 1764–1775. https://doi.org/10.1182/blood.2019001736

Lintz, M., Muñoz, A., & Reinhart-King, C. A. (2017). The mechanics of single cell and collective migration of tumor cells. *Journal of Biomechanical Engineering*, *139*(2), 0210051–0210059. https://doi.org/10.1115/1.4035121

Litvinov, R. I., Pieters, M., de Lange-Loots, Z., & Weisel, J. W. (2021). Fibrinogen and Fibrin. In J. R. Harris & J. Marles-Wright (Eds.), *Macromolecular Protein Complexes III: Structure and Function* (pp. 471–501). Springer International Publishing. https://doi.org/10.1007/978-3-030-58971-4_15

Liu, P., Wang, Y., Tong, L., Xu, Y., Zhang, W., Guo, Z., & Ni, H. (2015). Elevated preoperative plasma D-dimer level is a useful predictor of chemoresistance and poor disease outcome for serous ovarian cancer patients. *Cancer Chemotherapy and Pharmacology*, *76*(6), 1163–1171. https://doi.org/10.1007/s00280-015-2900-y

Locke, M., & Longstaff, C. (2021). Extracellular Histones Inhibit Fibrinolysis through Noncovalent and Covalent Interactions with Fibrin. *Thrombosis and Haemostasis*, *121*(4), 464–476. https://doi.org/10.1055/s-0040-1718760

Lüönd, F., Sugiyama, N., Bill, R., Bornes, L., Hager, C., Tang, F., Santacroce, N., Beisel, C., Ivanek, R., Bürglin, T., Tiede, S., van Rheenen, J., & Christofori, G. (2021). Distinct contributions of partial and full EMT to breast cancer malignancy. *Developmental Cell*, *56*(23), 3203-3221.e11. https://doi.org/10.1016/j.devcel.2021.11.006

Ma, M., Cao, R., Wang, W., Wang, B., Yang, Y., Huang, Y., Zhao, G., & Ye, L. (2021). The D-dimer level predicts the prognosis in patients with lung cancer: A systematic review

and meta-analysis. *Journal of Cardiothoracic Surgery*, *16*(1), 243. https://doi.org/10.1186/s13019-021-01618-4

Mailer, R. K., Rangaswamy, C., Konrath, S., Emsley, J., & Renné, T. (2022). An update on factor XII-driven vascular inflammation. *Biochimica et Biophysica Acta (BBA) - Molecular Cell Research*, *1869*(1), 119166. https://doi.org/10.1016/j.bbamcr.2021.119166

Majidpoor, J., & Mortezaee, K. (2021). Steps in metastasis: An updated review. *Medical Oncology (Northwood, London, England)*, *38*(1), 3. https://doi.org/10.1007/s12032-020-01447-w

Manon-Jensen, T., Kjeld, N. G., & Karsdal, M. A. (2016). Collagen-mediated hemostasis. *Journal of Thrombosis and Haemostasis*, *14*(3), 438–448. https://doi.org/10.1111/jth.13249

Mantovani, A., Marchesi, F., Malesci, A., Laghi, L., & Allavena, P. (2017). Tumour-associated macrophages as treatment targets in oncology. *Nature Reviews Clinical Oncology*, *14*(7), 399–416. https://doi.org/10.1038/nrclinonc.2016.217

Marchetti, M., Diani, E., ten Cate, H., & Falanga, A. (2012). Characterization of the thrombin generation potential of leukemic and solid tumor cells by calibrated automated thrombography. *Haematologica*, *97*(8), 1173–1180. https://doi.org/10.3324/haematol.2011.055343

Martinez-Torres, C., Grimbergen, J., Koopman, J., & Koenderink, G. H. (2024). Interplay of fibrinogen αEC globular domains and factor XIIIa cross-linking dictates the

extensibility and strain stiffening of fibrin networks. *Journal of Thrombosis and Haemostasis*, *22*(3), 715–726. https://doi.org/10.1016/j.jtha.2023.10.025

Mathivet, T., Bouleti, C., Van Woensel, M., Stanchi, F., Verschuere, T., Phng, L., Dejaegher, J., Balcer, M., Matsumoto, K., Georgieva, P. B., Belmans, J., Sciot, R., Stockmann, C., Mazzone, M., De Vleeschouwer, S., & Gerhardt, H. (2017). Dynamic stroma reorganization drives blood vessel dysmorphia during glioma growth. *EMBO Molecular Medicine*, *9*(12), 1629–1645. https://doi.org/10.15252/emmm.201607445

Matveeva, V. G., Senokosova, E. A., Sevostianova, V. V., Khanova, M. Yu., Glushkova, T. V., Akentieva, T. N., Antonova, L. V., & Barbarash, L. S. (2022). Advantages of Fibrin Polymerization Method without the Use of Exogenous Thrombin for Vascular Tissue Engineering Applications. *Biomedicines*, *10*(4), 789. https://doi.org/10.3390/biomedicines10040789

McLarnon, J. G. (2022). A Leaky Blood–Brain Barrier to Fibrinogen Contributes to Oxidative Damage in Alzheimer's Disease. *Antioxidants*, *11*(1), Article 1. https://doi.org/10.3390/antiox11010102

Metelli, A., Wu, B. X., Riesenberg, B., Guglietta, S., Huck, J. D., Mills, C., Li, A., Rachidi, S., Krieg, C., Rubinstein, M. P., Gewirth, D. T., Sun, S., Lilly, M. B., Wahlquist, A. H., Carbone, D. P., Yang, Y., Liu, B., & Li, Z. (2020). Thrombin contributes to cancer immune evasion via proteolysis of platelet-bound GARP to activate LTGF-β. *Science Translational Medicine*, *12*(525), eaay4860. https://doi.org/10.1126/scitranslmed.aay4860

Michael, J. V., Wurtzel, J. G. T., Mao, G. F., Rao, A. K., Kolpakov, M. A., Sabri, A., Hoffman, N. E., Rajan, S., Tomar, D., Madesh, M., Nieman, M. T., Yu, J., Edelstein, L. C., Rowley, J. W., Weyrich, A. S., & Goldfinger, L. E. (2017). Platelet microparticles infiltrating solid tumors transfer miRNAs that suppress tumor growth. *Blood*, *130*(5), 567–580. https://doi.org/10.1182/blood-2016-11-751099

Miller, P., Akama-Garren, E. H., Owen, R. P., Demetriou, C., Carroll, T. M., Slee, E., Al Moussawi, K., Ellis, M., Goldin, R., O'Neill, E., & Lu, X. (2023). P53 inhibitor iASPP is an unexpected suppressor of KRAS and inflammation-driven pancreatic cancer. *Cell Death & Differentiation*, *30*(7), 1619–1635. https://doi.org/10.1038/s41418-023-01168-3

Mondal, S., Adhikari, N., Banerjee, S., Amin, S. A., & Jha, T. (2020). Matrix metalloproteinase-9 (MMP-9) and its inhibitors in cancer: A minireview. *European Journal of Medicinal Chemistry*, *194*, 112260. https://doi.org/10.1016/j.ejmech.2020.112260

Morton, D., Seymour, M., Magill, L., Handley, K., Glasbey, J., Glimelius, B., Palmer, A., Seligmann, J., Laurberg, S., Murakami, K., West, N., Quirke, P., Gray, R., & FOxTROT Collaborative Group. (2023). Preoperative Chemotherapy for Operable Colon Cancer: Mature Results of an International Randomized Controlled Trial. *Journal of Clinical Oncology: Official Journal of the American Society of Clinical Oncology*, *41*(8), 1541–1552. https://doi.org/10.1200/JCO.22.00046

Mullin, J. L., Norfolk, S. E., Weisel, J. W., & Lord, S. T. (2006). Clot lysis of variant recombinant fibrinogens confirms that fiber diameter is a major determinant of lysis

rate. *Annals of the New York Academy of Sciences*, *936*(1), Article 1. https://doi.org/10.1111/j.1749-6632.2001.tb03519.x

Mushtaq, M. U., Papadas, A., Pagenkopf, A., Flietner, E., Morrow, Z., Chaudhary, S. G., & Asimakopoulos, F. (2018). Tumor matrix remodeling and novel immunotherapies: The promise of matrix-derived immune biomarkers. *Journal for Immunotherapy of Cancer*, *6*, 65. https://doi.org/10.1186/s40425-018-0376-0

Njock, M., O'Grady, T., Nivelles, O., Lion, M., Jacques, S., Cambier, M., Herkenne, S., Muller, F., Christian, A., Remacle, C., Guiot, J., Rahmouni, S., Dequiedt, F., & Struman, I. (2022). Endothelial extracellular vesicles promote tumour growth by tumour-associated macrophage reprogramming. *Journal of Extracellular Vesicles*, *11*(6), e12228. https://doi.org/10.1002/jev2.12228

Obonai, T., Fuchigami, H., Furuya, F., Kozuka, N., Yasunaga, M., & Matsumura, Y. (2016). Tumour imaging by the detection of fibrin clots in tumour stroma using an anti-fibrin Fab fragment. *Scientific Reports*, *6*(1), Article 1. https://doi.org/10.1038/srep23613

Ogunnaike, E. A., Valdivia, A., Yazdimamaghani, M., Leon, E., Nandi, S., Hudson, H., Du, H., Khagi, S., Gu, Z., Savoldo, B., Ligler, F. S., Hingtgen, S., & Dotti, G. (2021). Fibrin gel enhances the antitumor effects of chimeric antigen receptor T cells in glioblastoma. *Science Advances*, *7*(41), eabg5841. https://doi.org/10.1126/sciadv.abg5841

Oxford English Dictionary. (2023). Oxford University Press; Oxford English Dictionary. https://doi.org/10.1093/OED/3781091087

Papageorgiou, L., Alhaj Hussen, K., Thouroude, S., Mbemba, E., Cost, H., Garderet, L., Elalamy, I., Larsen, A., Van Dreden, P., Dimopoulos, M. A., Mohty, M., & Gerotziafas, G. T. (2019). Modelization of Blood-Borne Hypercoagulability in Myeloma: A Tissue-Factor-Bearing Microparticle-Driven Process. *TH Open: Companion Journal to Thrombosis and Haemostasis*, *3*(4), e340–e347. https://doi.org/10.1055/s-0039-1700885

Parrott, J. A., Whaley, P. D., & Skinner, M. K. (1993). Extrahepatic expression of fibrinogen by granulosa cells: Potential role in ovulation. *Endocrinology*, *133*(4), 1645–1649. https://doi.org/10.1210/endo.133.4.8404605

Parunov, L. A., Surov, S. S., Liang, Y., Lee, T. K., & Ovanesov, M. V. (2017). Can the diagnostic reliability of the thrombin generation test as a global haemostasis assay be improved? The impact of calcium chloride concentration. *Haemophilia*, *23*(3), 466–475. https://doi.org/10.1111/hae.13174

Petersen, M. A., Ryu, J. K., & Akassoglou, K. (2018). Fibrinogen in neurological diseases: Mechanisms, imaging and therapeutics. *Nature Reviews. Neuroscience*, *19*(5), 283–301. https://doi.org/10.1038/nrn.2018.13

Pieters, M., & Wolberg, A. S. (2019). Fibrinogen and fibrin: An illustrated review. *Research and Practice in Thrombosis and Haemostasis*, *3*(2), 161–172. https://doi.org/10.1002/rth2.12191

Pietsch, K., Storm-Johannsen, L., Schmidt-Thomée, A., & Pompe, T. (2023). Correlation between Fibrin Fibrillation Kinetics and the Resulting Fibrin Network Microstructure.

Advanced Healthcare Materials, *12*(8), 2202231. https://doi.org/10.1002/adhm.202202231

Porrello, A., Leslie, P. L., Harrison, E. B., Gorentla, B. K., Kattula, S., Ghosh, S. K., Azam, S. H., Holtzhausen, A., Chao, Y. L., Hayward, M. C., Waugh, T. A., Bae, S., Godfrey, V., Randell, S. H., Oderup, C., Makowski, L., Weiss, J., Wilkerson, M. D., Hayes, D. N., … Pecot, C. V. (2018). Factor XIIIA-expressing inflammatory monocytes promote lung squamous cancer through fibrin cross-linking. *Nature Communications*, *9*(1), 1988. https://doi.org/10.1038/s41467-018-04355-w

Qin, Y., & Xu, G. (2022). Enhancing CAR T-cell therapies against solid tumors: Mechanisms and reversion of resistance. *Frontiers in Immunology*, *13*, 1053120. https://doi.org/10.3389/fimmu.2022.1053120

Ramanujam, R. K., Maksudov, F., Litvinov, R. I., Nagaswami, C., Weisel, J. W., Tutwiler, V., & Barsegov, V. (2023). Biomechanics, Energetics, and Structural Basis of Rupture of Fibrin Networks. *Advanced Healthcare Materials*, *12*(27), 2300096. https://doi.org/10.1002/adhm.202300096

Rees, P. A., Castle, J., Clouston, H. W., Lamb, R., Singh, U., Duff, S. E., & Kirwan, C. C. (2023). The effects of coagulation factors and their inhibitors on proliferation and migration in colorectal cancer. *Cancer Medicine*, *12*(16), 17184–17192. https://doi.org/10.1002/cam4.6332

Rickles, F. R., Patierno, S., & Fernandez, P. M. (2003). Tissue factor, thrombin, and cancer. *Chest*, *124*(3 Suppl), 58S-68S. https://doi.org/10.1378/chest.124.3_suppl.58s

Rimal, R., Desai, P., Daware, R., Hosseinnejad, A., Prakash, J., Lammers, T., & Singh, S. (2022). Cancer-associated fibroblasts: Origin, function, imaging, and therapeutic targeting. *Advanced Drug Delivery Reviews*, *189*, 114504. https://doi.org/10.1016/j.addr.2022.114504

Risman, R. A., Belcher, H. A., Ramanujam, R. K., Weisel, J. W., Hudson, N. E., & Tutwiler, V. (2024). Comprehensive Analysis of the Role of Fibrinogen and Thrombin in Clot Formation and Structure for Plasma and Purified Fibrinogen. *Biomolecules*, *14*(2), 230. https://doi.org/10.3390/biom14020230

Risman, R. A., Paynter, B., Percoco, V., Shroff, M., Bannish, B. E., & Tutwiler, V. (2024). Internal fibrinolysis of fibrin clots is driven by pore expansion. *Scientific Reports*, *14*(1), 2623. https://doi.org/10.1038/s41598-024-52844-4

Rosenfeld, M. A., Leonova, V. B., Shchegolikhin, A. N., Bychkova, A. V., Kostanova, E. A., & Biryukova, M. I. (2015). Covalent structure of single-stranded fibrin oligomers cross-linked by FXIIIa. *Biochemical and Biophysical Research Communications*, *461*(2), 408–412. https://doi.org/10.1016/j.bbrc.2015.04.052

Rousseau, A., Larsen, A. K., Van Dreden, P., Sabbah, M., Elalamy, I., & Gerotziafas, G. T. (2017a). Differential contribution of tissue factor and factor XII to thrombin generation triggered by breast and pancreatic cancer cells. *International Journal of Oncology*, *51*(6), 1747–1756. https://doi.org/10.3892/ijo.2017.4172

Rousseau, A., Larsen, A. K., Van Dreden, P., Sabbah, M., Elalamy, I., & Gerotziafas, G. T. (2017b). Differential contribution of tissue factor and Factor XII to thrombin generation

triggered by breast and pancreatic cancer cells. *International Journal of Oncology*, *51*(6), 1747–1756. https://doi.org/10.3892/ijo.2017.4172

Rousseau, A., Van Dreden, P., Khaterchi, A., Mbemba, E., Larsen, A., Elalamy, I., & Gerotziafas, G. T. (2015). Acquision of Resistance to Doxorubicin By Breast Cancer Cells MCF7 Enhances Their Procoagulant Properties and Alters the Efficacy of Antithrombotic Agents to Inhibit Thrombin Generation. *Blood*, *126*(23), 1113. https://doi.org/10.1182/blood.V126.23.1113.1113

Rousseau, A., Van Dreden, P., Mbemba, E., Elalamy, I., Larsen, A., & Gerotziafas, G. T. (2015). Cancer cells BXPC3 and MCF7 differentially reverse the inhibition of thrombin generation by apixaban, fondaparinux and enoxaparin. *Thrombosis Research*, *136*(6), 1273–1279. https://doi.org/10.1016/j.thromres.2015.08.009

Rubenstein, D. A., & Yin, W. (2018). Platelet-Activation Mechanisms and Vascular Remodeling. In *Comprehensive Physiology* (pp. 1117–1156). John Wiley & Sons, Ltd. https://doi.org/10.1002/cphy.c170049

Ruf, W., & Graf, C. (2020). Coagulation signaling and cancer immunotherapy. *Thrombosis Research*, *191*, S106–S111. https://doi.org/10.1016/S0049-3848(20)30406-0

Ruggeri, Z. M. (2007). The role of von Willebrand factor in thrombus formation. *Thrombosis Research*, *120*(Suppl 1), S5–S9. https://doi.org/10.1016/j.thromres.2007.03.011

Ruggeri, Z. M., & Mendolicchio, G. L. (2007). Adhesion Mechanisms in Platelet Function. *Circulation Research*, *100*(12), 1673–1685. https://doi.org/10.1161/01.RES.0000267878.97021.ab

Saidak, Z., Soudet, S., Lottin, M., Salle, V., Sevestre, M.-A., Clatot, F., & Galmiche, A. (2021). A pan-cancer analysis of the human tumor coagulome and its link to the tumor immune microenvironment. *Cancer Immunology, Immunotherapy: CII*, *70*(4), 923–933. https://doi.org/10.1007/s00262-020-02739-w

Saito, H., Fushida, S., Miyashita, T., Oyama, K., Yamaguchi, T., Tsukada, T., Kinoshita, J., Tajima, H., Ninomiya, I., & Ohta, T. (2017). Potential of extravasated platelet aggregation as a surrogate marker for overall survival in patients with advanced gastric cancer treated with preoperative docetaxel, cisplatin and S-1: A retrospective observational study. *BMC Cancer*, *17*(1), 294. https://doi.org/10.1186/s12885-017-3279-4

Sandrine, T., Van Dreden, P., Gerotziafas, G. T., & Larsen, A. (2018). Chemoresistant Colorectal Cancer (CRC) Cells Show Increased Invasive Potential Which Is Part Is Mediated By VEGF-Signaling and Can be Attenuated By VEGF-Directed Agents. *Blood*, *132*, 4974. https://doi.org/10.1182/blood-2018-99-110202

Sanz-Horta, R., Matesanz, A., Gallardo, A., Reinecke, H., Jorcano, J. L., Acedo, P., Velasco, D., & Elvira, C. (2023). Technological advances in fibrin for tissue engineering. *Journal of Tissue Engineering*, *14*, 20417314231190288. https://doi.org/10.1177/20417314231190288

Schroeder, V., & Kohler, H. P. (2016). Factor XIII: Structure and Function. *Seminars in Thrombosis and Hemostasis*, *42*(4), 422–428. https://doi.org/10.1055/s-0036-1571341

Schumacher, D., Strilic, B., Sivaraj, K. K., Wettschureck, N., & Offermanns, S. (2013). Platelet-derived nucleotides promote tumor-cell transendothelial migration and metastasis via P2Y2 receptor. *Cancer Cell*, *24*(1), 130–137. https://doi.org/10.1016/j.ccr.2013.05.008

Sébert, M., Denadai-Souza, A., Quaranta, M., Racaud-Sultan, C., Chabot, S., Lluel, P., Monjotin, N., Alric, L., Portier, G., Kirzin, S., Bonnet, D., Ferrand, A., & Vergnolle, N. (2018). Thrombin modifies growth, proliferation and apoptosis of human colon organoids: A protease-activated receptor 1- and protease-activated receptor 4-dependent mechanism. *British Journal of Pharmacology*, *175*(18), 3656–3668. https://doi.org/10.1111/bph.14430

Seltana, A., Cloutier, G., Reyes Nicolas, V., Khalfaoui, T., Teller, I. C., Perreault, N., & Beaulieu, J.-F. (2022). Fibrin(ogen) Is Constitutively Expressed by Differentiated Intestinal Epithelial Cells and Mediates Wound Healing. *Frontiers in Immunology*, *13*, 916187. https://doi.org/10.3389/fimmu.2022.916187

Sensi, F., D'Angelo, E., D'Aronco, S., Molinaro, R., & Agostini, M. (2019). Preclinical three-dimensional colorectal cancer model: The next generation of in vitro drug efficacy evaluation: SENSI ET AL. *Journal of Cellular Physiology*, *234*(1), Article 1. https://doi.org/10.1002/jcp.26812

Seo, J., Al-Hilal, T. A., Jee, J.-G., Kim, Y.-L., Kim, H.-J., Lee, B.-H., Kim, S., & Kim, I.-S. (2018). *A targeted ferritin-microplasmin based thrombolytic nanocage selectively dissolves blood clots*. 10.

Seo, J., Do Yoo, J., Kim, M., Shim, G., Oh, Y.-K., Park, R.-W., Lee, B., Kim, I.-S., & Kim, S. (2021). Fibrinolytic nanocages dissolve clots in the tumor microenvironment, improving the distribution and therapeutic efficacy of anticancer drugs. *Experimental & Molecular Medicine*, *53*(10), 1592–1601. https://doi.org/10.1038/s12276-021-00688-7

Shaashua, L., Ben-Shmuel, A., Pevsner-Fischer, M., Friedman, G., Levi-Galibov, O., Nandakumar, S., Barki, D., Nevo, R., Brown, L. E., Zhang, W., Stein, Y., Lior, C., Kim, H. S., Bojmar, L., Jarnagin, W. R., Lecomte, N., Mayer, S., Stok, R., Bishara, H., … Scherz-Shouval, R. (2022). BRCA mutational status shapes the stromal microenvironment of pancreatic cancer linking clusterin expression in cancer associated fibroblasts with HSF1 signaling. *Nature Communications*, *13*(1), 6513. https://doi.org/10.1038/s41467-022-34081-3

Shaker, H., Bundred, N. J., Landberg, G., Pritchard, S. A., Albadry, H., Nicholson, S. L., Harries, L. J., Heah, J. Y. E., Castle, J., & Kirwan, C. C. (2020). Breast cancer stromal clotting activation (Tissue Factor and thrombin): A pre-invasive phenomena that is prognostic in invasion. *Cancer Medicine*, *9*(5), 1768–1778. https://doi.org/10.1002/cam4.2748

Sharma, V., Blackwood, K. A., Haddow, D., Hook, L., Mason, C., Dye, J. F., & García-Gareta, E. (2015). Method for estimating protein binding capacity of polymeric systems. *Biochimie Open*, *1*, 40–50. https://doi.org/10.1016/j.biopen.2015.10.001

Simpson-Haidaris, P. J., Courtney, M.-A., Wright, T. W., Goss, R., Harmsen, A., & Gigliotti, F. (1998). Induction of Fibrinogen Expression in the Lung Epithelium during

Pneumocystis carinii Pneumonia. *Infection and Immunity*, *66*(9), 4431–4439. https://doi.org/10.1128/iai.66.9.4431-4439.1998

Singh, R., Gautam, P., Sharma, C., & Osmolovskiy, A. (2023). Fibrin and Fibrinolytic Enzyme Cascade in Thrombosis: Unravelling the Role. *Life*, *13*(11), Article 11. https://doi.org/10.3390/life13112196

Starmans, L. W. E., van Mourik, T., Rossin, R., Verel, I., Nicolay, K., & Grüll, H. (2015). Noninvasive visualization of tumoral fibrin deposition using a peptidic fibrin-binding single photon emission computed tomography tracer. *Molecular Pharmaceutics*, *12*(6), Article 6. https://doi.org/10.1021/mp500673u

Stellos, K., Langer, H., Daub, K., Schoenberger, T., Gauss, A., Geisler, T., Bigalke, B., Mueller, I., Schumm, M., Schaefer, I., Seizer, P., Kraemer, B. F., Siegel-Axel, D., May, A. E., Lindemann, S., & Gawaz, M. (2008). Platelet-derived stromal cell-derived factor-1 regulates adhesion and promotes differentiation of human CD34+ cells to endothelial progenitor cells. *Circulation*, *117*(2), 206–215. https://doi.org/10.1161/CIRCULATIONAHA.107.714691

Stock, K., Estrada, M. F., Vidic, S., Gjerde, K., Rudisch, A., Santo, V. E., Barbier, M., Blom, S., Arundkar, S. C., Selvam, I., Osswald, A., Stein, Y., Gruenewald, S., Brito, C., van Weerden, W., Rotter, V., Boghaert, E., Oren, M., Sommergruber, W., … Graeser, R. (2016). Capturing tumor complexity in vitro: Comparative analysis of 2D and 3D tumor models for drug discovery. *Scientific Reports*, *6*(1), Article 1. https://doi.org/10.1038/srep28951

Sun, S., Campello, E., Zou, J., Konings, J., Huskens, D., Wan, J., Fernández, D. I., Reutelingsperger, C. P. M., Ten Cate, H., Toffanin, S., Bulato, C., de Groot, P. G., de Laat, B., Simioni, P., Heemskerk, J. W. M., & Roest, M. (2023). Crucial roles of red blood cells and platelets in whole blood thrombin generation. *Blood Advances*, *7*(21), 6717–6731. https://doi.org/10.1182/bloodadvances.2023010027

Tan, M. H., Nowak, N. J., Loor, R., Ochi, H., Sandberg, A. A., Lopez, C., Pickren, J. W., Berjian, R., Douglass, H. O., & Chu, T. M. (1986). Characterization of a New Primary Human Pancreatic Tumor Line. *Cancer Investigation*, *4*(1), 15–23. https://doi.org/10.3109/07357908609039823

Thielmann, C. M., Costa da Silva, M., Muley, T., Meister, M., Herpel, E., & Muckenthaler, M. U. (2019). Iron accumulation in tumor-associated macrophages marks an improved overall survival in patients with lung adenocarcinoma. *Scientific Reports*, *9*(1), 11326. https://doi.org/10.1038/s41598-019-47833-x

Thijs, T., Nuyttens, B. P., Deckmyn, H., & Broos, K. (2010). *Platelet physiology and antiplatelet agents*. *48*(s1), S3–S13. https://doi.org/10.1515/cclm.2010.363

Tiruvannamalai Annamalai, R., Rioja, A. Y., Putnam, A. J., & Stegemann, J. P. (2016). Vascular Network Formation by Human Microvascular Endothelial Cells in Modular Fibrin Microtissues. *ACS Biomaterials Science & Engineering*, *2*(11), 1914–1925. https://doi.org/10.1021/acsbiomaterials.6b00274

Tomaiuolo, M., Brass, L. F., & Stalker, T. J. (2017). Regulation of platelet activation and coagulation and its role in vascular injury and arterial thrombosis. *Interventional Cardiology Clinics*, *6*(1), 1–12. https://doi.org/10.1016/j.iccl.2016.08.001

Tomashefski, J. F., Abramowsky, C. R., Chung-Park, M., Wisniewska, J., & Bruce, M. C. (1992). Immunofluorescence studies of lung tissue in cystic fibrosis. *Pediatric Pathology*, *12*(3), 313–324. https://doi.org/10.3109/15513819209023312

Ukan, Ü., Delgado Lagos, F., Kempf, S., Günther, S., Siragusa, M., Fisslthaler, B., & Fleming, I. (2022). Effect of Thrombin on the Metabolism and Function of Murine Macrophages. *Cells*, *11*(10), 1718. https://doi.org/10.3390/cells11101718

van der Meijden, P. E. J., & Heemskerk, J. W. M. (2019). Platelet biology and functions: New concepts and clinical perspectives. *Nature Reviews Cardiology*, *16*(3), Article 3. https://doi.org/10.1038/s41569-018-0110-0

Varjú, I., Sótonyi, P., Machovich, R., Szabó, L., Tenekedjiev, K., Silva, M. M. C. G., Longstaff, C., & Kolev, K. (2011). Hindered dissolution of fibrin formed under mechanical stress. *Journal of Thrombosis and Haemostasis: JTH*, *9*(5), 979–986. https://doi.org/10.1111/j.1538-7836.2011.04203.x

Versteeg, H. H. (2015). Tissue Factor: Old and New Links with Cancer Biology. *Seminars in Thrombosis and Hemostasis*, *41*(7), 747–755. https://doi.org/10.1055/s-0035-1556048

Wahab, R., Hasan, M. M., Azam, Z., Grippo, P. J., & Al-Hilal, T. A. (2023). The role of coagulome in the tumor immune microenvironment. *Advanced Drug Delivery Reviews*, *200*, 115027. https://doi.org/10.1016/j.addr.2023.115027

Wautier, J.-L., & Wautier, M.-P. (2022). Vascular Permeability in Diseases. *International Journal of Molecular Sciences*, *23*(7), 3645. https://doi.org/10.3390/ijms23073645

Weisel, J. W., & Litvinov, R. I. (2017). Fibrin Formation, Structure and Properties. *Sub-Cellular Biochemistry*, *82*, 405–456. https://doi.org/10.1007/978-3-319-49674-0_13

Weisel, J. W., & Nagaswami, C. (1992). Computer modeling of fibrin polymerization kinetics correlated with electron microscope and turbidity observations: Clot structure and assembly are kinetically controlled. *Biophysical Journal*, *63*(1), 111–128.

Welsh, J. (2013). Chapter 40—Animal Models for Studying Prevention and Treatment of Breast Cancer. In P. M. Conn (Ed.), *Animal Models for the Study of Human Disease* (pp. 997–1018). Academic Press. https://doi.org/10.1016/B978-0-12-415894-8.00040-3

Wolberg, A. S. (2007). Thrombin generation and fibrin clot structure. *Blood Reviews*, *21*(3), 131–142. https://doi.org/10.1016/j.blre.2006.11.001

Wolberg, A. S. (2023). Fibrinogen and fibrin: Synthesis, structure, and function in health and disease. *Journal of Thrombosis and Haemostasis: JTH*, *21*(11), 3005–3015. https://doi.org/10.1016/j.jtha.2023.08.014

Wu, R., Ma, R., Duan, X., Zhang, J., Li, K., Yu, L., Zhang, M., Liu, P., & Wang, C. (2023). Identification of specific prognostic markers for lung squamous cell carcinoma based on tumor progression, immune infiltration, and stem index. *Frontiers in Immunology*, *14*, 1236444. https://doi.org/10.3389/fimmu.2023.1236444

Yau, J. W., Teoh, H., & Verma, S. (2015). Endothelial cell control of thrombosis. *BMC Cardiovascular Disorders*, *15*, 130. https://doi.org/10.1186/s12872-015-0124-z

Yeow, Y. L., Kotamraju, V. R., Wang, X., Chopra, M., Azme, N., Wu, J., Schoep, T. D., Delaney, D. S., Feindel, K., Li, J., Kennedy, K. M., Allen, W. M., Kennedy, B. F., Larma, I., Sampson, D. D., Mahakian, L. M., Fite, B. Z., Zhang, H., Friman, T., … Hamzah, J. (2019). Immune-mediated ECM depletion improves tumour perfusion and payload delivery. *EMBO Molecular Medicine*, *11*(12), e10923. https://doi.org/10.15252/emmm.201910923

Yin, T., He, S., Liu, X., Jiang, W., Ye, T., Lin, Z., Sang, Y., Su, C., Wan, Y., Shen, G., Ma, X., Yu, M., Guo, F., Liu, Y., Li, L., Hu, Q., Wang, Y., & Wei, Y. (2015). Extravascular Red Blood Cells and Hemoglobin Promote Tumor Growth and Therapeutic Resistance as Endogenous Danger Signals. *The Journal of Immunology*, *194*(1), 429–437. https://doi.org/10.4049/jimmunol.1400643

Yokota, N., Koizume, S., Miyagi, E., Hirahara, F., Nakamura, Y., Kikuchi, K., Ruf, W., Sakuma, Y., Tsuchiya, E., & Miyagi, Y. (2009). Self-production of tissue factor-coagulation factor VII complex by ovarian cancer cells. *British Journal of Cancer*, *101*(12), 2023–2029. https://doi.org/10.1038/sj.bjc.6605406

Yu, M., Ma, X., Jiang, D., Wang, L., Zhan, Q., & Zhao, J. (2021). CXC chemokine ligand 5 (CXCL5) disrupted the permeability of human brain microvascular endothelial cells via regulating p38 signal. *Microbiology and Immunology*, *65*(1), 40–47. https://doi.org/10.1111/1348-0421.12854

Ząbczyk, M., Natorska, J., & Undas, A. (2021). Factor XIII and Fibrin Clot Properties in Acute Venous Thromboembolism. *International Journal of Molecular Sciences*, *22*(4), Article 4. https://doi.org/10.3390/ijms22041607

Zhang, B., Pang, Z., & Hu, Y. (2020). Targeting hemostasis-related moieties for tumor treatment. *Thrombosis Research*, *187*, 186–196. https://doi.org/10.1016/j.thromres.2020.01.019

Zhang, S.-R., Yao, L., Wang, W.-Q., Xu, J.-Z., Xu, H.-X., Jin, W., Gao, H.-L., Wu, C.-T., Qi, Z.-H., Li, H., Li, S., Ni, Q.-X., Yu, X.-J., Fu, D.-L., & Liu, L. (2018). Tumor-Infiltrating Platelets Predict Postsurgical Survival in Patients with Pancreatic Ductal Adenocarcinoma. *Annals of Surgical Oncology*, *25*(13), 3984–3993. https://doi.org/10.1245/s10434-018-6727-8

Zhang, T., Ma, Z., Wang, R., Wang, Y., Wang, S., Cheng, Z., Xu, H., Jin, X., Li, W., & Wang, X. (2010). Thrombin facilitates invasion of ovarian cancer along peritoneum by inducing monocyte differentiation toward tumor-associated macrophage-like cells. *Cancer Immunology, Immunotherapy*, *59*(7), 1097–1108. https://doi.org/10.1007/s00262-010-0836-y

Zhmurov, A., Protopopova, A. D., Litvinov, R. I., Zhukov, P., Mukhitov, A. R., Weisel, J. W., & Barsegov, V. (2016). Structural Basis of Interfacial Flexibility in Fibrin Oligomers. *Structure*, *24*(11), 1907–1917. https://doi.org/10.1016/j.str.2016.08.009

Zhu, S., Chen, J., & Diamond, S. L. (2018). Establishing the Transient Mass Balance of Thrombosis: From Tissue Factor to Thrombin to Fibrin Under Venous Flow.

Arteriosclerosis, Thrombosis, and Vascular Biology, *38*(7), 1528–1536. https://doi.org/10.1161/ATVBAHA.118.310906

Zhu, X., Li, Q., & Zhu, X. (2022). Mechanisms of CAR T cell exhaustion and current counteraction strategies. *Frontiers in Cell and Developmental Biology*, *10*, 1034257. https://doi.org/10.3389/fcell.2022.1034257

Zou, Z., Denny, E., Brown, C. E., Jensen, M. C., Li, G., Fujii, T., Neman, J., Jandial, R., & Chen, M. (2012). Cytotoxic T lymphocyte trafficking and survival in an augmented fibrin matrix carrier. *PLoS ONE*, *7*(4), Article 4. https://doi.org/10.1371/journal.pone.0034652

ANNEX

PUBLICATIONS

1. Research article in Thrombosis Research (2024):

1.1. The procoagulant signature of cancer cells drives fibrin network formation in tumor microenvironment and impacts its quality. Implications in cancer cell migration and the resistance to anticancer agents

Thrombosis Research 238 (2024) 172–183

Contents lists available at ScienceDirect

Thrombosis Research

journal homepage: www.elsevier.com/locate/thromres

Full Length Article

The procoagulant signature of cancer cells drives fibrin network formation in tumor microenvironment and impacts its quality. Implications in cancer cell migration and the resistance to anticancer agents

Huong Chi Mai Tran [a,b], Elisabeth Mbemba [a], Noémie Mourot [a], Beshoy Faltas [a], Aurélie Rousseau [b], Elmina Lefkou [a], Michèle Sabbah [a], Patrick van Dreden [a,b], Grigoris Gerotziafas [a,c,*]

[a] Sorbonne University, INSERM UMR_S 938, Saint-Antoine Research Center (CRSA), Team "Cancer Biology and Therapeutics", Group "Cancer - Angiogenesis – Thrombosis", University Institute of Cancerology (UIC), 34 Rue du Crozatier, F-75012 Paris, France
[b] Clinical Research Department, Diagnostica Stago, 125 Avenue Louis Roche, 92230 Gennevilliers, France
[c] Thrombosis Center, Tenon - Saint Antoine University Hospital,Hôpitaux Universitaires Est Parisien, Assitance Publique Hôpitaix de Paris (AP-HP), 4 Rue de la Chine, 75020 Paris, France

ARTICLE INFO

Keywords:
Cancer
Thrombosis
Microenvironment
D-dimer
Fibrin
Fibrinolysis

ABSTRACT

Introduction: Cancer cells induce hypercoagulability in the tumoral microenvironment by expressing Tissue Factor (TF). We aimed to study the impact of the procoagulant signature of cancer cells on the quality and structure of fibrin network. We also studied the impact of fibrin clot shield (FCS) on the efficiency of anticancer agents and the migration of cancer cells.

Materials and methods: Pancreatic cancer cells BXPC3 and breast cancer cells MDA-MB231 and MCF7, were cultured in the presence of normal Platelet Poor Plasma (PPP), diluted 10 % in conditioning media. Their potential to induce thrombin generation and their fibrinolytic activity were assessed. The structure of fibrin network was analyzed with Scanning Electron Microscopy (SEM). Cancer cells' mobility with fibrin clot and their interactions with fibrin were observed. Cancer cells were treated with paclitaxel (PTX) or 4-hydroxy-tamoxifen (4OHTam) in the presence or absence of FCS.

Results: Cancer cells, in presence of PPP, induced fibrin network formation. High TF-expressing cancer cells (BXPC3 and MDA-MB23 cells), led to dense fibrin network with fine fibers. Low TF expressing cells MCF7 led to thick fibers. Exogenous TF enhanced the density of fibrin network formed by MCF7 cells. Cancer cells through their inherent profibrinolytic potential migrated within the fiber scaffold. The BXPC3 and MCF7 cells moved in clusters whereas the MDA-MB231 cells moved individually within the fibrin network. FCS decreased the efficiency of PTX and 4OHTam on the viability of cancer cells.

Conclusions: The procoagulant signature of cancer cells is determinant for the quality and structure of fibrin network in the microenvironment. Original SEM images show the architecture of "bird's nest"-like fibrin network being in touch with the cell membranes and surrounding cancer cells. Fibrin network constructed by triggering thrombin generation by cancer cells, provides a scaffold for cell migration. Fibrin clot shields protect cancer cells against PTX and 4OHTam.

Abbreviations: 4OHTam, 4-hydroxy-tamoxifen; BXPC3, biopsy xenograft of pancreatic carcinoma cell line; CAR-T cells, chimeric antigenic receptor-T cells; ELISA, enzyme-linked immunosorbent Assay; ETP, endogenous thrombin potential; FCS, fibrin clot shield; HMDS, hexamethyldisilazane; IC50, half maximal inhibitory concentration; ICAM-1, intercellular adhesion molecule; LSCM, Laser Scanning Confocal Microscopy; MCF7, Michigan Cancer Foundation-7 Cells; MDA-MB23, MD Anderson-Metastatic Breast-231 Cells; MMP, matrix metalloproteinases; MTT, 3-(4,5-dimethylthiazol-2-yl)-2,5-diphenyltetrazolium bromide; PBS, phosphate-buffered saline; PFA, paraformaldehyde; PPP, platelet poor plasma; PTX, paclitaxel; SEM, Scanning Electron Microscopy; TF, tissue factor; TGF-β, transforming growth factor-beta; TMB, 3,3′,5,5′-tetramethylbenzidine; tPA, tissue plasminogen activator; uPA, urokinase plasminogen activator; VEGF, vascular endothelial growth factor.

* Corresponding author at: Saint-Antoine Research Center, CRSA, AP-HP, Saint-Antoine Hospital, 34 Rue du Crozatier, F-75012 Paris, France.
E-mail address: grigorios.gerotziafas@inserm.fr (G. Gerotziafas).

https://doi.org/10.1016/j.thromres.2024.04.015
Received 16 January 2024; Received in revised form 2 April 2024; Accepted 15 April 2024
Available online 17 April 2024

1. Introduction

Solid tumor is a complex system, dominated by the interactions of cancer cells with the microenvironment, where vessels and blood components, including coagulation proteins, play an important role in tumor development and metastasis. Neoangiogenesis and vascular mimicry are essential procedures driven by cancer cells that allow tumor supply with nutrients and energy [1–6]. Some populations of cancer cells within the tumor are in contact with blood, and in consequence, with coagulation and fibrinolysis factors.

Cancer cells express tissue factor (TF), the principal activator of blood coagulation that drives thrombin generation, leading to fibrin clot formation [6–10]. The histological type and the aggressiveness of cancer cells are linked to TF expression and their procoagulant potential [9]. In addition, cancer cells release TF-bearing procoagulant exosomes, which amplify the procoagulant stimulus in the microenvironment [4,7,11].

Cleavage of fibrinogen by thrombin, polymerization of fibrin monomers and stabilization of the fibrin network by the thrombin-activated factor XIII are the ultimate steps of coagulation activation leading to clot formation [12–15]. Fibrin is degraded by plasmin, following the cleavage of plasminogen by urokinase plasminogen activator (uPA) or tissue plasminogen activator (tPA). Fibrinolysis and extracellular matrix remodeling are key mechanisms in the metastasis process [6,16].

The remodeling of the extracellular matrix by cancer cells supports proliferation, metastasis, angiogenesis, lymphangiogenesis, and immunosuppression [17–23]. Fibrin is a substantial element in the tumor microenvironment, evident in pathological specimens of tumors from patients [24–26]. Furthermore, a link has been established between the stage and aggressiveness of cancer and the quantity of fibrin in the tumor microenvironment [25].

The present study explores the qualitative and quantitative characteristics of fibrin clot formation upon the activation of coagulation by TF-expressing cancer cells. It presents original evidence proving that cancer cells lead to fibrin clot network formation that is structured like a "bird's nest" in contact with cancer cell membranes. Cancer cells with their proper procoagulant signature construct the fiber network that provides a scaffold for the migration. The histological type of TF-expressing cancer cells and their procoagulant signature are determinants of the architecture and structural characteristics of the fiber network. The fibrin network functions as a protecting barrier against the anticancer agents, such as paclitaxel and 4-hydroxy-tamoxifen. In addition, cancer cells by creating the "birds' nest"-like clot get a scaffold for their migration within the fibrin network.

2. Methods

2.1. Cancer cell conventional cultures

Pancreatic adenocarcinoma cells with high invasive potential BXPC3, the aggressive triple-negative breast adenocarcinoma cells MDA-MB231 and the estrogen receptor positive with lower invasive potential breast adenocarcinoma cells MCF7 were cultured in RPMI-1640 media, supplemented with 10 % Fetal Bovine Serum, 1 % Penicillin/Streptomycin, 1 % L-Glutamine, at 37 °C, 5 % CO_2 and 100 % humidity.

2.2. 3D cancer cell cultures

Cells were seeded (3×10^3 cells/well) in low-attachment 96-wells plate (Nucleon Sphera, Thermo Fisher, Massachusetts, USA). Spheroids were used at 4 days old.

2.3. Fibrin network formation in the presence of cancer cells

Fibrin network formation was induced by culturing cancer cells in the presence of platelet poor plasma (PPP) obtained from the French Blood Establishment (Saint Antoine Hospital, Paris, France). To determine the optimal dilution of PPP in culture media, cancer cells' viability and capacity to induce thrombin generation were measured in serial dilutions of PPP, ranging from 10 % to 75 %. The dilution of 10 % was selected to be used (PPP-conditioned media). In this condition the viability of the cells was preserved, thrombin generation was measurable and fibrin network formation was warranted (Supplementary Fig. S1).

2.4. Thrombin generation assessment

The Calibrated Automated Thrombogram assay (Thrombinoscope™, Diagnostica Stago, Asnières, France) was used to measure thrombin generation.

2.5. Thrombin generation experiments in the presence of increasing concentrations of TF

The PPP-Reagent HIGH® (Diagnostica Stago, Asnières, France) was diluted in the STA® Owren-Koller buffer (Diagnostica Stago, Asnières, France) to yield a final concentrations of 0.5 pM, 1 pM, and 2 pM of TF in the experimental milieu. In each well of a 96-wells microplate, a volume of 20 µl of TF solution was mixed with 80 µl of the PPP-conditioned media. Thrombin generation was initiated by the addition of 20 µl triggering solution comprising $CaCl_2$ (16.7 mM final concentration) and a fluorogenic substrate of thrombin (Z-Gly-Gly-Arg-AMC, 417 mM final concentration). Among thrombogram parameters, the lag-time, endogenous thrombin potential (ETP) and Peak were retrieved with the Calibrated Automated Thrombogram software (CAT®) and analyzed.

2.6. Thrombin generation in the presence of cancer cells

Cancer cells were seeded at a density of 5×10^3 cells/well in each well of the 96-well microplate. In the control experiment, PBS buffer (20 µl) was mixed with 80 µl of PPP-conditioned media. Exogenous TF (PRP Reagent®, Diagnostica Stago, Asnières, France) was added to MCF7 cells cultures in PPP-conditioned media at a final concentration of 1 pM. Thrombin generation was initiated by the addition of 20 µl triggering solution and thrombogram parameters were analyzed as described above.

2.7. Viability assessment of cancer cells within the fibrin clot

For MTT [3-(4,5-dimethylthiazol-2-yl)-2,5-diphenyltetrazolium bromide] assay, cells were seeded (12.5×10^4 cells/ml) in chambered coverglass (Nunc, Thermo Fischer, Massachusetts, USA). Fibrin clot was formed as described above, with the addition of 25 µg/ml of fluorescent fibrinogen (Thermo Fisher, Massachusetts, USA). After 24 h incubation, a MTT solution (4 g/l) was added. Images of formazan crystals and fibrin networks were obtained with a fluorescent microscope analysis (EVOS, Thermo Fisher, Massachusetts, USA).

Cell viability was studied by Resazurin assay by adding Resazurin solution to the final concentration of 0.2 mg/ml to each well, followed by incubation for 4 h at 37 °C, and fluorescence measurement at excitation/emission lengths at 530/590 nm.

2.8. Fibrin clot structure analysis

2.8.1. Scanning Electron Microscopy (SEM)

Cells were seeded in a 12-wells plate at density of 3×10^5 cells/well, on glass coverslips (φ 18 mm), for 24 h, before replacing their culture media with a media supplemented with 10 % PPP. After 24 h, culture media was carefully removed.

Clots were rinsed with PBS before being immersed overnight at 4 °C in a fixative solution of 2 % EM-grade glutaraldehyde in 0.1 M

cacodylate buffer pH 7.4 (Agar Scientific or Delta Microscopies). The samples were then rinsed with 0.1 M cacodylate buffer. Then, samples were incubated for 20 min in 0.1 M cacodylate buffer containing 1 % osmium tetroxide (Delta Microscopies, Mauressac, France), thoroughly rinsed with distilled water, and dehydrated using a graded concentration of ethanol (50 %–70 %–90 %–100 %). Samples were immersed in a 1:1 mixture of ethanol and hexamethyldisilazane (HMDS), before pure HMDS, followed by drying in a vacuum desiccator. Finally, samples were mounted on stubs, platinum-sputtered (ACE600, Leica microsystems, Nanterre, France), and inspected with a 3 kV high-resolution Field-Emission SEM (GeminiSEM500, Zeiss, Perigny, France) with a 20 μm objective aperture diameter. Secondary electrons were collected with in-lens or Everhart-Thornley detectors and scan speed and line integration were adjusted during observation.

Fiber diameters, pore sizes and the number of intersections were calculated using the Fiji software (version 1.53 t), using the DiameterJ plugin, as described elsewhere [27]. Fibers and pores in the bottom layers would seem smaller in pictures due to perspective. To avoid this artifact, only the top layers' fibers and pores were examined.

2.8.2. Laser Scanning Confocal Microscopy (LSCM)

Cells were cultured in a 12-wells plate (3×10^5 cells/well), on glass coverslips (φ 18 mm), for 24 h. Afterwards, the culture media was replaced with a media supplemented with 10 % PPP and 2.5 μg/ml of Fibrinogen coupled with Alexa Fluor 488 (Thermo Fisher, Massachusetts, USA). After 24 h, culture media was carefully removed, clots were fixed with 4 % Paraformaldehyde (PFA) in PBS, washed 3 times in PBS, and mounted between coverslip and slide. Images were obtained with FV3000 microscope (Olympus, Tokyo, Japan). Z positions for z-stack imaging were determined manually. Imaris software (version 10.1.0, Oxford Instruments) and Fiji (version 1.54f, NIH, USA) was used for deconvolution, and 3D reconstruction.

2.9. Study of fibrinolysis

Cells were cultured in a 12-well plate (3×10^5 cells/well) for 24 h before replacing the culture media with either PPP conditioned media or 10 % PBS (control experiment). Cell-free PPP conditioned media was also used as a control. Supernatants were collected at predefined intervals (0, 6, 10, 12, 14, 18, 24, 48, and 72 h) for D-Dimers and tPA measurement using commercially available ELISA methods (Asserachrom D-Di and Asserachrom tPA respectively, from Diagnostica Stago, Asnières, France). The assays were performed according to the manufacturer's instructions. Briefly, 200 μl of the pure supernatant or diluted in buffer solution, were deposited and incubated for 2 h in each well. After 5 washes, an anti-D-Dimer or anti-tPA antibody coupled to peroxidase was added, followed by another 2-h incubation. After 5 washes, 3,3′,5,5′-tetramethylbenzidine (TMB) was added. The reaction was stopped by the addition of H_2SO_4. The absorbance was measured at 450 nm (Tecan Infinite 200 Pro Spectrophotometer – Microplate reader, Männedorf, Suisse).

2.10. Fluorescence intensity quantification

Cells were cultured in a 12-wells plate (3×10^5 cells/well), on glass coverslips (φ 18 mm), for 24 h, then nuclei were marked with Hoechst 33342 (Thermo Fischer, Massachusetts, USA) and culture media was replaced by PPP conditioned media, in the presence or absence of 2.5 μg/ml of fibrinogen coupled with Alexa Fluor 488 (Thermo Fisher, Massachusetts, USA). After incubation for 24 h, fibrin clots were removed, and the remaining cells on the coverslip were fixed with 4 % paraformaldehyde in PBS, washed 3 times in PBS, and mounted between coverslip and slide.

Images of were obtained with a fluorescent microscope (Olympus IX83, Olympus, Tokyo, Japan). Cell Detection plugins in QuPath software (version 0.4.1) was used to isolate each individual cell base on the blue channel. Then, the intensity of the green channel was measured and divided by the total number of cells. No threshold or any contrast/brightness adjustments were conducted.

2.11. Efficacy of the anticancer treatments in the presence or absence of fibrin clot network

The anticancer effect of paclitaxel and 4-hydroxy-tamoxifen (4OHTam) was studied using the usual procedure for *in vitro* evaluation of the efficiency of the anticancer agents and in the presence of fibrin clot [28,29].

2.11.1. Conventional model for the evaluation of the efficiency of anticancer agents

Cancer cells were cultured at conditioning media followed by addition of the studied anticancer agent [28]. Herein BXPC3, MDA-MB231 and MCF7 cells were cultured in a 96-wells plate (3×10^3 cells/well) for 24 h in conditioned media (RPMI-1640) in order to achieve maximum cell adhesion. Subsequently, the conditioned media was replaced by a new solution of RPMI-1640 with the studied anticancer agents: paclitaxel (Taxol®) from Thermo Fisher (Massachusetts, USA) for the BXPC3, MDA-MB231 and MCF7 cells or 4-hydroxy-tamoxifen (4OHTam) obtained from Selleckchem, (Texas, USA) for the MCF7 at increasing concentrations. In the control experiment, cancer cells were treated with DMSO instead of anticancer agents. The concentration of the anticancer agents that reduced the viability of cancer cells by 50 % (IC50) as compared to the control condition was calculated after exposure for 72 h.

2.11.2. Fibrin clot shield model for the evaluation of the efficiency of anticancer agents

BXPC3, MDA-MB231 and MCF7 cells were cultured in a 96-wells plate (3×10^3 cells/well) for 24 h in conventional conditioned media (RPMI-1640) in order to achieve maximum cell adhesion. Subsequently, the conventional conditioned media was replaced by PPP-conditioned media (50 μl) and clot formation was formed. In 2 h after the addition of the PPP-conditioned media and following visual confirmation of clot formation, 50 μl of PPP-conditioned media containing the studied anticancer agents at the IC50 final concentration (calculated for the total volume of the PPP-conditioned media). In the control experiment, cancer cells were treated with DMSO instead of the anticancer agents. The cell viability was measured after 72 h of exposure to anticancer the agents, and compared to the control condition.

2.12. Statistical analysis

Statistical analysis was conducted using GraphPad Prism (version 9.5.1, GraphPad Software Inc., California, USA). Data were first verified for normal distribution. In case of normal distribution, parametric ANOVA test was used. Non-parametric Kruskal-Wallis test, followed by a post-hoc study, was used in case of non-normal distribution. The threshold for statistical significance (p) was set at 0.05.

3. Results

3.1. Impact of TF on the structure of fibrin clot

Increase of TF concentration (0.5 pM, 1 pM and 2 pM), in PPP-conditioned media, in the absence of cancer cells resulted in a concentration-dependent decrease of the lag-time and increase of the ETP and Peak of thrombin generation (Fig. 1A, B, C, D).

Clots were analyzed by SEM (Fig. 1E). Increase of TF concentrations resulted in decrease of fiber diameters (0.104 ± 0.007 μm, 0.094 ± 0.003 μm and 0.091 ± 0.001 μm for 0.5, 1 and 2 pM of TF respectively) and pore size (0.093 ± 0.005 μm^2, 0.075 ± 0.003 μm^2, and 0.067 ± 0.001 μm^2 for 0.5, 1 and 2 pM of TF respectively). On the other hand, the

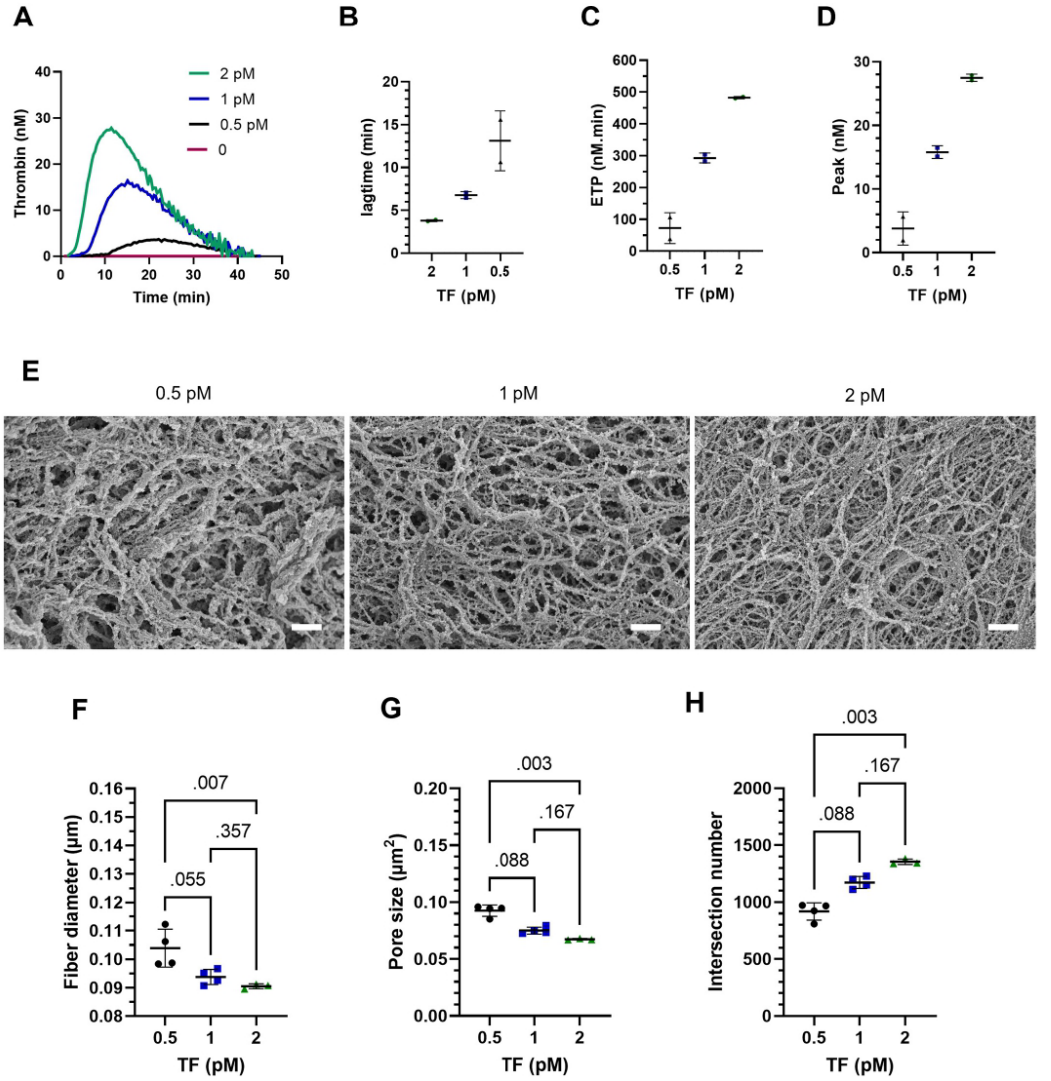

Fig. 1. Impact of increasing TF concentrations on thrombin generation and on the structure of fibrin clot in PPP-conditioned media (PPP diluted 10 % in RPMI-1640 as described in Materials and Methods section). (A): Representative thrombin generation curves (Mean curve from 2 experiments). (B, C, D): Thrombogram parameters. (E): SEM images of the fibrin network formed 2 h after triggering coagulation. (F, G, H): Analysis of the structure of fibrin network using images obtained from SEM. Each data point represents the mean value of an independent experiment. Bars represent Mean ± SD. SEM: scanning electron microscopy. SD: standard deviation.

augmentation of TF concentrations resulted in increase of the number of intersections: 918 ± 76 in the presence of 0.5 pM TF, 1173 ± 52 in 1 pM TF and 1356 ± 24 intersections in 2 pM of TF. For each parameter of fibrin clot produced in the presence of 2 pM TF the difference was significant ($p < 0.05$) as compared to the corresponding of the clot produced in the presence of 0.5 pM. Detailed comparisons are depicted in Fig. 1F, G, H.

3.2. Procoagulant signature of cancer cells

In the PPP-conditioned media, triggering coagulation in the absence of cancer cells (control experiment) no thrombin generation and clot formation was detected. The BXPC3 and MDA-MB231 cells induced higher thrombin generation as compared with MCF7 cells (Fig. 2A, B, C, D). The BXPC3 and MDA-MB231, at the same number of cells, had a similar effect on thrombin generation. In the presence of the same

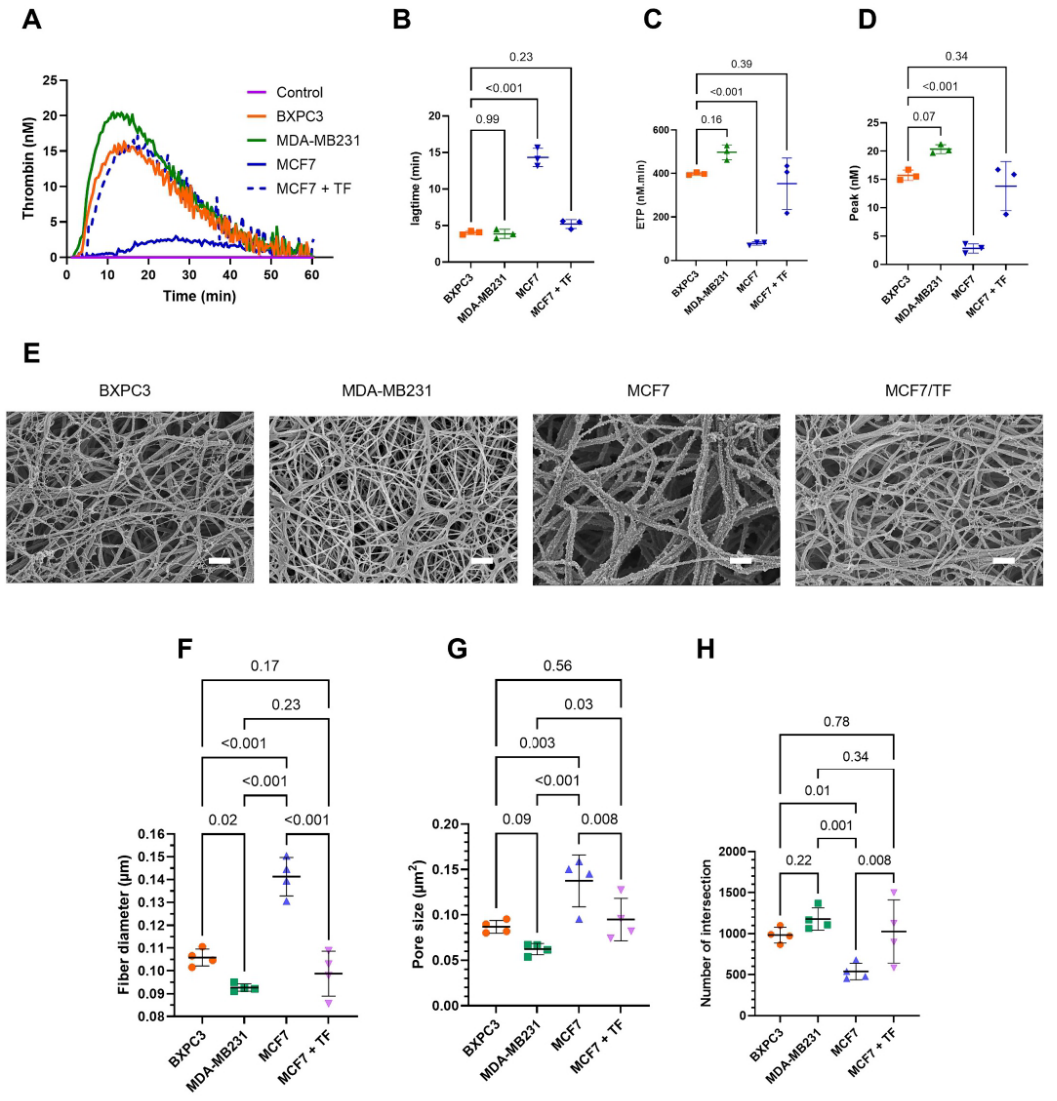

Fig. 2. Impact of cancer cell-induced thrombin generation on the structure of fibrin network. (A): Representative thrombin generation curves (one out of 4 experiments) after addition of $CaCl_2$ in PPP-conditioned media in the control experiment (absence of cancer cells), in the presence of cancer cells (BXPC3, MDA-MB231, MCF7) and in the presence of exogenous TF added in MCF7 cells (MCF7 + TF). (B, C, D): Parameters of thrombin generation in PPP-conditioned media in the presence of cancer cells. (E): SEM images of the network formed after clotting in PPP-conditioned media in the presence of cancer cells (BXPC3, MDA-MB231, MCF7) or MCF7 + TF. Scale bar: 1 µm. (F, G, H): Analysis of the fibrin network structure using images from SEM. Each data point represents the mean value of an independent experiment. Bars represent Mean ± SD of 4 independent experiments. SEM: scanning electron microscopy. SD: standard deviation.

number of MCF7 cells, the lag-time was 3.5 folds longer; the ETP and the Peak were 80 % lower as compared to the BXPC3 cells. In the experiment with the MCF7 cells, the addition of exogenous TF (1 pM) amplified thrombin generation at levels similar to those observed in the presence of BXPC3 cells.

3.3. Structural characteristics of fibrin clot induced by the cancer cells

Thrombin generation induced by cancer cells BXPC3, MDA-MB231, MCF7 and MCF7 + TF resulted in the formation of fibrin clot network. Original SEM images of clot formed in the presence of cancer cells are shown in Fig. 2E.

The structural characteristics of the fibrin network varied among the

three studied cancer cell lines (Fig. 2F, G, H).

The fiber diameters of clots formed by MDA-MB231 cells were significantly smaller than those formed by BXPC3 or MCF7 cells [0.093 ± 0.002 μm *versus* 0.106 ± 0.004 μm ($p = 0.02$) and 0.141 ± 0.008 μm ($p < 0.001$) respectively]. The fibers of fibrin clot formed by MCF7 cells had a significantly larger diameter than those formed by BXPC3 cells ($p < 0.001$) (Fig. 2F).

The pore sizes of clots formed in the presence of MDA-MB231 cells (0.062 ± 0.006 μm^2) were significantly smaller than those formed in the presence of MCF7 cells (0.138 ± 0.029 μm^2, $p < 0.001$), but not to those of BXPC3 cells (0.087 ± 0.007 μm^2, $p = 0.09$). Clots formed in the presence of MCF7 cells showed a significantly larger pore size compared to those formed in the presence of BXPC3 or MDA-MB231 cells ($p = 0.003$ and $p < 0.001$ respectively) (Fig. 2G).

The number of fibrin fiber intersections was significantly lower in clots formed in the presence of MCF7 cells (539 ± 101) compared to those formed in the presence of MDA-MB231 or BXPC3 cells (1177 ± 135 and 982 ± 96, $p = 0.001$ and $p = 0.01$ respectively). There was no significant difference in the number of fibrin intersections between clots formed in the presence of BXPC3 cells and MDA-MB231 cells ($p = 0.22$) (Fig. 2H).

The addition of 1 pM TF into MCF7 PPP-conditioned media led to the formation of clots that were similar to those formed in the presence of BXPC3 cells, in terms of fiber diameters (0.099 ± 0.010 μm *versus* 0.106 ± 0.004 μm respectively, $p = 0.17$), pore sizes (0.095 ± 0.023 μm^2 *versus* 0.087 ± 0.007 μm^2 respectively, $p = 0.56$) and the number of intersections (1026 ± 385 *versus* 982 ± 96 respectively, $p = 0.78$) (Fig. 2F, G, H).

3.4. Profibrinolytic signature of cancer cells and kinetics of fibrin clot lysis

In the control experiment, (cells cultured in conditioned media without PPP), a progressive release of tPA was observed in the presence of BXPC3 or MDA-MB231 cells, but not in the presence of MCF7 cells. At 72 h of incubation, MDA-MB231 cells released a 4-fold higher concentration of tPA as compared to BXPC3 cells. The time required to observe a detectable increase of tPA secretion was 14 h for MDA-MB231 cells ($p < 0.001$ between t0 and 14 h) and 72 h ($p < 0.001$ between t0 and 72 h) for BXPC3 cells (Fig. 3A).

During the observation period tiny concentrations of tPA were measured in plasma (0.06 ± 0.04 ng/ml at t0 and 0.24 ± 0.07 ng/ml after 72 h; $p > 0.99$) (Fig. 3B). In the presence of PPP, the release of tPA by BXPC3 or MDA-MB231 cells progressively increased. At 72 h, the levels of tPA released by MDA-MB231 (3.77 ± 2.18 ng/ml) were significantly higher as compared to those released by MCF7 cells (0.14 ± 0.01 ng/ml, $p = 0.02$) (Fig. 3B).

In the control experiment, in the absence of cancer cells, the levels of D-Dimer in PPP-conditioned media were 0.09 ± 0.11 μg/ml after 72 h (Fig. 3C). Following fibrin clot formation in the presence of BXPC3 or MDA-MB231 cells, a progressive increase in D-Dimer was observed. The increase in D-Dimer concentration became significant after 24 h from clot formation for BXPC3 cells ($p < 0.001$ as compared to t0) and 14 h for MDA-MB231 cells ($p < 0.001$ as compared to t0) (Fig. 3C). In the presence of MDA-MB231 and BXPC3 cells, the levels of D-Dimer continued to increase up to 72 h from clot formation. In the presence of MCF7 cells, after fibrin clot formation, no significant changes in D-Dimer concentration were observed ($p > 0.99$ between t0 and after 72 h). At the end of the observation period, the maximum concentration of D-Dimer in the presence of BXPC3 and MDA-MB231 was 160.77 ± 46.39 μg/ml and 56.19 ± 9.29 μg/ml, respectively.

3.5. Cancer cell mobility into the fibrin clot

In the beginning of the experiment cancer cells formed an adhesive monolayer at the bottom of the well. After clot formation, the observation by SEM showed of clusters of cells on the top layer of fibrin clots (Fig. 4C).

Clot observation under Laser Scanning Confocal Microscopy (LSCM) revealed the presence of BXPC3, MDA-MB231, or MCF7 cells at the bottom, inside, and on top of the fibrin clot (Fig. 4B).

Afterwards we confirmed the vitality of these cells and ruled out the possibility that they were dead cells detached from the culture plate and subsequently they were trapped within the fibrin clot. The viability of cells located at the top and at the bottom layers of the clot, was assessed with the MTT assay. These cells maintained their metabolic activity as documented by the ability to induce the formation of formazan crystals (Fig. 4D). Additionally, the absence of condensed or fragmented DNA in the nuclei (Fig. 4B), the intactness of the cell membranes, the maintenance of cell-cell adhesion (Fig. 4C), further substantiated that cells at all levels of the clot were alive.

3.6. 3D spheroid cultures: Cancer cell invasion into fibrin clot in

At 72 h after clot formation, the invasion of BXPC3, MDA-MB231, and MCF7 cells within the fibrin network was confirmed by the observation with phase-contrast microscopy of 3D spheroids (Fig. 5). In the control experiment performed in 3D cultures in conventional media (absence of PPP), cancer spheroids exhibited a symmetrical increase in size while they conserved the spherical structure. The structure of the 3D cultures of cancer cells was different in the PPP-conditioned media. The BXPC3 and MCF7 3D cultures showed and asymmetric expansion. In distinct regions of the initial spheroid cultures of BXPC3 and MCF7 cells

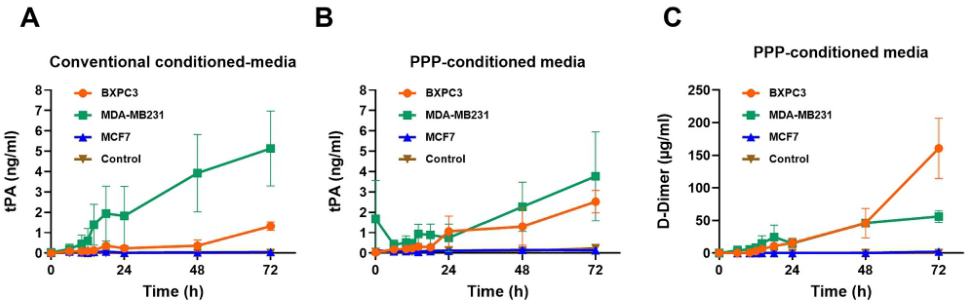

Fig. 3. Distinct fibrinolytic potential of BXPC3, MDA-MB213 and MCF7 cells. Control experiment: conditioned media without cells. Data are shown ad Mean ± SD; of 3 experiments. (A): Secretion of tPA from cancer cells (BXPC3, MDA-MB231, MCF7) cultured in conventional conditioned media. (B) Secretion of tPA from cancer cells (BXPC3, MDA-MB231, MCF7) cultured in PPP-conditioned media. (C) Release of D-Dimer in PPP-conditioned media in the control experiment and in the presence of BXPC3, MDA-MB231, or MCF7 cells.

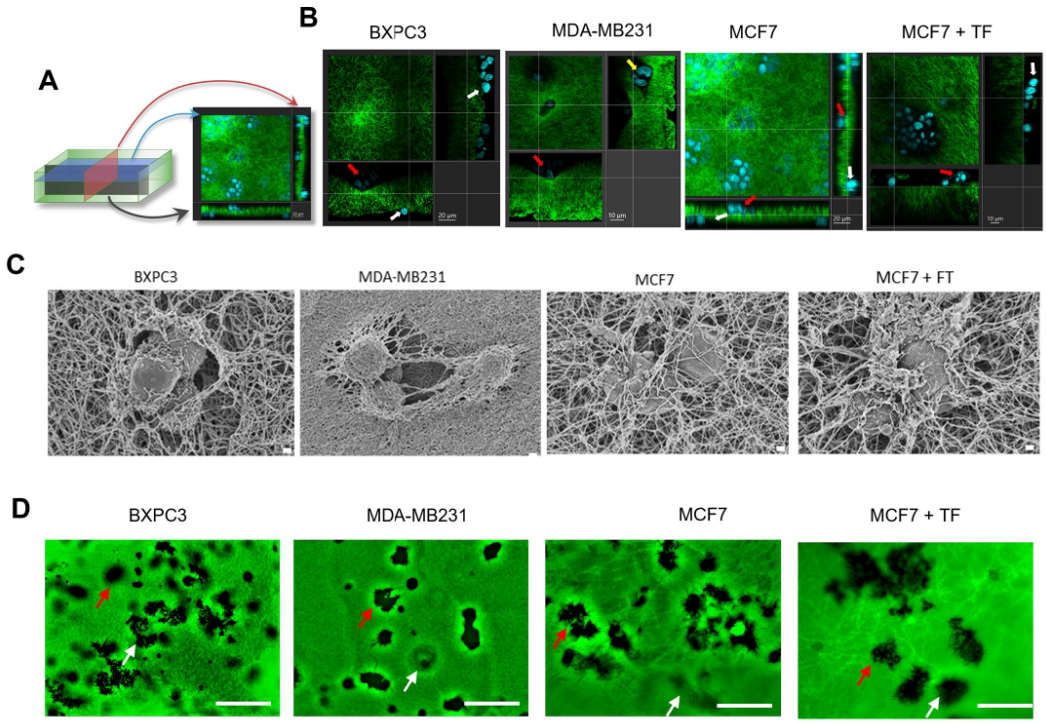

Fig. 4. Migration into fibrin clot of cancer cells from bottom to top layers. (A): Schema of orthogonal slides. (B): Orthogonal slides of fibrin clot formed from different cell lines. Cyan: nuclei. Green: Fibrin. White arrows: cells at bottom layer. Red arrows: cells at op layer. Yellow arrows: cells in the middle. (C): Cancer cells found on the top layer of the fibrin clot network. Scale bars: 2 μm. (D): Formazan crystals formed by cells in the bottom (white arrows) and top (red arrows) of fibrin clots. Scale bars: 50 μm. Images are representative of 4 independent experiments. (For interpretation of the references to colour in this figure legend, the reader is referred to the web version of this article.)

budding formations appeared indicating a pattern of collective migration of the cells. The addition of exogenous TF enhanced the invasion of MCF7 cells within the fibrin network.

In, 3D cultures of MDA-MB231, single cells were identified along the fibrin fibers indicating a cell migration that followed an individual pattern.

3.7. Presence of fibrin on the membrane of cancer cells

Fluorescence microscopy revealed the presence of fibrin fibers bound at the extracellular layer of the cancer cell membranes (Fig. 6).

In the 2D-culture model using fluorescent fibrinogen, the superposition of green and cyan channels demonstrated that fibrin was located at the extracellular layer of the cell membrane (Fig. 6A). Quantification of the fluorescence intensity at the extracellular layer of cell membrane after careful removal of the clot confirmed that thrombin generation induced by BXPC3 or MDA-MB231 cells leaded to fibrin deposition on the cell membrane. No signs of fibrin deposition were found in the experiment with MCF7 cells in the 2D-culture model, using fluorescent fibrinogen (Fig. 6B). The exogenous addition of TF induced detectable fibrin deposition on the extracellular layer of the cytoplasmic membrane of MCF7 cells.

An attempt to confirm that the fluorescent signal observed was fibrin and not its degradation products using an anti-fibrin antibody was made, however, due the low adherence of cells on glass coverslip, most of the cells were eliminated after many of washing steps in the immunofluorescence technic.

The presence of fibrin on the cell membrane was further confirmed by immunofluorescence observation in 3D cultures, using a specific anti-fibrin antibody that specifically recognized fibrin. Transversal slides showed that exclusively the cells located on the outer layer of the spheroids formed by the MCF7 or MDA-MB231 interacted with fibrin (Fig. 6D). In contrast, this type of interaction was found on cells located at both the outer and inner layers of BXPC3 spheroids (Fig. 6D).

3.8. Fibrin clot shields induced resistance to the anticancer agents

Applying the conventional experimental system for the study of the efficacy of anticancer agents, without fibrin, the IC50 of paclitaxel was 0.5 μM for BXPC3 and 0.1 μM for MDA-MB231 and MCF7 cells. The IC50 of 4-hydroxy-tamoxifen was 10 nM for MCF7 cells.

At 2 h after the clot formation the addition of paclitaxel at the IC50 did not induce any detectable decrease of the viability of the BXPC3, MDA-MB213 or MCF7 cells. Similarly, the addition of 4-hydroxy-tamoxifen did not induce any detectable decrease of the viability of the MCF7 cells (Fig. 7).

4. Discussion

Multiple lines of evidence from experiments in an original culture

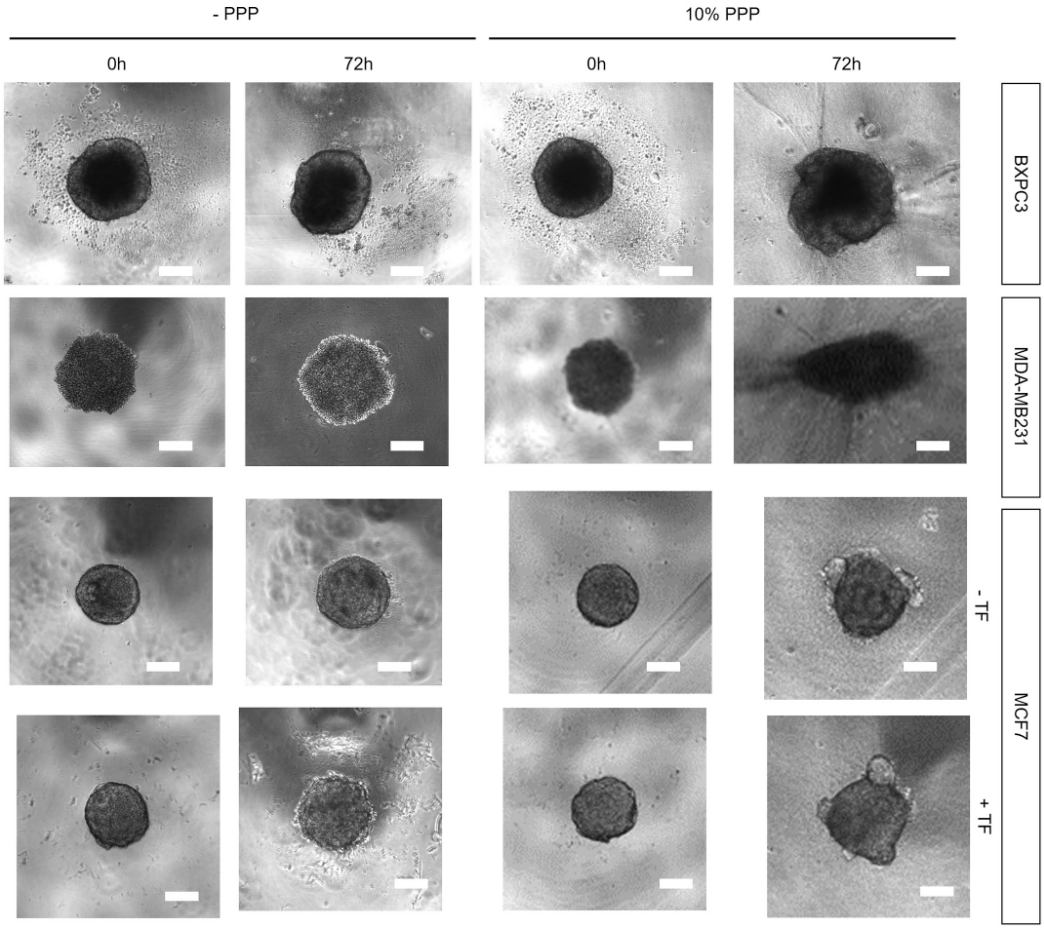

Fig. 5. Migration of BXPC3, MDA-MB231, and MCF7 from 3D from spheroid cultures towards the fibrin network. Images were taken at the beginning of the experiment (t0) and 72 h after triggering coagulation in PPP-conditioned media and were compared with images taken in 3D cultures in conventional conditioned media. Scale bars represent 200 μm. Images are representative of 4 independent experiments. -TF: no exogenous addition of TF. +TF: exogenous addition of TF (1 pM).

system of in the presence of human platelet poor plasma, show for the first time that the procoagulant signature of cancer cells determines the quality and structure of fibrin clot network which in turn acts as a protecting barrier that abrogates the efficacy of the anticancer agents.

Previous work from our group and others showed that the ability of cancer cells to trigger thrombin generation in normal human PPP is bent on TF expression. The BXPC3 and MDA-MB231 cells express higher amounts of TF and induce higher thrombin generation as compared to MCF7 cells [9,30].

Here, we set up and validated a new *in vitro* experimental system based on dilution of PPP in conditioning media that provides a sufficient amount of clotting factors to support TF-mediated thrombin generation without compromising cell viability. In these experimental conditions, as in normal PPP, the ETP and Peak of thrombin were high in the presence of pancreatic cancer cells BXPC3 or aggressive triple-negative breast cancer cells, MDA-MB231. Thrombin generation was lower in the presence of noninvasive, estrogen receptor-positive breast cancer cells, MCF7. These experimental conditions led to the formation of fibrin network and allowed a comprehensive study of its architecture as well as of its effects on the efficacy of the conventional chemotherapeutic drug paclitaxel of the targeted anticancer agent 4-hydroxy-tamoxifen.

The structural characteristics of the fibrin clot were evaluated according to established criteria based on fiber thickness, pore size, and the number of intersections [27,31]. Thrombin generation triggered by the high TF expressing cells BXPC3 or MDA-MB231, resulted in more robust clot structure with thinner fibers, smaller pores, and a higher number of intersections as compared to those obtained following coagulation activation by the low TF expressing MCF7 cells. The exogenous addition of TF in the MCF7 experimental microenvironment, resulted in thrombin generation levels comparable to those observed in the experiment with the BXPC3 cells. Accordingly, the fibrin network displayed a similar architecture and structure to that observed in the

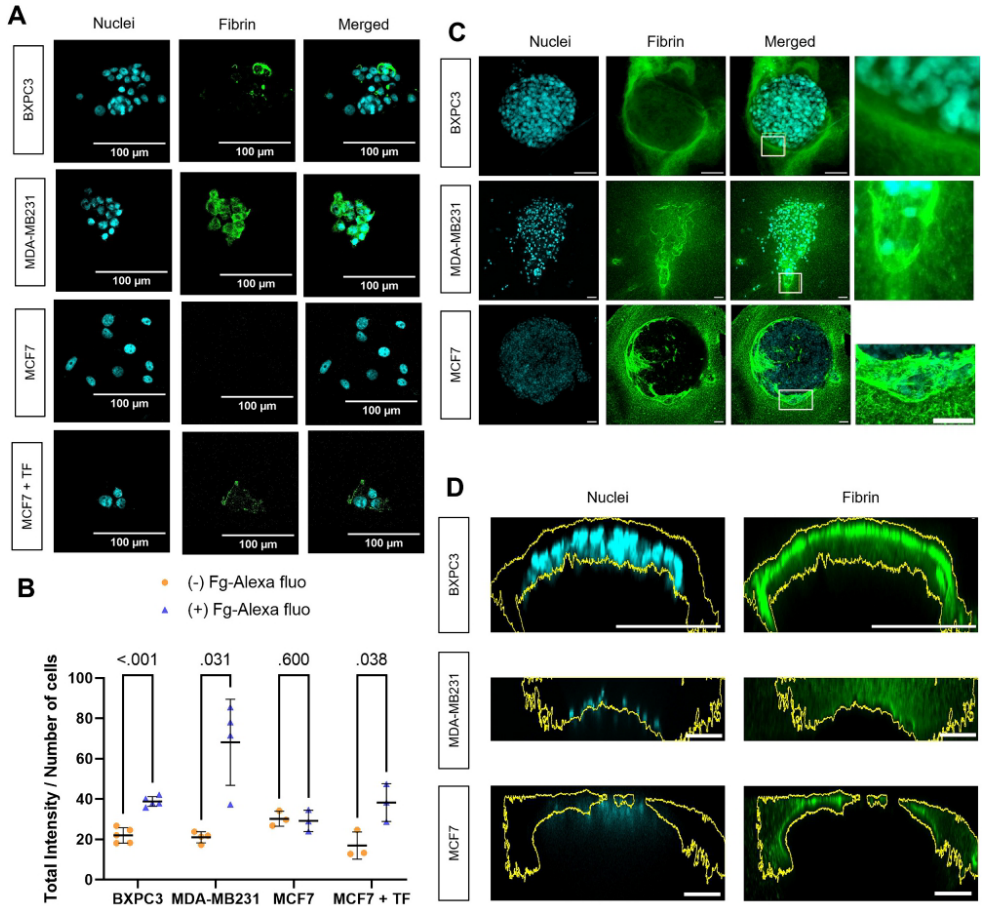

Fig. 6. Fibrin deposit on cancer cell membrane. (A): Detection of fibrin deposit on the cell membrane after 24 h of culture in the PPP-conditioned media, using 2.5 µg/ml of Fibrinogen coupled with Alexa Fluor 488 (in green). Nuclei were marked with Hoechst 33442 (in cyan). Scale bar represents 50 µm. (B): Fibrin deposit on cell membrane after 24 h was quantified by fluorescence intensity. The total fluorescence intensity of the green channel was normalized to the total number of cells. Each data point represents the mean value of each field from three independent experiments. Bars are Mean ± SD. (C): Detection of fibrin fibers on cell membrane in cancer cell spheroids, using anti-fibrin antibody. Scale bars represent 50 µm. (D): Transversal slides of cancer cells spheroids. Yellow lines represent regions where fibrin was detected. Scale bars represent 100 µm. (For interpretation of the references to colour in this figure legend, the reader is referred to the web version of this article.)

presence of BXPC3 cells. The analysis of SEM images, obtained by the addition of exogenous TF in the PPP-conditioned media (in the absence of cells) showed that the strengthening of the fibrin network was correlated with the concentration of TF and the increase of thrombin generation.

To the best of our knowledge, the present study provides for the first-time electron microscopy images of the architecture of the cancer cell-initiated fibrin network and its interaction with the cell membranes. This network develops in the form of "bird's nest" being in contact with the extracellular layer of the cell membrane. The envelopment of the cells and their contact with the fibrin network was further illustrated by immunofluorescence studies in 3D cultures. We suppose that fibrin fibers could cover specific receptors at the membrane of cancer cells which are potential aims of targeted anticancer therapies. This hypothesis must be investigated in appropriately designed studies.

The "bird's nest" organization of the fibrin network around the cancer cells could function as a protective shield against the conventional chemotherapy or targeted anticancer treatments. To control this hypothesis, we determined the concentrations of paclitaxel that halved the viability of BXPC3, MDA-MB213 or MCF7 cells in conventional cultures for pharmacological studies on anticancer drugs [28]. Similarly, we determined the concentration of 4-hydroxy-tamoxifen that halved the viability of MCF7 cells. Then, we evaluated the efficacy of the IC50 of these anticancer agents on the viability of the corresponding cells in the presence of fibrin network. This series of experiments documented that the fibrin clot shields generated by the cancer cells act as a protective barrier against the anticancer agents. Indeed, the presence of fibrin clot shields completely abrogated the effect of the conventional chemotherapeutic agent paclitaxel on the viability of the pancreatic cancer cells BXPC3, on the triple negative breast cancer cells MDA-

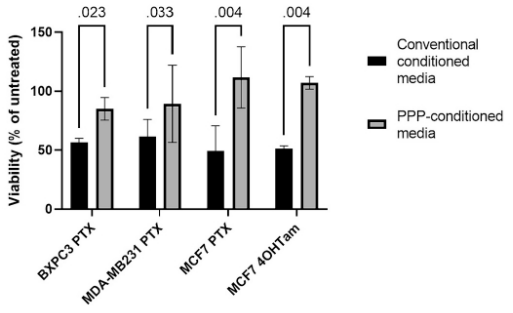

Fig. 7. Resistance to anticancer agents paclitaxel (PTX) and 4-hydroxy-tamoxifen (4OHTam) induced by the fibrin lot shields. The IC50 of PTX and 4OHTam on cancer cell viability were determined in conventional cancer cell cultures as described in Materials and Methods. Viability was evaluated after 72 h of treatment with 0.5 μM of PTX for BXPC3 cells, 0.1 μM of PTX for MDA-MB231 and MCF7 cells, and 10 nM of 4OHTam for MCF7 cells, in conventional conditioned media and in PPP-conditioned media. Values are Means ± SD of 3 independent experiments.

MB213 as well as on the estrogen receptor-positive breast cancer cells MCF7 cells. Similarly, the fibrin clot shields totally abrogated the effect of 4-hydroxy-tamoxifen on the viability of MCF7 cells. The capacity of fibrin clot shields generated by the procoagulant potential of cancer cells that we report here, might be a new pathway that leads to resistance to anticancer treatment. In the light of these experiments, the mechanisms of the resistance to the anticancer treatment induced by cancer cell generated fibrin clot shields as well as its clinical relevance needs to be studied. In the same line, a potential implication of fibrin clot shields in the exhaustion of CAR-T cells, should be investigated since this phenomenon is considered as a major mechanism of CAR-T cell treatment failure [32,33].

It is well established that cancer cells express profibrinolytic properties [5,16]. So, we controlled the rate of fibrinolysis upon fibrin network formation. We also studied the movement of cancer cells within the fibrin network. As it was expected, MDA-MB231 and BXPC3 cells, but not MCF7 cells, secreted tPA at when they were cultured either in conventional conditioned media or in PPP-conditioned media. In conventional conditioned media, MDA-MB231 cells released higher levels of tPA as compared to BXPC3 cells. Interestingly, in PPP-conditioned media, both types of cells released similar amount of tPA with comparable kinetics. This change reflects the differential impact of PPP on the proliferation rate of the two types of cells. Indeed, in the presence of PPP, the proliferation of BXPC3 was accelerated particularly after 48 h of exposure. (Supplementary Fig. S1).

The lysis of the fibrin network formed by MDA-MB231 or BXPC3 cells, as evidenced by the increase in D-Dimer, follows the release of tPA. While the secretion of tPA in MDA-MB231 cells surpassed that in BXPC3 cells, the rate of increase in D-Dimer levels in the former was notably slower than that observed in the latter. This observation is consistent with previous studies indicating that the lysis of clots composed of finer fibers is a prolonged process compared to clots formed by thicker fibers [12,34].

Neither significant tPA release nor a substantial increase in D-Dimer were observed in fibrin clots formed by MCF7 cells. Nevertheless, MCF7 cells were found within the fibrin clot at a distance from the original adhesive layer. We hypothesize that MCF7 move within the clot *via* an alternative, plasminogen-independent pathway for fibrin degradation. Indeed, various matrix metalloproteinases (MMPs) have the capacity to degrade not only fibrin but also D-Dimer [35–38].

It is well established that fibrin serves as a scaffold supporting cancer cell adhesion and migration [1]. The evidence presented herein confirms this concept and further demonstrates that cancer cells, *via* their inherent procoagulant properties, construct the fibrin scaffold utilized for their migration. Cell imaging using LSCM of fibrin clots revealed that BXPC3, MDA-MB231, or MCF7 cells detached from the initial adhesive monolayer and moved through the fibrin network. Within the 24-hours observation period, living cells were identified at a distance from the cell layer, within, and on the top of the clots. This phenomenon has been also observed by Andrade et al., who showed that breast cancer cells migrate within fibrin bundles formed in the presence of platelets [39]. According to this study platelets are a source of TGF-β and VEGF which guide the migration of breast cancer cells. Our study demonstrates that migration of pancreatic or breast cancer cells within the fibrin network occurs in the absence of platelets. Consequently, we hypothesize that the presence of fibrin scaffolds and/or the serine proteases of blood coagulation (*i.e.* activated factors X, IX, VII or thrombin) in concert with the inherent profibrinolytic activity of the cells, play a pivotal role in the selection of migrating cancer cells within the fibrin clot and the formation of distal colonies.

The observation with phase-contrast microscopy of 3D spheroids of the three studied cancer cell lines confirmed that the cells invaded and moved within the fibrin network. MDA-MB231 cells exhibited individual movement into the fibrin clot, whereas BXPC3 and MCF7 cells demonstrated collective movement and this is in accordance with previous findings [2,40–43]. According to a recent study, cancer cells move through the fibrin network by expressing ICAM-1 and forming a fibrinogen-dependent bridge [44].

A limitation of our study is that erythrocytes, platelets and endothelial cells were not included in the experimental system. In non-cancer experimental systems, erythrocytes, platelets neutrophil extracellular traps as well as TF expressing activated monocytes support thrombin generation and increases viscosity of the clot [45–47]. It is probable that blood cells alter the kinetics of cancer cells migration on the fibrin scaffold. This is a field of investigation in ongoing studies since it creates experimental conditions closer to the physiological cancer and vascular microenvironment. The impact of blood cells and endothelial cells on the capacity of fibrin clot shields to abrogate the effect of the anticancer agent is of particular interest.

In conclusion, the present study provides original experimental data documenting that the inherent procoagulant signature of cancer cells lead to the formation of a fibrin clot shields which are organized as a "bird's nest" enveloping cancer cells. The fibrin clot shields function as a protective barrier against the conventional chemotherapeutic agents such as paclitaxel or the targeted anticancer agent 4-hydroxy-tamoxifen. In addition, the fibrin clot shields offer a scaffold for the migration of cancer cells.

Supplementary data to this article can be found online at https://doi.org/10.1016/j.thromres.2024.04.015.

CRediT authorship contribution statement

Huong Chi Mai Tran: Writing – original draft, Visualization, Software, Project administration, Methodology, Formal analysis, Data curation. **Elisabeth Mbemba:** Methodology, Investigation. **Noémie Mourot:** Methodology. **Beshoy Faltas:** Methodology. **Aurélie Rousseau:** Resources. **Elmina Lefkou:** Writing – review & editing, Writing – original draft. **Michèle Sabbah:** Writing – review & editing. **Patrick van Dreden:** Writing – review & editing, Writing – original draft, Validation, Resources, Funding acquisition, Formal analysis, Data curation, Conceptualization. **Grigoris Gerotziafas:** Writing – review & editing, Writing – original draft, Validation, Supervision, Resources, Methodology, Investigation, Funding acquisition, Formal analysis, Data curation, Conceptualization.

Declaration of competing interest

The authors declare that they have no known competing financial

interests or personal relationships that could have appeared to influence the work reported in this paper.

Acknowledgements

We thank Michaël Trichet from the IBPS electron microscopy core facility, with the support of "Région Île-de-France", Sorbonne-University and CNRS, for SEM technics, as well as Romain Morichon from the CISA platform with financial support from Sorbonne Université, ITMO Cancer of Aviesan, and INCA on funds administrated by INSERM, for LSCM technics. We also would like to thank Dr. Clémence Gentner from the Kastler Brossel Laboratory, ENS-Université PSL, CNRS, Sorbonne Université, Collège de France for her kind help in imaging methods, as well as Dr. Coralie Dorard for advices on 3D cell cultures.

References

[1] H.F. Dvorak, Tumors: wounds that do not heal, N. Engl. J. Med. 315 (1986) 1650–1659, https://doi.org/10.1056/NEJM198612253152606.
[2] J. Majidpoor, K. Mortezaee, Steps in metastasis: an updated review, Med. Oncol. 38 (2021) 3, https://doi.org/10.1007/s12032-020-01447-w.
[3] M. Shoji, K. Abe, K.A. Casper, J.N. Wilcox, D.L. Dillehay, J. Contrino, Activation of Coagulation and Angiogenesis in Cancer 152, 1998, p. 13.
[4] H. ten Cate, A. Falanga, Overview of the postulated mechanisms linking cancer and thrombosis, Pathophysiol. Haemost. Thromb. 36 (2008) 122–130, https://doi.org/10.1159/000175150.
[5] A. Galmiche, J. Rak, L.T. Roumenina, Z. Saidak, Coagulome and the tumor microenvironment: an actionable interplay, Trends Cancer 8 (2022) 369–383, https://doi.org/10.1016/j.trecan.2021.12.008.
[6] H.C. Kwaan, P.F. Lindholm, Fibrin and fibrinolysis in cancer, Semin. Thromb. Hemost. 45 (2019) 413–422, https://doi.org/10.1055/s-0039-1688495.
[7] A. Falanga, L. Russo, V. Milesi, A. Vignoli, Mechanisms and risk factors of thrombosis in cancer, Crit. Rev. Oncol. Hematol. 118 (2017) 79–83, https://doi.org/10.1016/j.critrevonc.2017.08.003.
[8] J.I. Zwicker, B.C. Furie, B. Furie, Cancer-associated thrombosis, Crit. Rev. Oncol. Hematol. 62 (2007) 126–136, https://doi.org/10.1016/j.critrevonc.2007.01.001.
[9] G.T. Gerotziafas, V. Galea, E. Mbemba, et al., Tissue factor over-expression by human pancreatic cancer cells BXPC3 is related to higher prothrombotic potential as compared to breast cancer cells MCF7, Thromb. Res. 129 (2012) 779–786, https://doi.org/10.1016/j.thromres.2011.07.049.
[10] M. Marchetti, E. Diani, H. ten Cate, A. Falanga, Characterization of the thrombin generation potential of leukemic and solid tumor cells by calibrated automated thrombography, Haematologica 97 (2012) 1173–1180, https://doi.org/10.3324/haematol.2011.055343.
[11] C. Zhang, Z. Yang, P. Zhou, et al., Phosphatidylserine-exposing tumor-derived microparticles exacerbate coagulation and cancer cell transendothelial migration in triple-negative breast cancer, Theranostics 11 (2021) 6445–6460, https://doi.org/10.7150/thno.53637.
[12] E.L. Hethershaw, A.L. Cilia La Corte, C. Duval, et al., The effect of blood coagulation factor XIII on fibrin clot structure and fibrinolysis, J. Thromb. Haemost. 12 (2014) 197–205, https://doi.org/10.1111/jth.12455.
[13] A.S. Wolberg, Fibrinogen and fibrin: synthesis, structure, and function in health and disease, J. Thromb. Haemost. 21 (2023) 3005–3015, https://doi.org/10.1016/j.jtha.2023.08.014.
[14] A.S. Wolberg, Thrombin generation and fibrin clot structure, Blood Rev. 21 (2007) 131–142, https://doi.org/10.1016/j.blre.2006.11.001.
[15] I. Lal, K. Dittus, C.E. Holmes, Platelets, coagulation and fibrinolysis in breast cancer progression, Breast Cancer Res. 15 (2013) 207, https://doi.org/10.1186/bcr3425.
[16] Z. Saidak, S. Soudet, M. Lottin, et al., A pan-cancer analysis of the human tumor coagulome and its link to the tumor immune microenvironment, Cancer Immunol. Immunother. 70 (2021) 923–933, https://doi.org/10.1007/s00262-020-02739-w.
[17] E. Henke, R. Nandigama, S. Ergün, Extracellular matrix in the tumor microenvironment and its impact on cancer therapy, Front. Mol. Biosci. 6 (2020) 160, https://doi.org/10.3389/fmolb.2019.00160.
[18] J. Huang, L. Zhang, D. Wan, et al., Extracellular matrix and its therapeutic potential for cancer treatment, Sig. Transduct. Target Ther. 6 (2021) 1–24, https://doi.org/10.1038/s41392-021-00544-0.
[19] M.U. Mushtaq, A. Papadas, A. Pagenkopf, et al., Tumor matrix remodeling and novel immunotherapies: the promise of matrix-derived immune biomarkers, J. Immunother. Cancer 6 (2018) 65, https://doi.org/10.1186/s40425-018-0376-0.
[20] Y. Yang, Y. Wang, X. Che, et al., Integrin α5 promotes migration and invasion through the FAK/STAT3/AKT signaling pathway in icotinib-resistant non-small cell lung cancer cells, Oncol. Lett. 22 (2021) 556, https://doi.org/10.3892/ol.2021.12817.
[21] E. Cruz da Silva, M. Dontenwill, L. Choulier, M. Lehmann, Role of integrins in resistance to therapies targeting growth factor receptors in cancer, Cancers (Basel) 11 (2019) 692, https://doi.org/10.3390/cancers11050692.
[22] L.M. Knowles, L.A. Gurski, C. Engel, J.R. Gnarra, J.K. Maranchie, J. Pilch, Integrin αvβ3 and fibronectin upregulate slug in cancer cells to promote clot invasion and metastasis, Cancer Res. 73 (2013) 6175–6184, https://doi.org/10.1158/0008-5472.CAN-13-0602.
[23] H. Mao, Y. Ito, Growth factors and protein-modified surfaces and interfaces, in: P. Ducheyne (Ed.), Comprehensive Biomaterials II, Elsevier, Oxford, 2017, pp. 321–359, https://doi.org/10.1016/B978-0-12-803581-8.10191-2.
[24] T. Obonai, H. Fuchigami, F. Furuya, N. Kozuka, M. Yasunaga, Y. Matsumura, Tumour imaging by the detection of fibrin clots in tumour stroma using an anti-fibrin Fab fragment, Sci. Rep. 6 (2016) 23613, https://doi.org/10.1038/srep23613.
[25] Y. Hisada, M. Yasunaga, S. Hanaoka, et al., Discovery of an uncovered region in fibrin clots and its clinical significance, Sci. Rep. 3 (2013) 2604, https://doi.org/10.1038/srep02604.
[26] A.R. Kirtane, T. Sadhukha, H. Kim, V. Khanna, B. Koniar, J. Panyam, Fibrinolytic enzyme co-therapy improves tumor perfusion and therapeutic efficacy of anticancer nanomedicine, Cancer Res. 77 (2017) 1465–1475, https://doi.org/10.1158/0008-5472.CAN-16-1646.
[27] A. Daraei, M. Pieters, S.R. Baker, et al., Automated fiber diameter and porosity measurements of plasma clots in scanning electron microscopy images, Biomolecules 11 (2021) 1536, https://doi.org/10.3390/biom11101536.
[28] J.E. Liebmann, J.A. Cook, C. Lipschultz, D. Teague, J. Fisher, J.B. Mitchell, Cytotoxic studies of paclitaxel (Taxol) in human tumour cell lines, Br. J. Cancer 68 (1993) 1104–1109.
[29] Y. Berthois, J.A. Katzenellenbogen, B.S. Katzenellenbogen, Phenol red in tissue culture media is a weak estrogen: implications concerning the study of estrogen-responsive cells in culture, Proc. Natl. Acad. Sci. U. S. A. 83 (1986) 2496–2500.
[30] A. Rousseau, A.K. Larsen, P. Van Dreden, M. Sabbah, I. Elalamy, G.T. Gerotziafas, Differential contribution of tissue factor and factor XII to thrombin generation triggered by breast and pancreatic cancer cells, Int. J. Oncol. 51 (2017) 1747–1756, https://doi.org/10.3892/ijo.2017.4172.
[31] W. Li, J. Sigley, M. Pieters, et al., Fibrin fiber stiffness is strongly affected by fiber diameter, but not by fibrinogen glycation, Biophys. J. 110 (2016) 1400–1410, https://doi.org/10.1016/j.bpj.2016.02.021.
[32] X. Zhu, Q. Li, X. Zhu, Mechanisms of CAR T cell exhaustion and current counteraction strategies, Front. Cell Dev. Biol. 10 (2022) 1034257, https://doi.org/10.3389/fcell.2022.1034257.
[33] T. Kouro, H. Himuro, T. Sasada, Exhaustion of CAR T cells: potential causes and solutions, J. Transl. Med. 20 (2022) 239, https://doi.org/10.1186/s12967-022-03442-3.
[34] J.L. Mullin, S.E. Norfolk, J.W. Weisel, S.T. Lord, Clot lysis of variant recombinant fibrinogens confirms that fiber diameter is a major determinant of lysis rate, Ann. N. Y. Acad. Sci. 936 (2006) 331–334, https://doi.org/10.1111/j.1749-6632.2001.tb03519.x.
[35] A. Bini, Y. Itoh, B.J. Kudryk, H. Nagase, Degradation of cross-linked fibrin by matrix metalloproteinase 3 (stromelysin 1): hydrolysis of the γ gly 404–ala 405 peptide bond, Biochemistry 35 (1996) 13056–13063, https://doi.org/10.1021/bi960730c.
[36] A. Bini, D. Wu, J. Schnuer, B.J. Kudryk, Characterization of stromelysin 1 (MMP-3), matrilysin (MMP-7), and membrane type 1 matrix metalloproteinase (MT1-MMP) derived fibrin(ogen) fragments D-dimer and D-like monomer: NH2-terminal sequences of late-stage digest fragments, Biochemistry 38 (1999) 13928–13936, https://doi.org/10.1021/bi991096g.
[37] K.B. Hotary, I. Yana, F. Sabeh, et al., Matrix metalloproteinases (MMPs) regulate fibrin-invasive activity via MT1-MMP–dependent and –independent processes, J. Exp. Med. 195 (2002) 295–308, https://doi.org/10.1084/jem.20010815.
[38] K. Alexander, A. Banos, S. Abro, et al., Levels of matrix metalloproteinases in arthroplasty patients and their correlation with inflammatory and thrombotic activation processes, Clin. Appl. Thromb. Hemost. 22 (2016) 441–446, https://doi.org/10.1177/1076029616639704.
[39] S.S. Andrade, J.T. Sumikawa, E.D. Castro, et al., Interface between breast cancer cells and the tumor microenvironment using platelet-rich plasma to promote tumor angiogenesis - influence of platelets and fibrin bundles on the behavior of breast tumor cells, Oncotarget 8 (2017) 16851–16874, https://doi.org/10.18632/oncotarget.15170.
[40] F. Lüönd, N. Sugiyama, R. Bill, et al., Distinct contributions of partial and full EMT to breast cancer malignancy, Dev. Cell 56 (2021) 3203–3221.e11, https://doi.org/10.1016/j.devcel.2021.11.006.
[41] M. Lintz, A. Muñoz, C.A. Reinhart-King, The mechanics of single cell and collective migration of tumor cells, J. Biomech. Eng. 139 (2017) 0210051–0210059, https://doi.org/10.1115/1.4035121.
[42] C. De Pascalis, S. Etienne-Manneville, Single and collective cell migration: the mechanics of adhesions, MBoC 28 (2017) 1833–1846, https://doi.org/10.1091/mbc.e17-03-0134.
[43] P. Friedl, D. Gilmour, Collective cell migration in morphogenesis, regeneration and cancer, Nat. Rev. Mol. Cell Biol. 10 (2009) 445–457, https://doi.org/10.1038/nrm2720.
[44] E. Angelidakis, S. Chen, S. Zhang, Z. Wan, R.D. Kamm, S.E. Shelton, Impact of fibrinogen, fibrin thrombi, and thrombin on cancer cell extravasation using in vitro microvascular networks, Adv. Healthc. Mater. 12 (2023) 2202984, https://doi.org/10.1002/adhm.202202984.

[45] A.F. Guedes, F.A. Carvalho, M.M. Domingues, et al., Impact of γ′γ′ fibrinogen interaction with red blood cells on fibrin clots, Nanomedicine (London) 13 (2018) 2491–2505, https://doi.org/10.2217/nnm-2018-0136.
[46] A.F. Guedes, F.A. Carvalho, M.M. Domingues, et al., Sensing adhesion forces between erythrocytes and γ′ fibrinogen, modulating fibrin clot architecture and function, Nanomedicine 14 (2018) 909–918, https://doi.org/10.1016/j.nano.2018.01.006.
[47] K.C. Gersh, C. Nagaswami, J.W. Weisel, Fibrin network structure and clot mechanical properties are altered by incorporation of erythrocytes, Thromb. Haemost. 102 (2009) 1169–1175, https://doi.org/10.1160/TH09-03-0199.

2. International Society on Thrombosis and Haemostasis (ISTH) 2024 : Posters

2.1. The procoagulant signature of cancer cells drives fibrin network formation in tumor microenvironment and impacts its quality. Implications in cancer cell migration

Huong Chi Mai Tran[1, 2], Elisabeth Mbemba[1], Noémie Mourot[1], Beshoy Faltas[1], Aurélie Rousseau[2], Elmina Lefkou[1], Michèle Sabbah[1], Patrick Van Dreden[1,2], Grigoris Gerotziafas[1,3]

[1] Sorbonne University, Inserm UMR_S_938, Saint-Antoine Research Center, CRSA, Team "Cancer Biology and Therapeutics", Group "Cancer - Angiogenesis - Haemostasis", Institut Universitaire de Cancérologie, AP-HP, Saint-Antoine Hospital, 34 Rue du Crozatier, F-75012 Paris, France.

[2] Clinical Research Department, Diagnostica Stago, 125 Avenue Louis Roche, 92230 Gennevilliers, France.

[3] Thrombosis Center, Service of Biological Hematology, AP-HP, Hôpitaux Universitaires de l'Est Parisien, Tenon Hospital, Faculty of Medecine Sorbonne University, 4 Rue de la Chine, 75020 Paris, France

Background

Cancer cells induce hypercoagulability in the tumoral microenvironment by expressing Tissue Factor (TF).

Aims

We aim to study the impact of the procoagulant signature of cancer cells on the structure of fibrin clot, and the migration of cancer cells within the fibrin network.

Materials and Methods

Pancreatic cancer cells BXPC3 and breast cancer cells MCF7, MDA-MB23 were cultured in the presence of normal Platelet Poor Plasma (PPP) (diluted 10% in conditioning media). Their potential to induce thrombin generation and their fibrinolytic activity were assessed. The structure of fibrin clots was analyzed with Scanning Electron Microscopy (SEM). Cancer cells' mobility with fibrin clot and their interactions with fibrin were observed.

Results

Cancer cells, in presence of PPP, induced fibrin network formation. Cancer cells expressing high procoagulant potency (BXPC3 cells and MDA-MB23 cells), led to dense fibrin network with fine fibers. MCF7 cells with low procoagulant potential led to thick fibers. Exogenous TF enhanced the density of fibrin network formed by MCF7 cells. Cancer cells through their inherent profibrinolytic potential migrated within the fiber scaffold. The BXPC3 and MCF7 cells moved in clusters whereas the MDA-MB231 cells moved individually within the fibrin network.

Conclusions

The procoagulant signature of cancer cells is determinant for the formation of fibrin clot network in the microenvironment and the clot's structure. Original SEM images show the architecture of "bird's nest"-like fibrin network being in touch with the cell membranes and surrounding cancer cells. Fibrin network constructed by triggering thrombin generation by cancer cells, provides a scaffold for cell migration.

2.2. Effect of tinzaparin, apixaban, enoxaparin and quercetin and on the expression of procoagulant properties of cancer cells and endothelial cells exposed to cancer cell derived microvesicles

Mohammed Baghdadi[1], Huong Chi Mai Tran[1, 2], Patrick Van Dreden[1,2], Grigoris Gerotziafas[1,3]

[1] Sorbonne University, Inserm UMR_S_938, Saint-Antoine Research Center, CRSA, Team "Cancer Biology and Therapeutics", Group "Cancer - Angiogenesis - Haemostasis", Institut Universitaire de Cancérologie, AP-HP, Saint-Antoine Hospital, 34 Rue du Crozatier, F-75012 Paris, France.

[2] Clinical Research Department, Diagnostica Stago, 125 Avenue Louis Roche, 92230 Gennevilliers, France.

[3] Thrombosis Center, Service of Biological Hematology, AP-HP, Hôpitaux Universitaires de l'Est Parisien, Tenon Hospital, Faculty of Medecine Sorbonne University, 4 Rue de la Chine, 75020 Paris, France

Background

Flavonoid Quercetin, has some anti-inflammatory and anti-oxidation activity. And exerts a significant proapoptotic effect on cancer cells as well as a protective effect on endothelial cells.

Aims

Explore the effect of quercetin on the procoagulant potential of pancreatic cancer cells (BXPC3) and breast cancer cells (MCF7) as well as its effect on endothelial cells (HUVEC) exposed to cancer cell derived microvesicles (CaCe-dMV) from BXPC3 and MCF7 cells.

Method

BXPC3, MCF7 and cells HUVEC cells were pretreated with Quercetin and clinically relevant concentrations of antithrombotic agents (apixaban, enoxaparin, or tinzaparin). The thrombin generation process was studied. Crystal violet was used to assess cell viability.

Results

Quercetin and tinzaparin significantly reduced the viability of BXPC3 or MCF7 cells. Treatment of cancer cells with enoxaparin or apixaban did not significantly affect the viability of BXPC3 or MCF7 cells.

Exposure of BXPC3 cells to quercetin and tinzaparin as compared to the control experiment resulted in significant prolongation of the lag-time, while no significant changes were observed with enoxaparin and apixaban. (Table 1)

The lag-time of thrombin generation induced by HUVEC pre-treated with quercetin and exposed to BXPC3 CaCe-dEVs was significantly longer and the peak was significantly lower as compared to those obtained by HUVEC non-treated with quercetin exposed to BXPC3 CaCe-dEVs. The lag-time of HUVEC pre-treated with apixaban and exposed to BXPC3 CaCe-dEVs was similar to that observed in the experiments with HUVEC non-treated with apixaban and exposed to BXPC3 CaCe-dEVs. Pretreatment with either quercetin or apixaban did not significantly modify the effect of HUVEC exposed to MCF7 CaCe-dEVs. (Table 2)

Conclusion(s)

This study showed that quercetin prevents endothelial cell activation and possible TF expression upon exposure to a potent stimulus such as CaCe-dEV from aggressive pancreatic cancer cells (BXPC3).Quercetin and tinzaparin decrease the viability of cancer cells.

3. ISTH 2023 : Posters

3.1. Impact of the Procoagulant Fingerprint of Cancer Cells on the Structure of Fibrin Clot Formed in Tumor Microenvironment

1. Huong Chi Mai Tran (Role: Co-Author)
2. Noémie Mourot (Role: Co-Author)
3. Beshoy Faltas (Role: Co-Author)
4. Elisabeth Mbemba (Role: Co-Author)
5. Ismail Elalamy (Role: Co-Author)
6. Michele Sabbah (she/her/hers) (Role: Co-Author)
7. Jawed Fareed (Role: Co-Author)
8. Patrick Van Dreden (Role: Presenting Author)
9. Grigorios Gerotziafas (Role: Co-Author)

Background

Cancer cells according to their histological type and the aggressivity trigger thrombin generation (TG) in their microenvironment via tissue factor (TF) expression and microvesicles release leading to fibrin clot formation.

Aims

In the present study we modelized the fibrin clot network in function of the histological type and the aggressivity of cancer cells.

Methods

Cells from invasive pancreatic and breast cancer (BXPC3 and MDA-MB231 respectively) and from less invasive breast cancer (MCF7), were put in contact with normal human platelet poor plasma (PPP). In some experiments fluorescent Fibrinogen (AlexaFluo488, Invitrogen™, USA) was added. Thrombin generation was assessed with Calibrated Automated Thrombogram® (Stago France). Fibrin network was observed and analyzed with fluorescent microscopy.

Results

The BXPC3 and MDA-MB231 cells expressed significantly higher amount of TF induced significantly higher endogenous thrombin potential (ETP) as compared to MCF7 cells and as compared to MCF73 cells (ETP: 729.64±28.79 nM.min, 96.95±39.53 nM.min, and 65.44±6.41 nM.min, respectively). The BXPC3 cells induced higher ETP as compared to MDA-MB231 cells. Fibrin clots formed by BXPC3 and MDA-MB231 cells showed a dense structure with fine fibers, whereas clots formed by MCF7 cells are less dense with thicker fibers. No significant differences were observed between fibrin network formed by BXPC3 and MDA-MB321 cells.

Conclusion(s)

The procoagulant fingerprint of cancer cell lines was associated with variations in their potential to induce thrombin generation, which influences the structure of the fibrin clot. Fibrin network derived from aggressive cancers of pancreas (BXPC3) or the breast (MDA-MB231) showed a more dense structure as compared to those derived from less aggressive breast cancer cells (MCF7). The fibrin network could provide a protection of cancer cells against natural immunosurveillance system and could be a mechanism contributing to resistance to anticancer treatment.

3.2. Colonization of Fibrin Clot Formed by Cancer Cells in Tumor Microenvironment. A Mechanism Potentially Related with Resistance to the Anticancer Treatment

1. Huong Chi Mai Tran (Role: Co-Author)
2. Noémie Mourot (Role: Co-Author)
3. Beshoy Faltas (Role: Co-Author)
4. Elisabeth Mbemba (Role: Co-Author)
5. Ismail Elalamy (Role: Co-Author)
6. Michele Sabbah (she/her/hers) (Role: Co-Author)
7. Jawed Fareed (Role: Co-Author)
8. Patrick Van Dreden (Role: Presenting Author)
9. Grigorios Gerotziafas (Role: Co-Author)

Background

Cancer cells via Tissue Factor (TF) expression and release of TF-bearing microvesicles trigger thrombin generation (TG) leading to fibrin clot formation in their microenvironment. The fibrinolytic potential of cancer cells is a key property for invasion, migration and metastasis.

Aims

Investigation of the colonization of fibrin clot by cancer cells

Methods

Cells from pancreatic and breast cancer (BXPC3, MDA-MB231, MCF7), were put in contact with normal human platelet poor plasma (PPP) enriched with fluorescent fibrinogen. The concentrations of tPA and D-Dimer in conditional media were measured at 2h intervals for an

observational period of 72h. Fluorescent microscopy was used for the study of cancer cell invasion in the fibrin network and MTT assay was used for the assessment of cell viability.

Results

BXPC3 and MDA-MB231 but not MCF7 cells expressed tPA. In the presence of BXPC3 and MDA-MB231 cells, within 20h, the concentration of tPA in the conditioned media significantly increased by 3- and 1.5-fold respectively and that of D-Dimers increased by 50 folds. D-Dimers expotentially increased until the end of the observation period. In the presence of MCF7 no significant increase of tPA and D-dimers was observed. Fluorescent microscopy analysis showed the presence of numerous clusters of BXPC3 or MDA-MB231 cells within the clot. Lower number of MCF7 clusters were discovered. Cancer cells of the intra-clot clusters were alive and migrated from the initial monolayer of the cell culture.

Conclusion(s)

This study documents the presence of cancer cells clusters within the fibrin clot which is related with their constitutional capacity to express tPA and to induce fibrinolysis. Aggressive pancreatic and breast cancer cells possessed significant highly fibrinolytic potential. This proof-of-concept study provides evidence of a new mechanism which could contribute to the development of resistance to anticancer treatment.

4. ISTH 2022 : Poster

4.1. Impacts of antithrombotic agents on cellular physiology in the tumoral microenvironment

HCM. Tran1,2, R. Amrane1,2, E. Mbemba1, M. Sabbah1, P. Van Dreden2, 1, G. Gerotziafas1

1INSERM, UMR_S 938, Centre de Recherche Saint-Antoine - Cancer Biology and Therapeutics Team, «Cancer-Hemostasis-Angiogenesis» Group, Institut Universitaire de Cancérologie, F-75012, Sorbonne Université, PARIS.

2Clinical Research, Diagnostica Stago, Gennevilliers.

Background

In prevention and treatment of cancer-associated thrombosis, antithrombotic agents in some cases are prescribed for cancer patients. Recent emerging studies suggest that their involvements in the tumoral microenvironment could go beyond their catalytic activities in the cascade of coagulation.

Aim

The aim of this study is to investigate the role of Low Molecular Weigh Heparins (LMWH), Unfractionated Heparin (UFH), and Direct Oral Anticoagulants (DOAC) on the cellular physiology in the tumoral microenvironment.

Methods

BXPC3 cells were exposed to enoxaparin (2 anti-Xa UI/ml), tinzaparin (2 anti-Xa UI/ml), fondaparinux (2 µg/ml), or Apixaban (2 µg/ml) for 48h. A thrombin generation (TG) assay was conducted to investigated the coagulant properties of cells and their conditioned media after treatment. Cells were also tested for their viability by MTT assay. mRNA expression of Tissue Factor (TF), Vascular Endothelial Growth Factor (VEGF), and Thrombospondin 1 (THSB1) were evaluated by RT-qPCR. An specific amidolytic assay was used to measure the residual anti-Xa activity in the conditioned media.

HUVEC cells were exposed to Lipopolysaccharide (LPS) for 24h, then to either danaparoid or enoxaparin at 1 UI/ml for another 24h. Their viability was evaluated using the MTT assay.

Results

Antithrombotic agents significantly impair TG capacity of the conditioned media, but not that of BXPC3 cells. A significant decrease of mRNA expression of TF by apixaban, of VEGF by fondaparinux and enoxaparin, and a significant increase of mRNA expression of THBS1 by apixaban, were observed. Cell viability was reduced by enoxaparin (14%), tinzaparin (11%), fondaparinux (12%), and apixaban (30%). Exposure to BXPC3 induced a decrease of the concentration of fondaparinux (27%), enoxaparin (48%) and tinzaparin (26%) in the conditioned media, but did not significantly impact that of apixaban.

Conclusions

Antithrombotic agents interfere with tumoral microenvironment not only by impairing the pro-coagulant properties of cancer cells' secretome, but also by altering cell viability, and gene expression of pro- and antiangiogenic factors VEGF and THBS1. Nonetheless, a degradation of LMWH and fondaparinux was observed after two days of exposure to cancer cells.

5. American Society of Hematology (ASH) 2022 : Poster

5.1. Cancer Cells and Platelets Have a Synergistic Role on the Acceleration of Clot Formation and Fibrin Polymerization. A Thromboelastometric Study

Elisabeth Mbemba[1], Huong Chi Mai Tran[1, 2], Noemie Mourot[1], Beshoy Faltas[1], Mohammed Baghdadi[1], Ismail Elalamy[1,3], Patrick Van Dreden[1, 2], Grigoris T Gerotziafas[1, 3]

[1]Sorbonne Université, INSERM, UMR_S 938, Centre de recherche Saint-Antoine (CRSA), Research Group "Cancer, Biology and Therapeutics", Research Team "Cancer, Haemostasis, Angiogenesis", Paris, France; Institut Universitaire de Cancérologie, Sorbonne Université, Paris, France.

[2]Clinical Research Department, Diagnostica Stago, Gennevilliers, France.

[3]Thrombosis Center, Service d'Hématologie Biologique Hôpital Tenon, Hôpitaux Universitaires de l'Est Parisien, Assistance Publique Hôpitaux de Paris, Faculté de Médecine Sorbonne Université, Paris, France.

Introduction

The histological type and the aggressiveness of cancer cells as well as the acquisition of resistance to chemotherapy are significant predictors for the high risk of cancer associated thrombosis (CAT).

It is well established that cancer cells, by expressing tissue factor (TF) trigger thrombin generation. Cancer cell derived extracellular vesicles (CaCa-dEV) bearing TF, in the microenvironment, further enhance thrombin generation. The impact of cancer cells on clot formation kinetics and the qualitative characteristics of the clot has not been evaluated yet.

Aim

The present study aimed to analyze the variables which influence the kinetics and the qualitative characteristics of the clot after triggering thrombin generation by cells from pancreatic cancer

(BXPC3), breast cancer (MCF7 and MCF7R10) and multiple myeloma (RPMI-8226 and U266) - associated with different risk of CAT. The impact of the resistance to chemotherapy on the clot characteristics was also studied.

Methods

Cancer cell lines (BXPC3, MCF7, MCF7R10, RPMI-8226 and U266) and primary umbilical vein endothelial cells (HUVEC) for the control experiments were used according to standardized and validated experimental procedure. Doxorubicin resistant breast cancer cells (MCF7R10) were obtained by treating native breast cancer cells (MCF7) by increasing concentrations of Doxorubicin from 5 nM to 10 µM..

Thromboelastometry, using the ROTEM® delta device (from Warfen Paris, France), was used for the study of clot formation and firmness in whole blood (WB), platelet rich and platelet poor plasma (PRP and PPP respectively) in the presence of cancer cells or HUVEC (control). A suspension of 200 µL with 10^5 cells was placed in each sterilized cup. Following an incubation of 4 hour, culture media was removed and 330 µL of WB, PRP or PPP were added followed by addition of 20 µM of $CaCl_2$ (0.2 M). Clotting time (CT), α-angle and maximum clot firmness (MCF) were analyzed.

Results

In PPP, pancreatic cancer cells BXPC3 as well as chemotherapy sensitive and resistant breast cancer cells (MCF7 and MCF7R10), significantly reduced the CT. MCF7R10 cells significantly reduced the CT as compared to MCF7. In contrast, myeloma cells (RPMI8226 and U266), did not significantly affect the CT. All studied cancer cell lines significantly increased the α-angle as compared to HUVEC, with the most potent effect from BXPC3 cells. The studied cancer cell lines did not significantly affect MCF.

In PRP, BXPC3 cells significantly reduced the CT whereas MCF7 and MCF7R10 did not significantly change the CT, and myeloma cells significantly prolonged the CT as compared to HUVEC. BXPC3 cells significantly increased the α-angle as compared to the HUVEC, whereas the other studied cancer cell lines did not have any significant effect on this parameter. BXPC3,

MCF7 and MCF7R10 cells did not significantly affect the MCF whereas the myeloma cells significantly decreased the MCF as compared to HUVEC.

In WB, BXPC3 and MCF7 cells significantly decreased the CT whereas MCF7R10 did not show any significant effect and the myeloma cells significantly prolonged it. The α-angle significantly increased in the presence of BXPC3 cells whereas the other cell lines did not show any significant effect on this parameter. The presence of cancer cells resulted in significant decrease of the MCF as compared to the control (HUVEC), with the most potent effect from myeloma.

In the control experiment (HUVEC), the comparison of the thromboelastometric profile of the three experimental systems (PPP, PRP and WB) showed that platelets (PRP) had a substantial impact on CT, α-angle and MCF whereas the erythrocytes (in WB) did not further modify these parameters. The same pattern of the role of platelets was observed in the presence of the studied cancer cell lines.

Discussion

The present study provides experimental evidence documenting that cancer cells impact clot formation kinetics without affecting clot firmness. The impact of cancer cells on clot formation kinetics is determined principally by the histological type. The pancreatic adenocarcinoma cells have a more pronounced effect on clot formation kinetics as compared to the breast cancer cells (sensitive or resistant to Doxorubicine). In contrast, multiple myeloma cells delay fibrin formation and polymerization and decrease the clot firmness. Platelets have a synergistic effect with cancer cells on the acceleration of the clot formation kinetics.

Table : Impact of cancer cells on clot formation kinetics and clot firmness. Results are expressed as Mean ± SD, n = 3. CT: Clotting Time. MCF: Maximum Clot Firmness. PPP: Platelet Poor Plasma. PRP: Platelet Rich Plasma. WB: Whole Blood. BXPC3 : Pancreatic cancer cells. MCF7: Breast cancer cells. MCF7R10: Breast cancer cells resistant to 10 µM of Doxorubicin. RPMI 8226 and U266: myeloma cells. HUVEC: primary human umbilical vein cells.

*p < 0.05 vs PPP ; $ p < 0.05 vs HUVEC; £ p < 0.05 vs MCF7 or MCF7R10

Thrombo-elastometry parameters	Experimental system	HUVEC	BXPC3	MCF7	MCF7R	RPMI 8226	U266
CT (sec)	PPP	636 ± 114	228 ± 20$£	490 ± 30$	413 ± 50$	642 ± 28	709 ± 33$
	PRP	424 ± 70*	136 ± 18*$£	435 ± 32*$	363 ± 58*$	588 ± 92*$	651 ± 79*$
	WB	322± 50*	142 ± 15*$£	206 ± 25*$	390 ± 32*	461 ± 30*$	435 ± 41*$
α-angle (°)	PPP	24 ± 11	45 ± 12$£	32 ± 2$	35 ± 6$	35 ± 6$	34 ± 3$
	PRP	56 ± 5*	69 ± 3*$	54 ± 9*	58 ± 1*	53 ± 11*	52 ± 8*
	WB	52 ± 7*	61 ± 8*$	53 ± 4*	57 ± 4*	54 ± 6*	57 ± 8*
MCF (mm)	PPP	23 ± 4	21 ± 2	18 ± 2	23 ± 5	30 ± 4	28 ± 3
	PRP	60 ± 3*	51 ± 7*	52 ± 3*	52 ± 4*	30 ± 10	38 ± 13*
	WB	55 ± 5*	45 ± 1*	41 ± 4*	47 ± 5*	31 ± 7	40 ± 6*

6. ASH 2021 : Poster

6.1. Impact of LMWH and Specific Factor Xa Inhibitors, Apixaban and Fondaparinux, on Cancer Cell Biology and Procoagulant Properties of Cancer Microenvironment

HCM. Tran1, R. Amrane1, E. Mbemba1, M. Sabbah1, P. Vandreden2, 1, G. Gerotziafas1

1INSERM, UMR_S 938, Centre de Recherche Saint-Antoine - Cancer Biology and Therapeutics Team, «Cancer-Hemostasis-Angiogenesis» Group, Institut Universitaire de Cancérologie, F-75012, Sorbonne Université, PARIS.

2Clinical Research, Diagnostica Stago, Gennevilliers.

Due to high risk of cancer-associated thrombosis risk, cancer patients in some case are treated with antithrombotic agents. In the present study, we investigated the interaction between these agents with pancreatic cancer cells, as well as with their microenvironment. The impact of apixaban, fondaparinux, enoxaparin and tinzaparin on the procoagulant properties of pancreatic cancer cells BXPC3 was examinated. Reciprocally, we also investigated the impact of BXPC3 on the potency of these antithrombotic agents.

After 48 hours of exposure to apixaban (2 µg/ml), fondaparinux (2 µg/ml), enoxaparin, or tinzaparin (2 anti-Xa IU/ml) at density of 400 cells/ml, supernatants and BXPC3 cells were harvested, separated, and tested for thrombin generation (TG) experiments in normal platelet-poor plasma (PPP). Cells' viability was also assessed with the MTT assay. Gene expression for Tissue Factor (TF), Vascular Endothelial Growth Factor (VEGF), Thrombospondin 1 (THSB1) was assessed with RT-qPCR. Expression of TF protein and activity of cancer cells, as well as of cancer-cell-released Microparticles (MP) was assessed using ELISA method. Residual anti-Xa activity in supernatant was measured using specific amidolytic assays.

TG was enhanced by BXPC3 cells. Antithrombotic agents did not significantly modify this TG capacity after 48 hours of incubation. Apixaban resulted in significant TF mRNA expression decrease. However, protein expression of TF was not significantly modified by any of the antithrombotic agents. VEGF's mRNA expression was significantly decreased by fondaparinux

and enoxaparin. THBS1's mRNA expression was significantly increased by apixaban. Apixaban, fondaparinux, enoxaparin, and tinzaparin reduced cell viability respectively by 25%, 12 %, 14%, and 11%. MP generation by cancer cells was not impacted by exposure to antithrombotic agents. The potency of inducing TG of the supernatants was decreased by apixaban (70%), fondaparinux (30%), enoxaparin (40%) and tinzaparin (90%). After 48 hours of exposure, BXPC3 cells reduced the concentration of fondaparinux, enoxaparin and tinzaparin in the supernatant by 27%, 48% and 26% respectively, but did not significantly impact the concentration of apixaban.

Although antithrombotic agents did not have any impact on the expression of TF, nor on the release of MP of cancer cells, they could inhibit the procoagulant potency of cancer microenvironment. Nonetheless, a degradation of low-molecular-weight-heparins and fondaparinux was observed after two days of exposure to cancer cells. The mRNA expression of pro- and antiangiogenic factor, as well as the viability of pancreatic cancer cells were also impaired by these antithrombotic agents.

Table: Impact of antithrombotic agents on BXPC3 cells, on their MP, and on the capacity of trigger thrombin generation of their culture supernatants. Cells were treated with 2 UI/ml of fondaparinux/apixaban, or 2 µg/ml of tinzaparin/enoxaparin for 48 hours. mRNA expression were normalized using the 2^(- Δ(ΔCq)) method. *: $p < 0.05$ as compare to Control experiment.

	Cells				
	Control	Fondaparinux	Enoxaparin	Tinzaparin	Apixaban
Peak of Thrombin Generation (nM)	120,57 ± 26,36	136,95 ± 35,96	135,71 ± 28,87	135,70 ± 32, 98	126,71 ± 29,52
TF normalized mRNA expression rate	1,00 ± 0,35	0,64 ± 0,10	1,41 ± 0,13	0,62 ± 0,77	0,50 ± 0,19 *
TF protein expression (pg/ml)	0,71 ± 0,36	0,79 ± 0,60	1,02 ± 0,58	0,99 ± 0,45	0,74 ± 0,41
Viability rate	1,00 ± 0,00	0,88 ± 0,03 *	0,86 ± 0,06 *	0,89 ± 0,03 *	0,75 ± 0,05 *
VEGF normalized mRNA expression rate	1,00 ± 0,12	0,27 ± 0,00 *	0,69 ± 0,08 *	0,55 ± 0,83	0,88 ± 0,01
THBS1 normalized mRNA expression rate	1,00 ± 0,21	0,65 ± 0,25	0,57 ± 1,17	0,51 ± 0,45	1,40 ± 0,03 *
	MP				
PS (nM)	0,71 ± 0,36	0,79 ± 0,60	1,02 ± 0,58	0,99 ± 0,45	0,74 ± 0,41
TF protein expression (pg/ml)	1,42 ± 0,40	1,53 ± 0,60	2,87 ± 1,35	2,85 ± 0,70	1,10 ± 0,63
	Supernatant				
Lagtime (min)	3,23 ± 0,56	4,45 ± 1,07 *	5,04 ± 1,57 *	3,73 ± 1,75	5,23 ± 1,10 *
ETP (nM.min)	1472,05 ± 269,96	1174,79 ± 265,83	471,15 ± 207,88 *	154,63 ± 19,63 *	508,37 ± 258,51 *
Peak (nM)	194,18 ± 29,22	145,34 ± 24,36 *	42,80 ± 11,96 *	9,48 ± 2,00 *	49,67 ± 16,76 *
ttPeak (min)	6,26 ± 0,80	7,73 ± 1,32 *	8,37 ± 2,13	14,30 ± 5,16 *	7,99 ± 1,55 *

Vellocity Index (nM/min)	63,92 ± 5,25	44,22 ± 5,31 *	14,12 ± 7,01 *	1,29 ± 0,69 *	19,22 ± 8,26 *
MRI (nM/min)	63,87 ± 5,26	44,10 ± 5,05 *	14,03 ± 7,07 *	1,24 ± 0,72 *	19,15 ± 8,27 *

7. Haemostasis And Thrombosis Association (GTH) 2021 : Oral communication :

7.1. Modelization the impact of antithrombotic agents on pancreatic tumoral micro-environment

H-C-M. Tran[1], R. Amrane[1], E. Mbemba[1], M. Sabbah[1], P. Vandreden[2, 1], G. Gerotziafas[1]

[1]INSERM, UMR_S 938, Centre de Recherche Saint-Antoine- Team Cancer Biology and Therapeutics,Group « Cancer-Hemostasis-Angiogenesis », Institut Universitaire de Cancérologie, F-75012, Sorbonne Université, PARIS.

[2]Clinical Research, Diagnostica Stago, Gennevilliers.

Interactions between cancer cells and their micro-environment with antithrombotic agents is an emerging field of research. In the present study we investigated the impact of apixaban, fondaparinux, enoxaparin and tinzaparin on the procoagulant properties of pancreatic cancercells BXPC3. Reciprocally, we investigated the impact of BXPC3 on the potency of these antithrombotic agents.

BXPC3 (400 cells/ml) were exposed to apixaban (2 microgram/ml), fondaparinux (2 microgram/ml), enoxaparin, or tinzaparin (2 anti-Xa IU/ml) for 48h. Then, cells and supernatants were separated and added in normal platelet poor plasma (PPP) for thrombin generation (TG) experiments. Viability of cancer cells (assessed with the MTT assay), gene expression for TF, VEGF, THSB1 (assessed with RT-qPCR) and expression of TF protein and activity were also examined. Microparticles (MP) were tested for TF with specific ELISA. Residual anti-Xa activity was measured in the supernatant using specific amidolytic assays.

BXPC3 enhanced TG. Incubation of the BXPC3 cells with all antithrombotic agents did not significantly modify their TG capacity. Apixaban resulted in significant TF mRNA expression decrease by BXPC3 cells. None of the antithrombotic agents significantly modified the amountof BXPC3 cells -TF protein. Fondaparinux and enoxaparin significantly decreased VEGF mRNA expression and apixaban significantly increased the expression of THBS1. The viability of BXPC3 cells was significantly reduced following exposure to apixaban (25%), fondaparinux (12%), enoxaparin (14%) or tinzaparin (11%). Exposure of BXPC3 to antithrombotic agents did not significantly modify the release of MP. Apixaban, fondaparinux, enoxaparin and tinzaparindecreased TG induced by the supernatant by 70%, 30%, 40%, 90% respectively. After exposure to BXPC3 cells the concentration of fondaparinux, enoxaparin and tinzaparin in the supernatant reduced by 27%, 48% and 26% respectively. In contrast the concentration of apixaban did not significantly change.

Antithrombotic agents do not alter cancer cells' TF expression or procoagulant MP release, but inhibit the procoagulant potency of microenvironment. Nevertheless, a LMWHs and fondaparinux degradation occurs following two days of exposure to cancer cells. Antithrombotic agents reduced tumour cells' viability and impaired mRNA expression of pro-and antiangiogenic factors.

Table: Impact pf antithrombotic agents on BXPC3 cells, on their MP, and on the capacity of trigger thrombin generation of their culture supernatants. Cells were treated with 2 UI/ml ofFondaparinux/Apixaban, or 2 micro gram/ml of Tinzaparin/Enoxaparin for 48h. mRNA expression were normalized using the 2^(-delta(deltaCq)) method. *: $p < 0.05$ as compare toControl experiment.

	Cells				
	Control	Fondaparinux	Enoxaparin	Tinzaparin	Apixaban
Peak of Thrombin Generation (nM)	120,57 ± 26,36	136,95 ± 35,96	135,71 ± 28,87	135,70 ± 32,98	126,71 ± 29,52
TF normalized mRNA expression rate	1,00 ± 0,35	0,64 ± 0,10	1,41 ± 0,13	0,62 ± 0,77	0,50 ± 0,19 *
TF protein expression (pg/ml)	0,71 ± 0,36	0,79 ± 0,60	1,02 ± 0,58	0,99 ± 0,45	0,74 ± 0,41
Viability rate	1,00 ± 0,00	0,88 ± 0,03 *	0,86 ± 0,06 *	0,89 ± 0,03 *	0,75 ± 0,05 *
VEGF normalized mRNA expression rate	1,00 ± 0,12	0,27 ± 0,00 *	0,69 ± 0,08 *	0,55 ± 0,83	0,88 ± 0,01
THBS1 normalized mRNA expression rate	1,00 ± 0,21	0,65 ± 0,25	0,57 ± 1,17	0,51 ± 0,45	1,40 ± 0,03 *
	MP				
PS (nM)	0,71 ± 0,36	0,79 ± 0,60	1,02 ± 0,58	0,99 ± 0,45	0,74 ± 0,41
TF protein expression (pg/ml)	1,42 ± 0,40	1,53 ± 0,60	2,87 ± 1,35	2,85 ± 0,70	1,10 ± 0,63
	Supernatant				
Lagtime (min)	3,23 ± 0,56	4,45 ± 1,07 *	5,04 ± 1,57 *	3,73 ± 1,75	5,23 ± 1,10 *
ETP (nM.min)	1472,05 ± 269,96	1174,79 ± 265,83	471,15 ± 207,88 *	154,63 ± 19,63 *	508,37 ± 258,51 *

Peak (nM)	194,18 ± 29,22	145,34 ± 24,36 *	42,80 ± 11,96 *	9,48 ± 2,00 *	49,67 ± 16,76 *
ttPeak (min)	6,26 ± 0,80	7,73 ± 1,32 *	8,37 ± 2,13	14,30 ± 5,16 *	7,99 ± 1,55 *
Vellocity Index (nM/min)	63,92 ± 5,25	44,22 ± 5,31 *	14,12 ± 7,01 *	1,29 ± 0,69 *	19,22 ± 8,26 *
MRI (nM/min)	63,87 ± 5,26	44,10 ± 5,05 *	14,03 ± 7,07 *	1,24 ± 0,72 *	19,15 ± 8,27 *